

NASA Tech Briefs

National
Aeronautics and
Space
Administration

Have You Requested
The 1978 NASA Tech Briefs Index?
[See Page A2.]

Computer-processed satellite images are helping planners evaluate the potential impact of increasing agricultural irrigation on the ecology of Florida's Suwannee Sound area, shown in this color-coded Landsat view. Assistance in using satellite data is offered by NASA to Government and private industry for such programs as environmental assessment and monitoring, land-use planning, agriculture, forestry, mineral exploration, and other resource management. To find out how to obtain information about these programs, see the bottom of page A1.

About the NASA Technology Utilization Program

The National Aeronautics and Space Act of 1958, which established NASA and the United States civilian space program, requires that "The Administration shall provide for the widest practicable and appropriate dissemination of information concerning its activities and the results thereof."

To help carry out this objective, NASA's Technology Utilization (TU) Program was established in 1962. Now, as an element of NASA's Technology Transfer Division, this program offers a variety of valuable services to help transfer aerospace technology to nonaerospace applications, thus assuring American taxpayers maximum return on their investment in space research; thousands of spinoffs of NASA research have already occurred in virtually every area of our economy.

The TU program has worked for engineers, scientists, technicians, and businessmen; and it can work for you.

NASA Tech Briefs

Tech Briefs is published quarterly and is free to engineers in U.S. industry and to other domestic technology transfer agents. It is both a current-awareness medium and a problem-solving tool. Potential products . . . industrial processes . . . basic and applied research . . . shop and lab techniques . . . computer software . . . new sources of technical data . . . concepts . . . can be found here. The short section on New Product Ideas highlights a few of the potential new products contained in this issue. The remainder of the volume is organized by technical category to help you quickly review new developments in your areas of interest. Finally, a subject index makes each issue a convenient reference file.

Further Information on Innovations

Although some new technology announcements are complete in themselves, most are backed up by Technical Support Packages (TSP's). TSP's are available without charge and may be ordered by simply completing a TSP Request Card found at the back of this volume. Further information on some innovations is available for a nominal fee from other sources, as indicated. In addition, Technology Utilization Officers at NASA Field Centers will often be able to lend necessary guidance and assistance.

Patent Licenses

Patents have been issued to NASA on some of the inventions described, and patent applications have been submitted on others. Each announcement indicates patent status, if applicable.

Other Technology Utilization Services












To assist engineers, industrial researchers, business executives, city officials, and other potential users in applying space technology to their problems, NASA sponsors Industrial Applications Centers. Their services are described on page A7. In addition, an extensive library of computer programs is available through COSMIC, the Technology Utilization Program's outlet for NASA-developed software.

Applications Program

NASA conducts applications engineering projects to help solve public-sector problems in such areas as safety, health, transportation, and environmental protection. Applications teams, staffed by professionals from a variety of disciplines, assist in this effort by working with Federal agencies and health organizations to identify critical problems amenable to solution by the application of existing NASA technology.

Reader Feedback

We hope you find the information in *NASA Tech Briefs* useful. A reader-feedback card has been included because we want your comments and suggestions on how we can further help you apply NASA innovations and technology to your needs. Please use it; or if you need more space, write to the Director, Technology Transfer Division, P. O. Box 8757, Baltimore/Washington International Airport, Maryland 21240.

NASA TU Services	A3	Technology Utilization services that can assist you in learning about and applying NASA technology.	
New Product Ideas	A9	A summary of selected innovations of value to manufacturers for the development of new products.	
Tech Briefs	131	Electronic Components and Circuits	
	147	Electronic Systems	
	159	Physical Sciences	
	177	Materials	
	185	Life Sciences	
	189	Mechanics	
	211	Machinery	
	229	Fabrication Technology	
	249	Mathematics and Information Sciences	
	Subject Index	257	Items in this issue are indexed by subject; a cumulative index will be published yearly.

COVERS: The photographs on the front and back covers illustrate developments by NASA and its contractors that have resulted in commercial and nonaerospace spinoffs. To find out more about the application of satellite images [Regional Remote-Sensing Applications Program], Circle 100 on the TSP Request Card at the back of this issue of NASA Tech Briefs. To find out more about the metalized products, Circle 101.

About This NASA Publication

NASA Tech Briefs, a quarterly publication, is distributed free to qualified U.S. citizens to encourage commercial application of U.S. space technology. For information on publications and services available through the NASA Technology Utilization Program, write to the Director, Technology Transfer Division, P. O. Box 8757, Baltimore/Washington International Airport, Maryland 21240.

"The Administrator of National Aeronautics and Space Administration has determined that the publication of this periodical is necessary in the transaction of the public business required by law of this Agency. Use of funds for printing this periodical has been approved by the Director of the Office of Management and Budget."

Change of Address

If you wish to have NASA Tech Briefs forwarded to your new address, use one of the Subscriptions cards enclosed in the back of this volume of NASA Tech Briefs. Be sure to check the appropriate box indicating change of address.

Communications Concerning Editorial Matter

For editorial comments or general communications about NASA Tech Briefs, you may use the Feedback card in the back of NASA Tech Briefs, or write to: The Publications Manager, Technology Transfer Division (ETD-6), NASA Headquarters, Washington, DC 20546. Technical questions concerning specific articles should be directed to the Technology Utilization Officer of the sponsoring NASA Center (addresses listed on page A4).

1978 Index

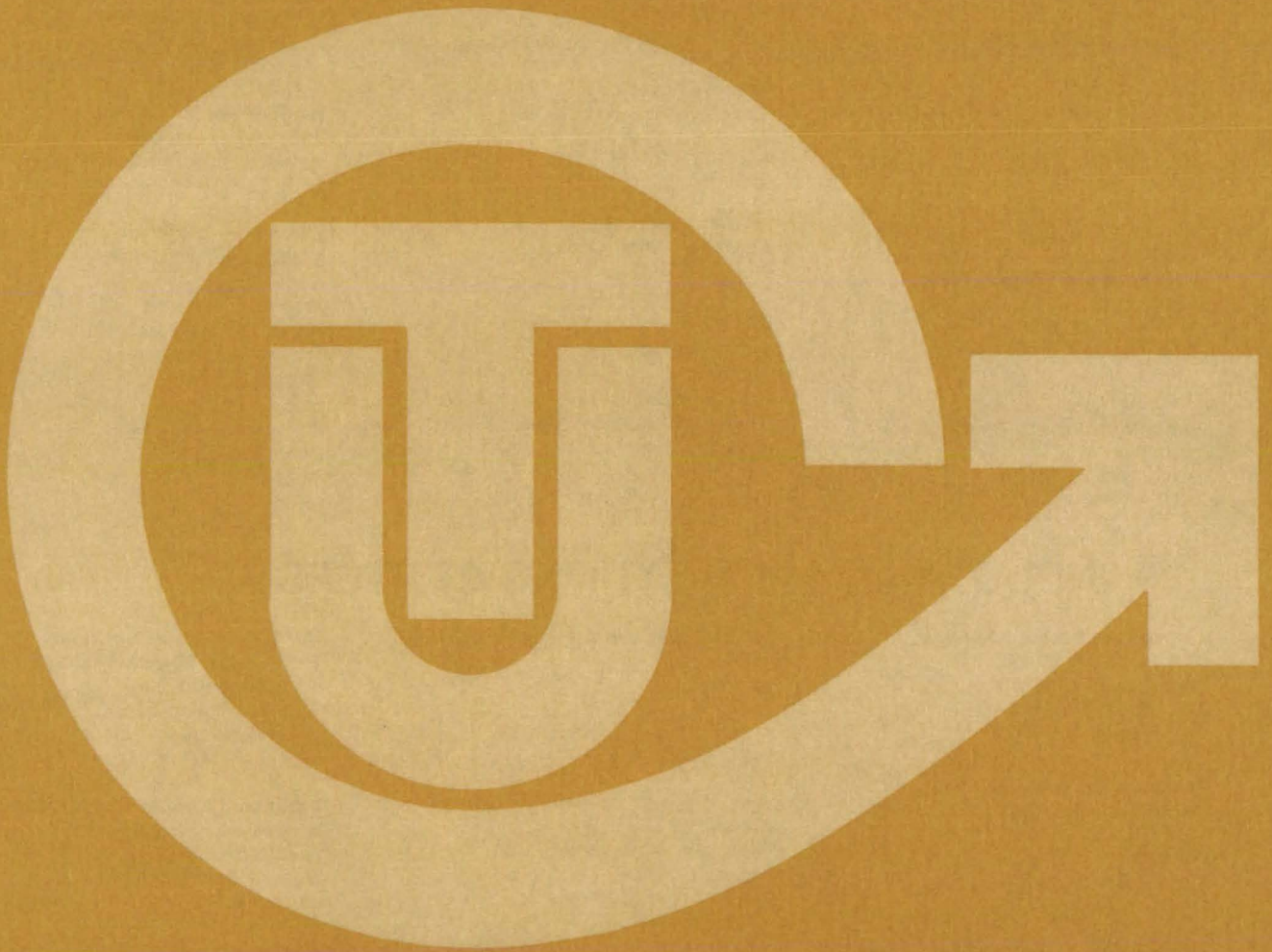
Readers who wish to request a copy of the 1978 Index to NASA Tech Briefs may still do so by Circling 102 on the TSP Request Card at the back of this issue.

Acknowledgements

NASA Tech Briefs is published quarterly by the National Aeronautics and Space Administration, Technology Utilization Branch, Washington, DC: Administrator: **Robert A. Frosch**; Director, Technology Transfer Division: **Floyd I. Roberson**; Publications Manager: **D. W. Orrick**. Prepared for the National Aeronautics and Space Administration by **Logical Technical Services Corp.**: Editor-in-Chief: **Jay Kirschenbaum**; Art Director: **Ernest Gillespie**; Assistant Editor: **Jerome Rosen**; Chief Copy Editor: **Oden Browne**; Staff Editors: **Donald Blattner, Ted Selinsky, George Watson**; Graphics: **Concetto Auditore, Luis Martinez**; Editorial & Production: **Richard Johnson, Rose Giglietti, Beth Rogers, Vincent Susinno, John Tucker, Ernestine Walker**.

This document was prepared under the sponsorship of the National Aeronautics and Space Administration.. Neither the United States Government nor any person acting on behalf of the United States Government assumes any liability resulting from the use of the information contained in this document, or warrants that such use will be free from privately owned rights.

NASA TU SERVICES



NASA TECHNOLOGY UTILIZATION NETWORK

★ TECHNOLOGY UTILIZATION OFFICERS

Charles C. Kubokawa
Ames Research Center
Code AU: 240-2
Moffett Field, CA 94035
(415) 965-5333

Gussie Anderson
Hugh L. Dryden Flight Research Center
Code OD/TU Office - Room 2015
Post Office Box 273
Edwards, CA 93523
(805) 258-3311, Ext. 787

Donald S. Friedman
Goddard Space Flight Center
Code 702.1
Greenbelt, MD 20771
(301) 344-6242

John T. Wheeler
Lyndon B. Johnson Space Center
Code AT-3
Houston, TX 77058
(713) 483-3809

Raymond J. Cerrato
John F. Kennedy Space Center
Code PT-STA-1
Kennedy Space Center, FL 32899
(305) 867-2780

John Samos
Langley Research Center
Mail Stop 139A
Hampton, VA 23665
(804) 827-3281

Harrison Allen, Jr.
Lewis Research Center
Mail Code 7-3
21000 Brookpark Road
Cleveland, OH 44135
(216) 433-4000, Ext. 6422

Aubrey D. Smith
George C. Marshall Space Flight Center
Code AT01
Marshall Space Flight Center, AL 35812
(205) 453-2224

D. W. Orrick
NASA Headquarters
Code ETD-6
Washington, DC 20546
(202) 755-2244

John H. Warden
NASA Pasadena Office
4800 Oak Grove Drive
Pasadena, CA 91103
(213) 354-6420

Gilmore H. Trafford
Wallops Flight Center
Code OD
Wallops Island, VA 23337
(804) 824-3411, Ext. 201

● INDUSTRIAL APPLICATIONS CENTERS

Aerospace Research Applications Center
1201 East 38th Street
Indianapolis, IN 46205
E. G. Buck, director
(317) 264-4644

Computer Software Management and Information Center (COSMIC)
Suite 112, Barrow Hall
University of Georgia
Athens, GA 30602
(404) 542-3265

Kerr Industrial Applications Center
Southeastern Oklahoma State University
Durant, OK 74701
Robert Oliver, director
(405) 924-0121, Ext. 413

NASA Industrial Applications Center
LIS Building
University of Pittsburgh
Pittsburgh, PA 15260
Edmond Howie, director
(412) 624-5211

New England Research Applications Center
Mansfield Professional Park
Storrs, CT 06268
Daniel Wilde, director
(203) 486-4533

North Carolina Science and Technology Research Center
Post Office Box 12235
Research Triangle Park, NC 27709
Peter J. Chenery, director
(919) 549-0671

Technology Applications Center
University of New Mexico
Albuquerque, NM 87131
Stanley Morain, director
(505) 277-3622

Western Research Applications Center
University of Southern California
University Park
Los Angeles, CA 90007
Robert Mixer, acting director
(213) 741-6132

■ STATE TECHNOLOGY APPLICATIONS CENTERS

NASA/University of Florida State Technology Applications Center
311 Weil Hall
University of Florida
Gainesville, FL 32611
Ronald J. Thornton, director
Gainesville: (904) 392-6760
Orlando: (305) 275-2706
Tampa: (813) 974-2499

NASA/University of Kentucky State Technology Applications Program
109 Kinkead Hall
University of Kentucky
Lexington, KY 40506
William R. Strong, manager
(606) 258-4632



◆ PATENT COUNSELS

Robert F. Kempf
Asst. Gen. Counsel for patent matters
NASA Headquarters
 Code GP-4
 400 Maryland Avenue, S.W.
 Washington, DC 20546
 (202) 755-3954

Darrell G. Brekke
Ames Research Center
 Mail Code: 200-11A
 Moffett Field, CA 94035
 (415) 965-5104

Paul F. McCaul
Hugh L. Dryden Flight Research Center
 Code OD/TU Office - Room 2015
 Post Office Box 273
 Edwards, CA 93523
 (213) 354-2734

John O. Tresansky
Goddard Space Flight Center
 Mail Code: 204
 Greenbelt, MD 20771
 (301) 344-7351

Marvin F. Matthews
Lyndon B. Johnson Space Center
 Mail Code: AM
 Houston, TX 77058
 (713) 483-4871

James O. Harrell
John F. Kennedy Space Center
 Mail Code: SA-PAT
 Kennedy Space Center, FL 32899
 (305) 867-2544

Howard J. Osborn
Langley Research Center
 Mail Code: 279
 Hampton, VA 23665
 (804) 827-3725

Norman T. Musial
Lewis Research Center
 Mail Code: 500-311
 21000 Brookpark Road
 Cleveland, OH 44135
 (216) 433-4000, Ext. 346

Leon D. Wofford, Jr.
George C. Marshall Space Flight Center
 Mail Code: CC01
 Marshall Space Flight Center, AL 35812
 (205) 453-0020

Monte F. Mott
NASA Pasadena Office
 Mail Code: 180-601
 4800 Oak Grove Drive
 Pasadena, CA 91103
 (213) 354-2700

▲ APPLICATION TEAMS

William N. Fetzner, director
**Advisory Center for Medical
 Technology and Systems**
 University of Wisconsin
 1500 Johnson Drive
 Madison, WI 53706
 (608) 263-2735

Edmund R. Bangs, director
IIT Research Institute
 10 West 35th Street
 Chicago, IL 60616
 (312) 567-4191

Doris Rouse, director
Research Triangle Institute
 Post Office Box 12194
 Research Triangle Park, NC 27709
 (919) 541-6256

Tom Anyos, director
SRI International
 333 Ravenswood Avenue
 Menlo Park, CA 94026
 (415) 326-6200, Ext. 2864

Eugene Schmidt, program coordinator
Stanford University School of Medicine
 Cardiology Division
 Biomedical Technology Transfer
 703 Welch Road, Suite E-4
 Palo Alto, CA 94304
 (415) 497-5353

David MacFadyen, project director
Technology + Economics
 2225 Massachusetts Avenue
 Cambridge, MA 02140
 (617) 491-1500

TECHNOLOGY UTILIZATION OFFICERS

Technology transfer experts can help you apply the innovations in NASA Tech Briefs.

The Technology Utilization Officer at each NASA Field Center is an applications engineer who can help you make use of new technology developed at his center. He brings you NASA Tech Briefs and other special publications, sponsors conferences, and arranges for expert assistance in solving technical problems.

Technical assistance, in the form of further information about NASA innovations and technology, is one of the services available from the TUO. Together with NASA scientists and engineers, he can often help you find and implement NASA technology to meet your specific needs.

Technical Support Packages (TSP's) are prepared by the center TUO's. They provide further technical details for articles in NASA Tech Briefs. This additional material can help you evaluate and use NASA technology. You may receive most TSP's free of charge by using the TSP Request Card found at the back of this issue.

Technical questions about articles in NASA Tech Briefs are answered in the TSP's. When no TSP is available, or you have further questions, contact the Technology Utilization Officer at the center that sponsored the research [see page A4].



NASA INVENTIONS AVAILABLE FOR LICENSING

Over 3,500 NASA inventions are available for licensing in the United States — both exclusive and nonexclusive.

Nonexclusive licenses

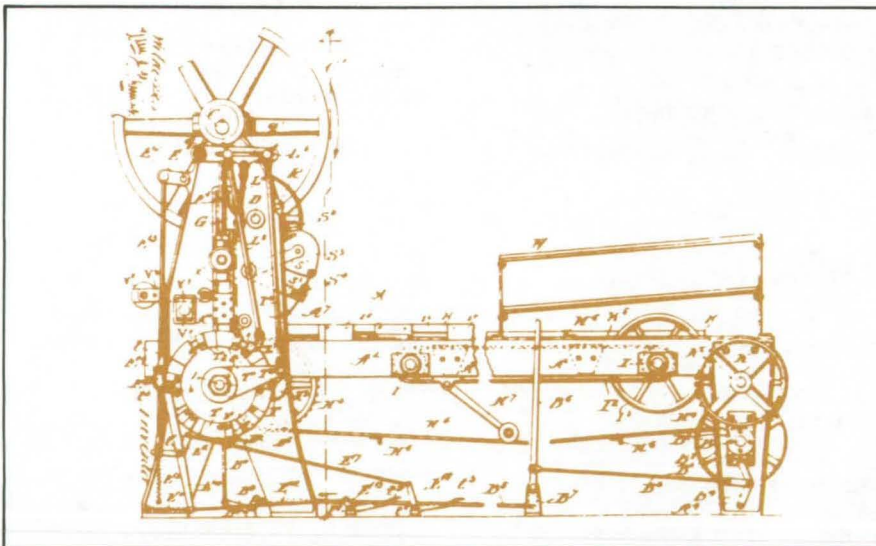
for commercial use of NASA inventions are encouraged to promote competition and to achieve the widest use of inventions. They must be used by a negotiated target date but are usually royalty-free.

Exclusive licenses

may be granted to encourage early commercial development of NASA inventions, especially when considerable private investment is required. These are generally for 5 to 10 years and usually require royalties based on sales or use.

Additional licenses available

include those of NASA-owned foreign patents. In addition to inventions described in NASA Tech Briefs, "NASA Patent Abstract Bibliography" (PAB), containing abstracts of all NASA inventions, can be purchased from National Technical Information Service, Springfield, VA 22161. The PAB is updated semiannually.



Patent licenses for Tech Briefs

are frequently available. Many of the inventions reported in NASA Tech Briefs are patented or are under consideration for a patent at the time they are published. The current patent status is described at the end of the article; otherwise, there is no statement about patents. If you want to know more about the patent program or are interested in licensing a particular invention, contact the Patent Counsel at the NASA Field Center that sponsored the research [see page A5]. Be sure to refer to the NASA reference number at the end of the Tech Brief.

APPLICATION TEAMS

Technology-matching and problem-solving assistance to public-sector organizations

Application engineering projects

are conducted by NASA to help solve public-sector problems in such areas as safety, health, transportation, and environmental protection. Some application teams specialize in biomedical disciplines; others, in engineering and scientific problems. Staffed by professionals from various disciplines, these teams work with other Federal agencies and health organizations to



identify critical problems amenable to solution by the application of existing NASA technology.

Public-sector organization

representatives can learn more about application teams by contacting a nearby NASA Field Center Technology Utilization Office [see page A4].

INDUSTRIAL APPLICATIONS CENTERS

Computerized access to nearly 10 million documents worldwide

Computerized information retrieval

from one of the world's largest banks of technical data is available from NASA's network of Industrial Applications Centers (IAC's). The IAC's give you access to 1,800,000 technical reports in the NASA data base and to more than 10 times that many reports and articles found in 140 other computerized data bases.

The major sources include:

- 750,000 NASA Technical Reports
- Selected Water Resources Abstracts
- NASA Scientific and Technical Aerospace Reports
- Air Pollution Technical Information Center
- NASA International Aerospace Abstracts
- Chem Abstracts Condensates
- Engineering Index
- Energy Research Abstracts
- NASA Tech Briefs
- Government Reports Announcements

and many other specialized files on food technology, textile technology, metallurgy, medicine, business, economics, social sciences, and physical science.

The IAC services

range from tailored literature searches through expert technical assistance:



•*Retrospective Searches:* Published or unpublished literature is screened, and documents are identified according to your interest profile. IAC engineers tailor results to your specific needs and furnish abstracts considered the most pertinent. Complete reports are available upon request.

•*Current-Awareness Searches:* IAC engineers will help design a program to suit your needs. You will receive selected monthly or quarterly abstracts on new developments in your area of interest.

•*Technical Assistance:* IAC engineers will help you evaluate the results of your literature searches. They can help find answers to your technical problems and put you in touch with scientists and engineers at appropriate NASA Field Centers.

Prospective clients

can obtain more information about the services offered by NASA IAC's by contacting the nearest IAC [see page A4] or by checking the IAC box on a TSP Request Card in this issue.

STATE TECHNOLOGY APPLICATIONS CENTERS

Technical information services for industry
and state and local government agencies

Local government and industry

in Florida and Kentucky can utilize the services of NASA's State Technology Applications Centers (STAC's). The STAC's differ from the Industrial Applications Centers described on page A7, primarily in that they are integrated into existing state technical assistance programs and serve only

the host state, whereas the IAC's serve multistate regions.

Many data bases,

including the NASA base and several commercial bases, are available for automatic data retrieval through the STAC's. Other services such as document retrieval and special

searches are also provided. (The STAC's normally charge a fee for their services.)

To obtain information

about the services offered by NASA STAC's, write or call the STAC in your state [see page A4].

COSMIC[®]

An economical source of computer programs
developed by NASA and other government agencies

A vast software library

is maintained by COSMIC — the Computer Software Management and Information Center. COSMIC gives you access to approximately 1,600 computer programs developed for NASA and the Department of Defense and selected programs for other government agencies. Programs and documentation are available at reasonable cost.

Available programs

range from management (PERT scheduling) to information science (retrieval systems) and computer operations (hardware and software). Hundreds of engineering programs perform such tasks as structural analysis, electronic circuit design, chemical analysis, and the design of fluid systems. Others determine building energy requirements and optimize mineral exploration.

COSMIC services

go beyond the collection and storage of software packages. Programs are checked for completeness; special announcements and an indexed software catalog are prepared; and programs are reproduced for distribution. Customers are helped to

identify their software needs; and COSMIC follows up to determine the successes and problems and to provide updates and error corrections. In some cases, NASA engineers can offer guidance to users in installing or running a program.

Information about programs

described in NASA Tech Briefs articles can be obtained by completing the COSMIC Request Card at the back of this issue. Just circle the letters that correspond to the programs in which you are interested.

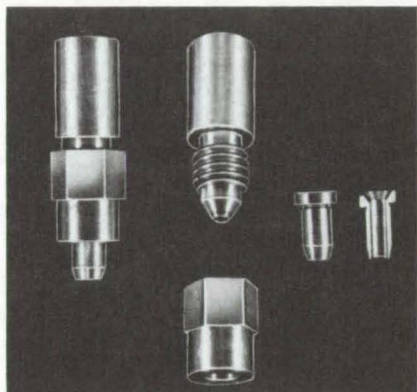


NEW PRODUCT IDEAS



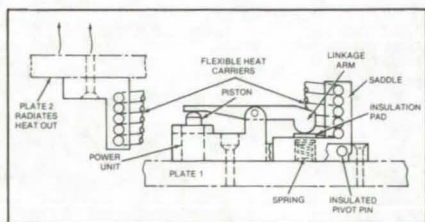
NEW PRODUCT IDEAS are just a few of the many innovations described in this issue of NASA Tech Briefs and having promising commercial applications. Each is discussed further on the referenced page in the appropriate section in this issue. If you are interested in developing a product from these or other NASA innovations, you can receive further technical information by requesting the TSP referenced at the end of the full-length article or by writing the Technology Utilization Office of the sponsoring NASA center (see page A4). NASA's patent-licensing program to encourage commercial development is described on page A8.

Flared-Tube Attachment Fitting



Tubes can be flared first, then attached to valves and other flow-line components, with a new fitting that can be disassembled and reused. The installed fitting can be disassembled so that the parts can be inspected. It can be salvaged and reused without damaging the flared tube; and the tube can be coated, tempered, or otherwise treated after it has been flared, rather than before, as was previously required. The fitting consists of a threaded male portion with a conical seating surface, a hexagonal nut with a hole larger than the outer diameter of the flared end of the tube, and a split ferrule. (See page 213.)

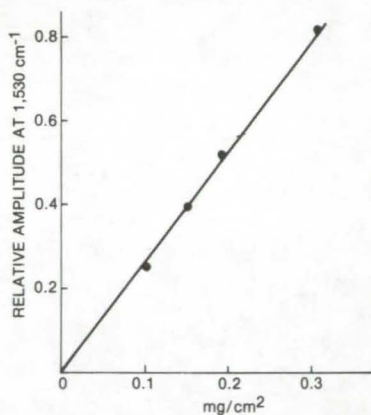
Automatic Thermal Switches



Two new automatic switches control heat flow from one thermally conductive plate to another. One switch permits heat flow to the

outside; the other limits heat flow. Mechanically simple and reliable, the switches can be used in almost any situation in which temperature can be controlled by regulating heat flow. In one switch, heat on a conductive plate activates a piston that forces a saddle against the plate. Heat carriers then conduct the heat to a second plate that radiates it away. After the temperature in the first plate drops, the piston contracts and a spring breaks thermal contact with the plate. In the second switch, the action is reversed. (See page 191.)

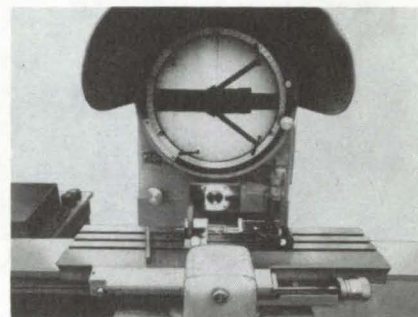
UV Actinometer Film



Cumulative UV radiation can be measured by a proposed low-cost polymer film that is unaffected by visible light. Useful for virtually any surface, the film can help paint and plastics manufacturers determine how well their products stand up against UV radiation. The proposed actinometer film uses a photochemically sensitive compound that changes its chemical composition in response to solar UV radiation. The extent of this chemical conversion depends on the length of the exposure and can be measured by examining the film samples with a spectrophotometer. The film can be exposed from several seconds up to a month. (See page 165.)

Tube-Flare Inspection Tool

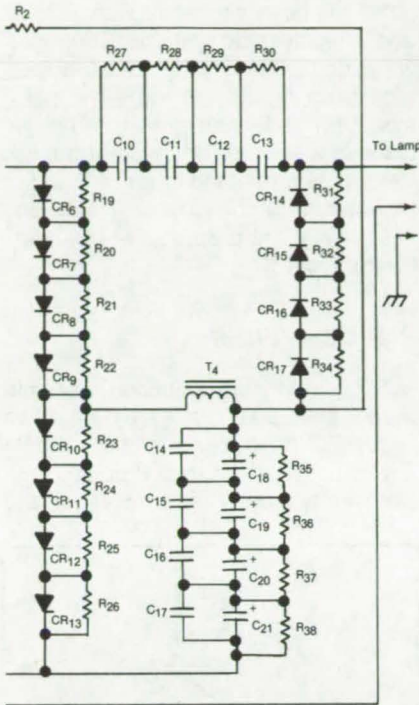
The flare angle and symmetry of tube ends can be checked by a simple tool that consists of two stainless-steel pins bonded to a rubber plug. The primary function of the tool is to inspect tubes before they are installed, thereby eliminating the expense and inconvenience of repairing leaks caused by imperfect flares.



Measuring hole tapers, countersink angles, and bearing-race angles are other possible uses. The tool is used with an optical comparator. The axis of the tool is aligned with the centerline of the tube. The shadow of the seated pins on the comparator screen allows the operator to verify that the flare angle is within tolerance. (See page 213.)

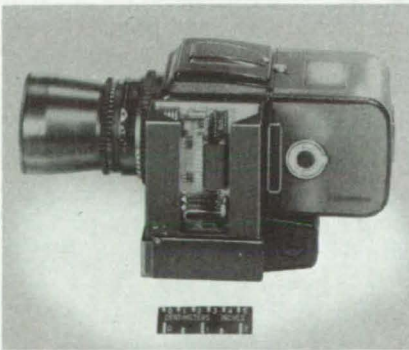
Direct-Current Converter for Gas-Discharge Lamps

Metal/halide and similar gas-discharge lamps can be powered from a low-voltage dc source, using a small efficient converter. The converter can be useful wherever 60-cycle ac power is not available or where space and weight allocations are limited. Possible applications are in offshore platforms, mobile homes, and emergency lighting. Several design innovations give the new supply high reliability and an efficiency of up to 75 percent. The instantaneous high voltage available



with the circuit makes the lamp less likely to "blow out" because of transients in the power source. The circuit also stabilizes the lamp current, thus eliminating the need for an external "ballast." (See page 140.)

Camera Add-On Records Time of Exposure

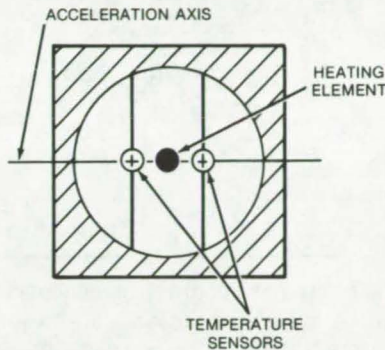


A compact module attached to a camera contains all the electronics and optics needed to print the time a photograph is taken on the edge of that photograph. The module can be used wherever it is necessary to document the exact time a photo is taken. The module includes an eight-digit LED display that continuously shows the time to an accuracy of a hundredth of a second. The normally blanked display is unblanked when the camera shutter switch is activated.

Light from the display is reflected off two flat mirrors, through a focusing lens, into the camera, and onto the film. (See page 168.)

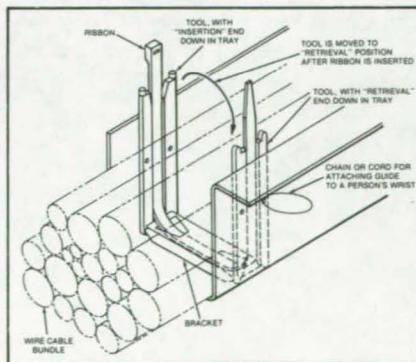
Electrofluidic Accelerometer

An electrofluidic accelerometer senses components of a linear or angular acceleration field. A typical application of such an accelerometer is as an active controlling element in



an airplane autopilot. In contrast to conventional accelerometers, an electrofluidic accelerometer is lightweight, small, inexpensive, rugged, and requires little power. It consists of two temperature sensors on opposite sides of a heating element. The sensors detect the temperature gradient created by an acceleration field on the fluid; and when the device is accelerated, the gradient changes because of the buoyant force on the hotter (thus lighter) portion of the fluid. (See page 201.)

Handtool Assists in Bundling Cables

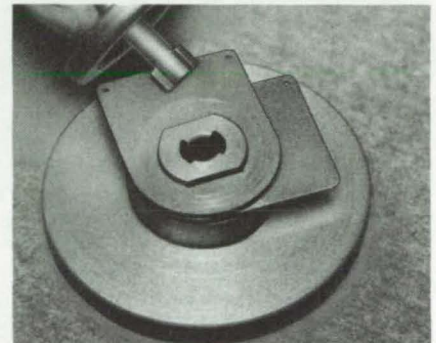


A simple tool makes it possible to bundle electrical cables in a channel or "tray" without requiring that the cables be lifted out of the tray. The procedure for bundling is faster and

less awkward than the old method of lifting the cables for wrapping. Used with commercially-available plastic ribbons that tie the cables together, the tool guides the ribbon along a tray wall, through a bracket at the bottom of the tray, and up the opposite wall. One end of the ribbon locks in the other end, securing the cable bundle. (See page 225.)

Bayonet Plug With Ramp-Activated Lock

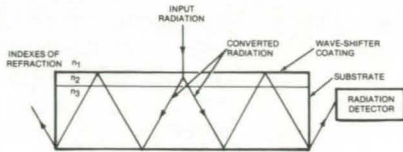
A matched pair of washers with broad surface ramps is the locking mechanism in a new bayonet plug. It can be used where threaded fasteners and springs are impractical because of extreme temperatures or other environmental incompatibility. The matched pair of ramped washers is placed on the plug and the bayonet inserted. The inner slot of one washer



matches the contour of the plug; this washer is stationary. The inner slot of the second washer is circular. When the second washer is rotated, the washers push against the bayonet plug, locking it in place. A retaining wire secures the plug. (See page 218.)

Fluorescent Radiation Converter

A new fluorescent radiation converter uses an optically transparent substrate. One side of the substrate is coated with a plastic film containing fluorescent organic dyes that absorb optical radiation at one wavelength and emit it at a longer one. The coating is formulated to respond to specific wavelengths. The emitted radiation is reflected internally inside the substrate, amplifying the intensity that reaches the radiation detector.

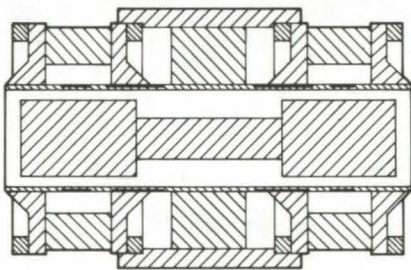


The converter can be made in several sizes and shapes; round or square bars coated all around their lengths are useful in converting relatively intense radiation and transmitting it through the substrate over lengthy distances.

(See page 166.)

A Linear Magnetic Motor and Generator

In a proposed linear magnetic motor and generator, suitable for remote and hostile environments, magnetic forces drive a reciprocating shaft along its axis. The actuator shaft is located in the center of a cylindrical body and may be supported by either contacting or noncontacting bearings. When the device operates as a bidirectional motor, the drive coil selectively adds

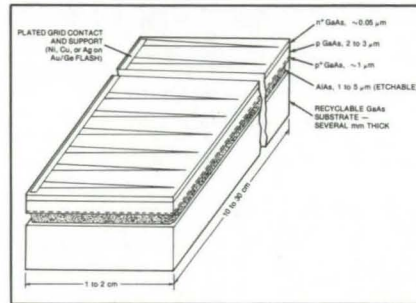


and subtracts magnetic flux to and from the flux paths to produce the forces that drive the actuator back and forth along the axis. When the actuator is driven by an external reciprocating engine, the device becomes an ac generator.

(See page 226.)

"Peeled-Film" Solar Cells

Proposed "peeled-film" solar cells could be lighter and less expensive than conventional cells. The GaAs cells would be deposited on a GaAs substrate coated with a thin etchable layer that would allow the completed cell film to be peeled away from the substrate. At an estimated conversion efficiency of 18 percent, an array of such cells would deliver about 1 kW of



electricity per kilogram of cell material. A blanket of these cells would deliver energy at a power-to-weight ratio about 4 times that of conventional 2-mil (0.5-mm) silicon solar cells. In addition, GaAs solar cells have better radiation resistance than silicon cells.

(See page 135.)

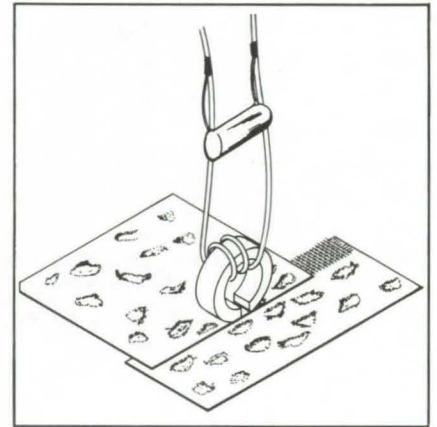
Plasticizer for Polyimide Composites

The problem of maintaining good prepreg tack and drape has been solved by a new modification of an addition polyimide. Tack and drape are the ability of the prepreg to adhere to adjacent plies and to conform to a desired shape during the layup process. This alternate approach will allow both longer life of the polymer prepreg and the processing of low-void lami-

nates. It appears to be applicable to all addition polyimide systems. The modified addition polyimide takes advantage of a reactive liquid plasticizer, monoethylphthalate, which is used in place of a solvent. Because of the low vapor pressure of the reactive liquid, it is retained and, thereby, tack and flexibility of the prepreg are retained. (See page 180.)

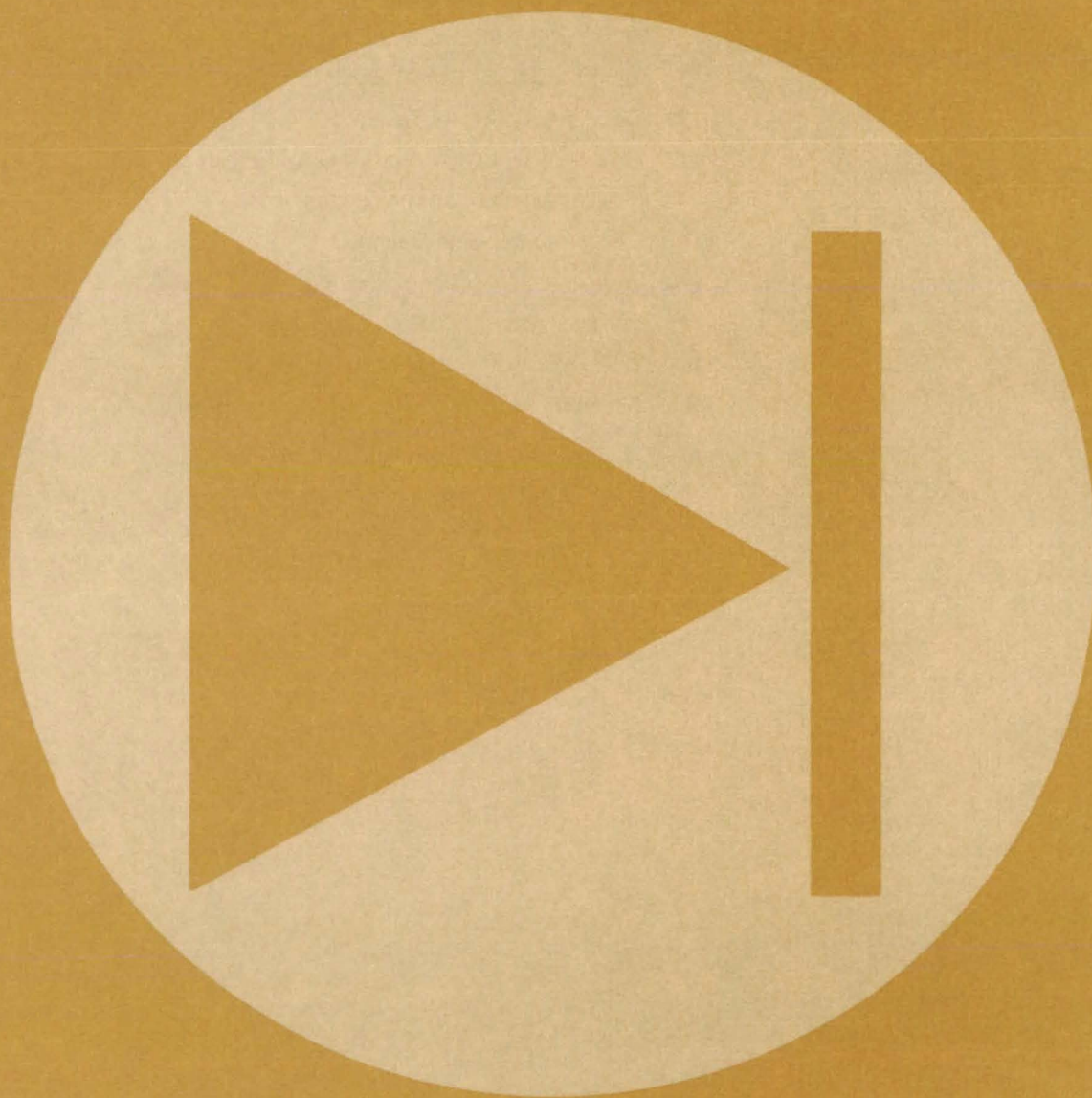
Plastic Welder

A low-cost, self-contained, portable welder joins plastic parts by induction heating. The welder can be used in any atmosphere or in a vacuum, with almost any type of thermoplastic; and



the plastic components can be joined in situ. Possible uses are in the aerospace industry and in the automobile, furniture, and construction industries. The low power requirements can be easily met by battery or solar power. In the welder, a toroidal inductor transfers magnetic flux through the thermoplastic to a screen. The heated screen causes the plastic surface on either side of it to melt and flow into it to form the joint. (See page 242.)

Electronic Components and Circuits



Hardware, Techniques, and Processes

- 133 Improved Power-Factor Controller
- 134 Energy Saving in ac Generators
- 135 "Peeled-Film" Solar Cells
- 136 Temperature-Compensating dc Restorer
- 137 Aliasing Filter for Multirate Systems
- 138 Dual-Frequency Bidirectional Antenna
- 139 Computer-Controlled Warmup Circuit
- 140 Direct-Current Converter for Gas-Discharge Lamps
- 141 Position Monitor for Mining Machines
- 141 11-Line to 512-Line Decoder
- 143 Input/Output Interface Module
- 144 Smoothing the Output From a DAC
- 144 LSI Logic for Phase-Control Rectifiers
- 145 Model for MOS Field-Time-Dependent Breakdown

Computer Programs

- 146 DDL: Digital Systems Design Language

Improved Power-Factor Controller

Two improvements increase energy savings in ac motors without sacrificing performance.

Marshall Space Flight Center, Alabama

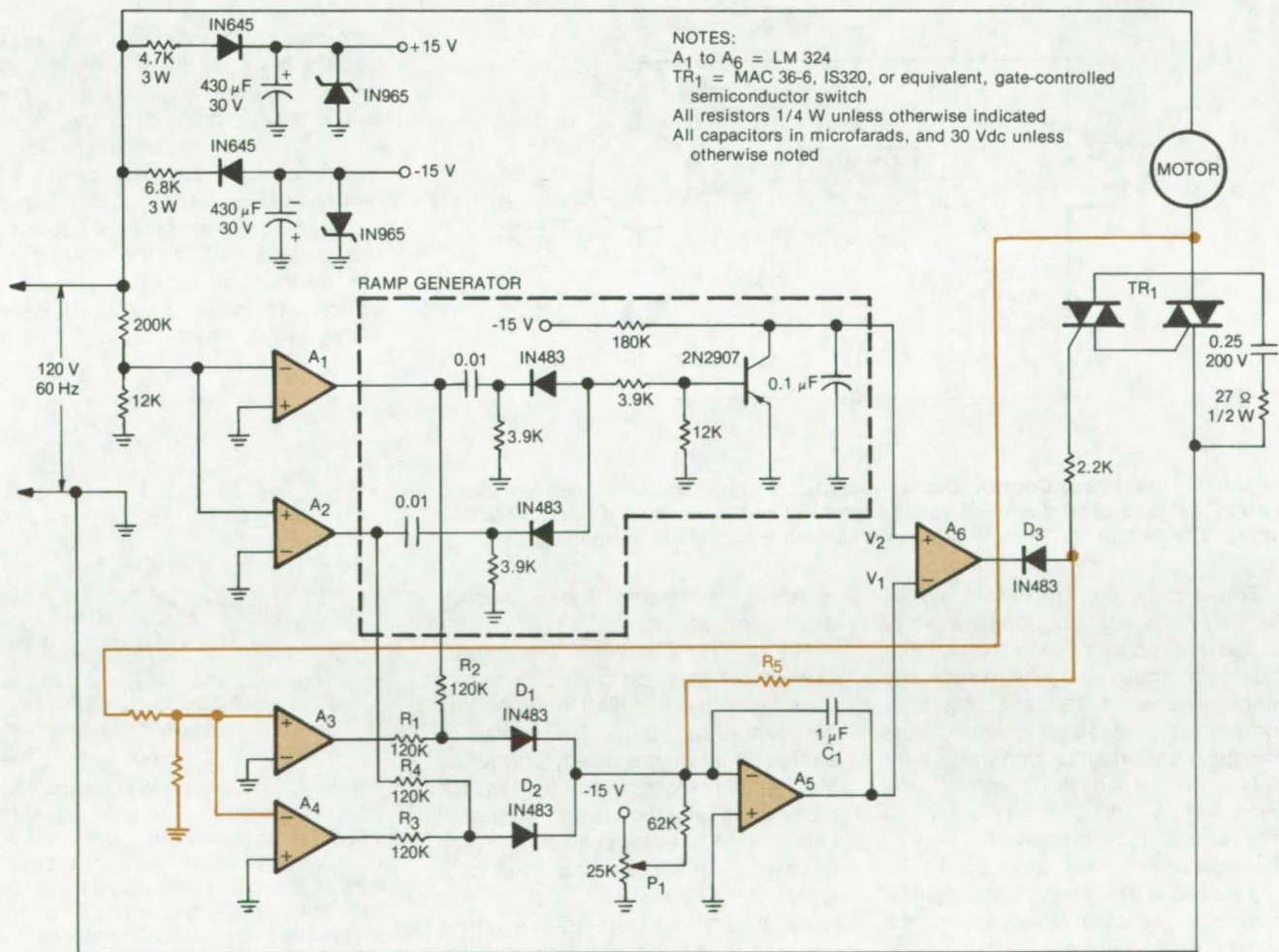
An improved power-factor controller for ac motors saves more energy, yet is simpler and less expensive than the original circuit. Motor performance is unaffected by the modifications. [The first *NASA Tech Briefs* article on the power-factor controller, "Save Power in AC Induction Motors" (MFS-23280), appeared on page 179 of Vol. 2, No. 2. An improved circuit is described in "Fast-Response Power Saver for Induction Motors" (MFS-23988) on page 6 of Vol. 4, No. 1.]

The power-factor controller, in either its original or improved form, reduces ac losses in an induction motor by lowering the applied voltage when the motor is unloaded or lightly loaded. It does so by phase-controlling the "on" time of a gate-controlled semiconductor switch installed in series with the motor. The circuit monitors the phase angle between the applied voltage and the lagging current (an indicator of the level of loading) and adjusts the timing of the switch gate signal accordingly.

In the original circuit, the voltage across a high-power resistor in series with the motor was used to sense the current. This resistor is removed in the new circuit and instead, the voltage across the semiconductor switch is monitored (see figure). Thus, the cost and effort of wiring the high-power resistor are eliminated.

The voltage across the semiconductor switch is low, typically 1 volt, when the switch is on. When the current through it goes to zero, the switch

(continued on next page)



In the Improved Power-Factor Controller, A₆ delivers a gate pulse that turns on the semiconductor switch. The voltage across the switch, an indicator of the motor current, is fed back to op-amps A₃ and A₄. Resistor R₅ adds feedback of the gate pulse.

automatically shuts off, and the voltage rises to almost the full line voltage. This abrupt rise marks the zero-crossing point of the current.

The time interval between the current and voltage zero crossings is a measure of the phase angle. The circuit associated with op-amps A₃ and A₄, resistors R₁, R₂, R₃, and R₄, and diodes D₁ and D₂ develops a positive voltage proportional to this interval at the inverting input to A₅. A negative voltage from potentiometer P₁ is also fed to this input. Thus, the output

voltage of A₅, a measure of how much the phase angle departs from a pre-selected value set by P₁, is an error signal that can be used to control the turn-on point of the switch. This voltage (V₁) is compared with ramp voltage V₂ at A₆, and the output of A₆ delivers the gate pulse.

Resistor R₅ is also an improvement not present on the original circuit. It adds a small amount of positive feedback of the gate signal to the inverting input of A₅. This further decreases the switch "on" time when the motor is

unloaded, without sacrificing full-load performance. In tests, no-load savings were increased by over 70 percent by adding just this one resistor.

This work was done by Frank J. Nola of **Marshall Space Flight Center**. For further information, Circle 1 on the TSP Request Card.

Inquiries concerning rights for the commercial use of this invention should be addressed to the Patent Counsel, Marshall Space Flight Center [see page A5]. Refer to MFS-25323.

Energy Saving in ac Generators

Circuit cuts no-load losses, without sacrificing full-load power.

Marshall Space Flight Center, Alabama

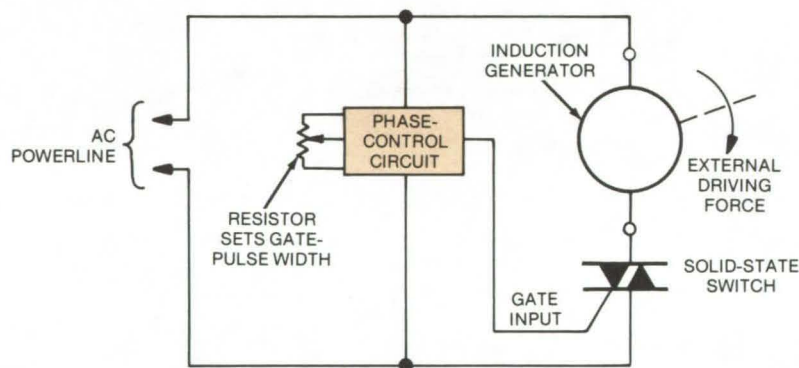


Figure 1. The **Phase-Control Circuit** includes a gate-controlled semiconductor switch that cuts off the applied voltage for most of the ac cycle if the generator is idling. The switch "on" time increases when the generator is in operation.

Three previous articles in *NASA Tech Briefs* described a phase-control circuit that reduces power losses in ac induction motors. (See preceding article.) Recent tests have now confirmed that the same circuit saves energy in an induction generator connected to an ac powerline. If the generator is idling (that is, if no mechanical force is applied), it nonetheless draws power because the ac line rotates it like a motor. In a typical unloaded induction generator, the idling current can be quite large, and no-load losses can be substantial. The circuit reduces the losses by lowering the applied voltage when the generator

is idling, increasing it only when a driving force is applied.

Figure 1 illustrates the circuit concept. A gate-controlled semiconductor switch is installed in series with the generator. Once the switch is energized by a gate pulse, control by the gate is lost, and the switch remains on until the current through it falls to zero. At that point, the switch turns off, waiting for the next gate signal.

As shown in Figure 2, the gating signal is synchronized with the line voltage so that the generator is out of the circuit except for a short period that begins just before the voltage

zero-crossing point in each half cycle. Current flows during this period until the lagging current passes through its zero-crossing point and the switch turns off. No additional power is consumed until the next gate signal reopens the switch.

When a driving force is applied to the generator shaft, the current and the phase lag increase. Thus, the switch remains on for a longer period during each half cycle, allowing

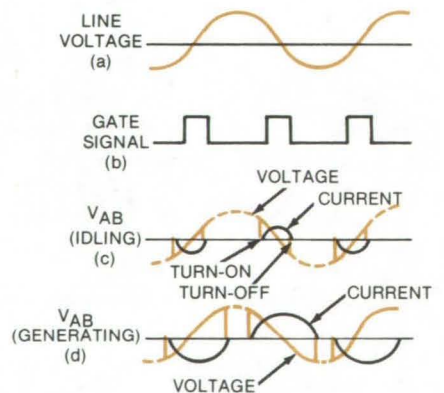


Figure 2. The **Circuit Waveforms** illustrate its operation. The gate signal (b), which is synchronous with the line voltage (a), turns on the switch, applying voltage to the generator during the periods indicated in (c). Each "on" period ends when the generator current goes through its zero-crossing point. Curve (d) shows the increased "on" time registered when the generator is driven.

energy from the generator to be transferred to the ac line. If the current and phase lag increase sufficiently, the switch can remain on for a full cycle.

Using this method for a 1/2-horsepower (746-watt) induction generator

driven by a dc motor, idling losses were reduced from 210 watts to 70 watts, with no sacrifice in performance when the generator is driven at full output.

This work was done by Frank J. Nola of **Marshall Space Flight**

Center. For further information, Circle 2 on the TSP Request Card.

Inquiries concerning rights for the commercial use of this invention should be addressed to the Patent Counsel, Marshall Space Flight Center [see page A5]. Refer to MFS-25302.

“Peeled-Film” Solar Cells

Proposed GaAs cells would be lighter and more economical than conventional cells.

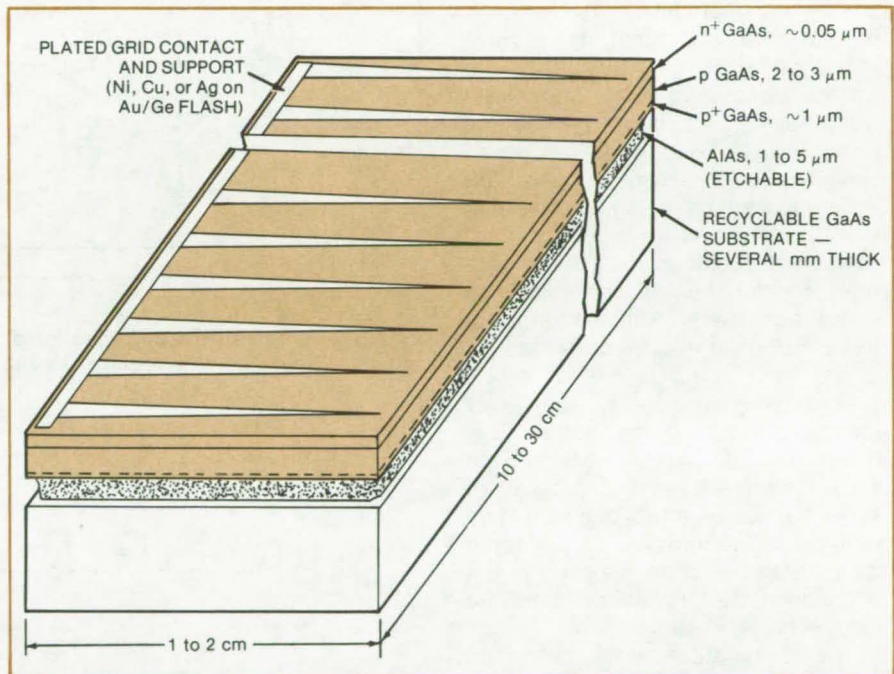
NASA's Jet Propulsion Laboratory, Pasadena, California

Proposed “peeled-film” solar cells could be lighter and less expensive than conventional cells. At an estimated conversion efficiency of 18 percent, an array of such cells would deliver about 1 kW of electricity per kilogram of cell material.

The proposed GaAs n^+p cell structure (see figure) would be deposited on a GaAs substrate coated with a thin, etchable AIAs layer. When the cell is complete, the AIAs interlayer would be etched away, and the $4\text{-}\mu\text{m}$ cell film would be peeled away. The GaAs substrate could then be reused. Possible etchants of AIAs, which would not attack GaAs, are hydrofluoric acid, redox solutions of potassium iodide with iodine, or potassium ferricyanide plus potassium ferrocyanide.

The n^+pp^+ cell structure was chosen because more-conventional Al(Ga)As/GaAs p^+n heteroface cell structures would require special masking to avoid etching of the Al(Ga)As layer. Also, the conventional cell would “curl” after being peeled away since there is a slight mismatch between the substrate and cell crystal lattices.

The problem of handling the ultra-thin solar cells would be reduced by bonding a glass or plastic layer on the top surface before the etching step. Such a layer might also prevent curling, allowing use of the Al(Ga)As heteroface structure.



The **Peeled-Film Cell** is separated from the GaAs substrate by an AIAs layer. The AIAs is etched away, freeing the cell and allowing the substrate to be reused.

The solar-cell blanket would be given an ohmic back contact by electroplating or vacuum deposition. It could then be placed on a thin metalized Kapton (or equivalent) backing.

The peeled-film solar-cell blanket would deliver energy at a power-to-weight ratio roughly 4 times that of conventional 2-mil (0.5-mm) silicon

solar cells. In addition, GaAs solar cells have better radiation resistance and temperature stability than silicon cells.

This work was done by Richard J. Stirn of Caltech for **NASA's Jet Propulsion Laboratory.** For further information, Circle 3 on the TSP Request Card. NPO-14734

Temperature-Compensating dc Restorer

Circuit provides stable reference restoration in addition to temperature compensation.

Langley Research Center, Hampton, Virginia

In a closed-loop computerized control system, analog-to-digital converters may be used to condition analog sensor signals. These analog-to-digital converters have a fixed operating range that determines the limits of the sensor signals. In order to improve resolution, the sensor signals are set equal to the operating range of the analog-to-digital converter. The lower limit of the sensor signal, or the zero-reference level, must be stable to maintain resolution for low-level signals since a varying zero-reference level would swamp out low-level signals. Some sensor signals are superimposed on a bias signal that must be removed. The dc restorer removes the bias signal. If the zero reference for the sensor signal level varies significantly with temperature, this effect must also be corrected.

The most common method of dc restoration is to couple capacitively the signal to a diode clamp. This technique adequately restores the zero-reference level, but it does not solve the temperature compensation problem. Furthermore, it adds a temperature drift because of the variation of the forward voltage of the diode with temperature.

The temperature-compensating dc restorer shown in Figure 1 provides stable zero-reference restoration and compensates for temperature variations. It was developed for an autonomous Earth-observation experiment aboard the Space Shuttle. CCD cameras are used as sensors; their outputs are digitized and recorded on magnetic tape for later evaluation.

When light strikes the image sensor elements, a packet of electrons proportional to the incident light is generated at each sensing element. ϕH clocking sequentially delivers the charge packets to a gated charge integrator, which produces an output signal proportional to the input charge (see Figure 2). The ϕR clock resets the charge integrator prior to the arrival of the next charge packet. A portion of the ϕR clock is coupled

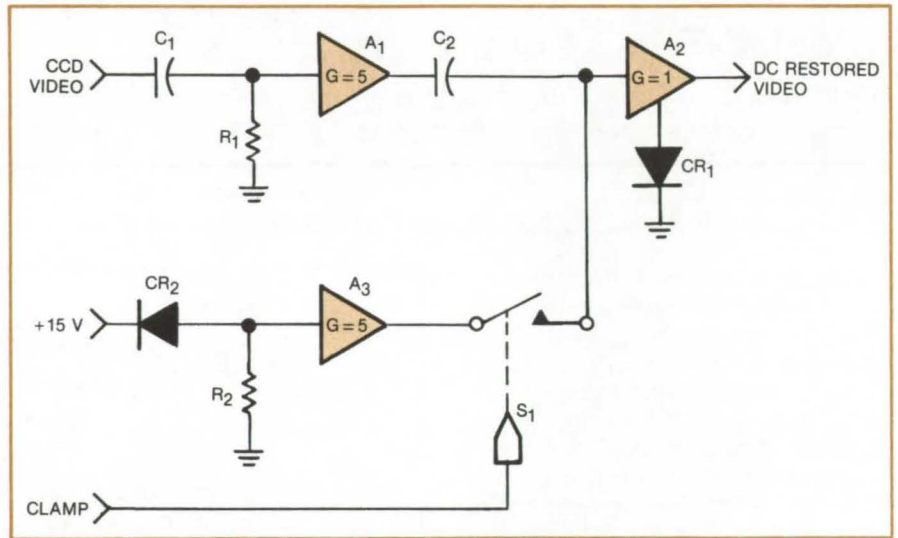


Figure 1. **Temperature-Compensating dc Restorer** circuit was designed to condition the video signal of a Fairchild CCD 202 area-image sensor.

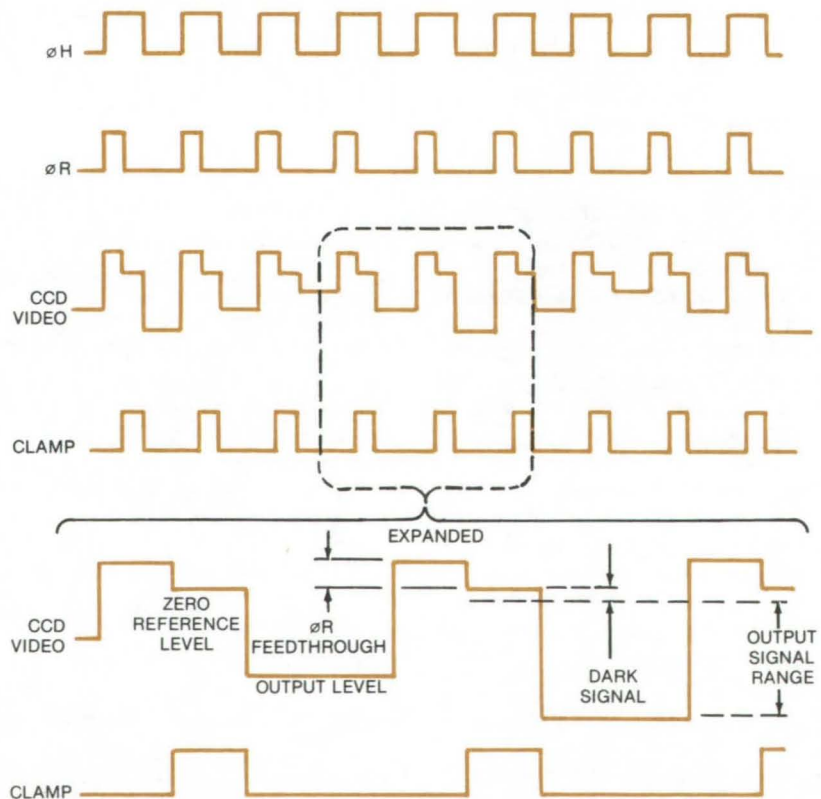


Figure 2. **Timing Diagram** of CCD 202 video output appears as a pulse-amplitude-modulated data stream.

through to the video output. Following the $\emptyset R$ feedthrough is a reference-level pedestal for the output video pulse.

Although it was designed for solid-state optical sensors, the temperature-compensating dc restorer could be adapted to any sensor with bias and temperature drift similar to those described; e.g., in closed-loop computerized process-control systems.

While closed-circuit TV applications do not require the output to be digitized for display on a TV monitor, this circuit would be advantageous if the observer did not have access to the monitor controls to adjust for reference-level changes. Possible TV monitor applications include traffic and security surveillance systems, where cameras are subject to environmental extremes, as in unheated

warehouses or outdoors.

This work was done by H. M. Thomas of Martin Marietta Corp. for **Langley Research Center**. For further information, Circle 4 on the TSP Request Card.

Inquiries concerning rights for the commercial use of this invention should be addressed to the Patent Counsel, Langley Research Center [see page A5]. Refer to LAR-12549.

Aliasing Filter for Multirate Systems

Adding a rolloff filter is an inexpensive way of reducing aliasing in digital control systems.

Lyndon B. Johnson Space Center, Houston, Texas

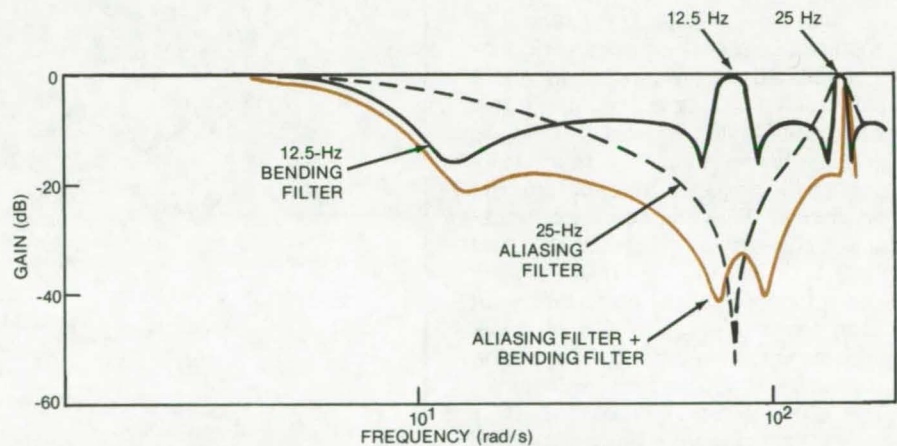
Digital control systems operating at single or multiple sampling rates are susceptible to foldback, or "aliasing," for signals above the half-sampling frequency. A rolloff filter operating at the faster sample rate (or rates) of a system with a 2:1 rate ratio gives infinite attenuation at the half-sample rate of the fast-rate loop. Tested successfully on the Space Shuttle primary flight-control system, the filter technique could be applied to other multirate sampled-data systems.

Three methods have previously been used to reduce or at least account for the effects of aliasing:

1. analyzing the high-frequency effects in the sampled-data domain,
2. using a faster sample rate such that all significant dynamics are within the half-sample-rate bandwidth, and
3. using a digital filter operating at the lower sampling frequency and accepting the degradation of the lower frequency characteristics.

Compared to these approaches, the rolloff filter is a relatively-inexpensive software function that eliminates aliasing without requiring an extensive foldback analysis, as in method 1.

The Shuttle flight-control system experiences significant bending modes over (at least) the range from 2



A 25-Hz Rolloff Filter reduces aliasing in the Shuttle flight-control system. The solid curve in black is the response of a 12.5-Hz bending filter. The dashed curve is the characteristic of the added rolloff filter. The response of the combination, shown in color, has increased attenuation in the vicinity of 12.5 Hz.

to 12-1/2 Hz. Core limitations in the central-processing unit required that a 25-Hz rate-fill function in the attitude-control loop be reduced to 12-1/2 Hz; however, aliasing was a potential problem because of high-frequency bending-mode foldback.

As shown in the figure, adding the 25-Hz rolloff filter between the rate gyro and the 12.5-Hz bending filter increases the attenuation at 12.5 Hz.

The end-to-end transfer function is virtually insensitive to dynamics in the vicinity of 12.5 Hz, and the impact on the low-frequency dynamics is minimal.

This work was done by John F. L. Lee of Honeywell Inc. for **Johnson Space Center**. For further information, Circle 5 on the TSP Request Card.

MSC-18472

Dual-Frequency Bidirectional Antenna

Simultaneous two-way communication at 20 and 30 GHz is possible with a versatile paraboloid-dish antenna.

Goddard Space Flight Center, Greenbelt, Maryland

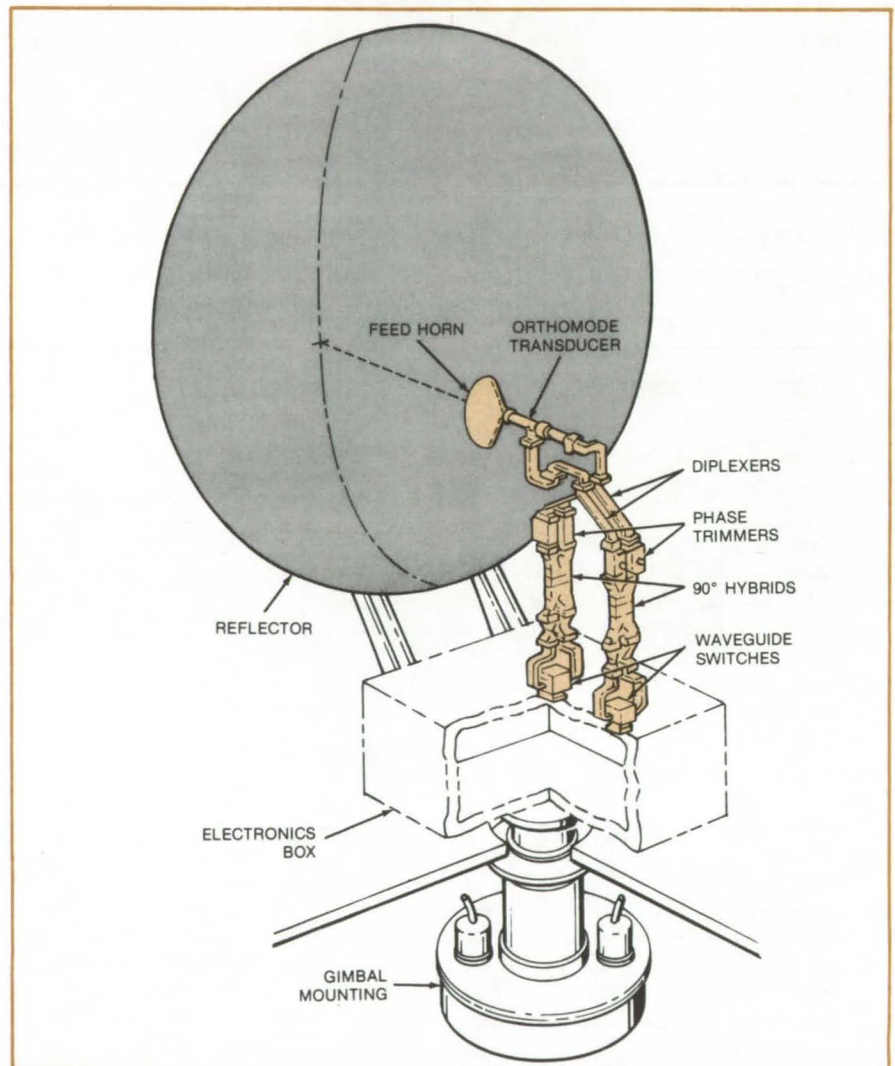
A versatile communications antenna transmits left-circularly-polarized or right-circularly-polarized signals at one frequency and simultaneously receives either polarization at another frequency. Developed for two-way communications between the Space Shuttle and a ground station, the antenna includes a parabolic reflector, a feed horn, a waveguide network, and a single-axis gimbal mounting.

The waveguide network separates the two frequency components — 20 GHz and 30 GHz in the Shuttle system — and selects one polarization at each frequency. It includes an orthomode transducer, two diplexers, and a pair of single-pole, double-throw solenoid-actuated switches. Using a gradual finline transition from TE_{11} circular waveguide to separate the orthogonal TE_{11} modes, the transducer converts the incoming 20- and 30-GHz circularly polarized signals into orthogonal linear polarizations at each frequency. One TE_{11} mode is coupled vertically out of the main line into a WR34 rectangular waveguide. The other component of the TE_{11} mode is coupled horizontally to another WR34 waveguide. Identical diplexers separate the 20- and 30-GHz signals in each arm.

A 90° hybrid reconstitutes the circularly-polarized 20-GHz wave from the two 20-GHz linear components, and another hybrid does the same for the 30-GHz signal. Phase trimmers between the output arms of the diplexers and the hybrids compensate for phase deviations that can arise from minor differences in waveguide dimensions. The two waveguide switches select either sense of polarization at each frequency.

Small grooves in the flared section of the feed horn adjust the impedance relationships to give nearly-equal field amplitudes in the E- and H-planes. The flare angle is 53.0° , and the corrugations are 0.150 inch (0.38 centimeter) deep.

An iterative numerical procedure established the optimum reflector



This **Bidirectional Antenna** transmits at 20 GHz and receives at 30 GHz. Peak system gain at 20 GHz is 29.8 dB; at 30 GHz, gain is 32.3 dB. The nominal paraboloid-dish reflector focal length is 14.76 in., with an $f/D = 0.5$. The edge of the dish subtends an angle of 53° with the position of the feed horn. The actual dish departs slightly from a true paraboloid of revolution.

shape. The reflector has different curvatures in two perpendicular planes: In one plane it is parabolic; in the other, it is distorted to give the required far-field pattern.

The feed horn is located 14.76 inches (37.49 centimeters) from the vertex of the reflector. It is displaced 2.40 inches (6.10 centimeters) from the central axis of the dish in the direction of maximum edge elevation.

The antenna and its electronics are

positioned by a single-axis gimbal driven by a stepper motor. The gimbal drive is run open loop, with its position indicated by a potentiometer output. The system resolution and accuracy are better than 1° .

This work was done by W. H. Kummer of Hughes Aircraft Co. for **Goddard Space Flight Center**. For further information, Circle 6 on the TSP Request Card. GSC-12501

Computer-Controlled Warmup Circuit

Filament of high-power radio transmitter can be brought to operating temperature automatically.

NASA's Jet Propulsion Laboratory, Pasadena, California

A special circuit automatically heats the filament of a klystron tube to operating temperature, relieving a human operator of the 15-minute task of slowly turning the knob of a variable transformer to maintain current at its maximum safe level while filament temperature (and resistance) increases. The warmup controller circuit, which was developed for the klystron transmitting tubes used in Deep-Space Network stations, is activated by a pushbutton. It thus reduces the operator's role to a one-step command and is compatible with various forms of computer control.

The klystron filament floats at the beam potential, which can be as high as 70 kV, so an isolation transformer is used to deliver ac filament power. Filament current and voltage are sensed through windings on the isolation transformer. The power to the isolation transformer is supplied by a motor-driven variable transformer that is controlled, in turn, by a circuit board.

Figure 1 is a photograph of the Local Control Console (LCC), and

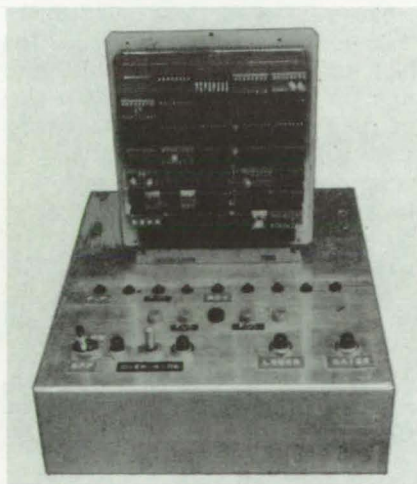


Figure 1. **Automatic Control** of heater power to a klystron filament is furnished by the circuit board. After the operator pushes the RAISE button on the console panel, the filament temperature is raised to the operating level at a rate that prevents excessive filament current or voltage.

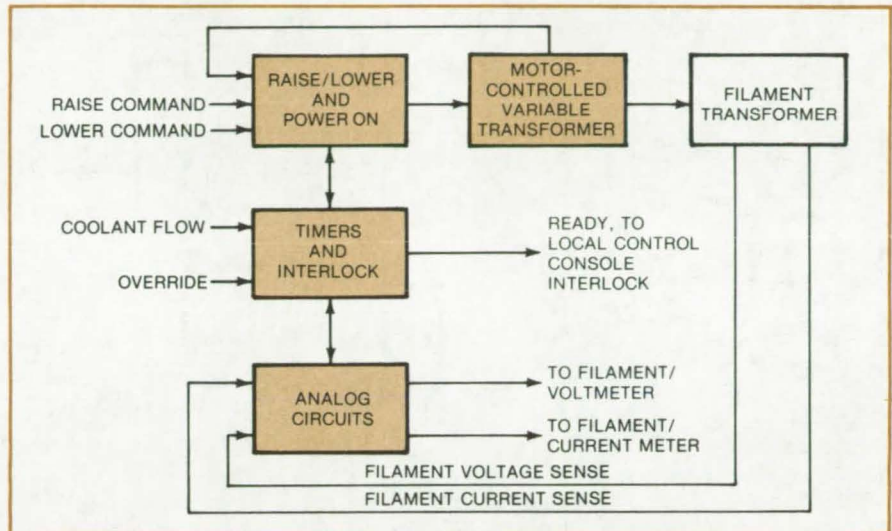


Figure 2. This **Block Diagram** shows how the warmup control circuit monitors the filament current and voltage of the high-power transmitting tube and governs a motor to raise or lower the voltage from a variable transformer that drives the filament transformer.

Figure 2 is a block diagram of the warmup controller. When the user issues a warmup command (RAISE) at the LCC, the circuit applies power to the variable transformer via a solid-state relay and turns the motor on in the "up" direction. The motor continues to run until the maximum programmed current limit or the operating voltage limit is reached. When the filament is cold and the resistance low, the current limit will always be reached first; so the controller will pulse the motor every few seconds, maintaining the current at the limit as the filament warms up. When the filament reaches 70 percent of its operating voltage, a 20-minute timer is started. After 20 minutes the filament-ready signal closes the beam voltage interlock, allowing dc operating voltages to be applied to the klystron. When the filament is hot and current limiting no longer occurs, the filament voltage is regulated to within ± 0.1 volt.

A filament shutdown can be initiated by three events: (1) a "down" command from the operator, (2) a failure of the cooling system, or (3) a power failure for more than a few

seconds. The operator can command a shutdown by pressing the LOWER button twice, which changes the circuit mode from "up" to "halt" to "down." A cooling failure forces a "down" mode, but only after a 1-minute time delay. A power failure longer than 5 seconds causes the circuit to reset, removing filament power and mechanically lowering the variable transformer setting when power returns. The variable transformer must be turned all the way down before it can be raised again.

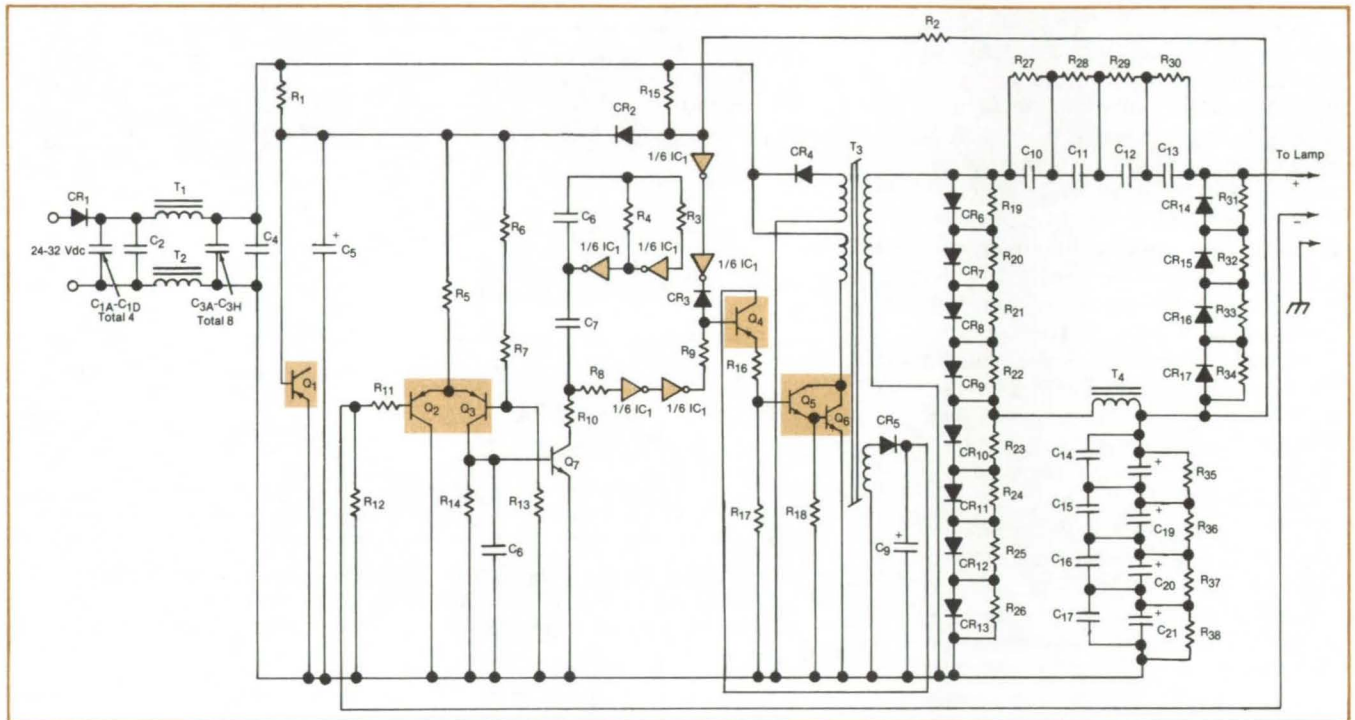
An override function allows either manual or external computer control. When override is enabled, the RAISE and LOWER buttons at the LCC control the motor that is connected to the variable transformer. (The control is constrained by the current and voltage limits set by switches in the filament supply chassis.) This feature allows an operator or a computer to control the filament power directly.

This work was done by John J. Daeges of Caltech for NASA's Jet Propulsion Laboratory. For further information, Circle 7 on the TSP Request Card.
NPO-14815

Direct-Current Converter for Gas-Discharge Lamps

No ballast is required with a new dc supply for metal/halide and other gas-discharge lamps.

Lyndon B. Johnson Space Center, Houston, Texas



The **Lamp Power Supply** consists of a high-frequency inverter switched by a waveform generator, a current-regulating loop, and associated circuitry driven by direct-current sources. Prototypes are used at power levels of 175 watts for mercury-vapor lamps doped with halides of sodium and scandium. The lamps contain argon as a start gas.

Metal/halide and similar gas-discharge lamps can be powered from a low-voltage dc source, using the small efficient converter shown in the figure. The circuit also stabilizes the lamp current, thus eliminating the need for an external "ballast," a standard component with conventional ac-powered lamps. The prototype converter can be useful wherever 60-cycle ac power is not available or where space and weight allocations are limited. (It was developed for discharge lamps aboard the Space Shuttle.) Possible terrestrial applications are in offshore platforms, mobile homes, and emergency lighting.

Several design innovations give the new supply high reliability and an efficiency of up to 75 percent. The heart of the circuit is a 20-kHz power-switching inverter (a "forward converter") that changes the input dc power to high-voltage alternating cur-

rent, which is then rectified and integrated to supply direct current to the lamp.

The forward converter is the middle portion of the circuit, shown in the figure. It instantaneously develops the high starting voltages (typically 1,200 V for the Shuttle lamps) necessary to turn the lamp on. It is a rapid-response circuit that is inherently efficient because the single output transistor (Q₆) is either fully on or fully off at all times.

A lamp-current control loop is formed with transistors Q₂, Q₃, and Q₇ sensing the lamp current and feeding signals back to the waveform generator that controls the inverter duty cycle. The inverter duty cycle is thus lengthened or shortened to compensate for changes in the lamp current.

The instantaneous high voltages available with the circuit make the

lamp less likely to "blow out" because of transients in the power source. The high voltages also reduce restart times to about 5 minutes if the lamp is shut off and then reenergized. (Typical restart times for conventional ac-powered lamps are 10 to 15 minutes.) In addition, whereas conventional power sources require a three-electrode lamp, for which the third electrode is a starting electrode, the new supply can directly energize simpler, two-electrode lamps.

This work was done by P. Lutus of ILC Technology for **Johnson Space Center**. For further information, Circle 8 on the TSP Request Card.

Inquiries concerning rights for the commercial use of this invention should be addressed to the Patent Counsel, Johnson Space Center [see page A5]. Refer to MSC-18407.

Position Monitor for Mining Machines

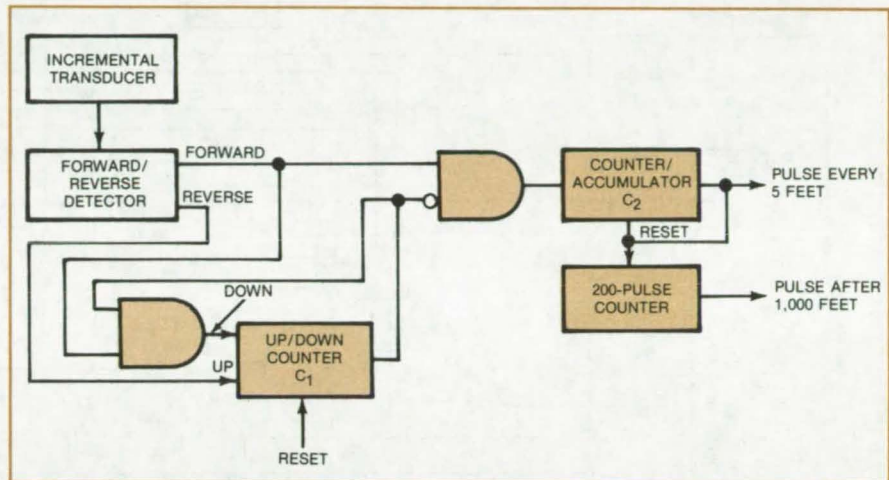
A simple circuit at the output of an incremental transducer records the progress of a longwall shearer.

Marshall Space Flight Center, Alabama

Faced with the problem of monitoring the forward progress of a longwall shearer (a coal-mining machine), engineers under contract to Marshall Space Flight Center developed a simple digital circuit that could have applications in other harsh environments. Shown in the figure, the circuit attaches to the output of a rotary-motion transducer and develops a pulse for rotation equivalent to each 5-foot (1.5-m) increment of forward progress of the machine. A reset pulse is derived after the shearer has moved 1,000 feet (304 meters). In contrast to mechanical shaft encoders, the electronic circuit can be easily packaged to withstand the shock and vibration of the mining machine as it cuts across the coal seam.

The circuit delivers pulses only when true forward progress has been made. If the mining machine should reverse direction, as happens periodically, the pulses cease until the point of maximum forward progress is returned to and exceeded.

Referring to the figure, the stream of pulses from the transducer (e.g., optoelectronic or magnetic) is channeled along one of two paths, depending on whether the machine is moving forward or backward. Forward-motion pulses clock the "down" input of an up/down counter/accumulator (C1) and also the input of another counter/accumulator (C2),



This **Block Diagram** of the position monitor could be converted to a working circuit by using standard IC's. Increments of 5 feet along a 600-foot (182-meter) path are resolved to within 0.06 in. (0.15 cm) by the system.

which delivers one output pulse when the number of input pulses corresponds to 5 feet of forward motion. Reverse-motion pulses clock the "up" input of C1.

When the C1 output is reset to "0," AND gate 1 prevents pulses from reaching the "down" input, while AND gate 2 allows forward-motion pulses to reach C2. In this mode, the forward motion is continuously monitored.

If the machine should reverse direction, no pulses reach C2, and C1 is incremented to a count that corresponds to the net backward motion. When forward progress resumes,

AND gate 1 prevents pulses from reaching C2 until "down" pulses decrement C1 back to its "zero" state. When this happens, the AND gate 2 is reopened and normal operation resumes.

This work was done by Joseph Lubich of Benton Corp. for Marshall Space Flight Center. No further documentation is available.

Inquiries concerning rights for the commercial use of this invention should be addressed to the Patent Counsel, Marshall Space Flight Center [see page A5]. Refer to MFS-25342.

11-Line to 512-Line Decoder

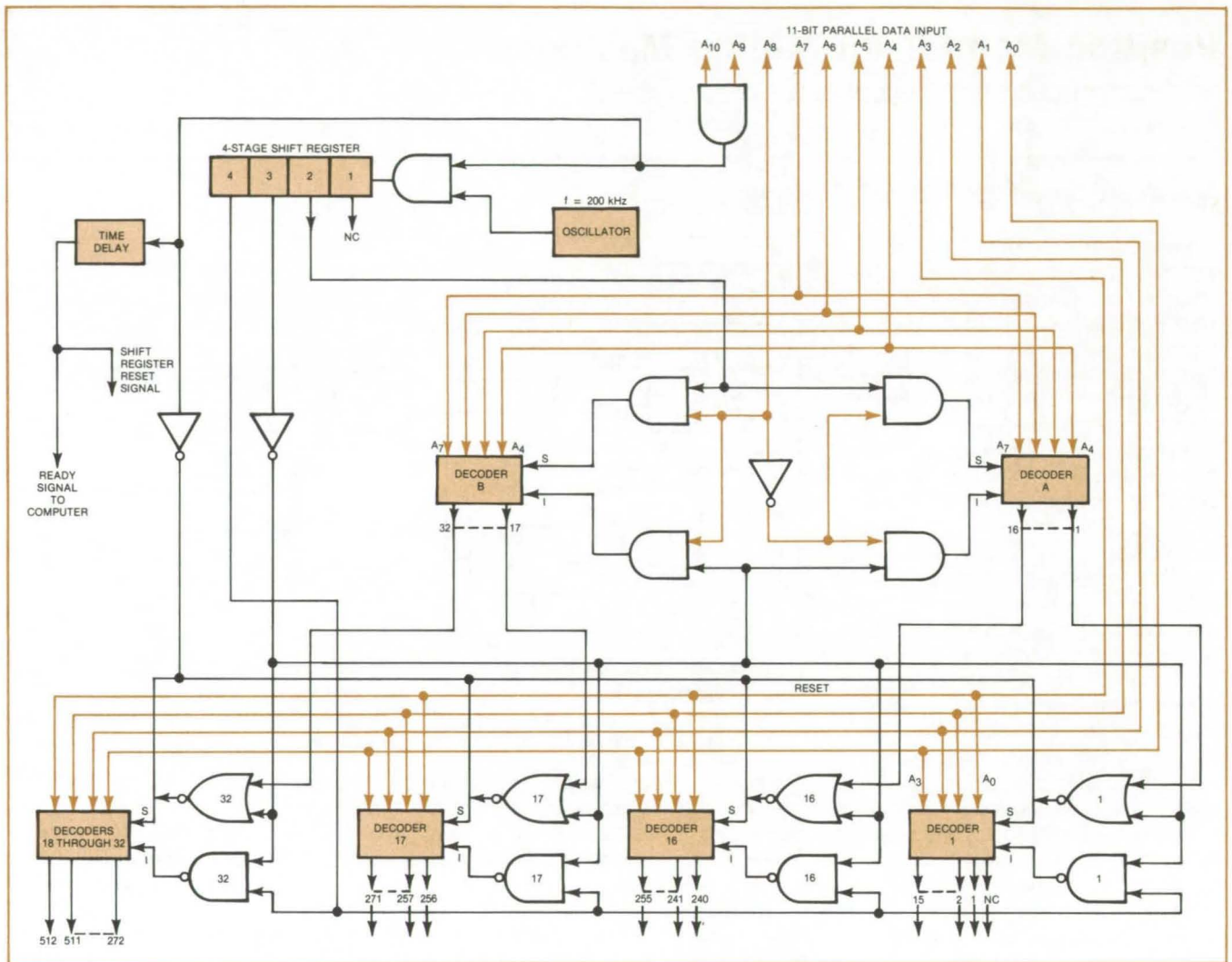
CMOS decoder is assembled from standard 4-line to 16-line decoder/demultiplexer IC's.

Lyndon B. Johnson Space Center, Houston, Texas

The matrix of logic integrated circuits shown is an 11-line to 512-line parallel decoder assembled from standard 4-line to 16-line decoders. It can be expanded by adding more 4-line to 16-line decoders. The matrix

may also be used to generate 256 latched-on or latched-off logic signals instead of 512 discrete unlatched signals. By using conventional CMOS IC's, the circuit consumes only about 30 milliwatts.

An input word to the decoder consists of two groups of bits: nine numerical bits and two execute bits. The binary word comprised of bits A₉ through A₈ designates which of the 512 discrete outputs will change from
(continued on next page)



11-Line to 512-Line Decoder Is Composed of complementary metal-oxide-semiconductor integrated circuits. Pairs of output signals can be wired as latch-on and latch-off commands, to remember the most recent output state after the input is switched off.

a 0 to a 1. The execute bits A_9 and A_{10} turn the decoder "on" when both are 1's.

When a valid 11-bit word is presented to the matrix, the two 1's in the execute group enable a 200-kHz clock oscillator that starts a four-stage shift register (see figure). Shift register position 1 is held for roughly one clock period to allow the 11-bit input data to settle. When the shift register

reaches position 2, it generates a strobe signal that enters data bits A_4 through A_7 into decoder blocks A and B. If A_8 is 0, the data enter block A; if A_8 is 1, data enter block B.

Data bits A_0 through A_3 are connected to the input terminals of decoders 1 through 32. When the shift register is stepped to position 3, it switches off the inhibit line from decoder block A. This enables the

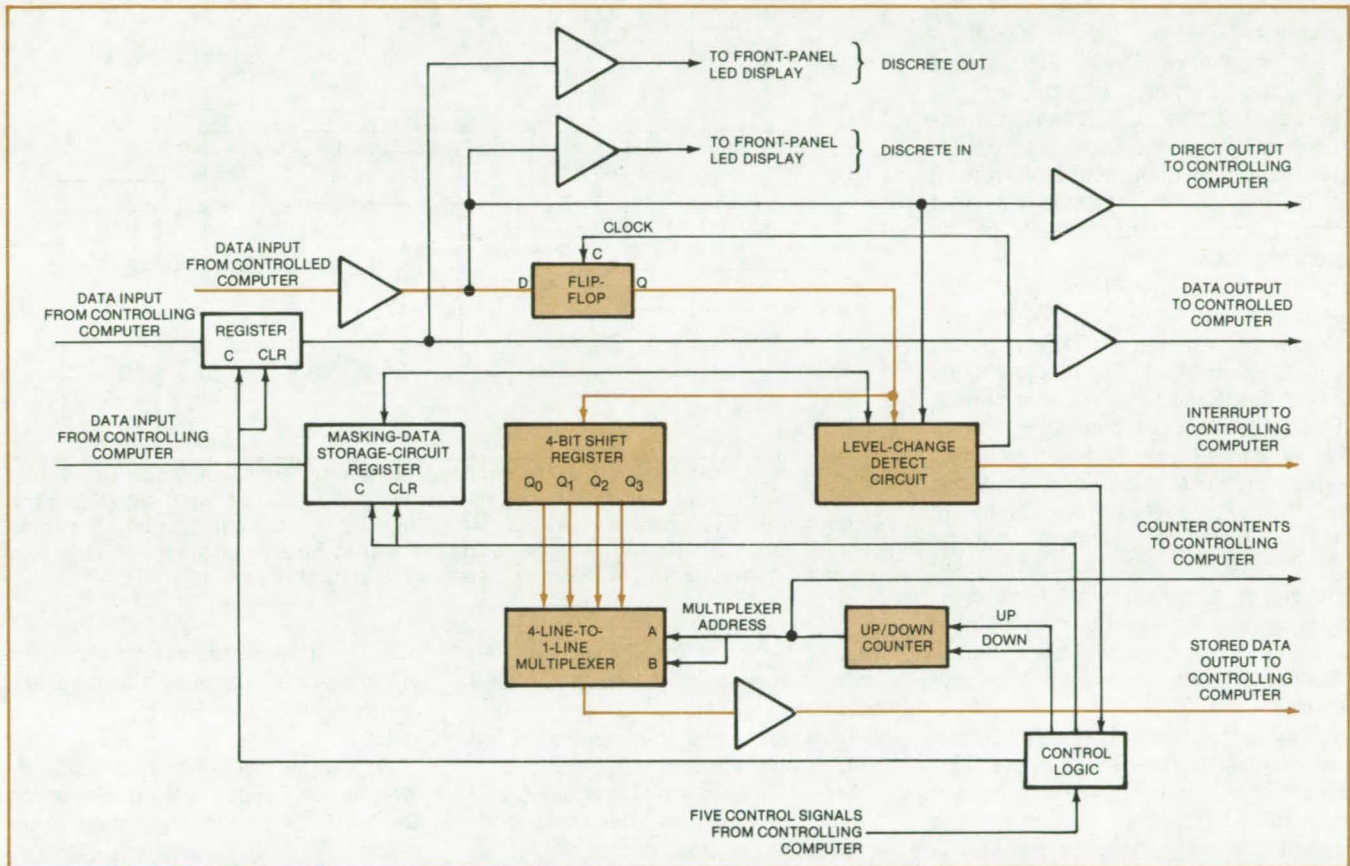
appropriate decoder so that it produces a logic "1" at the output terminal corresponding to the word at bits A_0 through A_8 . The output of the selected decoder is enabled when the shift register reaches position 4.

This work was done by Wilson N. Miller of Rockwell International Corp. for Johnson Space Center. For further information, Circle 9 on the TSP Request Card. MSC-19751

Input/Output Interface Module

Module stores up to 4 consecutive changes on each of 16 I/O lines.

Lyndon B. Johnson Space Center, Houston, Texas



One of Sixteen I/O Circuits is shown in this simplified diagram. The circuit stores up to 4 changes in state in each of the 16 circuits.

An input/output module that transfers up to 16 parallel logic signals between computer systems is useful in computer-to-computer operations, such as flight simulation, and in industrial process control. The module detects level changes in any of its 16 input lines, transfers these to its output lines, and generates interrupts when level changes are detected.

As shown in the simplified block diagram of 1 of the 16 lines, the

module contains a counter and a shift register that stores up to 4 changes in state per line. When the maximum number of changes has been reached, the controlling computer can retrieve the stored data by decrementing the count. The computer has access at all times to the current value of all 16 signals and to the contents of the counter.

The I/O module is packaged in a rack-mounted chassis 3.5 inches (8.9

centimeters) high and 21 inches (53.3 centimeters) deep. It fits into a standard 19-inch-wide (48.3-centimeter) console. The module uses standard TTL logic.

This work was done by Emin M. Ozyazici of Rockwell International Corp. for Johnson Space Center. For further information, including logic diagrams of the I/O module, Circle 10 on the TSP Request Card. MSC-18180

Smoothing the Output From a DAC

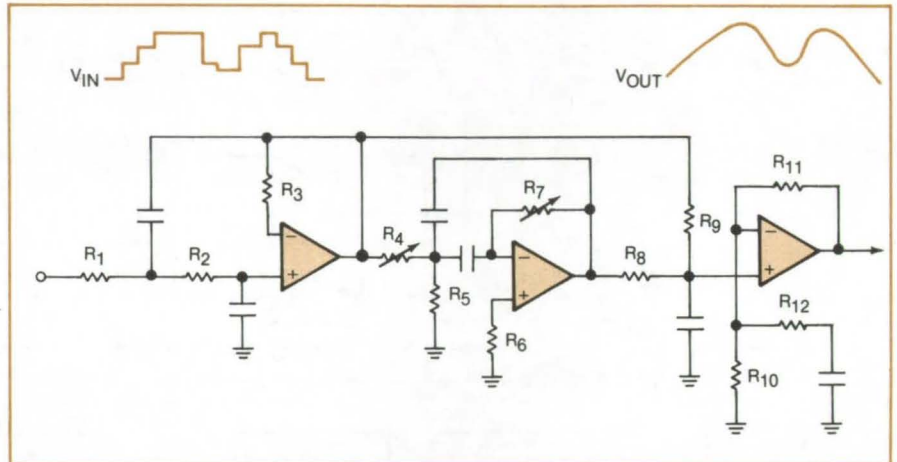
A simple filter conditions the waveform from a digital-to-analog converter for use in control systems.

Dryden Flight Research Center, Edwards, California

A three-stage electronic filter smooths the output from a digital-to-analog converter (DAC), producing a waveform suitable for driving the controls used in manufacturing processes, aerospace systems, and automobiles. The smooth output waveform is in phase with the stepped input signal and is independent of its stepping rate.

A computer or other digital data processor produces an output that is a series of values in binary form, generated at equally spaced intervals called the frame time or clock period. The output is held constant at each value for one frame and then switches rapidly to the next value. Each of these values is converted from digital to analog form virtually instantaneously, so the analog output is a stepped waveform. Unfortunately, such stepped waveforms are unacceptable in many applications; therefore the filter circuit has been developed to smooth them.

The figure shows the stepped input waveform, the three-stage active filter circuit, and the smoothed output waveform. The first section of the circuit is a noninverting low-pass filter. The second is an inverting stage that passes a narrow frequency band centered at the stepping frequency (frame rate), with sharp cutoff on either side of that narrow band. The third section adds the noninverted output of the first section to the inverted output of the second section.



This **Filter Circuit** smooths the stepped waveform from an analog-to-digital converter without appreciable phase shift between the stepped input signal and the smoothed output signal and without any effect from the stepping rate. The three operational amplifiers can be three-fourths of a quad op-amp package, and the only precision components are the four resistors R_8 through R_{11} .

This third section includes a lead/lag characteristic to eliminate phase shift between the signal at its output terminal and the stepped signal at the input to the filter.

This filter, which is noninverting overall, has several desirable constructional features. It uses only three operational amplifiers, which can be three-fourths of a quad op-amp package. Nearly all of the components can have tolerances as large as 5 percent; the only exceptions are the four resistors R_8 through R_{11} . Precision capacitors are not required. Calibration is easily done by simply

injecting a sinusoidal input that has the stepping-rate frequency and adjusting resistors R_4 and R_7 to give zero output.

*This work was done by Charles Wagner of **Dryden Flight Research Center**. For further information, including full design equations, Circle 11 on the TSP Request Card.*

*This invention is owned by NASA, and a patent application has been filed. Inquiries concerning nonexclusive or exclusive license for its commercial development should be addressed to the Patent Counsel, Dryden Flight Research Center [see page A5]. Refer to *FRC-11025*.*

LSI Logic for Phase-Control Rectifiers

Large-scale-integrated components reduce the size of control circuitry.

Marshall Space Flight Center, Alabama

The signals for controlling a phase-controlled rectifier circuit are generated by combinatorial logic that can be implemented in large-scale integration

(LSI). The LSI circuit saves space, weight, and assembly time compared to previous controls that employ one-shot multivibrators, latches, and

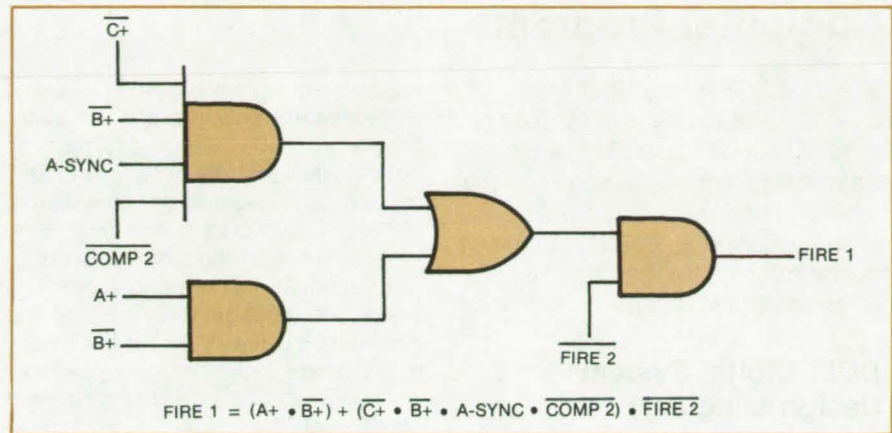
capacitors. The LSI logic functions by sensing the three phases of the ac power source and by comparing actual currents with the intended currents.

The LSI components required for the logic operations are:

- operational amplifiers (for integrating waveforms and for comparing magnitudes),
- inverters,
- AND gates, and
- OR gates.

These elements are arranged to generate several variables and combine the variables in logical operations that determine when firing pulses should be applied to the control terminals of six silicon-controlled rectifiers (SCR's).

For example, the figure shows the logic equation and part of the circuitry that determines the signal called "Fire 1," which is the control voltage applied to SCR 1. The logic equation states that the logic level at that control electrode is determined by applying several variables (that are not defined here) to the combinatorial circuit shown. The complete circuit diagram, showing the formation of all



Combinatorial Logic, using large-scale-integrated components, generates the firing pulses for a phase-controlled rectifier circuit.

the variables and their interconnection to produce the firing pulses for the six SCR's, may be obtained by requesting the Technical Support Package (TSP) referenced below.

This work was done by Carlisle Dolland of Airsearch Manufacturing Co. of California for **Marshall Space**

Flight Center. For further information, Circle 12 on the TSP Request Card.

Inquiries concerning rights for the commercial use of this invention should be addressed to the Patent Counsel, Marshall Space Flight Center [see page A5]. Refer to MFS-25208.



Model for MOS Field-Time-Dependent Breakdown

A quantitative model for MOS breakdown is derived and correlated with experiments.

NASA's Jet Propulsion Laboratory, Pasadena, California

A dominant mechanism in MOS time-dependent breakdown is sodium emission from the metal/oxide interface, which occurs during the application of a positive gate bias. This breakdown is related to the clustering of the emitted ions at localized defect sites at the oxide/silicon interface. Therefore, much smaller ion densities than normally associated with ion-charge stabilities can initiate breakdown.

The existing physical model describing this breakdown in terms of a single trapping energy has been extended to include the effect of a range of ion-trapping energies, leading to a logarithmic time dependence and a Schottky field dependence for breakdown to occur. The initial breakdowns have been related to a Fowler-Nordheim field dependence. Experimental data on MOS breakdown probability, enhanced by implantation damage, have been ob-

tained and correlated with the predicted time and field dependencies. The results can be applied to evaluate the reliability of an MOS process.

The theoretical analysis indicates that the breakdown probability is

$$P_1(t, F) = B \ln(t/t_0)$$

where t is the elapsed time after a field F is applied. The parameter t_0 , the time delay until onset of breakdown is related exponentially to the trapping energy barrier, which is lowered by a factor proportional to the square root of the applied field (Schottky field dependence); and the coefficient B is proportional to the area of the silicon interface, the defect density per unit area, the density of trapped ions, the effective ion-capture cross section, the Boltzmann constant, and the temperature.

The logarithmic time-dependent breakdown probability does not include

the effects of initial breakdowns at localized defects. These are characterized by a Fowler-Nordheim field dependence given by the probability

$$P_0(F) = b \exp(-a/F)$$

where a and b are constants. The total probability $P(t, F)$ of breakdown is therefore

$$P(t, F) = P_0(F) + P_1(t, F).$$

The modified model was verified by testing 24 wafers containing MOS capacitor arrays. The wafers were n-type silicon having 1- to 3-ohm-cm values, a 5-cm diameter, and a 100 orientation. A linear regression analysis of the tested initial breakdown and time-dependent breakdown probabilities correlated well with the model.

This work was done by Seung P. Li, Joseph Maserjian, and Simon Prussin of Caltech for **NASA's Jet Propulsion Laboratory**. For further information, Circle 13 on the TSP Request Card. NPO-14701

Computer Programs

These programs may be obtained at very reasonable cost from COSMIC, a facility sponsored by NASA to make new programs available to the public. For information on program price, size, and availability, circle the reference letter on the COSMIC Request Card in this issue.

DDL: Digital Systems Design Language

A block-oriented hardware description language

Hardware description languages are valuable tools in such applications as hardware design, system documentation, and logic design training. Just as software designers use high-level languages to express algorithms in concise language statements, digital hardware designers use hardware description languages to describe the system they are designing.

The Digital Systems Design Language (DDL) is a convenient medium for inputting design details into a

hardware-design automation system. A translator program and a simulator program allow hardware designers to benefit from the use of DDL. In DDL, the structural elements of the system are explicitly declared. At a lower level of description, functional and structural elements correspond directly to the actual physical elements of the system. DDL is suitable for describing digital systems at the gate, register transfer, and major combinational block level.

DDL is a "block-oriented" language that the designer can use to describe the functional specifications of a digital system. The blocks usually correspond to the natural divisions of the hardware being described. Thus a DDL description of a computer might have a major block called an "ALU," which contains a block called "adder," which consists of interconnected logic blocks called "full adders." The DDL language can describe parallel operations as well as synchronous and asynchronous behaviors.

The DDL translator program (DDLTRN) translates the user-

supplied DDL description of a system into a set of Boolean equations and register-transfer statements. The output from DDLTRN is used as input for the DDL simulation program (DDLSIM). DDLSIM enables the designer to test and verify the design of the digital system. DDLSIM is a table-driven, event-oriented simulator. Time is treated as a discrete quantity and advance on an event-by-event basis. Through command statements, the response of the simulated system to a wide variety of input signals may be determined.

The DDLTRN and DDLSIM programs are written in FORTRAN IV for batch execution on the SEL-32 computer. Each program requires approximately 64K of 8-bit bytes on the SEL-32. These digital system design aids were developed in 1979.

*This program was written by Sajjan G. Shival of the University of Alabama at Huntsville for **Marshall Space Flight Center**. For further information, Circle A on the COSMIC Request Card.*
MFS-25352

Electronic Systems



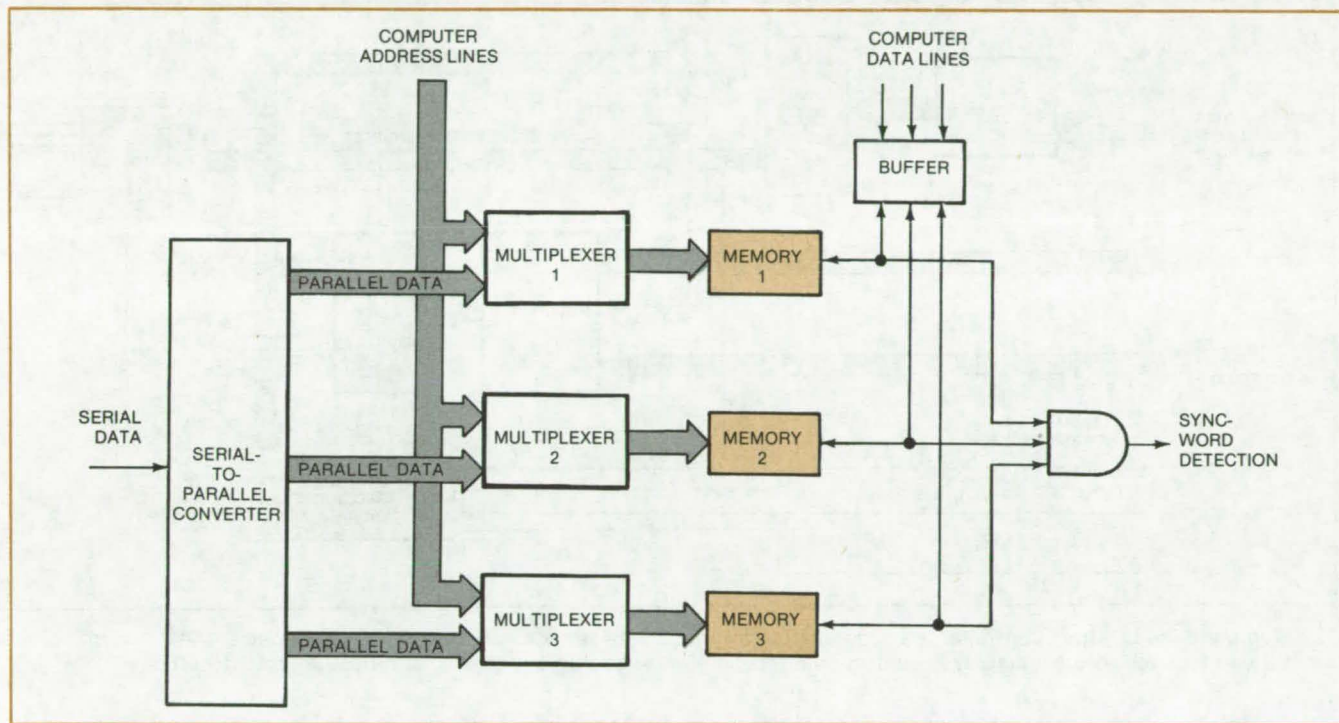
Hardware, Techniques, and Processes

- 149 RAM-Based Frame Synchronizer
- 150 RAM-Based Parallel-Output Controller
- 151 Microcomputer-Based Doppler System for Weather Monitoring
- 152 Linearizing Magnetic-Amplifier dc Transducer Output
- 153 Better-Quality CCD-Array Images
- 154 Real-Time Film Recording From Stroke-Written CRT's
- 155 Torque Control for Electric Motors
- 156 Frequency-Controlled Voltage Regulator
- 157 A Redundant Regulator Control With Low Standby Losses
- 158 Frequency Response of Multiple-Sampling-Rate Systems

RAM-Based Frame Synchronizer

A frame synchronizer for serial telemetry can be rapidly reconfigured for changing formats.

Goddard Space Flight Center, Greenbelt, Maryland



The **Sync-Word Recognizer**, containing memory blocks 1, 2, and 3, is the heart of the frame synchronizer. The synchronizer generates signals marking data-word boundaries (word sync), the beginning of each frame (frame sync), and the beginning of each paragraph (subframe sync). Also derived are search, check, and lock status signals. An existing unit is assembled from standard random-access memory elements and MOS and low-power-Schottky logic.

Random-access memories are the key elements in a versatile new frame synchronizer for serial-data telemetry. The use of memories makes it possible to reconfigure the system rapidly for changing formats and sync words, while offering wide flexibility in the specification of these parameters.

The memory-based frame synchronizer consists of a serial-to-parallel converter, sync-word recognizers, and control logic. The sync-word recognizers are segmented memory elements that are set up with the patterns of "1's" and "0's" necessary to identify the sync word, including its length and allowable bit error. A "true" output from any recognizer implies that there is a successful match between the parallel data and the sync-word segment.

As shown in the figure, the sync-word recognizer is made up of input multiplexers and memory elements. The inputs to the memory address lines are either from an external microprocessor, or a computer, or from the telemetry parallel data. In the control subsystem, memory arrays used as counters define the word bit length, frame word length, and paragraph frame length.

The frame synchronizer has an initialization mode and a processing mode. During initialization, the microprocessor or a computer loads the sync and format information into the memory-array elements, by memory mapping. When the memory modules are loaded, the frame synchronizer enters the processing mode. Incoming serial data are scanned continuously

by presenting the data in parallel to the address line inputs of the memory arrays. A sync is detected by gating of the recognizer-memory data outputs and the control-subsystem counters. The processing mode continues until the memories are reaccessed by the microprocessor or computer to change the matrix format.

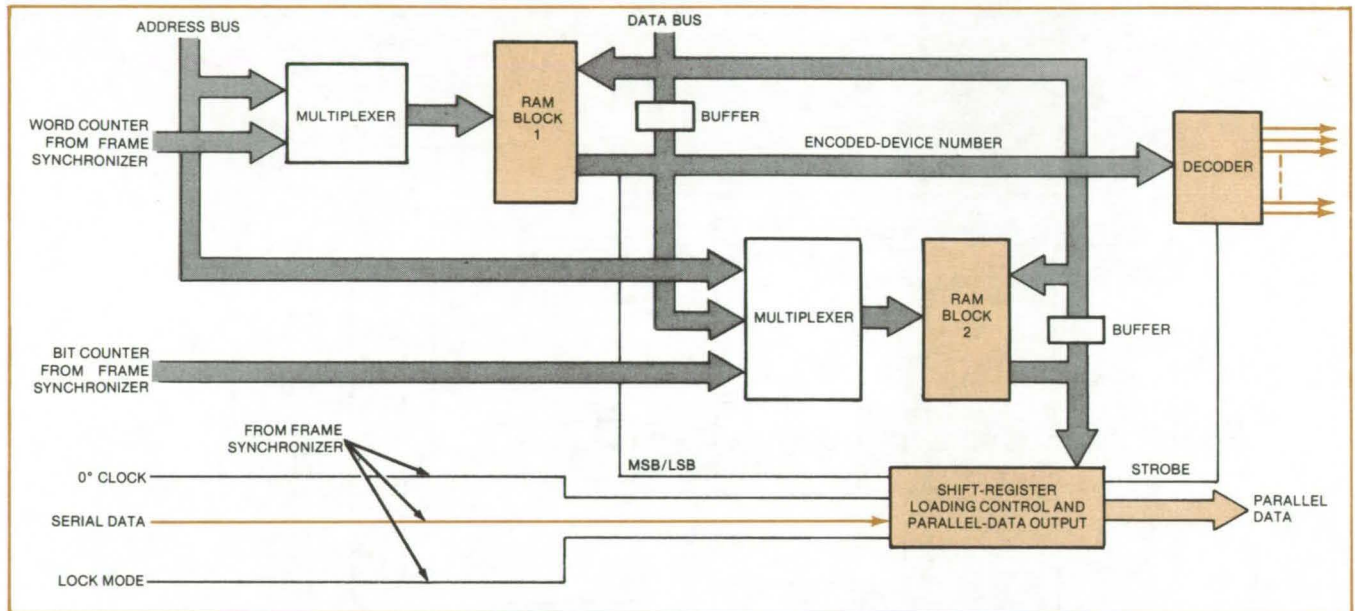
This work was done by James K. Niswander and Raymond J. Stattel of Goddard Space Flight Center. For further information, Circle 14 on the TSP Request Card.

This invention is owned by NASA, and a patent application has been filed. Inquiries concerning nonexclusive or exclusive license for its commercial development should be addressed to the Patent Counsel, Goddard Space Flight Center [see page A5]. Refer to GSC-12430.

RAM-Based Parallel-Output Controller

Selected bit strings in a serial-data link are extracted for processing.

Goddard Space Flight Center, Greenbelt, Maryland



The **Memory-Based Output Controller** is a programmable interface between a serial-data link and peripherals that accept parallel data. It can be used to drive displays, printers, plotters, digital-to-analog converters, and parallel-output ports.

A memory-based controller (see figure) selects bit strings from a stream of formatted serial data and directs the strings to peripherals as parallel data. It has several unique features:

- The configuration of the bit-string selector can be easily changed to accommodate changing formats. (This is especially useful for time-shared data links.)
- Any sequence of bits in a data word, or overlapping more than one word, can be selected for any peripheral.
- The data can be transferred either most-significant-bit first or least-significant-bit first.
- Costs are reduced below those of previous designs because of lowered parts count.

The output controller contains a block of random-access memory (RAM) that has at least as many

address locations as the number of words in a paragraph. The word counter input from a frame synchronizer addresses the RAM block, which provides as its output: (1) an encoded peripheral device number and (2) a most-significant-bit first/least-significant-bit first (MSB/LSB) flag.

The encoded device number and the bit counter from a frame synchronizer are address lines to another RAM block, which contains start and stop flags to pick out the required bits from the specified word number(s). The MSB/LSB and start and stop flags, along with the serial data, go into a control block, which selectively fills a shift register to drive the parallel-data output bus. A strobe pulse is also generated, enabling a decoder to select the appropriate peripheral using the encoded device number.

A microcomputer sets the contents of the RAM blocks during an initialization phase, using the technique of memory mapping. After the RAM blocks are loaded, the output controller operates completely independently of the microcomputer. The speed of operation is limited only by the access times required for operation of the memories.

This work was done by James K. Niswander and Raymond J. Stattel of Goddard Space Flight Center. For further information, Circle 15 on the TSP Request Card.

This invention is owned by NASA, and a patent application has been filed. Inquiries concerning nonexclusive or exclusive license for its commercial development should be addressed to the Patent Counsel, Goddard Space Flight Center [see page A5]. Refer to GSC-12447.

Microcomputer-Based Doppler System for Weather Monitoring

A microcomputer processes satellite Doppler data to determine the locations of weather beacons.

Goddard Space Flight Center, Greenbelt, Maryland

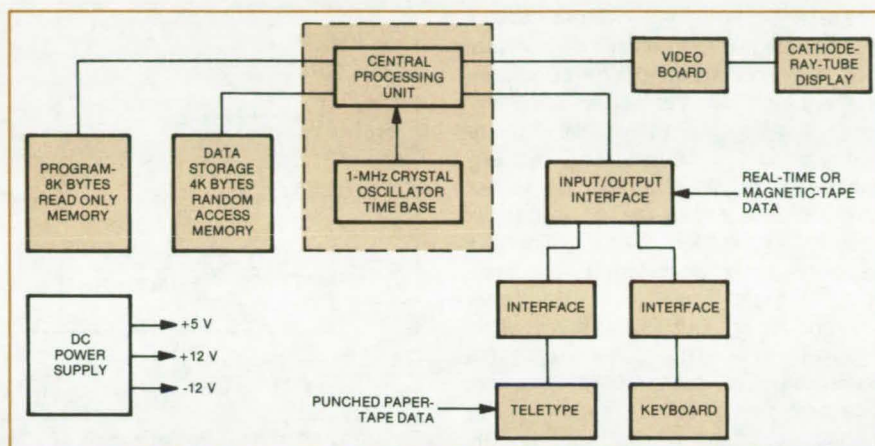
A ground-based microcomputer processes Doppler data from weather satellites to determine geographical positions of weather beacons interspersed around the globe. These beacons, such as weather balloons and buoys, collect local weather information and transmit it to orbiting satellites. The satellites in turn relay this information to ground-based monitoring stations. Each station equipped with the microcomputer can print out both beacon location and accurate weather data collected from various points around the globe.

The microcomputer as shown in the block diagram includes a central processing unit (CPU), memory, and input/output peripherals. The CPU is a single large-scale-integration (LSI) microprocessor chip that addresses up to 2^{16} bytes of memory.

A built-in 1 MHz timing oscillator and clock driver eliminate the need for an external clock generator. The time base generates the required two-phase clock pulses. Address lines and read/write commands are set up during the first pulse period, and data are transferred (either read or write) during the second pulse.

Internally, the processor is organized into two sections. The instructions obtained from program memory are executed by implementing a series of data transfers in the register section of the chip. The lines that cause the data transfers are in the control section.

Most of the program execution occurs in the register section. Input data from the program memory, the data memory, or from peripheral devices appear during the last 100 ns of the second (or phase two) positive clock pulse. These data are simply transferred into the input-data latch for use during the next cycle.



A **Ground-Based Microcomputer** determines geographical positions of beacons, using Doppler data from weather satellites. The system requires only 7 W and incorporates least-squares iteration to compute the positions. Results are printed out in alphanumeric characters either on the CRT or on the teletype. A 6502 CPU was used, although an equivalent processor could be substituted (with appropriate modification to the hardware).

The microcomputer memory section stores the satellite Doppler measurements in 4K bytes of random-access memory (RAM). The RAM has two distinct segments: the data storage and the working storage. Data are stored anytime the satellite passes over a radio beacon and can be loaded into the computer, using punched paper tape, via the teletype, magnetic tape, real-time satellite receiver tie, or by manual entry via the keyboard. The working storage segment is used for intermediate results in arithmetic operations for peripheral output data storage.

A position-location least-squares program is stored in read-only-memory (ROM) chips. These chips are permanently programmed to compute beacon latitude and longitude positions either on a single or two successive satellite passes. A minimum

of three Doppler measurements is needed for a single-pass solution, to solve for three unknowns: latitude, longitude, and frequency bias. Typically, however, about 15 data points are obtained per pass. That represents a 10-min observation interval, and it takes about 20 s to compute a beacon position for that interval.

The microcomputer can be interfaced with a number of peripherals. One typical interface is with a keyboard and a cathode-ray-tube (CRT) display. The results are printed out in alphanumeric characters on the keyboard and on the CRT.

This work was done by Paul E. Schmid of Goddard Space Flight Center and Joe J. Lynn of Old Dominion Systems, Inc. for further information, Circle 16 on the TSP Request Card.
GSC-12448

Linearizing Magnetic-Amplifier dc Transducer Output

A diode corrects nonlinearity at small currents in a magnetic-amplifier dc transducer circuit.

NASA's Jet Propulsion Laboratory, Pasadena, California

Magnetic-amplifier direct-current transducers used to monitor important points in spacecraft power-conditioning systems have exhibited nonlinear outputs at low current levels. Nonlinearity occurs in the miniature versions that are used, in quantity, to monitor many points where the dc is usually less than 1 A. These miniature versions have exhibited a relatively-linear transfer function in the higher current region, but as can be seen in Figure 1, they are nonlinear at the lower end. This can result in incorrect interpretation of actual readings. This nonlinear effect is caused by the magnetizing current, flowing through winding 6-5 and R_2 , in parallel with R_1 , and by the characteristics of the core material. The problem was corrected by adding a diode (CR_3) in series with the output stage between winding 6-5 and resistors R_2 in the circuit in Figure 2. The forward voltage drop of this diode minimizes the shunting effect on R_1 and reduces the magnetizing current flowing through R_2 .

The magnetic amplifier shown has the properties of a current transformer: The amplitude of the current in winding 5-6 equals the amplitude of the dc current being monitored (in winding 7-8), divided by the ratio of the turns of winding 5-6 to winding 7-8. During each respective Q and \bar{Q} , switching half cycle of the ac square-wave excitation applied sequentially to windings 1-2 and 3-4, the cores A and B each have two distinct operating phases: an unsaturated phase and a saturated one.

When a magnetic amplifier operates in the switching mode, desaturation can only occur if the voltage at the primary winding (e.g., 1-2) is of the same amplitude but of opposite polarity as the voltage across the secondary winding (e.g., 6-9). Hence the voltage that "resets" each of the cores in turn must not be allowed to reach a level that would overbias either core to produce saturation in the wrong direction. If this should

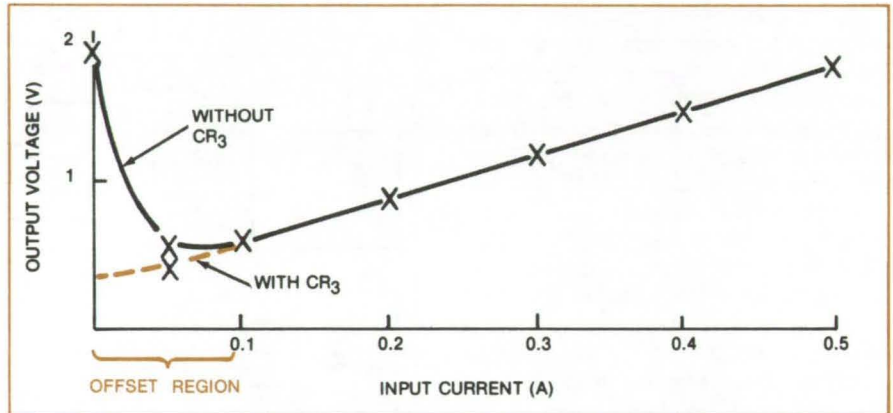


Figure 1. Nonlinear Performance of a Magnetic-Amplifier dc Transducer that occurs at low current levels is corrected by inserting a diode in series with the output stage.

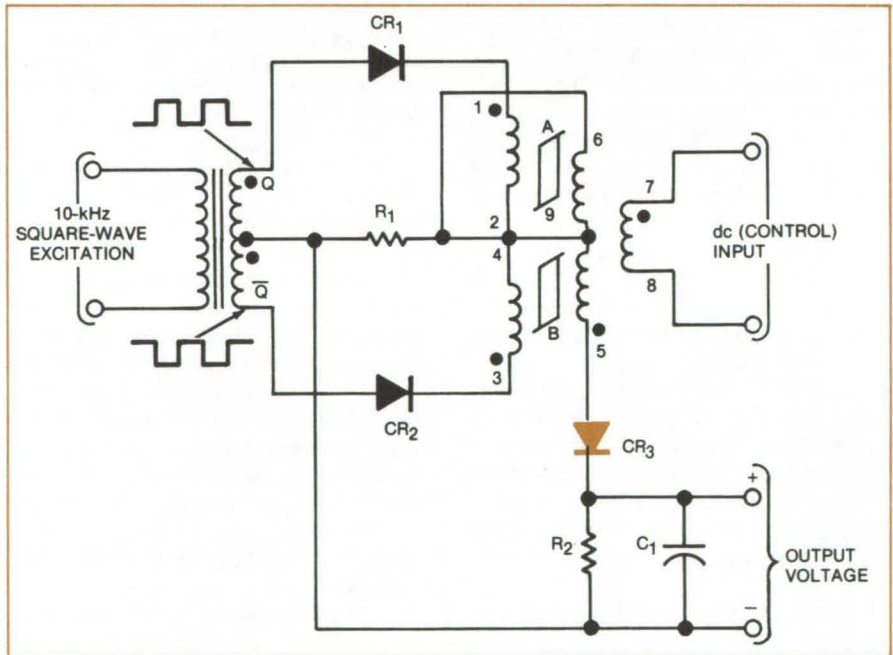


Figure 2. Circuit Schematic of a Magnetic-Amplifier dc Transducer shows where the diode is inserted to produce linear output at small current levels. The diode in series with the output stage corrects the nonlinear performance of the transducer in the offset region as shown on the graph.

occur with either core, both cores would thereafter remain saturated, defeating the desired switching action.

The diode drop (depending upon the number of diodes in series) in series with resistors R_2 and R_1 has a threefold effect: (1) It limits the indicating voltage that appears across

R_2 to provide the output indication and linearizes in the offset region; (2) it limits the voltage needed to reset the cores and thus lessens the possibility of overbiasing in the wrong direction (which could produce reverse saturation); and (3) it gives leeway in selecting the value of R_1 . After the

value of R_1 is determined, the number of diodes used in series to produce the desired diode drop is determined experimentally.

Resistor R_1 is used to provide the desired transformer action. The value of R_1 must be a compromise, small enough to provide the return path for

the magnetizing current instead of the alternate path through winding 6-5 yet high enough to minimize power loss.

This work was done by Satoshi Nagano of Caltech for **NASA's Jet Propulsion Laboratory**. For further information, Circle 17 on the TSP Request Card.

This invention is owned by NASA, and a patent application has been filed. Inquiries concerning nonexclusive or exclusive license for its commercial development should be addressed to the Patent Counsel, NASA Resident Legal Office-JPL [see page A5]. Refer to NPO-14617.

Better-Quality CCD-Array Images

Quadruple sampling increases the signal-to-noise ratio of charge-coupled-device imagers.

NASA's Jet Propulsion Laboratory, Pasadena, California

The quality of the image from an array of charge-coupled devices (CCD's) is improved by about 40 percent by a four-step sampling scheme. The scheme is easily implemented using simple logic circuits.

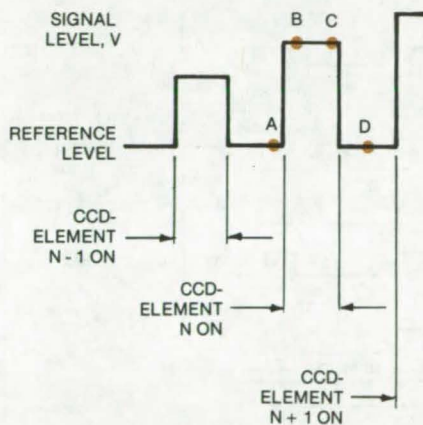


Figure 1. The **Signal From Contiguous Elements of a CCD Array** is sampled at points A, B, C, and D. The difference pairs $V_B - V_A$ and $V_C - V_D$ are added to double the signal level.

Previous CCD image processors used single or double sampling of the array output, as illustrated in Figure 1, which shows the signal derived from two contiguous CCD elements. In single sampling, only the signal level (B) during the "on" phase of each array element is measured; the "on" level and a reference level (B and A) are measured and subtracted in double sampling, improving the signal-to-noise level by a factor of 8 in one CCD imaging star tracker.

In quadruple sampling, the signal from each element in the array is sampled once before the element is

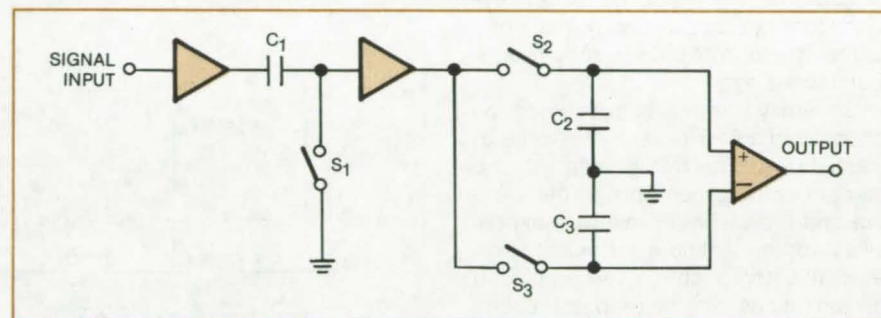


Figure 2. **Quadruple-Sampling Processor** is triggered by timing signals from the CCD array. The signals open and close electronic switches S_1 , S_2 , and S_3 .

clamped on, twice during the "on" period, and once again after the element is turned off. Thus, in Figure 1, one sample pair is taken at points A and B (as in double sampling), and another pair is taken at points C and D. The differences $V_B - V_A$ and $V_C - V_D$ are then added.

Adding the difference voltages effectively doubles the signal; and, since ideally the noise levels before and after the on period are uncorrelated, the noise increases only by a factor of $\sqrt{2}$, for an overall increase in signal-to-noise of $2/\sqrt{2}$, or 1.414, above its value if double sampling is used.

Figure 2 shows a simple implementation of a quadruple-sampling processor. Switch 1 clamps the reference level at time A, and switch 2 samples the signal at time B. Switch 1 also clamps the signal level at C; and the reference level is sampled at D with switch 3. The negative signal on capacitor C_3 is subtracted from the positive signal on capacitor C_2 by the differential amplifier, producing a net signal gain of 2. The timing signals to open and close the switches are easily de-

rived from the CCD-array timing, using standard logic.

In practice, there is usually some correlation between the "before" and "after" noise levels. However, calculations for a worst-case noise spectrum in one star tracker showed the added noise to be only 11 percent above the uncorrelated noise level; and for a more typical noise spectrum, the added noise is only about 2 percent. Thus, the quadruple-sampling scheme should increase the overall signal-to-noise by about 40 percent above the level for double sampling, a prediction verified by measurements on the star-tracking imager.

This work was done by Steve D. Gaalema of Caltech for **NASA's Jet Propulsion Laboratory**. For further information, Circle 18 on the TSP Request Card.

This invention is owned by NASA, and a patent application has been filed. Inquiries concerning nonexclusive or exclusive license for its commercial development should be addressed to the Patent Counsel, NASA Resident Legal Office-JPL [see page A5]. Refer to NPO-14426.

Real-Time Film Recording From Stroke-Written CRT's

A simple method for phasing ensures flicker-free recordings.

Langley Research Center, Hampton, Virginia

Real-time simulation studies often require motion-picture film recording of the events directly from stroke-written cathode-ray tubes (CRT's). The main difficulty presented is the prevention of "flicker," which results from the lack of synchronization between the display sequence on the CRT and the shutter motion of the camera. A simple programmatic method has been devised for phasing the display sequence to the shutter motion, ensuring flicker-free recordings.

Generally, flicker is prevented by choosing the CRT refresh rate to be at least twice the frame rate of the camera or by synchronizing the camera and the CRT with relatively-expensive interconnecting electronics. However, this approach may be precluded by limitations of the graphics equipment or by the unavailability of the interconnectors. Most computer graphics systems operate on a priority interrupt basis: The graphical computations are interrupted at fixed intervals of time to display the image on the CRT. For flicker-free film recording at 24 frames/second, a display refresh rate of at least 60 Hz is required. However, at this refresh rate, too little time may be available for an acceptable update rate for the graphical computations.

In the new technique, a motion-picture camera with a synchronous ac motor, running at a fixed frame rate of 24 frames/second and a shutter speed of 1/60 second, is used. The refresh rate of the display is set at 24 Hz (five intervals of 1/120 second each). Since the camera and the graphics terminal are both connected to the same power system, they are fully synchronized. In order to record the image on film, the phase lag between the shutter motion and display sequence must be such that the CRT image is displayed during the interval in which the shutter is fully open.

In Figure 1, pulse train I is the camera shutter sequence; pulse trains II are the display sequences for fully invisible, partially visible, and fully visible images. The problem of phasing

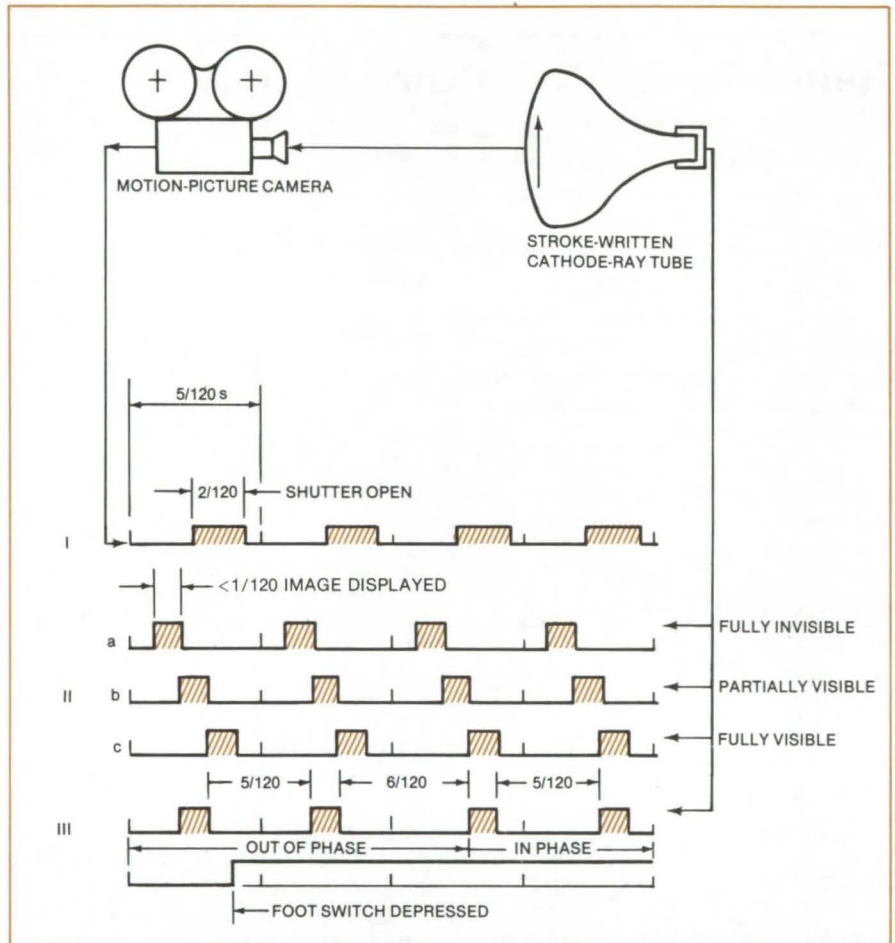


Figure 1. **Display Sequence** can be delayed by depressing a foot switch a sufficient number of times to phase the CRT image to the open shutter.

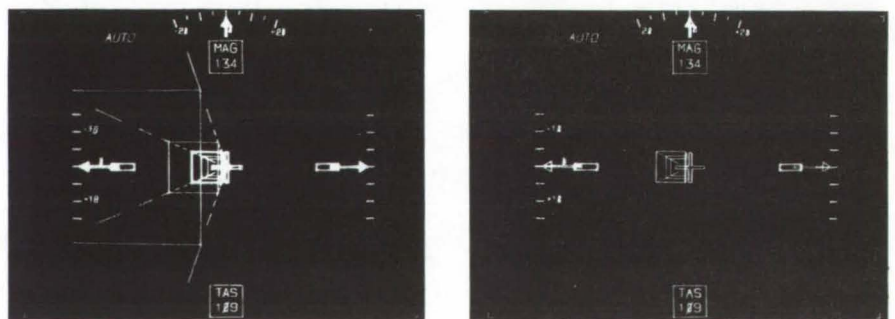


Figure 2. **Flicker-Free Phasing** is shown correctly in the single-frame image on the left. The image on the right, with incorrect phasing, shows an image only partly visible.

the camera and the graphics system is solved by programmatically delaying the display sequence. A simple foot switch, standard to most graphics systems, is used to initiate the delay. The number of 1/120-second intervals between interrupts is normally five. By depressing the foot switch, the display sequence is delayed by an interval of another 1/120 second, as shown in sequence III.

After releasing the foot switch, this process can be repeated, and the sequence is delayed by an additional 1/120 second. After pressing the foot switch five times, the phasing is again

the same as at the start. While observing the image through the viewfinder with running camera, the foot switch is pressed several times until the image is fully visible. Figure 2 shows single frames from a motion picture made using both correct and incorrect phasing. This method requires that the viewfinder image is identical to the image recorded on film.

The motion-picture recordings obtained with this method are absolutely free of flicker, with an adequate computational update rate. The image appears only slightly dimmer than with the more-wasteful 60-Hz refresh rate.

This work was done by Robert L. Hunt of Langley Research Center and Arthur J. Grunwald of the National Research Council. For further information, in the form of a film, 15 minutes long, taken using this technique, request film L-1266 from the NASA Langley Research Center, Film Lending Library, MS 425, Hampton, Virginia 23665.

Inquiries concerning rights for the commercial use of this invention should be addressed to the Patent Counsel, Langley Research Center [see page A5]. Refer to LAR-12529.

Torque Control for Electric Motors

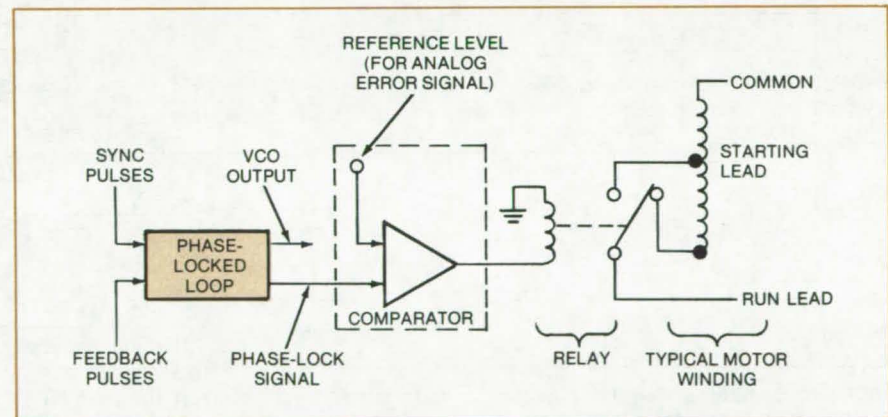
Torque output is varied to accommodate various loads.

Lyndon B. Johnson Space Center, Houston, Texas

A new method for adjusting electric-motor torque output to accommodate various loads utilizes a phase-lock loop to control a relay connected to the starting circuit. As the load is imposed, the motor slows down, and the phase lock is lost. The phase-lock signal then triggers the relay to power the starting coil and generate additional torque. Once the phase lock is recovered, the relay restores the starting circuit to its normal operating mode.

The phase-lock loop controls the motor starting coil. This eliminates the centrifugal switch and insures maximum torque whenever the motor is started or whenever additional torque is needed to restore the phase lock. This approach gives more positive control than the timed application of a starting torque and can generate additional torque when the motor is at operating speed.

The phase-lock signal may serve as a digital indication of the phase lock or as an analog indication of a phase error. As shown in the figure, the signal can drive the relay directly; in the second case the signal is compared to a reference level corre-



Motor Control Circuit uses a phase-locked loop to supply additional power to the motor shaft to accommodate various loads. When the load is applied, phase lock is lost, and a relay is triggered to feed power to the starting coil to generate the extra torque. When the phase lock is restored, the relay opens, and power is applied directly to the run lead.

sponding to the desired maximum in-lock phase error, and the comparator controls the relay.

Motor drive signals on the run lead are applied to the starting coil when the relay is activated (loop out of lock) to produce extra torque. Motor drive signals are applied to the run lead of the motor when the relay is not activated (loop in lock). The method

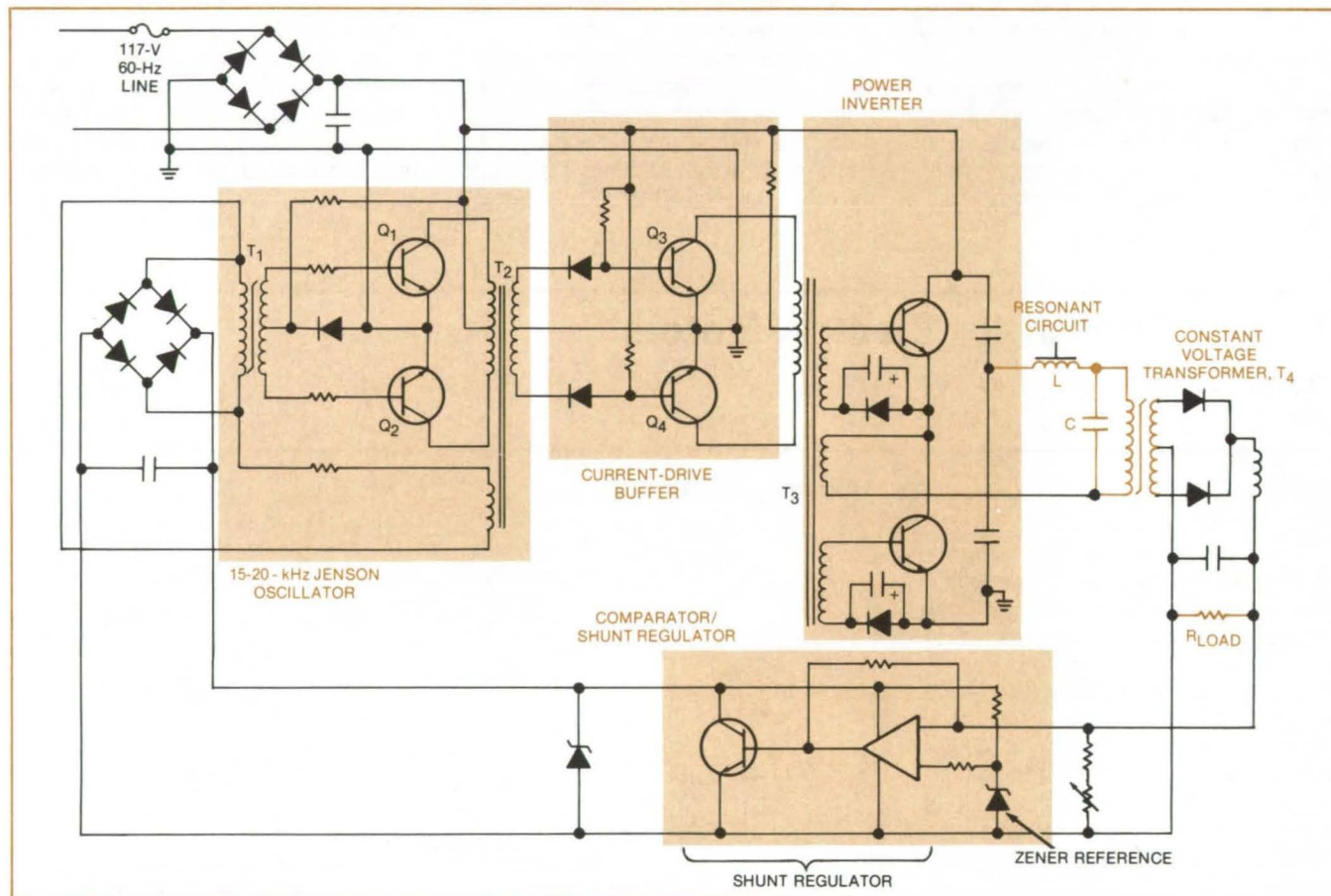
can save power because the running torque can match the load more closely, and additional torque (requiring additional power) is only generated when it is needed.

This work was done by Clement A. Berard of RCA Corp. for Johnson Space Center. No further documentation is available. MSC-18635

Frequency-Controlled Voltage Regulator

Converting input ac to a higher frequency reduces size and weight and makes possible a unique kind of regulation.

NASA's Jet Propulsion Laboratory, Pasadena, California



The new **Switching Regulator** uses a Jenson oscillator to convert the 60-Hz line voltage to 20 kHz. Stepping up to higher frequency makes possible the use of lightweight passive components.

A proposed power supply would be smaller and lighter than conventional supplies because it converts its ac line input to a much higher frequency before regulating it and rectifying it. At the higher frequency, the size and weight of the inductive and filter components are reduced by a factor of 100 or more; and since the conversion frequency is above the range of human hearing, the supply generates no audible noise. The supply also exploits the high-frequency conversion feature to regulate its output voltage in a novel way.

In the circuit (see figure), the 60-hertz, 117-volt line power is converted to a 15 to 20 kilohertz square wave. This signal drives a resonant circuit

(inductor L and capacitor C) at the input to saturable-core transformer T₄. A feedback leg returns part of the load voltage to the oscillator to vary its frequency in response to output voltage changes.

By operating the circuit at a frequency near the resonant point of the LC circuit, the voltage input to transformer T₄ is made large enough to drive the transformer into saturation. At that point on its operating curve, the transformer is insensitive to voltage fluctuations at its input, and the voltage at its output is "hard-limited" to the required value.

In the saturation mode, the transformer voltage varies proportionally to its drive frequency, and this effect is

used to regulate the circuit output. The error signal obtained by monitoring the load voltage is fed to one input of an op amp. The other input is a reference Zener diode. Any difference between these inputs is amplified and applied to a shunt regulator to vary the resistance across a bridge rectifier. Changes in the bridge impedance at the input to transformer T₁ adjust the oscillator frequency to compensate for changes in the load voltage. The ferroresonant circuit is inherently short-circuit proof.

This work was done by Colonel W. T. McLyman of Caltech for NASA's Jet Propulsion Laboratory. For further information, Circle 19 on the TSP Request Card.
NPO-13633

A Redundant Regulator Control With Low Standby Losses

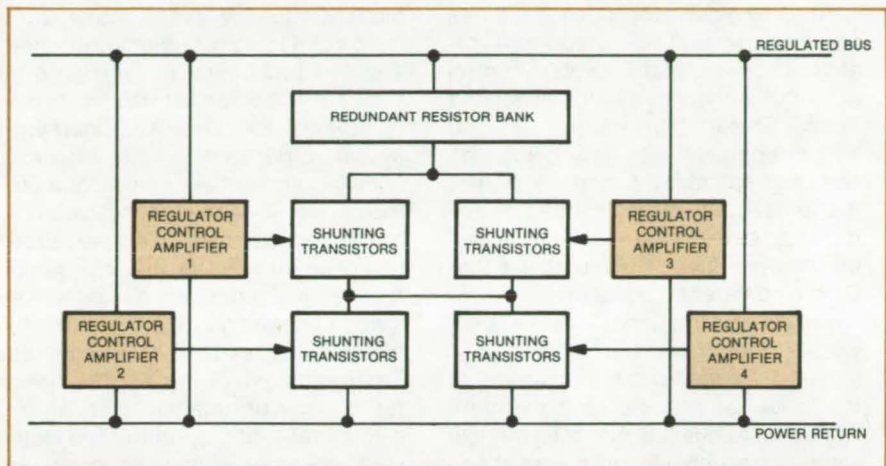
A shunt regulator minimizes power-conditioning losses.

NASA's Jet Propulsion Laboratory, Pasadena, California

A new shunt regulator circuit for an outer-planet-spacecraft radioisotope thermoelectric generator minimizes power-conditioning losses. The unit consists of a bank of duplicate regulator control amplifiers and their associated shunt transistors connected across a power-supply line. Its high-gain circuitry arranged in a redundant configuration is very reliable and is characterized by low standby loss. The circuit can be used in other power-supply applications where size, weight, and reliability are important.

The unit is based on a simple regulator control amplifier designed to minimize the power losses. Regulated bus voltage is sampled and compared to a voltage reference; an error signal proportional to the difference is produced by the operational amplifier. This output error signal drives shunting transistors to maintain the regulated bus voltage.

Four of these control amplifiers and their shunt transistors are arranged as shown in the figure, forming a highly reliable regulator. Each circuit has a standby loss of approximately 15 mW nominal and 25 mW worst-case maximum. The shunt regulator controls a maximum of 600 W regulating the bus voltage through all the spacecraft operational modes. With approximately 60 mW of power in the four regulator control amplifiers, an efficiency of 99.99 percent is realized when the full 600-W source power is delivered to the load.



Shunt Regulator block diagram shows the arrangement of control amplifiers and their shunt transistors. Because each regulator control amplifier has high gain, only one of the four governs shunting at any time. This highly reliable circuit features a very low standby power loss.

Because each regulator control amplifier has a sufficiently high gain, only one of the four governs shunting operations at any time. The one in series with the controlling unit is fully on; the one in parallel with the controlling unit is fully off; and the one diagonal to the controlling unit is either fully off or fully on. This quad redundant configuration makes the regulator highly tolerant to failures.

Partial failures, short or open, are accommodated without affecting the regulator performance. Control is transferred automatically from the failed unit to either its series or parallel unit, depending upon the mode of failure (fully on or fully off).

The 21-V output voltage swing of the operational amplifier causes the shunting circuitry to translate from the fully off to the fully on condition. The large signal-voltage gain, typically 300 V/mV, of the amplifier and the 5:1 voltage-sense divider network require only 35 mV deviation on the regulated voltage bus to produce a 21-V change in the amplifier output. Hence, the regulation change versus load change is nearly immeasurable.

This work was done by Roman W. Andryczyk and Stephen R. Peck of General Electric Co. for NASA's Jet Propulsion Laboratory. For further information, Circle 20 on the TSP Request Card.
NPO-13165

Camera Add-On Records Time of Exposure

The time a photograph is taken is permanently recorded on the edge of the exposure by a compact electronics module that attaches to the camera case. A single-chip timing circuit drives an LED display, which is imaged on the film plane. The normally blanked display is unblanked when the shutter switch is activated. (See page 168.)

Input/Output Interface Module

An input/output module detects level changes in any of its 16 inputs, transfers the changes to its outputs, and generates interrupts when the changes are detected. Up to four changes-in-state per line are stored for later retrieval by a controlling computer. Using standard TTL logic, the module fits in a 19-inch rack-mounted console. (See page 143.)

Improved Power-Factor Controller

Power dissipation in an ac induction motor is reduced by an improved circuit that lowers the applied voltage when the motor is idling or only lightly loaded. Timing voltages in phase with the motor current are sensed across a gate-controlled semiconductor switch in series with the motor, rather than across a high-power resistor, as in an earlier version. (See page 133.)

Frequency Response of Multiple-Sampling-Rate Systems

A new procedure makes a complex problem tractable.

Lyndon B. Johnson Space Center, Houston, Texas

An analytical procedure simplifies the prediction of the frequency response of multirate digital control systems. Although developed for the Space Shuttle flight-control system, which operates at two gyroscope sampling rates (12.5 and 25 hertz), the procedure is applicable to any multirate system describable by linear, constant-coefficient differential equations or difference equations.

Previously, frequency-domain analysis of multirate sampled-data systems has either been performed at the lower sample rate (and therefore limited in frequency range to the low sample frequency), or it has been performed at the higher sample rate by the use of a method that effectively increases the order of continuous- or

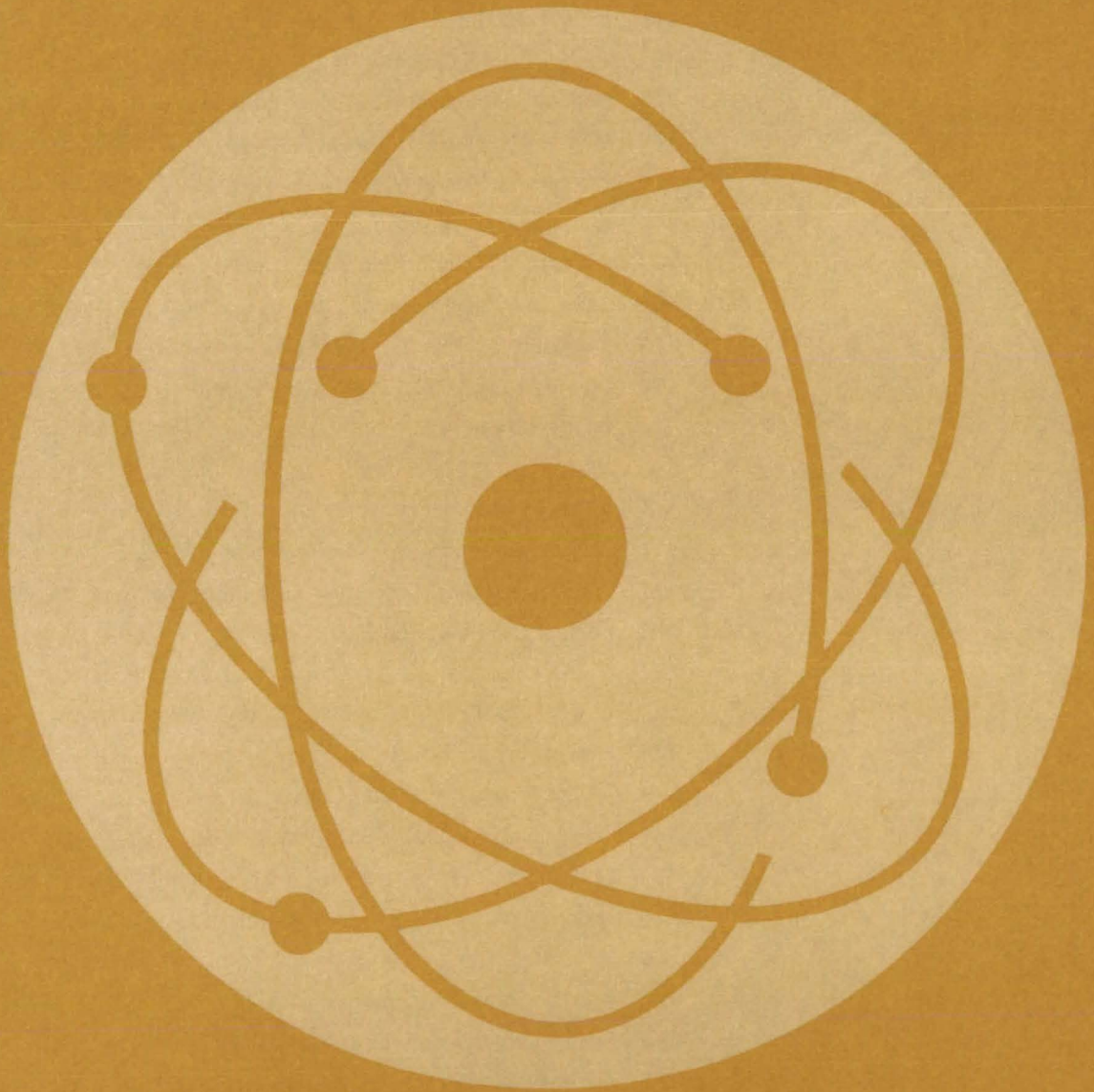
higher-frequency piece parts by a factor of n in an $n:1$ multirate system. The new procedure also analyzes the frequency domain at the fast rate; however, it does so without increasing system order (which presents root-finding problems and computer-memory overloads in many cases).

The previous method for frequency-response analysis at the fast sample rate is to construct a single rate system operating at the fast rate. This method requires the construction of a "mirror image" of the original system (or n "mirror images" for an $n:1$ sample-rate-ratio system). The loop is then broken at a selected point, and the frequency-response characteristics of the enlarged system are determined.

The new procedure replaces the enlarged system with the computation of two separate frequency responses based on the original system. The two frequency responses are vector-summed at discrete frequencies to produce the total system frequency response at the faster sample rate. The advantage is a reduction in problem size and, consequently, the emergence of a problem that fits within many existing analysis tools and that does not present multiple-root determination problems.

This work was done by David K. Scharmack of Honeywell, Inc., for Johnson Space Center. For further information, Circle 21 on the TSP Request Card.
MSC-18473

Physical Sciences



Hardware, Techniques, and Processes

- 161 An Equation of State for Liquids
- 162 High-Resolution Spectrometer/Interferometer
- 163 Instrument Remotely Measures Wind Velocities
- 164 Far-Field Radiation Pattern of Tunable Diode Lasers
- 164 Optical Calibrator for TDL Spectrometers
- 165 UV Actinometer Film
- 166 Fluorescent Radiation Converter
- 166 Automated Holographic Drop-Size Analyzer
- 167 Photographic Measurement of Droplet Density
- 168 Camera Add-On Records Time of Exposure
- 169 Improved Multispectral Solar-Cell Array
- 169 Low-Cost Calibration of Acoustic Locators
- 170 Integral Storage-Bulb and Microwave Cavity for Masers

Books and Reports

- 171 A Survey of Photovoltaic Systems
- 171 Thermal Stratification in Liquid-Storage Tanks
- 171 Final Report on Development of a Programmable Controller
- 172 Fresnel Lens Tracking Solar Collector
- 172 Outdoor Tests of the Concentric-Tube Collector
- 173 Selective Optical Coatings for Solar Collectors
- 173 Finned-Absorber Solar Collector
- 173 A Test Program for Solar Collectors
- 174 Operational Tests of a Solar-Energy System in Georgia
- 174 Operational Tests of a Solar-Energy System — Florida Site
- 174 A Solar-Energy System in Pennsylvania
- 175 Installation Guidelines for the Pennsylvania System
- 175 A Solar-Energy System in Minnesota
- 175 Solar-Energy System Evaluation — Pennsylvania Site
- 175 A Hot-Water System Tested Onsite — Togus, Maine
- 176 A Reliable Solar-Heating System — Huntsville, Alabama
- 176 Solar-Heating and Cooling Demonstration Project

An Equation of State for Liquids

A closed expression for volume as a function of pressure and temperature has been verified for over 250 liquids.

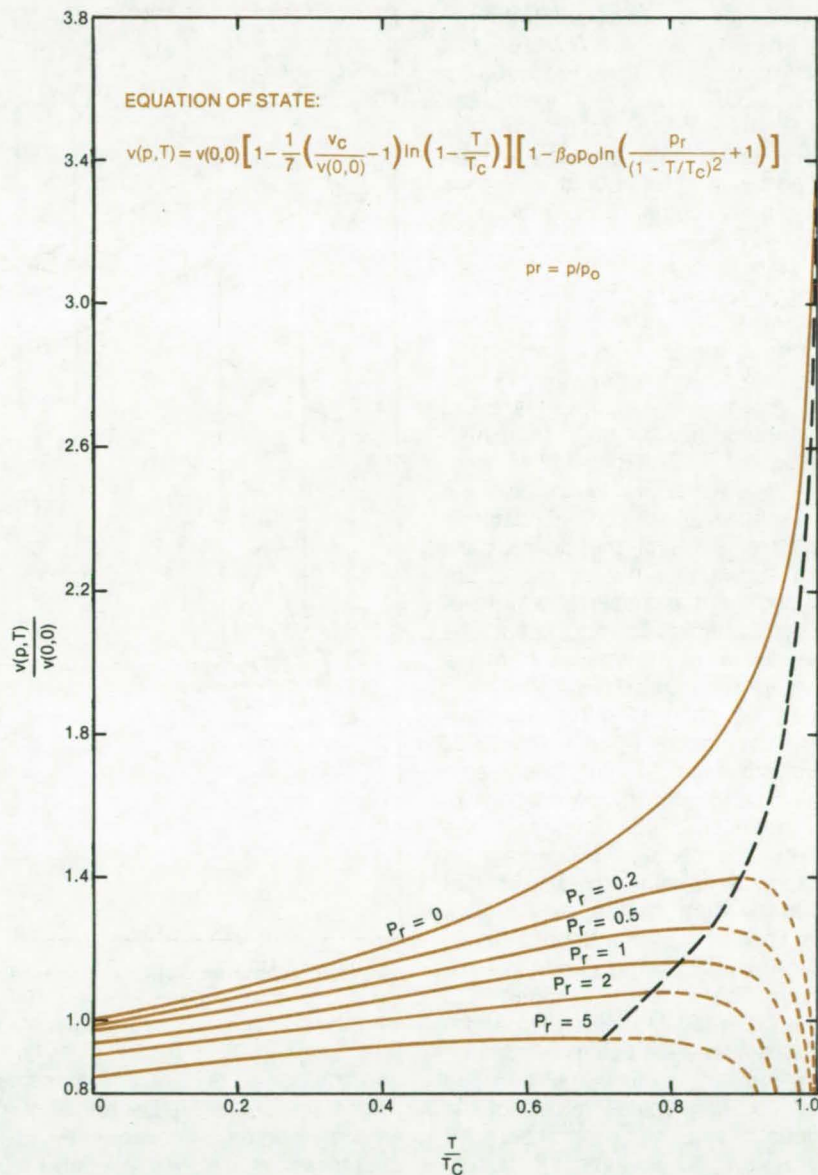
NASA's Jet Propulsion Laboratory, Pasadena, California

While several equations of state are known for gases, much less success has been achieved in describing the pressure, volume, and temperature interrelationship for liquids. Recently, however, researchers at the Jet Propulsion Laboratory discovered a relatively simple equation that works well for a wide group of liquid metals, molten salts, polymeric liquids, and inert liquids. The equation can assist chemical engineers, solid-state researchers, and others with interest in the thermodynamic behavior of liquids.

The new equation is given in the figure, where it is also plotted for several representative pressure values. It contains two constant parameters, β_0 and p_0 , which are determined by fitting the equation to experimental data. Three other constants are taken either from tabulated data or are estimated using established schemes. These constants are v_c and T_c , the volume and temperature at the critical point, and $v(0,0)$, a hypothetical volume of the liquid at $T = 0$.

In tests of the equation on data for 250 liquids near atmospheric pressure, only the behavior of water below about 140° C could not be fitted. For a few liquids, including organics, metallics, and fused salts, for which the $v(T)$ response is known as a function of pressure, volumes predicted by the equation agree to within 1 percent with measured values.

The figure shows $v(p,T)$ for $p/p_0 = 0, 0.2, 0.5, 1, 2,$ and 5 . The monotonically increasing curve for $p/p_0 = 0$ corresponds to behavior near atmospheric pressure. For higher pressures, the equation predicts a point of inflection in $v(p,T)$ and decreasing slope above that point. This general behavior is known for all liquids for which sufficient data exist. The new equation is one of only a few closed-form expressions that predict the inflection point.



Equation of State for Liquids is plotted as $v(p,T)$ for several values of pressure. The behavior in the region of dashed lines at the lower right, including the maximums of $v(p,T)$, is not observed in real liquids, and the equation is not valid in this region.

This work was done by Robert F. Fedors, Robert F. Landel, and Jovan Moacanin of Caltech for NASA's Jet Propulsion Laboratory. For further in-

formation, Circle 22 on the TSP Request Card. NPO-14821

High-Resolution Spectrometer/Interferometer

Proposed design compensates for tilt errors and minimizes spectrum channeling.

NASA's Jet Propulsion Laboratory, Pasadena, California

A modified double-pass interferometer has several new features that maximize its resolution. Proposed for rocket-borne probes of the upper atmosphere, it includes cat's-eye retroreflectors in both arms, a wedge-shaped beam splitter, and a wedged optical-path compensator. Among its advantages are:

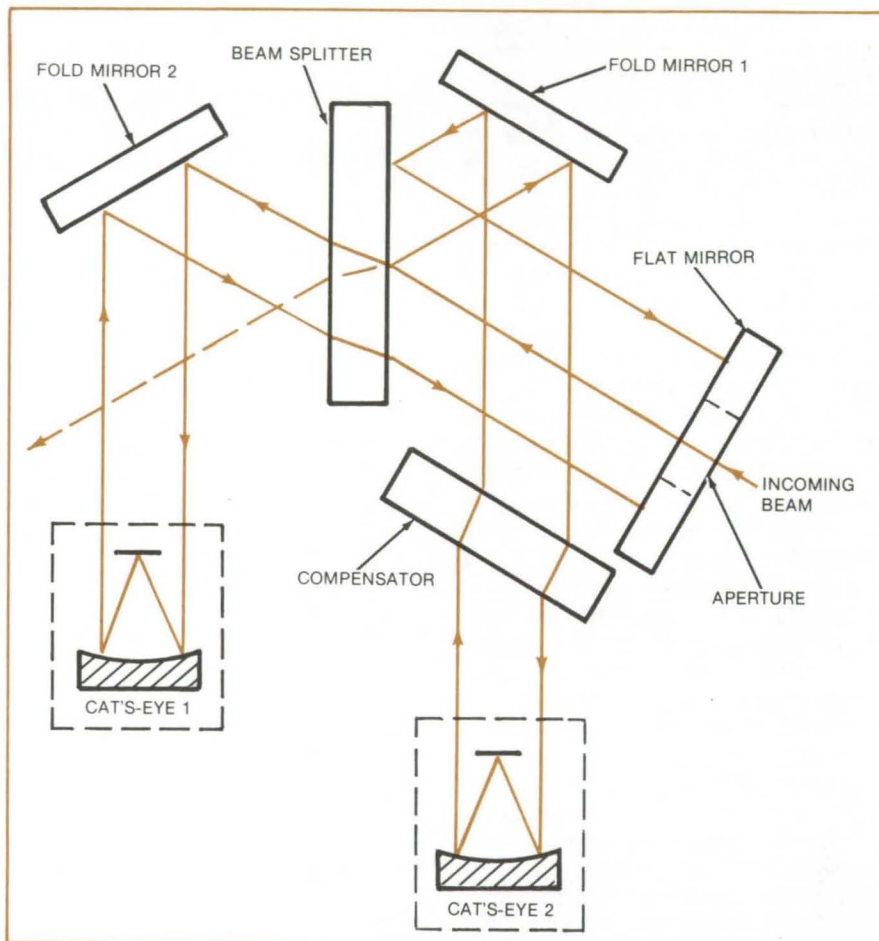
- full tilt compensation,
- minimal spectrum "channeling,"
- easy tunability,
- maximum fringe contrast, and
- even two-sided interferograms.

As shown in the figure, the basic configuration has only five freestanding elements: two flat "fold" mirrors, an entrance-aperture flat mirror, the beam splitter, and the compensator. A detailed analysis of the double-pass optics shows that the design is tilt-canceled — reasonable tilt errors of the components do not upset the superposition of the images from the two interferometer arms.

Spectrum channeling in some interferometers occurs when light makes multiple passes through the beam splitter and forms a spurious image of the foreoptics field-of-view on the cat's-eye secondary. This image is displaced by a small angle from that formed by light that makes only a single pass through the beam splitter. Thus, the interferogram becomes a superposition of several images, and an artificial modulation of the pattern — channeling — is observed.

This problem is eliminated by using a wedged beam splitter to deflect the spurious beams out of the detector field-of-view. To equalize the optical paths in both arms, the compensator is also wedged. For the proposed system, the required wedge angle is only 0.2° .

Because both the compensator and the beam splitter cover the input and the output of the cat's-eyes, precise matching of the wedge angles is not necessary. An analysis of the geometry shows that the total optical path through the wedge, including ingoing



The **Interferometer Optics** has only five freestanding components (other than the cat's-eyes) that could be misaligned by vibration or shock. By combining fold mirror 1 with the compensator in a single (Mangin) element, the number can be reduced to four.

and outgoing rays, is the same, regardless of the wedge angle or of wedge rotation. Consequently, the tolerances on the wedge angles and their alignment are not particularly critical. In the proposed design the angles do not have to be matched to better than 5 arc-minutes out of 0.2° .

The optical configuration shown has the smallest practical angles of incidence on the mirrors and on the dielectric/air interfaces. Thus, polarization on reflection is minimal, and the loss of contrast due to such polarization is reduced.

This work was done by James B. Breckinridge, Robert H. Norton, and Rudolf A. Schindler of Caltech for NASA's Jet Propulsion Laboratory. For further information, Circle 23 on the TSP Request Card.

This invention is owned by NASA, and a patent application has been filed. Inquiries concerning nonexclusive or exclusive license for its commercial development should be addressed to the Patent Counsel, NASA Resident Legal Office-JPL [see page A5]. Refer to NPO-14448.

Instrument Remotely Measures Wind Velocities

Gas velocity is determined by measuring the Doppler shift of its spectrum.

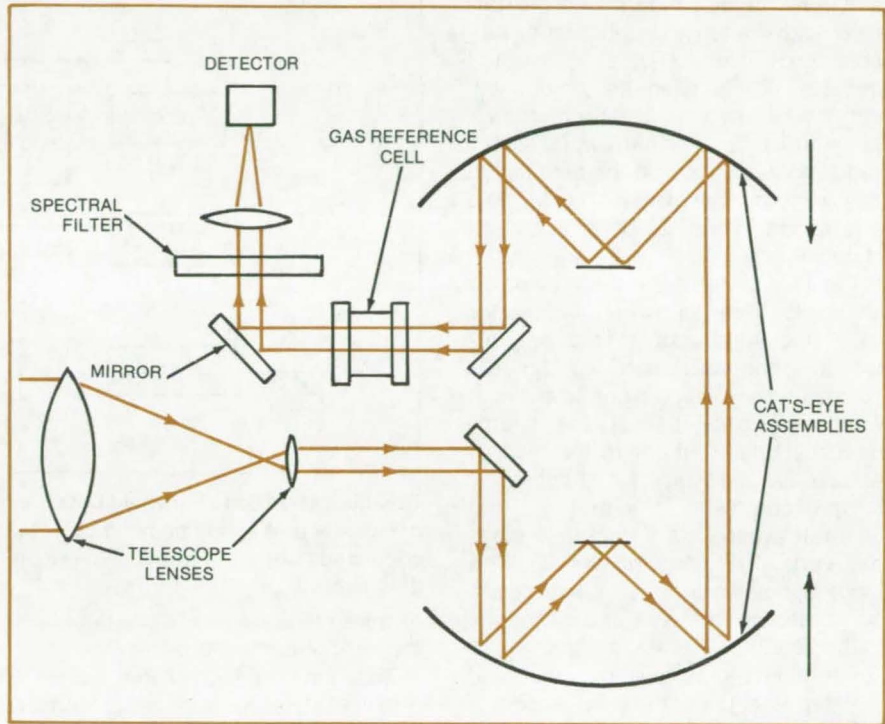
NASA's Jet Propulsion Laboratory, Pasadena, California

A Doppler-shift spectrometer makes remote satellite measurements of atmospheric wind velocity and temperature at specified altitudes. As in a correlation spectrometer, the spectrum of a gas in a reference cell and the spectrum of the same gas in the atmosphere are correlated both in emission and absorption. Correlation, usually lost due to Doppler-shifted spectra because of relative velocities between the measured and reference gases, is retained by a mechanically-modulated cat's-eye assembly. Acoustic/optic or electro-optic devices have also been considered and show promise in this application.

As shown in the figure, light coming in through the telescope established the field-of-view of the instrument. The light is reflected off two cat's-eye assemblies that oscillate with opposed motions in a direction normal to their faces.

Each reflection from the cat's-eye primary mirrors induces a Doppler shift in frequency by an amount of $\delta\nu$, where $\delta\nu = 2v(v/c)$ and where v is the velocity of the mirror, c is the speed of light, and ν is the unshifted frequency. The use of two cat's-eyes increases the Doppler shift and also eliminates the motion of the center of mass of the assembly. The Doppler-shifted light is bent away from the cat's-eyes by a mirror and is directed through a gas-reference cell, deflected by another mirror through a spectral filter, and onto the detector.

At some instant the motion of the cat's-eye will cancel out the Doppler shift due to the relative motion of the



Doppler-Shift Spectrometer determines wind velocities of the atmosphere. The altitudes at which these velocities are measured can be determined using a radiometer and color filter-wheel combination or by changing gas pressure in the reference cell that corresponds to pressure of the same gas at the specific altitude.

instrument and the atmosphere. This canceled shift will be apparent in the signal in the detector.

The linear velocity of the cat's-eye assembly depends on the angular position of a rotating drive wheel. At the instant that the reference and atmospheric spectra are correlated, the angular position of the driver wheel is a measure of the atmospheric velocity. A suitable shaft encoder may be used to read out the shaft position.

This work was done by Jack S. Margolis, Daniel J. McCleese, Clay H. Seaman, and Michael S. Shumate of Caltech for NASA's Jet Propulsion Laboratory. For further information, Circle 24 on the TSP Request Card.

This invention is owned by NASA, and a patent application has been filed. Inquiries concerning nonexclusive or exclusive license for its commercial development should be addressed to the Patent Counsel, NASA Resident Legal Office-JPL [see page A5]. Refer to NPO-14524.

Far-Field Radiation Pattern of Tunable Diode Lasers

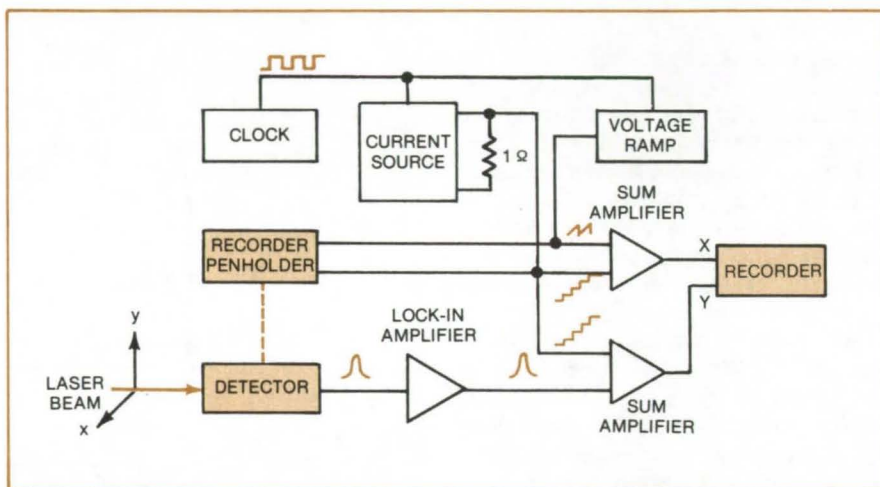
An improved technique rapidly determines the far-field spatial energy distribution.

Langley Research Center, Hampton, Virginia

A new method determines the far-field spatial energy distribution of tunable diode lasers (TDL's) in about 3 minutes. TDL's used as local oscillators in heterodyne measurement systems must have a narrow Gaussian radiation output so that the beat signal has a narrow bandwidth. The far-field distribution serves as an indicator in choosing the TDL.

Far-field patterns are taken by using an x-y recorder to sweep a detector mechanically across a field perpendicular to the laser beam (see figure). To mount the detector and to move it without slippage across the beam, modifications are made to the recorder carriage, penholder, and cables.

Upon completion of each horizontal (x-axis) sweep, the detector is stepped vertically (along the y-axis). The input signals to the recorder pen are synchronous with the x and y motions of the detector: The x-axis signal is the summation of the sweep signal and the detector output, and the y-axis signal is the summation of the step signal and the detector output. By adding the step signal to the x-axis motion, the graphical display is displaced to the right or left after each sweep, making the pattern appear to be three-dimensional. The step amplitude de-



Tunable Laser Diode Far-Field Data are obtained by using an x-y recorder to sweep a detector across a field perpendicular to the laser beam. The sweep, step, and pen lift commands are all controlled by a common clock, with adjustable frequency and duty cycle.

termines the degree of skew angle and the resolution of the display.

The new method takes about 3 minutes. It is optically simple and is economical, using standard laboratory parts and equipment. It records automatically without operator control and is easily adaptable to computer control of input instructions and computer treatment of output data. The degree of data resolution is limited only by the

width of the recorder pen, and data are repeatable.

This work was done by Thomas J. Lash of Langley Research Center. For further information, Circle 25 on the TSP Request Card.

Inquiries concerning rights for the commercial use of this invention should be addressed to the Patent Counsel, Langley Research Center [see page A5]. Refer to LAR-12631.

Optical Calibrator for TDL Spectrometers

Two etalons and a monochromator mode selector help calibrate the spectrometer in the selected laser mode.

Goddard Space Flight Center, Greenbelt, Maryland

Spectrometers using a tunable diode laser (TDL) source are difficult to calibrate in some laser modes. The frequency range of these modes does not include any frequency generated by standard molecular sources, leaving the spectrometer without the reference frequency.

A new approach of transferring and extending the absolute frequency calibration from one lasing mode to

another spectrally isolated from the first resolves that problem. TDL's emit in many modes; each is approximately 1 cm^{-1} wide, distributed over a range of up to 200 cm^{-1} . If two Fabry-Perot etalons (see figure) of unequal lengths and a monochromator mode selector are arrayed in tandem within the laser path, they can be used to establish the number of fringes between any two

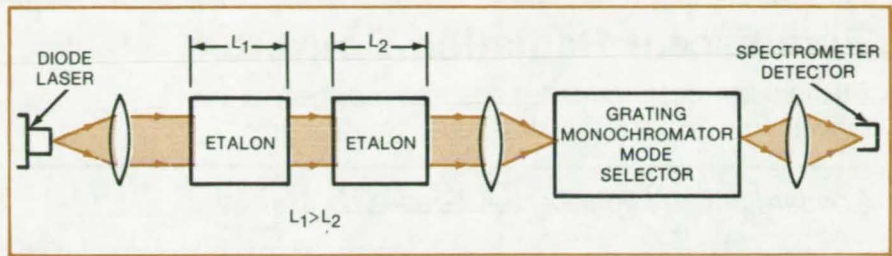
spectral points separated by a large frequency interval.

The etalons are the germanium type: One is 1 in. (2.5 cm) long, and the other is 0.8 in. (2 cm) long, although other lengths and materials can be used. If the first has a 0.05-cm^{-1} free spectral range and the second a 0.0625-cm^{-1} , the two combined in tandem will cause the

fringes to coincide every 0.25 cm^{-1} . The fringes that coincide are the most intense and are clearly identified with the aid of the monochromator, displaying every fifth fringe of the longer etalon and every fourth fringe of the shorter one.

The Ebert monochromator mode selector has a 0.1-cm^{-1} calibration accuracy and easily resolves the 0.25-cm^{-1} spaced undulations of the combined fringe pattern. Thus, if a peak fringe of one laser mode is precisely calibrated, the precise frequency of a peak fringe in any other mode can be determined, provided the free spectral range of one of the etalons is known. In this way, the absolute calibration of one laser mode can be extended to other modes separated from the first by arbitrarily large spectral intervals.

This technique also accurately determines the free spectral range of an



Spectrometer Frequency Calibrator comprises two etalons and a monochromator aligned in tandem in the laser path. The arrangement is used to establish the number of fringes between any two spectral points separated by a large frequency interval. It extends the absolute calibration of a single laser mode to other modes separated from the first by arbitrarily large spectral intervals.

etalon. By establishing the number of fringes between two modes, both of which have been calibrated with molecular line standards, one finds the free spectral range with an error inversely proportional to the spectral interval between the calibration points. This procedure establishes the

free spectral range of an etalon without prior knowledge of its length or its refractive index.

This work was done by Donald E. Jennings of Goddard Space Flight Center. For further information, Circle 26 on the TSP Request Card. GSC-12562

UV Actinometer Film

Low-cost polymer film measures cumulative UV radiation.

NASA's Jet Propulsion Laboratory, Pasadena, California

A proposed UV actinometer film using a photochemically sensitive compound changes its chemical composition in response to solar UV radiation. The extent of this chemical conversion depends on the length of the exposure and can be measured by examining the film samples with a spectrophotometer. The film can be exposed from several seconds up to a month. Paint and plastics manufacturers can use this film to determine total UV irradiance on their products to see how well they stand up against the UV radiation.

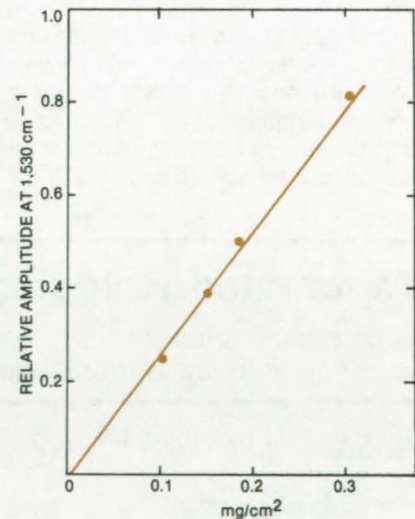
The film is cast from dichloromethane using polymethylmethacrylate containing 10 percent o-nitrobenzaldehyde (NBA). The NBA undergoes a photochemical rearrangement in response to the 300- to 430-nm UV region, forming o-nitrobenzoic acid. After the exposure to solar radiation, the film samples are mounted on 35-mm slides and examined with a spectrophotometer via absorption spectroscopy. The amount of remaining NBA is determined by observing the height of the $1,530\text{-cm}^{-1}$ band (see figure). This quantity is compared

with the amount of NBA present prior to exposure. The difference between the two shows how much of the NBA has been converted and hence the cumulative UV irradiance responsible for this conversion.

It is important not to overexpose the NBA. If more than 50 percent of the NBA is converted, the film response loses linearity.

The film is unaffected by visible light. It can be used on any surface, in areas inaccessible to bulky instruments (e.g., radiometers), and can also measure solar ultraviolet radiation as a function of wavelength and bandwidth using appropriate filters. Although less sensitive than radiometers, the film needs no direct or hemispherical irradiance to work and, of course, no calibration — a frequent necessity with the radiometers.

This work was done by Clifford D. Coulbert and Amitava Gupta, of Caltech and James N. Pitts of the University of California, Riverside, for NASA's Jet Propulsion Laboratory. For further information, Circle 27 on the TSP Request Card. NPO-14479



Calibration Curve for NBA shows the height of the absorbance band as a function of NBA density. This curve is used to determine the amount of NBA left on a film following its exposure to solar UV radiation. The amount, in turn, is used to compute the total solar UV irradiance on the film as a function of time.

Fluorescent Radiation Converter

Efficient low-cost converter absorbs radiation at one wavelength and emits it at a longer wavelength.

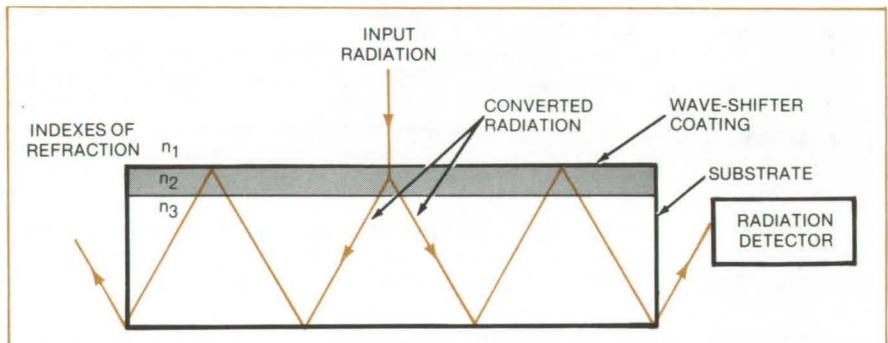
Goddard Space Flight Center, Greenbelt, Maryland

A fluorescent radiation converter (see figure) uses an undoped optically transparent substrate. One side of the substrate is coated with a plastic film containing fluorescent organic dyes that absorb optical radiation at one wavelength and emit it at a longer one. The emitted radiation is reflected internally inside the substrate, amplifying the intensity that reaches the radiation detector.

The transparent substrate can be fused silica, glass, or polymethylmethacrylate. Its index of refraction must be greater than that of the surrounding medium to trap the emitted radiation.

The coating is formulated to respond to specific wavelengths. Typically, one liter of the coating solution contains 1,000 g of toluene or xylene solvent, 70 to 200 g of organic polymer (e.g., isobutyl methacrylate or ethylmethacrylate), and 0.2 to 25 g of at least one fluorescent organic dye. The organic polymer gives the coating the necessary adhesion and proper hardness.

The optical density of the coating within the fluorescent-dye absorption band depends on the dye concentration and coating thickness. Typical thicknesses are less than $10\ \mu\text{m}$, which can be applied with a single dipping.



New Fluorescent Radiation Converter uses optically transparent substrate coated with a wave-shifter material. The wave-shifter coat absorbs radiation at one wavelength and emits it at a longer wavelength. Emitted radiation is more intense than the original input and is more easily detected.

The converters can be made in sizes and shapes other than the one illustrated. Round or square bars coated all around their lengths are useful in converting relatively intense radiation and transmitting it through the substrate over lengthy distances.

The new converter is also more efficient and economical than earlier models. Conventionally, substrates were doped with radiation conversion material, a more expensive process, which absorbed and scattered much of the emitted radiation, resulting in unnecessary losses.

*This work was done by Walter Viehmann of **Goddard Space Flight Center**. For further information, Circle 28 on the TSP Request Card.*

This invention is owned by NASA, and a patent application has been filed. Inquiries concerning nonexclusive or exclusive license for its commercial development should be addressed to the Patent Counsel, Goddard Space Flight Center [see page A5]. Refer to GSC-12528.

Automated Holographic Drop-Size Analyzer

A proposed automated system analyzes drop-size distribution in liquid-droplet-spray combustion fields.

NASA's Jet Propulsion Laboratory, Pasadena, California

A proposed system for studying particulate or droplet combustion spray fields uses a holographic camera for taking a "stop-motion" hologram of the combustion volume. The hologram is then reconstructed and viewed by a vidicon camera connected to a digital data-processing system that identifies the particles or droplets, determining their size and

count, and displays a histogram of the drop-size distribution in the holographic field.

Two processes are involved: one to construct the hologram and the other to process data in the viewed field. A three-dimensional snapshot, or hologram, is taken of the combustion volume containing the droplets. The hologram is illuminated by a laser

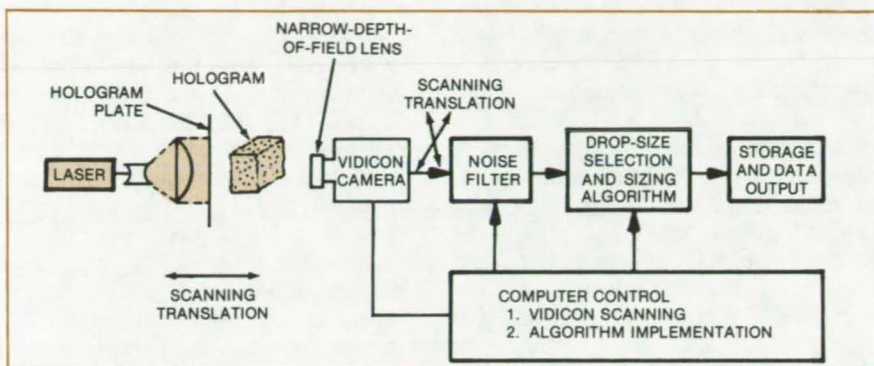
through an expanding collimating system of lenses to form a hologram. The hologram is a three-dimensional still picture translatable along one axis, as shown in the illustration.

The hologram is examined by a narrow depth-of-field vidicon camera fitted with a narrow-depth-of-field lens. By translating the hologram back and forth, different planes can be

imaged by the camera. The camera is controlled by a two-dimensional translation mechanism and views only a small piece of the cross section of the field at a time.

The camera output is applied to an analog-to-digital converter (ADC) for digital processing by computer algorithms. The information may be processed via fast Fourier transform filter to eliminate the high-frequency noise while retaining the low-frequency information. Algorithms locate the droplets, which are then sized and stored. The size distributions are displayed on the output histogram.

This work was done by Samuel P. Feinstein and Michael A. Girard of Caltech for NASA's Jet Propulsion Laboratory. For further information, Circle 29 on the TSP Request Card. NPO-14676



Proposed Drop-Size-Distribution Analysis System can be used for studying particle or droplet distribution in a liquid-droplet-spray combustion field. A hologram of the combustion volume is examined by a vidicon camera, which feeds the data to a digital processing system. The system using algorithms produces a histogram of particle distribution according to size within the examined field.

Photographic Measurement of Droplet Density

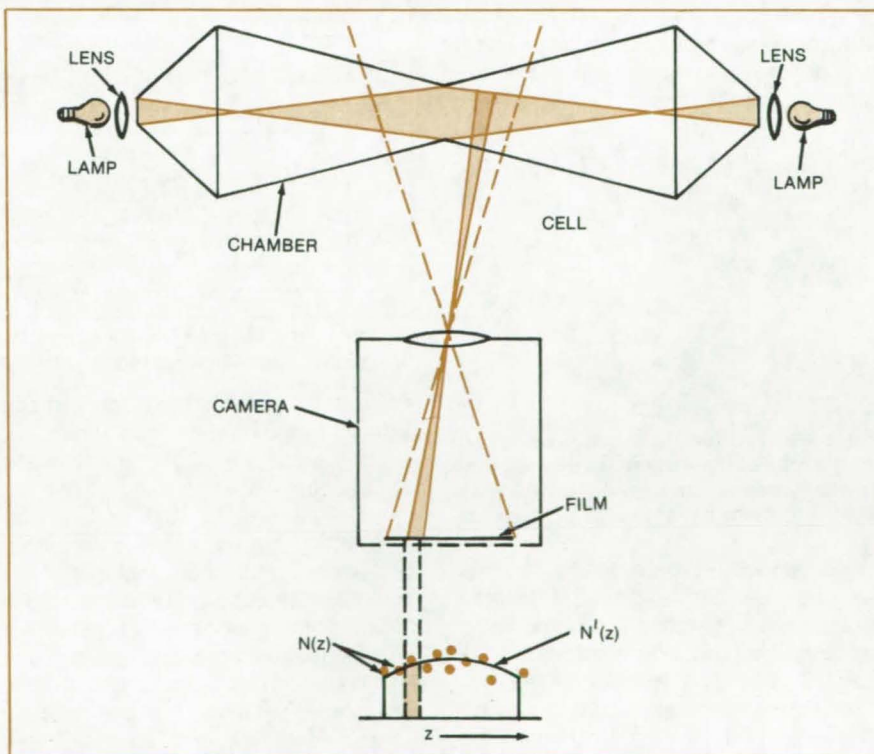
Pollutant analysis, fine-particles research, and aerosol and cloud studies should benefit from new accurate method.

Marshall Space Flight Center, Alabama

The density of cloud droplets in an expansion chamber or static diffusion liquid chamber can be measured with an error of less than 3 percent by an improved photographic technique. Measurement of this density is one of the principal instrumentation requirements in laboratory studies of atmospheric physics; the newly achieved precision is a substantial advance over the 10-percent accuracy limitation in methods used in the past. The method should also be useful in pollutant analysis, fine-particles research, and aerosol studies.

The figure shows how the measurement is performed: Two identical flashlamps with projection lenses face each other from the ends of the chamber, and a camera in front focuses on a plane containing the common axis of the lamps. The lamp lenses produce a well-defined image of a slot at the center of the chamber. In the vicinity of this sharp image, it is possible to define a small test volume, V , where the illumination is uniform and above the threshold for the

(continued on next page)



The **Count of Droplet Images** on a photographic film, in an area corresponding to a particular volume in an expansion chamber, may be in error. By counting images for many areas and drawing a smooth curve $N'(z)$, the most likely "true" count for the center volume, can be found.

detection of droplets. If the corresponding area on the camera film in a flash picture shows the images of N droplets, the density of droplets might be taken to be N/V .

However, such a determination is subject to error in the value of N . Therefore, many other volumes (cells) on both sides of V are also used in the measurement. The illumination field varies in these regions, but the variation is smooth, continuous, and symmetrical about V (although its functional form is not known).

On the flash photograph, the number of droplets in the images of

each cell $N(z)$ is counted and then plotted against the distance from the center cell. (These points are shown as color dots at the bottom of the figure.) The set of cell counts may be regarded as samples drawn from a symmetrical distribution. A curve fitted to this sample set by least-squares analysis gives a statistically improved count N' for the number of droplets in volume V .

Because of the symmetry, the smoothness, and the continuity of the illumination field, a three-term polynomial generally will give a very satisfactory fit. If the number of cells

is about 30 and three parameters describe the fitted curve, then N' and V are found to within 2 percent, and their ratio, N'/V , is accurate to within 3 percent.

This work was done by W. C. Yager of General Electric Co. for **Marshall Space Flight Center**. For further information, Circle 30 on the TSP Request Card.

Inquiries concerning rights for the commercial use of this invention should be addressed to the Patent Counsel, Marshall Space Flight Center [see page A5]. Refer to MFS-25326.

Camera Add-On Records Time of Exposure

Module prints the time a photo is taken on the edge of the exposed film.

Langley Research Center, Hampton, Virginia

The compact module attached to the camera shown in Figure 1 contains all the electronics and optics needed to print the time a photograph is taken on the edge of that photograph. It was originally developed for in-flight photography of wing deflections in aircraft, but it can be used wherever it is necessary to document the exact time a photo is taken.

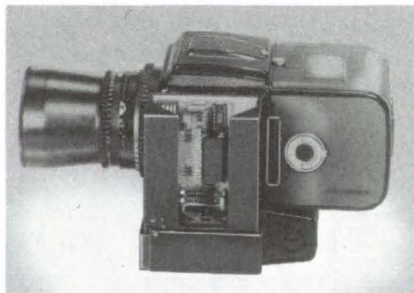


Figure 1. The **Timing Module**, attached to the side of the camera, is powered by a 4.2-V mercury battery. It draws less than 1 mA while the display is blanked.

As shown in Figure 2, the module includes an eight-digit LED display that continuously shows the time to an accuracy of one one-hundredth of a second. Two digits display the hours, two show the minutes, two show the seconds, and the last two show the fraction of a second. Leading zeros are blanked to conserve power.

Light from the display is reflected off two flat mirrors, through a focusing lens, and into the camera. A right-

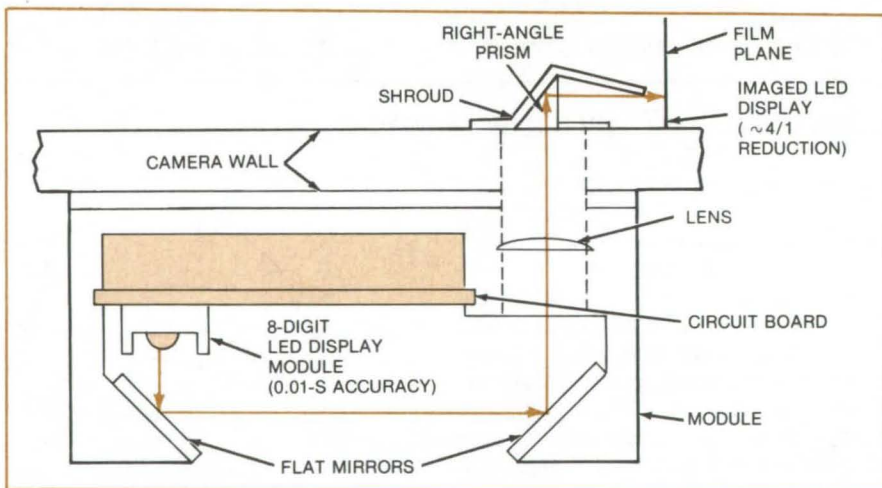


Figure 2. The **Module Optics** image the seven-segment display on the edge of the film plane. The display is blanked except at the time the camera shutter is actuated.

angle prism reflects the display image onto the edge of the film plane.

The electronics that drive the display are powered by a 4.2-V mercury battery. An ICM 7045 single-chip timing circuit is the main circuit component (equivalent timing circuits could be substituted). The IC is used in the split-timing mode, which records a time period between 0.01 second and 24 hours. All signals needed to multiplex the display digits and to energize the segments are generated by the timer.

The normally blanked display is unblanked when the camera shutter switch is actuated. A signal from the shutter switch triggers a monostable

multivibrator, which turns on the display drivers for a short period at the time of exposure. The monostable pulse width is adjustable to accommodate a range of shutter speeds and ASA film ratings.

The unit can be adapted to other cameras besides the one shown. Most of the changes would be in reconfiguring the optics.

This work was done by E. Conrad Compton, Philip C. Kassell, Jr., and Charles W. Knight of **Langley Research Center**. For further information, Circle 31 on the TSP Request Card.

LAR-12635

Improved Multispectral Solar-Cell Array

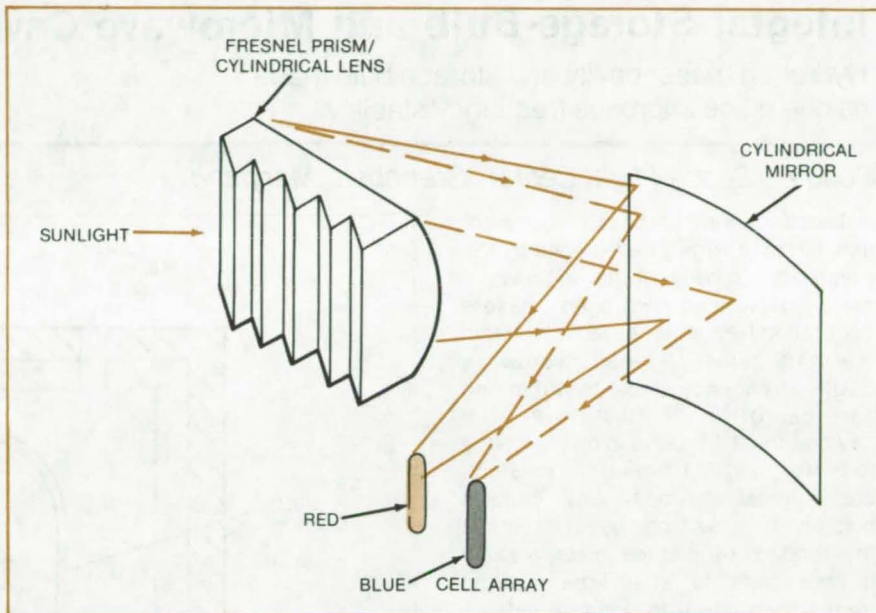
Proposed optics may optimize solar collection efficiency and reduce cell overheating.

NASA Headquarters, Washington, D.C.

A combined Fresnel prism/cylindrical lens along with a cylindrical reflector can be used to improve the efficiency of multispectral solar-cell arrays. These arrays consist of solar cells that have enhanced efficiencies at various single wavelengths. Previously these cells relied on a single type of optical dispersion/concentrator system which either resulted in cell overheating or poor energy concentration. The proposed system allows a more precise control over the dimension and distribution of the separated color bands onto the cell array.

The system (see figure) consists of a prism lens separating the incident solar energy into color components and focusing them on the reflector. The reflector projects each color band on the solar cells that operate most efficiently at that wavelength.

In essence the system combines the characteristics of both cylindrical and rotational optics to project oval images on the solar cells. The precise dimensions of the images may be controlled by varying the power of the Fresnel prism/cylindrical lens to match closely the specific requirements of the solar cells used. The arrangement would prevent cell overheating without signifi-



Proposed Solar-Collector System projects oval-shaped color-band images onto solar cells designed to be most efficient at specific wavelengths. The image size can be altered by changing the width of the reflecting mirror or the power of the lens. The image intensity is thus kept at an optimum level, preventing the cells from overheating.

cantly reducing the energy reaching each cell.

This work was done by Jerome J. Redmann of The Aerospace Corp. for

NASA Headquarters. For further information, Circle 32 on the TSP Request Card.
HQN-10937

Low-Cost Calibration of Acoustic Locators

Piezoelectric-torch lighter makes calibration easier.

Langley Research Center, Hampton, Virginia

A standard method of checking the sensitivity and accuracy of acoustic-emission-signal locators is not the most convenient one. An acoustic transducer (pulsar) used in this procedure simulates an acoustic-signal source. The pulsar, connected via long cable to a module built into the locator, converts a module-generated

fast-risetime voltage spike (about 30 V) to an acoustic spike. The locator is calibrated by determining the position of the pulsar signal and comparing it with the actual pulsar position.

A more convenient method is to use a modified commercially-available piezoelectric-torch lighter. This handheld lighter has a controlled spark gap

that can be easily adjusted to produce repeatable short-duration high-amplitude voltage spikes.

The pulsar and the lighter are coupled via a short coaxial cable, eliminating a long cable run, variations in cable attenuation, and a problem with the cable entangling with anything in its path.

(continued on next page)

The piezoelectric lighter is very reliable. It needs no batteries or external power and can be taken farther away unrestricted by the cable length.

Tests have shown that the lighter output is accurate within 1 percent.

The nominal unloaded output of the spark generator is in the range of 4 to 6 kV. The combination cable/transducer loading limits the excitation pulse to the range of 350 to 400 V. Because of the spark, the lighter can only be used

in nonexplosive environments.

This work was done by Robert F. Berry of Langley Research Center. No further documentation is available. LAR-12632

Integral Storage-Bulb and Microwave Cavity for Masers

Hydrogen maser cavity and storage bulb made as one piece improves frequency stability.

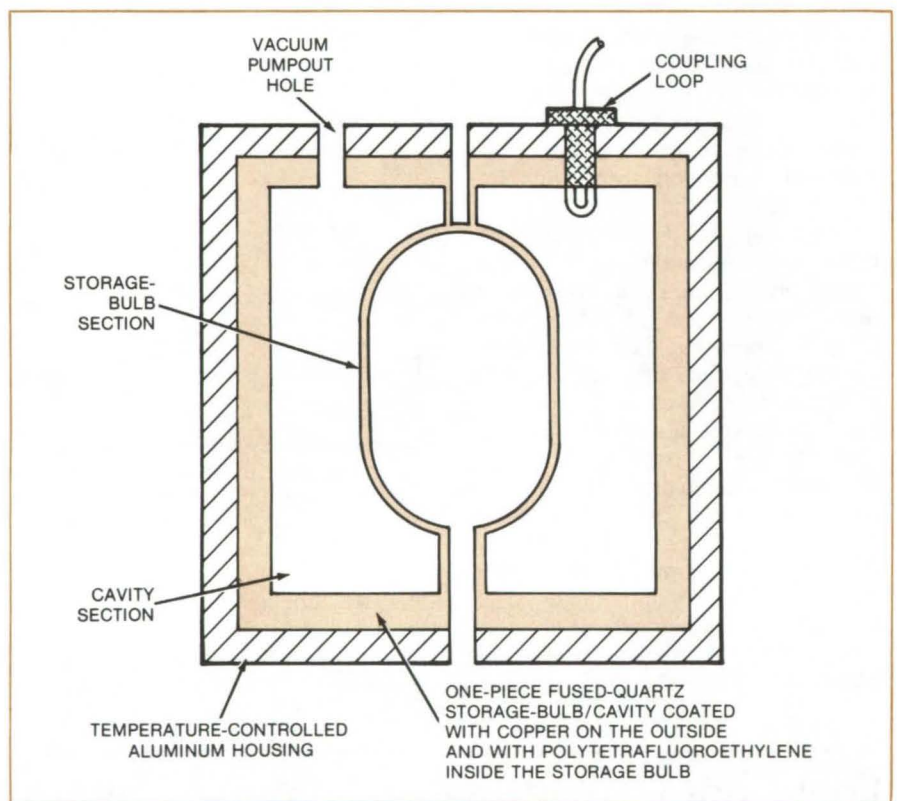
Goddard Space Flight Center, Greenbelt, Maryland

The frequency stability of a hydrogen maser is largely determined by the frequency stability of its microwave cavity. Advanced hydrogen masers generating frequencies stable to within one part per 10^{15} need microwave cavities frequency stable to within one part per 10^{11} . At that level, the cavities must be dimensionally stable to better than 0.1 nm. Unfortunately, conventional cavities and storage bulbs are made from several pieces that tend to creep at the joints, making it impossible to attain the needed frequency stability for long periods.

A mechanically-stable integral storage-bulb/microwave cavity (see figure) made out of a single piece of fused quartz can solve that problem. The single-piece construction eliminates the joints, making the cavity dimensionally and hence frequency-stable. Fused quartz is used because of its low thermal expansion coefficient.

To form the high Q (36,000) microwave cavity, the bulb cavity is vacuum-coated with copper on the outside instead of on the inside as in conventional designs, allowing the cavity to be coated after the complete one-piece assembly is fabricated. The cavity wall thickness can be at least 16 mm without appreciably affecting the Q. The cavity can be trimmed to the proper frequency by lapping its ends to change its length and recoating it with copper. The storage-bulb section is 1 to 2 mm thick and coated with PTFE on the inside as in conventional designs.

A temperature-controlled aluminum shell enclosing the quartz storage-



Integral Storage-Bulb and Microwave Cavity proposed for hydrogen masers can be built as one piece using fused quartz. The one-piece construction makes the assembly mechanically stable and therefore frequency-stable. This design can potentially attain a frequency coefficient of $1.3 \times 10^{-15}/^{\circ}\text{C}$ necessary for the future high-performance masers.

bulb/cavity enhances temperature stability. A hydrogen maser with an aluminum cavity showed a frequency coefficient of $4.5 \times 10^{-14}/^{\circ}\text{C}$ of room-temperature change. Using the same thermal design with the quartz cavity should therefore, yield a temperature

coefficient of $1.8 \times 10^{-15}/^{\circ}\text{C}$.

This work was done by Victor S. Reinhardt of Goddard Space Flight Center. No further documentation is available. GSC-12542

Books and Reports

These reports, studies, and handbooks are available from NASA as Technical Support Packages (TSP's) when a Request Card number is cited; otherwise they are available from the National Technical Information Service.

A Survey of Photovoltaic Systems

A compilation of suppliers, product data sheets, and other documentation

The results of an extensive telephone survey of photovoltaic manufacturers are compiled in a 220-page report that is available on request. The three-part report includes a catalog of suppliers, data sheets on specific products, and typical operating, installation, and maintenance procedures.

Photovoltaic technology — converting Sunlight into electricity — was applied just over 20 years ago when small photovoltaic cells were used to power one of the first U.S. satellites. Since that time, photovoltaics have been intensively researched to make them attractive for everyday use. Cost has been the primary barrier; however, in areas where electricity is unavailable or prohibitively expensive, photovoltaics have become economical and practical.

Three U.S. companies accounted for 77 percent of the total domestic photovoltaic sales in 1978. One firm surveyed reported that state regulations requiring a 30-year warranty on photovoltaic products are limiting its marketing efforts. Lacking extensive test data and field experience, such a warranty would be impractical or impossible, the firm said.

Another company reported that there is little or no domestic market for the systems but that there is an export demand. However, trade barriers are severely hampering exports. The export demand comes from countries where electricity costs are many times higher than in the United States and in applications where conventional electricity is unavailable, such as offshore or in underdeveloped countries. Typical applications include offshore

navigational aids and petroleum platforms; television, telemetry, and microwave transmitters and repeaters; and irrigation pumps. One manufacturer stated that he had sold several thousand units to recharge battery-operated television sets in weekend and summer cabins in Norway.

A few large-scale, photovoltaic demonstration projects are underway. One is in the Indian village of Schuchuli, Arizona, where a 768-ft² (71.3-m²) array provides 3.5 kW peak power, or 2,380 A-h of battery storage, to power the village water pump, home lighting, and domestic appliances. A remote village in Upper Volta, West Africa, has a 1.8-kW power supply that is used to drive a 1,200-gal/h (1.2-l/s) water pump.

This work was done by the University of Alabama in Huntsville for Marshall Space Flight Center. To obtain a copy of the report, "A Survey of Photovoltaic Systems," Circle 33 on the TSP Request Card.
MFS-25397

Thermal Stratification in Liquid-Storage Tanks

A comprehensive literature survey

Thermal stratification in a solar-energy/liquid-storage tank can improve system performance by as much as 15 percent. Collector efficiency increases when the collector inlet fluid is drawn from the bottom of the storage tank, where the fluid is coolest; the warmest liquid is drawn from the top of the tank to satisfy the thermal load.

A comprehensive survey of the literature on thermal stratification is compiled in a report that is available on request. Following an introductory section (section 1), the 30-page report assesses thermal-stratification effects on the performance of several solar-energy systems. In section 3, theoretical and experimental studies of "thermocline" tanks are reviewed; and in section 4, a brief discussion on the applicability of stratification techniques to solar heating and cooling is presented. Conclusions are given in section 5; the appendix lists the surveyed thermal-stratification literature.

Several simulation studies have quantified the net effects of thermal stratification on the total system performance, using a one-dimensional storage-tank model. The model assumes simple geometric shapes of conventional tanks, without short-circuited-flow phenomena, internal heat exchangers, or resistance heaters.

Transient temperatures and flow fields have been studied theoretically and, to a lesser extent, experimentally. Mathematical models for one, two, and three dimensions exist. Most of the one-dimensional models represent liquid-storage tanks in long-term computer-simulation studies, while two- and three-dimensional models are concerned with transient flow and heat transfer.

Detailed experimental studies on thermocline tanks are scarce. Flows that commonly prevail in thermocline liquid-storage tanks are very slow and hard to measure without expensive experimentation. Some rigorous temperature measurements in operating liquid-storage tanks have been made; however, the thermal stratification inside tanks is usually very small. Several researchers have studied enhancing thermal stratification by passive devices.

This work was done by D. L. Christensen and S. M. Han of the University of Alabama in Huntsville for Marshall Space Flight Center. To obtain a copy of the report, "Thermal Stratification of Solar Energy Liquid Storage Systems," Circle 34 on the TSP Request Card.
MFS-25416

Final Report on Development of a Programmable Controller

Microprocessor-based controller for solar-heating and cooling systems

The development of a sophisticated microprocessor-based controller for solar-heating and cooling systems is described in a new report. [Also see "Programmable Controller for Solar Heating" (MFS-23915) on page 204 of *NASA Tech Briefs*, Vol. 3, No. 2.]

(continued on next page)



Analog data from flow sensors, temperature sensors, and other devices are accepted by the programmable controller. It also receives digital input from relays and switches. Following a program stored in programmable read-only memory, the microprocessor commands 16 optically-coupled output relays that operate pumps, fans, and valves.

A five-digit LED display automatically displays the input channels in sequence or shows the date or time. Fifty-two constants in the program equations can be set through a 16-key keyboard.

The most obvious application of the controller is in complex residential, commercial, and industrial solar-energy systems. It can also be used for debugging and checkout during prototype work and early development of new systems.

The 23-page report describes the background of the development program. It also summarizes the operation, performance, and applications of the controller.

This work was done by James D. Hankins of Marshall Space Flight Center. To obtain a copy of the report, "Development and Testing of the Rho Sigma Incorporated Microprocessor Control Subsystem," Circle 35 on the TSP Request Card. MFS-25388

Fresnel Lens Tracking Solar Collector

A report on performance outdoors

A commercial tracking collector that uses acrylic Fresnel lenses to focus sunlight on copper absorber tubes was recently evaluated outdoors at Marshall Space Flight Center. Performed in accord with ASHRAE (American Society of Heating, Refrigerating, and Air-Conditioning Engineers) standards, the tests are documented in a 16-page report that is available on request. All tests were done at the Marshall Space Flight Center solar house. [Also see "Concentrating Solar Collector — Performance Tests" (MFS-25086) on page 60 of *NASA Tech Briefs*, Vol. 4, No. 1.]

The collector array consists of seven panels at an angle of 32° to the

horizontal. Each panel has four modules covered by 10.75 ft² (0.99m²) of transparent acrylic plastic Fresnel lenses. The complete assembly consists of the panels, supporting framework, insulated fluid manifolding, and a tracking drive. The panels are spaced 10 ft (0.93 m) between centers. The copper absorber tube has a selective coating with 0.95 absorptivity and 0.12 emissivity.

The Sun tracker is powered by photovoltaic cells. Collector panels, linked by galvanized cable and pulleys, are driven by a bidirectional motor through a chain drive, a stainless-steel (Acme) screw, and a drive nut.

The test array was operated over 10 months for heating and cooling of the solar house. It was then monitored for approximately 2 months under clear weather. On days with intermittent cloud cover or a high-density cloud cover, the tracking mechanism would either lag or would not track at all. Thus, the data presented in the report were obtained from selected clear days when the collector array was tracking properly.

Array performance at high inlet temperatures drops significantly in comparison to the single-panel curve offered by the manufacturer. The heat losses are attributed to losses from the large manifold area and from possible weathering of the array during exposure of almost 1 year.

This work was done by the Solar Energy Systems Division of Wyle Laboratories for Marshall Space Flight Center. To obtain a copy of the report, "Thermal Performance Evaluation of the Northrup Model NSC-01-0732 Concentrating Solar Collector Array at Outdoor Conditions," Circle 36 on the TSP Request Card. MFS-25419

Outdoor Tests of the Concentric-Tube Collector

The 72 element air-filled version is tested in a residential installation.

The 72-element, air-filled version of the concentric-tube solar collector

recently underwent a 2-month performance evaluation at the Marshall Space Flight Center solar house. A summary of the test results, along with other relevant data, is presented in a 27-page report that is now available. Performed in accord with ASHRAE Standard 93-77 ("Method of Testing to Determine the Thermal Performance of Solar Collectors"), the tests included measurements of thermal efficiency, incident-angle modifier, and time constant. [See related article "Indoor Tests of the Concentric-Tube Solar Collector," (MFS-25390) on page 39 of *NASA Tech Briefs*, Vol. 5, No. 1.]

Thermal efficiency was measured at air inlet temperatures of 0°, 70°, 90°, and 110° F (-18°, 21°, 32°, and 43° C) above ambient, at an airflow rate of 2 ft³/min per ft² (0.01 m³/s per m²) of collector area. Results are presented in tables and graphically. The efficiency ranged between 43.6 percent at 75.3° F (24.1° C) inlet air temperature and 34.0 percent at 200.2° F (93.4° C).

Permanently tilted at the 45° slope of the roof, the collector was measured for incident-angle modifier by logging its efficiency when the direction of the incident solar radiation was approximately 15°, 30°, 45°, 60°, and 67.5° with respect to the direction at solar noon. An average of the measurements on three clear days is shown as a graph of incident-angle modifier versus incident angle. For this collector, the efficiency is actually about one-third greater at an incident angle of 60° than it is at normal incidence. A time constant (the time for the differential temperature to drop to 0.368 of its initial value) of 15.6 minutes was measured for the collector. It was determined by shading the collector, while maintaining a constant flow rate and inlet temperature.

This work was done by Wyle Laboratories for Marshall Space Flight Center. To obtain a copy of the report, "Outdoor Test for Thermal Performance Evaluation of the Owens-Illinois Sunpak SEC-601 [Air] Solar Collector," Circle 37 on the TSP Request Card. MFS-25398

Selective Optical Coatings for Solar Collectors

Several chemical treatments and coatings are evaluated.

For best performance, the energy-absorbing surface of a solar collector should be characterized by a high ratio of solar absorptance to thermal emittance. Designers and users of solar-energy systems will therefore be interested in a new report on the optical characteristics of several chemical treatments and electrodeposited coatings for metal solar-absorbing surfaces. The moisture resistance of some of the coatings is also reported.

The coatings were produced by electroplating, by chemical conversion, and by anodizing (electrochemically converting a metal to its oxide). For proprietary processes, manufacturer's directions were followed; directions reported in the literature were followed for nonproprietary processes.

Optical measurements were made with a solar/infrared reflectometer or a ratio-recording spectrophotometer. The solar absorptance was determined by subtracting the solar reflectance from unity; the thermal emittance was determined by computing the difference between the infrared reflectance and unity. The moisture resistance was established by subjecting coated specimens to a relative humidity of 92 to 98 percent at a temperature of 98° to 100° F (37° to 38° C).

Of the coatings tested, black nickel showed the best combination of selective optical properties, although it was susceptible to degradation in high humidity. Electroplated black chrome has high solar absorptance, but its thermal emissivity varies between specimens and is quite high under some conditions. The black chrome also has very high moisture resistance. Black oxide coatings on copper and steel substrates showed the best combination of selective optical properties of any of the chemical conversion films.

This work was done by James R. Lowery of **Marshall Space Flight**

Center. To obtain a copy of the report, "Solar Absorption Characteristics of Several Coatings and Surface Finishes," Circle 38 on the TSP Request Card.
MFS-23589

Finned-Absorber Solar Collector

Report presents the results of a performance evaluation.

You can use the TSP Request Card at the back of this issue of *NASA Tech Briefs* to obtain a report summarizing performance tests on a commercial solar collector. The tests are part of a continuing study of solar-heating systems and components for NASA and the Department of Energy.

The tested collector is flat-plate, with water as the heat-transfer fluid. Its cover is tempered antireflective glass (one layer). The black-coated heat-absorbing surface consists of collared aluminum fins bonded to copper tubing.

Standard ASHRAE (American Society of Heating, Refrigerating, and Air-Conditioning Engineers) requirements were followed. Parameters measured, under simulated conditions, were thermal efficiency and time constant. A 30-day stagnation test (exposure to simulated Sunlight with no fluid flow) was also done. This is not a standard ASHRAE test. The collector absorptivity and heat-loss rate were measured before and after the 30-day exposure.

Test data are presented as graphs and tables. The report also summarizes the test procedures and a mathematical analysis of the results.

This work was done by the *Solar Energy Systems Division of Wyle Laboratories for Marshall Space Flight Center.* To obtain a copy of the report, "Thermal Performance Evaluation of the Suncatcher SH-11 (Liquid) Solar Collector," Circle 39 on the TSP Request Card.
MFS-25385

A Test Program for Solar Collectors

Rigorous environmental and performance tests qualify a solar collector for use in residential solar-energy systems.

Those using or testing solar collectors will be interested in a new report describing qualification tests on a particular commercial collector, described in a previous *NASA Tech Briefs* article. [See "Weathering of a Liquid-Filled Solar Collector" (MFS-25113) on page 60 of Vol. 4, No. 1.] Testing over a 7-month period examined pressurization effects, wind and snow loading, hail damage, solar and thermal degradation, the effects of pollutants, efficiency, and outgassing. The test procedures and results are summarized in tables, graphs, and text.

Some of the tests (pressure, loading, efficiency, hail, solar degradation, and outgassing) were done on a fully assembled collector. Coupon specimens of the absorber plate, cover glass, and other subcomponents were subjected to the pollutant and thermal-degradation tests.

Typical of the rigor with which this series was carried out is the test for thermal degradation. Coupon specimens of the essential collector subcomponents were each heated for at least 500 hours in a temperature-controlled chamber. Following the exposure, the specimens were tested for tensile strength or transmittance (for glass specimens). American Society for Testing Materials (ASTM) standards were applied in the tests. Unexposed specimens were also tested for comparison with the thermally treated samples.

This work was done by the *Energy Resources Center of Honeywell Inc. for Marshall Space Flight Center.* To obtain a copy of the report, "Qualification Test Procedures and Results for Honeywell Solar Collector Subsystem, Single-Family Residence," Circle 40 on the TSP Request Card.
MFS-25433



Operational Tests of a Solar-Energy System in Georgia

12-month performance of a hot-water heating system

A 73-page report describes the 1-year performance of a commercial solar-energy hot-water system. Installed in a public housing project in Macon, Georgia, the system is one of several at test sites throughout the country.

Silicone oil is the heat-exchange fluid in the tested system, designed to meet the needs of a family of four. A roll-bend heat exchanger is wrapped around the hot-water storage tank. The oil circulates through the exchanger and through flat-plate solar collectors. Auxiliary energy, to maintain a selectable minimum temperature in the storage tank, is supplied by a 4,500-watt resistance-heating element.

The manufacturer's specifications state that the system will supply up to 75 gallons (284 liters) of potable hot water per day at a temperature of 140° F (60° C), based on an average heating load of 1,313,000 Btu/month (1.385×10^9 J/month). Auxiliary hot-water requirements are 20 percent of the monthly load. The operating mode (collector-to-storage) begins when a differential controller recognizes a collector/storage-tank differential temperature of 20° F (11° C). The mode is terminated when the differential drops to 5° F (3° C). Both temperature settings are nominal.

For the test period, the incident solar-energy totaled 33.21×10^6 Btu (35.04×10^9 J) while the system was operating; the collected energy totaled 10.32×10^6 Btu (10.88×10^9 J), for an efficiency of 31 percent. Electrical-energy savings at the site were 8.98×10^6 Btu (9.47×10^9 J), after 1.34×10^6 Btu (1.41×10^9 J), required to operate the pump, are subtracted.

This work was done by the Federal Systems Division of IBM Corp. for Marshall Space Flight Center. To obtain a copy of the report, "Solar Energy System Performance Evaluation -- Seasonal Report for SEMCO, Macon, Georgia," Circle 41 on the TSP Request Card.
MFS-25420

Operational Tests of a Solar-Energy System — Florida Site

Projected annual electrical energy savings are above 10 million Btu.

The solar-energy hot-water system described in the preceding article has also been evaluated for performance at a test site in Loxahatchee, Florida. Results of these tests are available in a 76-page report.

Projected electrical energy savings at this site are above 10 million Btu (10.5 billion J) annually. Actual savings were less because the building was unoccupied for 8 months of the 11-month test period, and the hot-water load was abnormally low. Estimates based on results during the 3 months of nominal operation indicate that, during the summer, the system should deliver 90 percent of the hot-water load from solar energy.

The operating sequence for the system begins when the collector/storage-tank differential temperature exceeds 20° F (11° C). On one typical day (October 8, 1979), this occurred at 9:25 a.m., when the collector absorber plate was at 145° F (63° C). Collector-loop operation was continuous on that day until 4:31 p.m., when the absorber plate temperature was 163° F (73° C). At the time of turnoff, the storage tank was at approximately 164° F (73° C).

During the day, the incident solar energy was 135,000 Btu (142×10^6 J) of which 16,000 Btu (17×10^6 J) were supplied to meet the hot-water load. (The balance goes to replenishing the thermal-energy losses of the tank.)

This work was done by the Federal Systems Division of IBM Corp. for Marshall Space Flight Center. To obtain a copy of the report, "Solar Energy System Performance Evaluation — Seasonal Report for SEMCO, Loxahatchee, Florida," Circle 42 on the TSP Request Card.
MFS-25423

A Solar-Energy System in Pennsylvania

A specific case illustrates techniques that have general applicability.

A new report describes the development of a solar-heating system for a single-family residence at a site in Pennsylvania. The 143-page document, containing detailed drawings, performance specifications, cost tradeoff studies, and other material, can assist those planning similar systems in areas with comparable climate.

Components and design parameters were selected with the help of a computer simulation model, using weather and insolation data as inputs. The model computed the effect of collector area on the solar contribution to the total energy requirements of the dwelling. Using this information, an area of 504 ft² (47 m²) was selected as a compromise between architectural constraints and the required solar contribution. The storage-tank temperature set points were also selected with the help of the computer simulation.

For an average heating load of 4.0×10^6 Btu per month (4.2×10^9 joules per month), the system will deliver 46.5 percent from solar energy. In addition, 52 gallons (197 liters) of potable hot water will be delivered at 140° F (60° C), or greater, assuming a delivery rate of 3 gallons per minute (11 liters per minute) and a recovery time of 0.75 h.

Included in the report are a spare parts list and an outline of the projected installation, operation, and maintenance manual. Over 30 drawings of the system and its subcomponents are supplied.

This work was done by the Energy Resources Center of Honeywell, Inc., for Marshall Space Flight Center. To obtain a copy of the report, "Solar Energy Heating System Design Package for a Single-Family Residence at New Castle, Pennsylvania," Circle 43 on the TSP Request Card.
MFS-25427

Installation Guidelines for the Pennsylvania System

Detailed installation, operation, and maintenance procedures

The installation of the solar-energy system described in the preceding article is documented in a new report. Included are procedures for filling and testing the entire system, along with installation guidelines for each major subsystem.

The 170-page report describes operating procedures, controls, cautionary procedures, and maintenance. Information is in the form of text, schematics, detailed drawings, and photographs. An appendix contains 113 pages of manufacturers' literature, organized into separate sections for each subsystem.

When space heating is required and solar energy is available, the collectors supply heat directly. Energy is transferred through a heat exchanger and a heating coil; a blower moves the building air across the coil. Thermal energy is stored by circulating water from the bottom of the storage tank through the heat exchanger. The water is returned to the top of the tank. When required, auxiliary energy is supplied by an electrical resistance-heating coil.

This work was done by the Energy Resources Center of Honeywell Inc. for Marshall Space Flight Center. To obtain a copy of the report, "Installation Guidelines for Solar Heating System, Single-Family Residence at New Castle, Pennsylvania," Circle 44 on the TSP Request Card. MFS-25424

A Solar-Energy System in Minnesota

Design of a system for a Minnesota residence

A companion report to that described in the preceding article discusses a system for a Minnesota residence. Using similar procedures, a final design was arrived at that will meet 45 percent of the total average heating load and will supply 40 gallons (151 l) of potable water at 140° F

(60° C). The delivery rate is 3 gal/min (11 l/min), with a recovery time of 0.75 h. Optimum collector area for this site is 594 ft² (55 m²).

As in the report on the Pennsylvania site, this document contains detailed drawings, specifications, and cost tradeoff studies. Also included are an outline of the proposed installation, operation, and maintenance manual and an analysis of hazards.

This work was done by the Energy Resources Center of Honeywell, Inc., for Marshall Space Flight Center. To obtain a copy of the report, "Solar Heating System Design Package for a Single-Family Residence at William O'Brien State Park, Minnesota," Circle 45 on the TSP Request Card. MFS-25428

Solar-Energy System Evaluation — Pennsylvania Site

An in-depth evaluation of an installed system

A solar-heating and hot-water system installed in a single-family residence in Tunkhannock, Pennsylvania, has been evaluated for performance in a 1-year test program. Results of the tests are available as an 82-page report.

Tested previously under simulated conditions [see "Test and Evaluation of a Solar-Heating System" (MFS-25201) on page 360 of *NASA Tech Briefs*, Vol. 4, No. 3], the system has now been evaluated onsite from two perspectives: The first is an overall view to determine the net energy savings for prevailing and long-term climatic conditions and heating loads. The second is an in-depth look at the performance of individual subsystems.

The Tunkhannock solar-energy system supplies space heating and domestic-hot-water preheating for a 1,000-ft² (92.9-m²) single-family residence. Solar energy is collected with flat-plate collectors, using air as the transport fluid. The collector array has a gross area of 208.5 ft² (19.36 m²). Energy is transferred to and from storage by a liquid-to-air heat exchanger.

Storage capacity is 240 gallons (909 liters) of water in the main tanks and 40 gallons (151 liters) in the domestic-

hot-water tank. The system has five modes of operation: collector-to-space heating, storage-to-space heating, collector-to-storage, domestic-hot-water preheat, and collector-to-storage and auxiliary space heating.

During the 12-month test period, the daily average incident insolation in the plane of the collector array was 1,063 Btu/ft² (12.1x10⁶ J/m²). Solar energy satisfied 17 percent of the total measured load, which is considerably below the design prediction of 39 percent. The reduction in overall system solar fraction was due primarily to the space-heating subsystem. The space-heating solar fraction was only 7 percent. However, the computations do not account for uncontrolled energy losses from duct leakage. These losses are substantial and considerably reduce the measured space-heating load.

If the uncontrolled losses of solar energy are considered, the heating solar fraction becomes approximately 18 percent. This is a significant improvement, but is only about one-half of the value needed.

This work was done by the Federal Systems Division of IBM Corp. for Marshall Space Flight Center. To obtain a copy of the report, "Solar Energy System Performance Evaluation — Seasonal Report for Fern, Tunkhannock, Pennsylvania," Circle 46 on the TSP Request Card. MFS-25434

A Hot-Water System Tested Onsite — Togus, Maine

Performance close to design specifications was verified over a 1-year study.

A solar hot-water system described in several previous *NASA Tech Briefs* articles [see "Prototype Residential Solar-Energy System — Installation Package" (MFS-23956) on page 355 of Vol. 3, No. 3] has been evaluated during a 1-year onsite study. Described in a 69-page report that is now available, the study looked at the long-term operation of the system installed in a residential building in Togus, Maine.

Silicone fluid circulating through flat-plate collectors is the working
(continued on next page)



medium in this hot-water system. The water is preheated in a 120-gal (454-l) tank and is fed to a 40-gal (151-l) domestic-hot-water heater, which adds the balance of the energy. Solar power supplies about 51 percent of the hot-water energy.

Over the 1-year study, the system operated consistently well, experiencing no downtime. At the expected weather and hot-water load, the system operated very close to its design specifications.

This work was done by the Federal Systems Division of IBM Corp. for Marshall Space Flight Center. To obtain a copy of the report, "Solar Energy System Performance Evaluation — Seasonal Report for IBM System 2, Togus, Maine," Circle 47 on the TSP Request Card.
MFS-25435

A Reliable Solar-Heating System — Huntsville, Alabama

Silicone-liquid heat-exchange medium requires no freeze or stagnation protection.

The final report on a solar-heating demonstration project in Huntsville, Alabama, is rich in technical data, planning considerations, test and maintenance data, and other information. It can be a useful reference for those planning similar systems.

The solar facility installed at the Huntsville Senior Citizen Center is expected to supply 85 percent of the

building hot-water requirements. A silicone fluid was chosen as the heat-transfer medium. Since this liquid can be pumped at temperatures as low as -121°F (-85°C) and generates very little vapor pressure when its temperature is elevated to 600°F (316°C), it requires no freeze protection and can operate with a simple closed-loop flow path. No special provisions for stagnation are necessary. These features simplify maintenance and improve system reliability.

The report describes the major subsystems and includes relevant manufacturer's product literature. Each of the operating modes (e.g., direct-solar, heat-from-storage, stored-solar) is explained in detail. Drawings and photographs of the system are included.

This work was done by the City of Huntsville for Marshall Space Flight Center. To obtain a copy of the report, "Solar Heating and Hot Water System Installed at the Senior Citizen Center, Huntsville, Alabama," Circle 48 on the TSP Request Card.
MFS-25431

Solar-Heating and Cooling Demonstration Project

Design, operation, and installation details of a solar-heating and cooling system

The Florida Solar Energy Center has retrofitted an office building, approximately 5,000 square feet (465 square meters) of area, with solar heating and

air-conditioning. This demonstration project is viewed by hundreds of center visitors each day.

Information on the operation, installation, controls, and hardware for this system is contained in a report that is available on request. The 164-page document includes manufacturer's product literature and detailed drawings.

The major system subcomponents are:

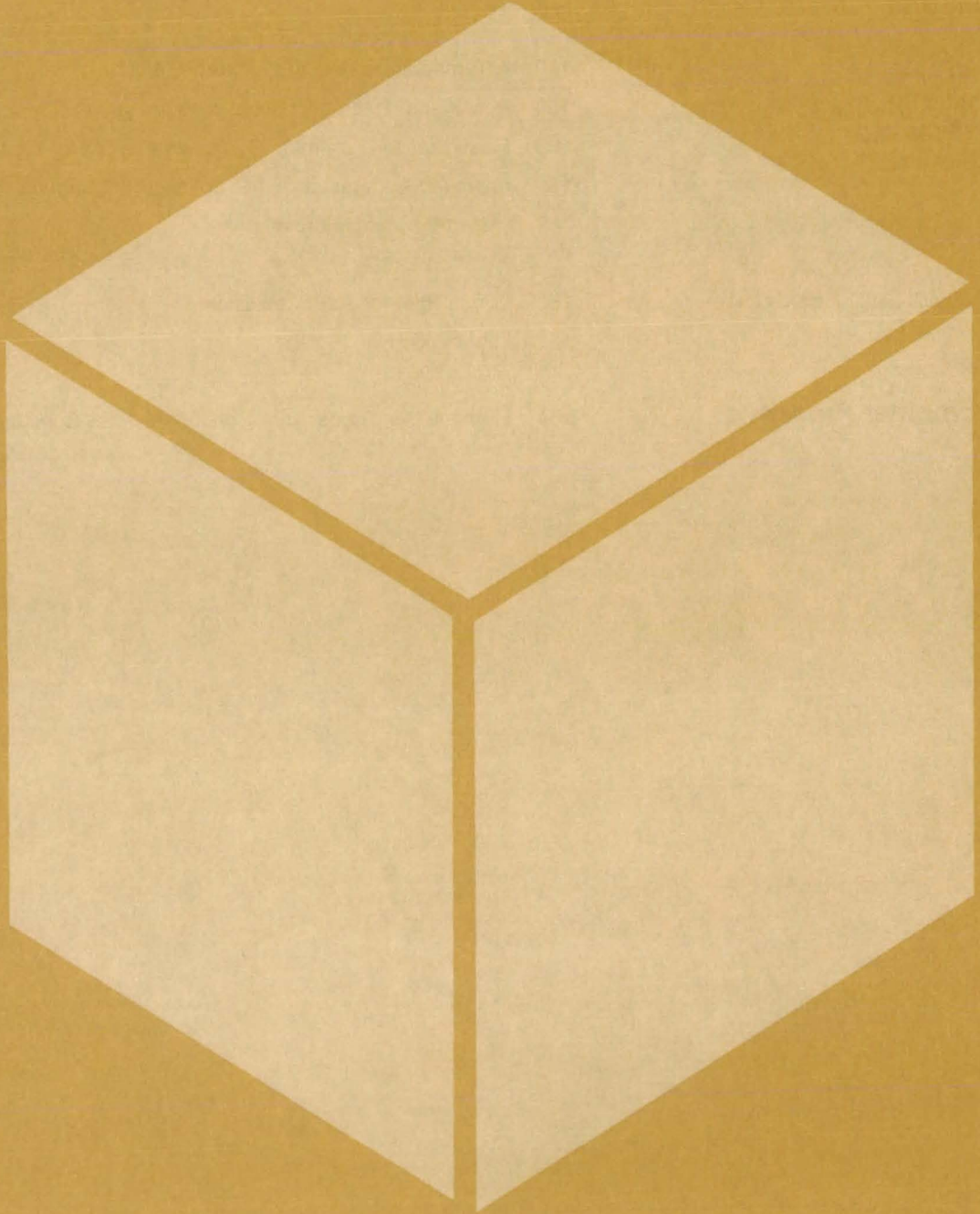
- solar collectors,
- an absorption chiller,
- storage tanks (for hot water and chilled water), and
- controls and piping.

A ten-tube commercial evacuated collector supplies the high-temperature water (at 80° to 90°C) needed for the absorption chiller. Rated at 25 tons ($2.2 \times 10^5\text{ N}$), the chiller is supplied with hot water from one storage tank and delivers its chilled water to another tank.

The system has operated without problems for almost 9 months. A count of the cooling hours from solar energy and of the total hours of space cooling indicates a solar fraction of between 50 and 60 percent during the summer.

This work was done by the Florida Solar Energy Center of the University of Florida for Marshall Space Flight Center. To obtain a copy of the report, "Solar Heating and Cooling Demonstration Project at the Florida Solar Energy Center." Circle 49 on the TSP Request Card.
MFS-25443

Materials



**Hardware,
Techniques, and
Processes**

- 179 A Temperature Fixed Point Near 58° C
- 180 Removal of Hydrogen Bubbles From Nuclear Reactors
- 180 Plasticizer for Polyimide Composites
- 181 Improved Adherence of TiC Coatings to Steel
- 182 Hybrid Polymer Microspheres

Books and Reports

- 183 Composites for Aeropropulsion
- 183 Lubrication Handbook

Computer Programs

- 184 Methane/Air Flames in a Concentric-Tube Combustor

A Temperature Fixed Point Near 58° C

The triple point of ultrapure succinonitrile could be used to calibrate thermometers between 0° and 100° C.

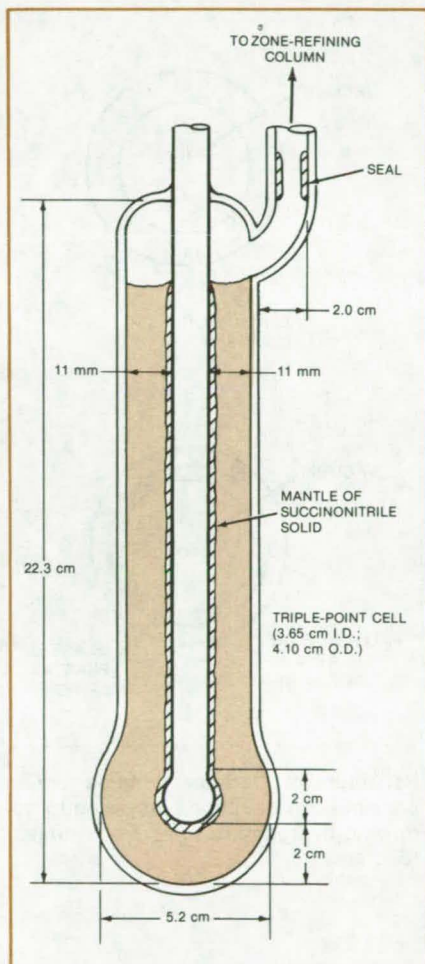
Marshall Space Flight Center, Alabama

A new secondary "fixed point" for defining the International Practical Temperature Scale has emerged from improved materials-processing methods for the organic substance succinonitrile $[\text{CN}(\text{CH}_2)_2\text{NC}]$. It has a reproducible triple point at $58.0810^\circ \pm 0.0004^\circ \text{C}$.

If adopted as a temperature standard, the new fixed point would improve the certainty of calibrations in the important temperature domain between 0° and 100° C. It would complement the primary fixed points of 0.010° and 100° C (the triple point and the boiling point of water) and the melting point of gallium metal at 29.770° C, the only other secondary fixed point in this range. Together, the secondary fixed points would bracket the clinically important temperature of 37° C (body temperature).

Techniques for preparing high-purity succinonitrile were developed as part of a study of the solidification of supercooled liquids (ultrapure liquids cooled to below their normal freezing points). The methods combine vacuum distillation and zone refining in a sealed system. To avoid recontamination, the pure material is directly transferred to a triple-point cell, where the fixed-point temperature is determined.

A mechanical pump isolated by a liquid-nitrogen cold trap is used for vacuum distillation of 99-percent-pure succinonitrile starting material. This step removes dust particles and impurities with vapor pressures higher or lower than that of succinonitrile at 80 to 90 C.



The **Triple-Point Cell** contains about 300 g of high-purity succinonitrile. Experiments show that the lower 4 cm of the thermometer well are virtually isothermal, making placement of the thermometer not very critical. The bulb at the bottom of the well helps to prevent the solid succinonitrile mantle from slipping.

Final zone refining of the distilled material is done in three stages, with 30 passages of 3 zones in each stage. The purer half of the material produced after each stage serves as the starting material for the next stage. The resulting product is at least 99.9999+ percent pure.

The borosilicate-glass triple-point cell (see figure) is first evacuated and then filled with approximately 300 g of the purified succinonitrile. It is immersed in a variable-temperature water bath at about 58° C. A thermometer is placed in the oil-filled well at the center of the cell. The cell wall becomes coated with a mantle of solid succinonitrile at the triple point, and good thermal contact between the cell and the thermometer is maintained through the oil.

The triple-point temperature is determined by observing the behavior of the specimen in the cell. At the triple point, the solid, liquid, and gaseous phases of the material are in equilibrium. If the temperature is raised above the triple point, liquid forms at the expense of solid; if the temperature is lowered, more material solidifies. Both the liquidus (melting) and solidus (freezing) temperatures were measured to look for any hysteresis that would indicate contamination. None was observed to within 0.001° C, verifying that the sample was at least 99.9999 percent pure.

This work was done by Martin E. Glicksman of Rensselaer Polytechnic Institute for **Marshall Space Flight Center**. For further information, Circle 50 on the TSP Request Card. MFS-25304

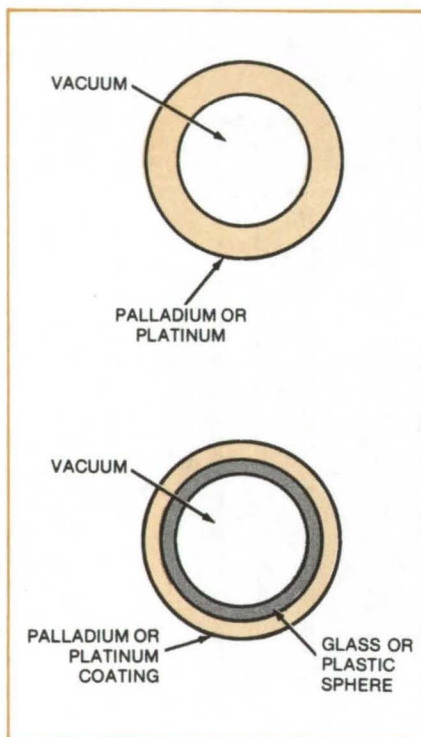
Removal of Hydrogen Bubbles From Nuclear Reactors

Palladium spheres could be used to absorb radioactive hydrogen.

Langley Research Center, Hampton, Virginia

During the recent crisis at the Three-Mile-Island nuclear electric-generating plant, a hydrogen bubble formed in Unit 2. It was considered dangerous since expansion would have uncovered the fuel rods from the core top down, causing further overheating of the core. The bubble was eventually reduced in size by allowing the radioactive hydrogen to escape into the containment building. This solution allowed additional radioactivity into the containment building and into the environment.

A novel method proposed for removing large hydrogen bubbles from the nuclear environment uses, in its simplest form, hollow spheres of palladium or platinum. At room temperature, palladium absorbs 900 times its own volume of hydrogen; when heated, it releases the hydrogen. A similar phenomenon occurs with platinum. The evacuated palladium or platinum spheres are introduced into the reactor with the cooling water where they rise to the top of the water and contact the hydrogen bubble. At low temperature, this contact results in the metal absorbing large volumes of hydrogen; and since the vapor pressure of hydrogen inside the spheres is initially zero, hydrogen also enters the vacuum of the spheres. At higher temperature, the metals absorb smaller volumes of hydrogen, but hydrogen passes through the metal more easily to the



Palladium or Platinum Spheres in two possible configurations proposed for removing hydrogen bubbles from nuclear reactors

hollow of the sphere. Hydrogen will pass through the metal until the vapor pressure inside the sphere equals that outside the sphere.

Such spheres cannot be used if an explosive mixture of hydrogen and oxygen is contained in the bubble. Platinum, in particular, would cause the mixture to explode. However, if the oxygen content is below the explosion limit, the metals will simply catalyze the formation of water from the hydrogen and oxygen. If the spheres are initially pressurized with pure oxygen, hydrogen entering through the metal shell will react with it to form water. Partially filling the spheres with water in this manner will cause them to sink. Gas-filled spheres, on the other hand, would sink only if critically balanced in buoyancy. Either method would result in the hydrogen bubble being reduced in size without letting more radioactivity outside the reactor.

An alternate technique would involve coating glass or plastic vacuum spheres with platinum and/or palladium and introducing these to the reactor. If the gas mixture is below the explosion limit, water will be formed, reducing the hydrogen bubble. The bubble can be completely removed by slowly adding oxygen to combine with the hydrogen to form water.

This work was done by Renaldo V. Jenkins of Langley Research Center. No further documentation is available. LAR-12597

Plasticizer for Polyimide Composites

Liquid plasticizer makes prepregs tacky and drapable.

Langley Research Center, Hampton, Virginia

A new modification of a NASA-developed addition polyimide, LaRC-160, is an essentially-solventless, high-viscosity laminating resin that is synthesized from low-cost liquid monomers. The modified version takes

advantage of a reactive liquid plasticizer, which is used in place of solvent, and helps to solve a major problem of maintaining good prepreg tack and drape, (or the ability of the prepreg to adhere to adjacent plies

and conform to a desired shape during the layup process). This alternate approach will allow both longer life of the polymer prepreg and the processing of low-void laminates. This approach appears to be applicable to all

addition polyimide systems. The reactive liquid that is used is monoethylphthalate (MEP), which is a liquid above 2° C that does not boil.

An added advantage to this material is that it has a very low vapor pressure at the temperatures that occur during normal fabrication (the laying up of prepreg in a shop area). This low vapor pressure allows essentially all of the MEP to be retained, and thereby, tack and flexibility of the prepreg are retained. When alcohol solvents are used, the solvents are so volatile at room temperature that they are rapidly lost to the atmosphere, leaving a brittle and dry prepreg with which it is impossible to work. High boiling

alcohols, such as *n*-butyl alcohol have been tried; but these solvents cannot be removed during processing and, therefore, lead to cracked or voidy composite parts.

The MEP is normally used in place of 10 percent of the benzophenone tetracarboxylic diester diacid (BTDE). Hence a nominal formulation for a liquid system would be 2.00 moles 5-norbornene-2,3-dicarboxylic methylester acid (NE); 1.50 moles BTDE; 0.34 mole MEP; and 2.67 moles 4,4'-methylenedianiline (MDA), or an amine mixture such as the one used in LaRC-160. Graphite-reinforced laminates prepared from prepreg containing MEP had mechanical properties

equal to the base LaRC-160 system both before and after aging at 600° F (315° C) for up to 500 hours.

This work was done by Terry L. St. Clair of Langley Research Center and John M. Butler of Virginia Polytechnic Institute and State University. For further information, Circle 51 on the TSP Request Card.

This invention is owned by NASA, and a patent application has been filed. Inquiries concerning nonexclusive or exclusive license for its commercial development should be addressed to the Patent Counsel, Langley Research Center [see page A5]. Refer to LAR-12642.

Improved Adherence of TiC Coatings to Steel

Use of a nitrogen-containing plasma improves adherence and reduces friction and wear.

Lewis Research Center, Cleveland, Ohio

A modified process for RF sputtering of titanium carbide coatings onto 440-C steel has resulted in improved adherence. A small partial pressure of nitrogen (~ 0.5 percent) during the first few minutes of deposition markedly improved adherence, friction, and wear properties when compared with coatings applied on sputter-etched surfaces, or oxidized surfaces, or in the presence of a small oxygen partial pressure. X-ray photoelectron spectroscopy and X-ray diffraction were used to characterize the resultant coatings.

Considerable interest in the use of hard coatings for wear resistance has prompted work on various coating methods. One of the most attractive methods is RF sputtering. Many different hard refractory compounds applied by sputtering have been studied for wear resistance. These studies have shown that coatings applied by sputtering can provide good wear protection and in many cases low friction. However, most coatings are limited not by coating properties but rather by the adherence of those coatings to the substrates. Failures generally occur at the coating/substrate interface.

Previous work showed that for certain refractory types of material,

significant improvement in adherence could be obtained if the steel surface was oxidized before coating. Recent tests have shown that a small nitrogen partial pressure during the first few minutes of sputter deposition promoted shear strength adherence for metal and ceramic couples.

In the present work, tests were conducted to determine if adding a small amount of nitrogen to the argon plasma during RF sputter deposition of titanium carbide was effective in promoting adherence and thereby improving friction and wear performance. A further objective was to contrast the effectiveness achieved with nitrogen when compared with the adherence gains achieved by oxidation.

The sputtering was done in a commercial, radio-frequency diode apparatus that operated at 13.56 MHz. Titanium carbide coatings were applied to several 440-C steel disk specimens under a variety of conditions so that comparisons could be made of the effectiveness of nitrogen and oxygen partial pressures and substrate preoxidation. A range of oxygen and nitrogen partial pressures was employed.

The RF-sputtered films were evaluated in a pin-on-disk apparatus, which

is often used for solid-film lubrication evaluation. The apparatus consisted of a pin loaded against a flat, rotating disk. The disk specimen was a 440-C bearing steel that had been RF sputter-coated with titanium carbide; the pin was 304 stainless steel. A strain gage measured the friction force. The combination of a 304 stainless-steel pin and a 440-C steel disk was chosen because the friction for this couple is very sensitive to any coating failure and transfer of the 304 steel to spalled regions accelerates the failure process.

The results obtained are shown in the figure. These results represent the best performance that was obtained for the particular gas listed. The oxidized substrates were prepared by furnace heating to 340° C for 18 to 20 hours. This treatment produced a thin, reddish-cast oxide but did not soften the 440-C disk. Also shown for comparison on the figure are data for coatings applied directly to sputter-etched surfaces without any oxygen or nitrogen partial pressure.

Both nitrogen and oxygen partial pressures provide some improvement over the sputter-etched-only values; however, the oxygen partial pressure technique did not yield results as good as furnace oxidation. At 2 N (newtons)

(continued on next page)

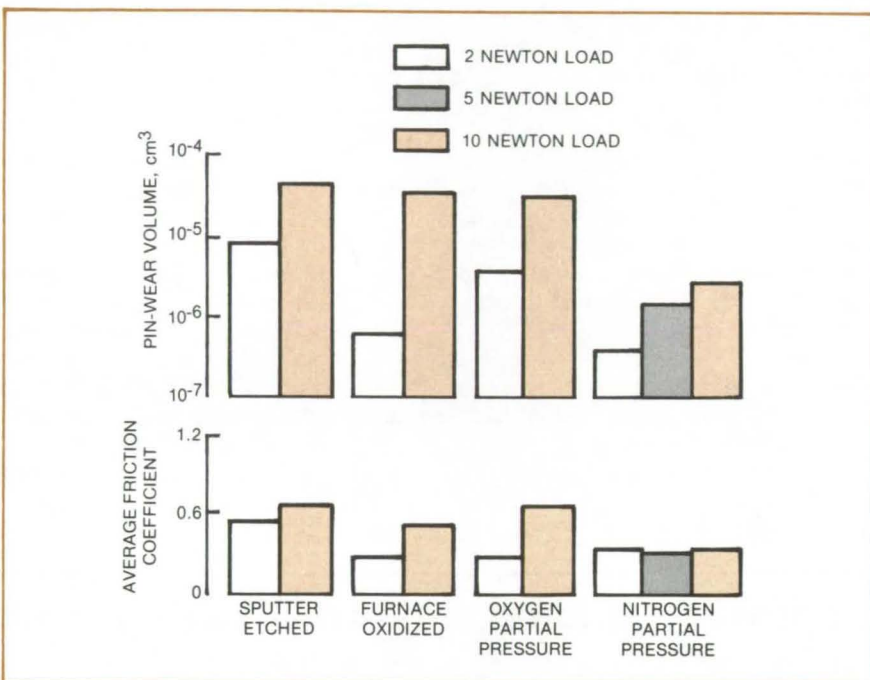


load, both the coatings on the oxidized 440-C steel disk and the coating prepared with an initial nitrogen partial pressure exhibited comparably low friction and wear.

At a high load of 5 N, only the sample prepared with nitrogen ran the entire 30 minutes without spalling. All other coatings, regardless of how prepared, failed, resulting in high friction and rider wear. The coating prepared with a nitrogen partial pressure ran without failure at loads of 10 N.

The friction and wear tests in conjunction with X-ray photoelectron spectroscopy and X-ray diffraction analyses yielded the following results:

- The addition of a small nitrogen partial pressure (~ 0.5 percent) during the initial stages of deposition (interface formation) yielded coatings with adherence, friction, and wear properties superior to coatings applied to oxidized surfaces or with an oxygen partial pressure instead of nitrogen.
- The improvement in adherence is related to the formation of an interface containing both titanium nitride and iron nitride.
- X-ray diffraction showed the RF-sputtered TiC coating done with a nitrogen partial pressure had a preferred orientation with the densest (111) planes parallel to the surface. In contrast, samples done with



Average Friction Coefficient and Pin Wear Volume for 440-C steel disks sputtered with titanium carbide, sliding speed 25 cm-s⁻¹, 30-min run, N₂ atmosphere

oxides present were more random in orientation.

This work was done by W. A. Brainard and D. R. Wheeler of **Lewis Research Center**. Further information may be found in NASA TP-1377 [N79-15184/NSP], "Effect of Nitrogen-Containing Plasma on Adherence, Friction, and Wear of Radiofrequency-

Sputtered Titanium Carbide Coatings" [5]. A copy may be purchased [prepayment required] from the National Technical Information Service, Springfield, Virginia 22161.

Inquiries concerning rights for the commercial use of this invention should be addressed to the Patent Counsel, Lewis Research Center [see page A5]. Refer to LEW-13169.

Hybrid Polymer Microspheres

Tiny polymeric spheres with even smaller spheres attached to their surfaces may be used for separation.

NASA's Jet Propulsion Laboratory, Pasadena, California

Several techniques have been successfully tested for bonding polymeric spheres, typically 0.1 micron in diameter, to spheres with diameters up to about 100 microns. The hybrids are being developed as improved packing material for ion-exchange columns, filters, and separators.

The polymers, including latex and poly-HEMA (poly-hydroxymethylmethacrylate), are prepared as microspheres by exposing a mixture of reagents to ionizing radiation (to promote polymerization) and then washing and filtering

the product. Solid and hollow glass spheres have also been used.

The polymeric spheres have attached carbonyl or other groups that are acceptor sites for extracting antibodies, enzymes, and other large molecules from aqueous suspensions and solutions. To enhance the possibility for binding in such applications, it is preferable to use spheres with small diameters, since this maximizes the exposed surface area in a given volume. However, if the spheres are too small and densely packed, they

impede the flow of liquid, which decreases the effectiveness of the separation process.

Compound spheres increase the effective surface area, while minimizing obstruction to the liquid flow. The initial experiments show that a stable hybrid consisting of a large sphere with many small spheres attached to its surface is formed by chemical bonding or electrostatic bonding.

In chemical bonding, glass spheres, typically 30 microns in diameter, are treated with silane or other agent that

introduces functional groups to the glass surface. The smaller poly-HEMA spheres (0.1 to 1.0 micron in diameter) form stable bonds to the treated glass. A similar treatment is used to prepare hybrid spheres of poly-HEMA and polystyrene.

Small poly-HEMA spheres were also attached to glass spheres by electrostatic attraction. The smaller spheres are prepared with positively-charged

dimethylamino surface groups. These form electrostatic bonds with the glass, which is negatively charged. Preliminary tests have also verified that some species of red blood cells can be extracted from an aqueous suspension by the glass/dimethylamino hybrids.

In another experiment, polyvinyl pyridine microspheres (5 microns in diameter), having amino groups on the surface, were mixed with magnetic

microspheres (0.2 micron in diameter) with aldehyde groups on the surface. The hybrid has a polyvinyl pyridine nucleus and a magnetic coating on the surface. A magnetic field is used to handle and separate these spheres.

This work was done by Alan Rembaum of Caltech for NASA's Jet Propulsion Laboratory. For further information, Circle 52 on the TSP Request Card.
NPO-14462

Books and Reports

These reports, studies, and handbooks are available from NASA as Technical Support Packages (TSP's) when a Request Card number is cited; otherwise they are available from the National Technical Information Service.

Composites for Aeropropulsion

Status report details significant advances made in the past several years.

A report has been published that summarizes the status of composite materials for aeropropulsion.

Composite materials are increasingly of interest for a variety of applications. A large potential exists for strategic material conservation and energy savings with composite materials. Research efforts in this field have resulted in major strides in the development of materials as well as in improved design and analysis capability. This report details significant advances made in the past several years. The applications discussed deal primarily with composites used in the cold and hot sections of aircraft turbine engines. Also reported is the current status of composite structural analysis technology. Although this report is concerned primarily with NASA-funded research, it also includes other investigations. Specific composites are described for both low- and high-temperature usage.

The most-widely-used low-temperature [less than 350° F (177° C)] composites utilize an epoxy resin

matrix and graphite fiber reinforcement. These materials exhibit good physical properties, low cost, and ease of processing into complex shapes. Use temperatures of non-metallic composites could be extended up to 600° F (315° C) if improved polyimide resins can be used as matrix materials.

Metal matrix composites are emerging as potential materials for both low- and high-temperature applications. For the former, boron/aluminum composites and for the latter, tungsten-fiber-reinforced superalloys show considerable promise.

This report describes key advances made in the past several years and lists 47 references published from 1971 to 1979.

This work was done by G. M. Ault and J. C. Freche of Lewis Research Center. To obtain a copy of the report, Circle 53 on the TSP Request Card.
LEW-13438

Lubrication Handbook

A ready reference for many of the solid and liquid lubricants used in the space industry

A lubrication handbook is divided into two major parts: Part A describes solid lubricants and part B liquid lubricants used in the aerospace industry. The listed materials cover a broad application spectrum from manufacturing and ground support to missile and spacecraft hardware. The handbook can serve as ready reference in the design and maintenance service of industrial equipment.

More than 250 lubricants are

covered in each section, with accompanying chemical and physical property data. The solid lubricants include bonded solid lubricants, dispersions, and composites; liquid lubricants include greases, oils, compounds, and fluids.

Part A of the handbook is divided into six major sections: Section I defines the solid lubricants and outlines their advantages and disadvantages. Section II lists the manufacturers in alphabetical order with their products and characterizes lubricant compatibility and usage tables for selected bonded solid lubricants and composite materials. Section III presents data sheets giving general composition and physical properties of selected lubricants; section IV presents data sheets listing manufacturer-supplied test and applications data. The data on selected solid film lubricants obtained from tests conducted by an independent laboratory are covered in section V. Section VI has three appendixes: one a glossary of terms, the second containing excerpts of solid lubricant applications, and the third describing test apparatus and procedures used in the laboratory evaluation of solid lubricants.

Part B consists of five sections: Section I instructs the reader on the use of part B, presents an index of all the liquid lubricants covered, and includes a series of charts describing the lubricant applications. A brief description of military specifications is given in section II, while section III presents data sheets listing physical and chemical properties of selected lubricants. Section IV shows the results of long-term evaluation of

(continued on next page)



selected grease lubricants. Section V contains three appendixes: one, a glossary of lubrication terms; two, a series of summaries of standard testing methods used to evaluate lubricating oils, greases, and fluids; and three, a detailed-conversion chart into international (SI) units.

The handbook is a valuable reference to designers, manufacturers, and maintenance crews of aerospace hardware. Much of the information is readily transferable to industrial and commercial hardware. It should be a welcome addition in any engineering library as well as to groups and

individuals involved with mechanical systems.

This work was done by Midwest Research Institute for Marshall Space Flight Center. To obtain a copy of the handbook, Circle 54 on the TSP Request Card.
MFS-25158

Computer Programs

These programs may be obtained at very reasonable cost from COSMIC, a facility sponsored by NASA to make new programs available to the public. For information on program price, size, and availability, circle the reference letter on the COSMIC Request Card in this issue.

Methane/Air Flames in a Concentric-Tube Combustor

Hydrodynamics and chemistry of confined turbulent flames are predicted.

This computer program gives a realistic prediction of the hydrodynamics and chemical reaction in a reverse-flow two-concentric-tube combustor. Special attention is given to the formation of oxides of nitrogen in the combustion process.

The combustor geometry considered is a two-concentric-tube combustor. Concentric streams of fuel (methane) and air enter the inner duct and mix. At the end of the inner duct, the flow expands radially outward and reverses its flow. Combustion occurs in this flow reversal region. Oxides of nitrogen and other combustion products are formed as a result of the chemical reaction. The flow is two-dimensional, axisymmetric, steady, and turbulent. Heat transfer between the combustion products in the annular passage between the tubes and the reactant stream in the center tube is considered.

The analysis involves the mathematical formulation of the flow in terms of partial differential and auxiliary algebraic equations. These equations are used in their finite-difference form for obtaining numerical solutions. The solution procedure is incorporated in the computer program to produce

profiles of velocity, temperature, and chemical species concentration throughout the combustor.

In this program two test cases were considered, cold flow (without chemical reaction) and hot flow. Possible modifications to this program include the use of more sophisticated heat transfer, chemical kinetics, and turbulence models.

This program is written in FORTRAN IV for batch execution and has been implemented on a UNIVAC 1100 computer with a central memory requirement of approximately 33K of 36-bit words. This combustor analysis program was developed in 1978.

This program was written by N. C. Markatos, D. B. Spalding, and S. K. Srivatsa of Concentration, Heat and Momentum Ltd. for Lewis Research Center. For further information, Circle B on the COSMIC Request Card.
LEW-13388

Life Sciences



**Hardware,
Techniques, and
Processes**

187 Testing EKG Electrodes On-Line

Books and Reports

187 Laser-Fluorescence Measurement of Marine Algae

Testing EKG Electrodes On-Line

A simple circuit verifies electrode-lead continuity and contact during an electrocardiograph recording.

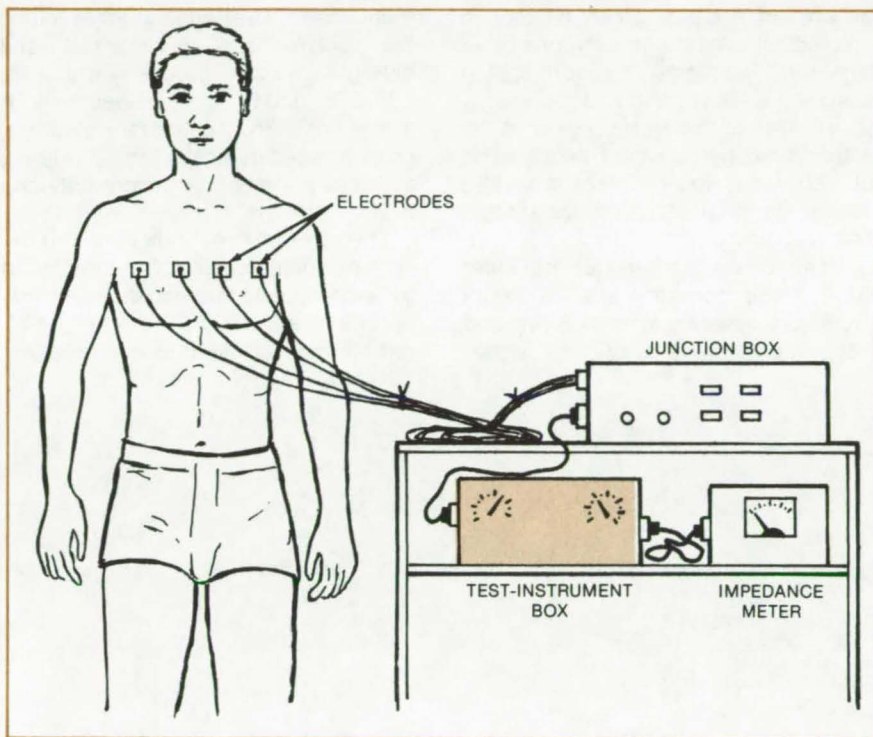
Lyndon B. Johnson Space Center, Houston, Texas

A simple test instrument allows an electrocardiograph operator to check individual electrodes while they are attached to the subject. Simply by rotating a switch and observing a meter, the operator verifies that each electrode is not short-circuited or open-circuited and does not present excessive contact resistance at its interface with the skin. The instrument also makes it convenient to check electrode cables that are subject to frequent bending and wear, such as cables used on patients who are exercising.

After the patient is instrumented (that is, after the skin is smeared with electrode paste, the electrodes are placed on the skin, and the leads are attached to the electrodes), the cable from the EKG junction box is attached to the test instrument (see figure). A current-limited impedance meter is plugged into another connector on the instrument.

Rotary switches allow the operator to select any electrode lead and measure the impedance between it and another lead or between it and the cable shield. The impedance is read directly on the meter.

An electrode-to-electrode impedance of less than 2,000 ohms is considered satisfactory, and a reading of 1,000 ohms is regarded as ideal. An open circuit, either in a lead or the junction box, shows up as infinite



Rotary Switches on Test Instrument allow an EKG operator to select individual electrode pairs for impedance measurements. The instrument also contains operational amplifiers that condition the EKG signals. Two 4-gang, 12-position rotary switches interconnect 14 electrode leads and 1 shield in a prototype. Improved versions will do all switching with a single rotary switch.

impedance. A short circuit appears as a zero reading. The electrode-to-shield impedance should be above 10 megohms.

This work was done by William G.

Crosier and Gordon S. Rutt of Technology Inc., for Johnson Space Center. For further information, Circle 55 on the TSP Request Card. MSC-18696



Books and Reports

These reports, studies, and handbooks are available from NASA as Technical Support Packages (TSP's) when a Request Card number is cited; otherwise they are available from the National Technical Information Service.

Laser-Fluorescence Measurement of Marine Algae

A thorough review of theory and experiment, plus some new information

Progress in the remote sensing of algae by laser-induced fluorescence is the subject of a comprehensive new

report. Existing single-wavelength and four-wavelength systems are reviewed, and a new expression for the power received by an airborne sensor is derived. The result differs by as much as a factor of 10 from those previously reported. A detailed error analysis evaluates factors affecting the accuracy of laser-fluorosensor systems.

Measurements of the concentration and distribution of algae in bodies of (continued on next page)

water are of ecological interest because they reflect chemical, thermal, and mechanical conditions in the marine environment. Algae presence is quantified by exciting the chlorophyll a pigment and detecting fluorescence at 685 nm.

Most algal species fall into one of four basic color groups: green, golden brown, red, and blue green; all contain chlorophyll a plus one or more other pigments. The pigments absorb light at specified wavelengths, and the energy is transferred between pigments toward chlorophyll a, where deexcitation at 685 nm occurs. There are also secondary deexcitation modes at other points in the cycle.

An airborne single-wavelength laser fluorosensor, operating at an optimum excitation wavelength of 600 nm and flying at an altitude of 500 m, is pre-

dicted to measure algae concentrations as low as 1 $\mu\text{g/liter}$. The calculations assume a 100-kW (peak power) laser.

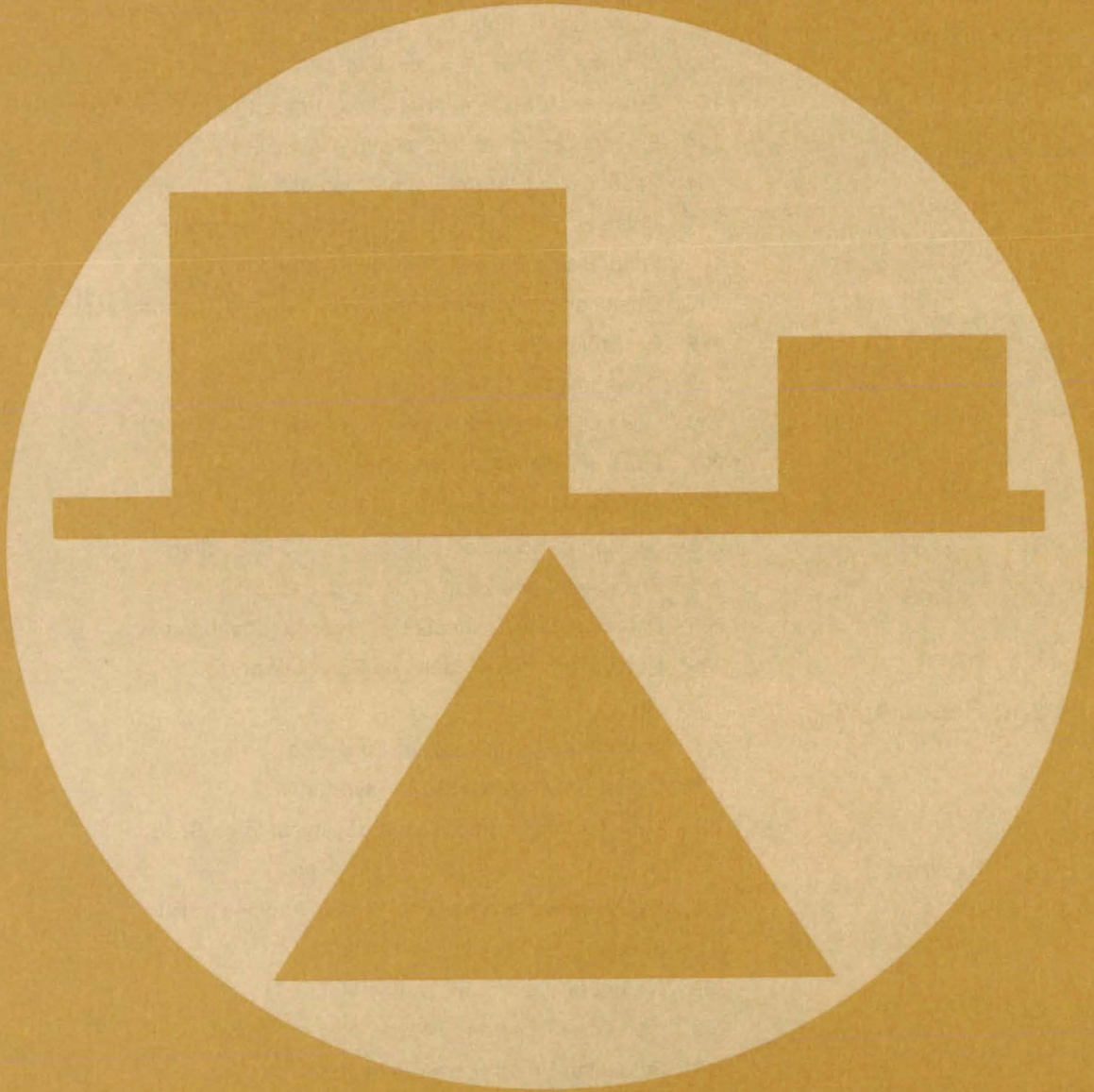
Four-wavelength laser fluorosensors give information on the distribution of algae in the four color groups. In a system previously developed at Langley Research Center, the optimum laser wavelengths for exciting the golden-brown, green, red, and blue-green color groups were 454, 539, 598, and 618 nm, respectively. A single flashlamp pumps four symmetrically-placed dye cells, and a rotating aperture permits lasing from only one cavity at a time.

The error analysis indicates that the remote quantification of chlorophyll a by laser-induced fluorescence requires optimum excitation wavelength(s), remote measurement of marine atten-

uation coefficients, and instrumentation to reduce uncertainties in fluorescence cross sections. Without these additional measurements, the systems only give qualitative information about the presence of chlorophyll a, and the results of single-wavelength measurements are comparable to those of multiple-wavelength sensors.

This work was done by Edward V. Browell of Langley Research Center. Further information may be found in NASA TND-8447 [N77-26480/NSP], "Analysis of Laser Fluorosensor Systems for Remote Algae Detection and Quantification" [\$6]. A copy may be purchased [prepayment required] from the National Technical Information Service, Springfield, Virginia 22161. LAR-12282

Mechanics



Hardware, Techniques, and Processes

- 191 Automatic Thermal Switches
- 192 Grooves Reduce Aircraft Drag
- 193 Efficient Measurement of Shear Properties of Fiber Composites
- 194 Fresnel Lenses for Ultrasonic Inspection
- 194 Passive Wing/Store Flutter Suppression
- 195 Changes in "Thermal Lens" Measure Diffusivity
- 196 Suppressing Buzz-Saw Noise in Jet Engines
- 196 Detection of Tanker Defects With Infrared Thermography
- 198 Recording Fluid Currents by Holography
- 199 Downhole Pressure Sensor
- 200 Oceanic-Wave-Measurement System
- 201 Electrofluidic Accelerometer
- 202 Flashback-Free Combustor
- 203 Measuring Radiation Effects on MOS Capacitors
- 204 Predicting Lifetime of Cast Parts
- 205 Detecting Contaminants by Ultraviolet Photography
- 205 Detecting Surface Faults on Solar Mirrors

Books and Reports

- 206 Refraction Corrections for Surveying
- 206 Digital Enhancement of X-Rays for NDT
- 207 Design Considerations for Mechanical Face Seals

Computer Programs

- 208 Regenerative Superheated-Steam Turbine Cycles
- 208 Stream-Tube Curvature Analysis
- 209 A Generalized Vortex Lattice Method
- 209 Vibration Modes and Frequencies of Structures
- 210 Predicting Propulsion-System Drag
- 210 Heat Conduction in Three Dimensions

Automatic Thermal Switches

Reliable and efficient switches control heat transfer from one area to another.

Goddard Space Flight Center, Greenbelt, Maryland

Two new switches control heat flow from one thermally conductive plate to another. One switch is activated to permit heat flow to the outside environment; the other is used to limit such heat flow. Both switches, developed for controlling payload temperatures in spacecraft, represent a practical answer to mechanically complex and less-reliable louvers that would close when facing the Sun and open when turned away from it. Mechanically simple and reliable, the switches can be used in almost any situation in which the temperature can be controlled by regulating the heat flow.

Figure 1 shows the switch that normally remains in the open position so long as the temperature of the plate (in contact with some internal system; e.g., the payload) it is resting on remains below the phase-change temperature of the power unit. The power unit has an internal reservoir containing a material (e.g., ammonia, deionized water, or some other material) that changes phase (liquid, solid, or gas) at a specific temperature.

When plate 1 is at a low temperature, the power-unit piston is retracted, and a spring biases a thermally-conductive switch saddle in an upward position, breaking the thermal contact with plate 1. When plate 1 heats up, the procedure is reversed. Heat expands the material in the power unit, forcing the piston up against the linkage arm. This force overcomes the spring, pressing the saddle against the plate. Heat is then transferred from plate 1 to plate 2 via flexible heat carriers (e.g., heat pipes). Plate 2 then radiates the heat to the outside.

Figure 2 shows the switch used for preventing excessive heat flow to or from the outside. The arrangement is similar; however, the switch action is reversed. When plate 1 is cold, the power-unit piston is retracted, and the spring biases the saddle to stay in contact with the plate. Heat coming in from plate 2 eventually warms up plate 1 to a level sufficient to activate the

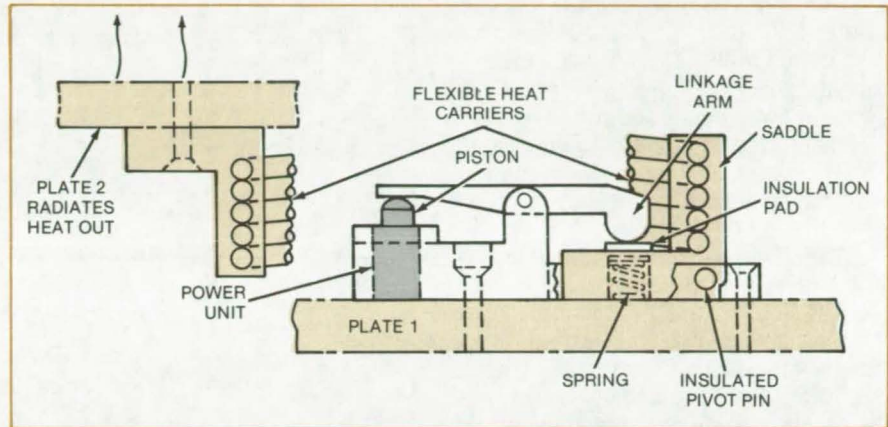


Figure 1. **Thermal Control Switch** eliminates excessive heat flow to the outside environment. Heat on conductive plate 1 (in thermal contact with some internal system) activates a piston that extends upward, forcing the saddle against plate 1. Flexible heat carriers conduct the heat to plate 2, which then radiates to the outside environment. After the plate 1 temperature drops, the piston contracts, and the spring forces the saddle to move clockwise, breaking the thermal contact with plate 1.

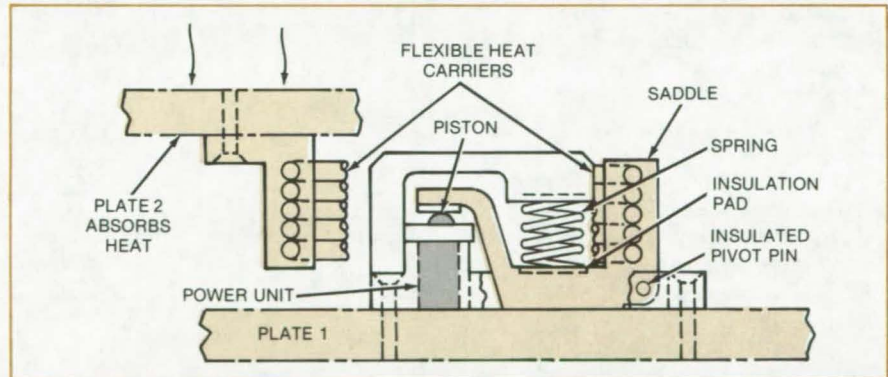


Figure 2. **Reverse Thermal Switch** regulates heat flow from the outside. The saddle remains in thermal contact with plate 1 until sufficient heat comes in from the outside (plate 2). When plate 1 heats up to a certain temperature, the heat extends the piston, forcing the saddle arm up, breaking the saddle contact with plate 1. As plate 1 cools, the piston contracts, and the spring forces the saddle counterclockwise into thermal contact with plate 1.

piston. The piston then forces the saddle arm upward, breaking the saddle contact with the plate and stopping the heat transfer.

Both switches are completely automatic and can be custom-designed to operate at specific temperatures. The material in the power unit determines at what temperatures the switches will trigger. The flexible heat carriers tolerate vibration and some relative displacement between the plates.

This work was done by Joseph W. Cunningham and Lawrence D. Wing of Goddard Space Flight Center. For further information, Circle 56 on the TSP Request Card.

This invention is owned by NASA, and a patent application has been filed. Inquiries concerning nonexclusive or exclusive license for its commercial development should be addressed to the Patent Counsel, Goddard Space Flight Center [see page A5]. Refer to GSC-12553.

Grooves Reduce Aircraft Drag

Tiny grooves in various cross-sectional shapes reduce aircraft fuel consumption.

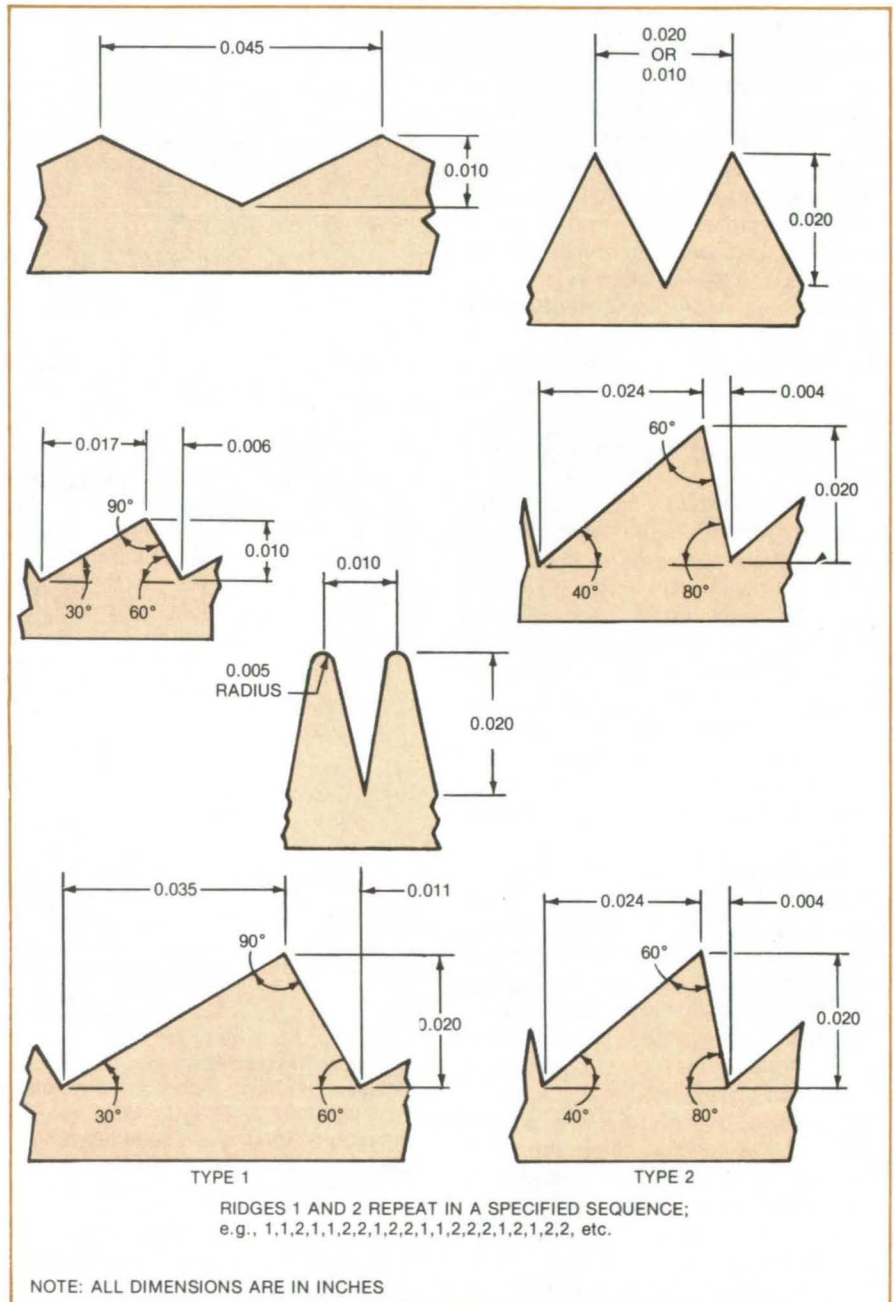
Langley Research Center, Hampton, Virginia

Aerodynamic drag can be reduced by many small longitudinal grooves machined in the aircraft skin. Experiments show that grooves parallel to the airflow reduce drag by 4 to 7 percent. The reduced drag translates into reduced engine power required to overcome the drag and ultimately to lower fuel consumption.

The grooves confine incipient bursts of turbulence so that they cannot expand and disrupt the boundary layer surrounding a moving aircraft. Most are V-shaped, but they may take a variety of dimensions (see figure). For example, they may have rounded or sharp peaks and symmetrical or asymmetrical cross sections. Asymmetrical grooves of various cross-sectional geometries may be arranged in some regular sequences to optimize the aerodynamic performance.

The most effective dimensions for reducing drag are indicated in the figure. The dimensions are small in comparison with those tested in previous experiments. In terms of law-of-the-wall (turbulent-flow) coordinates, the heights are less than 30 and the spacings are less than 40.

This work was done by Michael J. Walsh of Langley Research Center. For further information, Circle 57 on the TSP Request Card. LAR-12599



Most Effective Groove Shapes are shown with dimensions. The grooves inhibit the turbulent bursting process, thus reducing aerodynamic drag and aircraft fuel consumption.

Efficient Measurement of Shear Properties of Fiber Composites

10°-off-axis tensile-test specimen is recommended as a standard for developing design data.

Lewis Research Center, Cleveland, Ohio

Efficient intralaminar (in-plane) shear characterization (shear stress/strain relationships) of unidirectional fiber composites has been hampered by the difficulty of producing a state of pure shear in practical laboratory test specimens. The simplest test specimen in use today is the three-point-bend short-beam shear test specimen (ASTM D-2344-72). While adequate for material quality control, this specimen is not suitable for generating design data because shear stress is not uniform throughout its thickness and only the fracture stress, not the total shear stress/shear strain history, is recorded. The best test specimen, a thin tube subjected to torsion, is too expensive and time consuming to be practical.

The new proposed method is to use a 10°-off-axis tensile specimen (fibers oriented 10° from the load direction) in conjunction with simple transformation equations for intralaminar shear characterization of fiber composites. The geometry, dimensions, end reinforcements, and instruments are shown in the figure.

The procedures for generating the intralaminar shear properties, shear stress/strain curves, initial shear modulus, tangent shear modulus, secant shear modulus, fracture shear stress, and fracture shear strain are relatively straightforward.

Stress-vs.-strain curves are calculated from the outputs of three simultaneous strain-gage readings at increments of stress, using equations of the form:

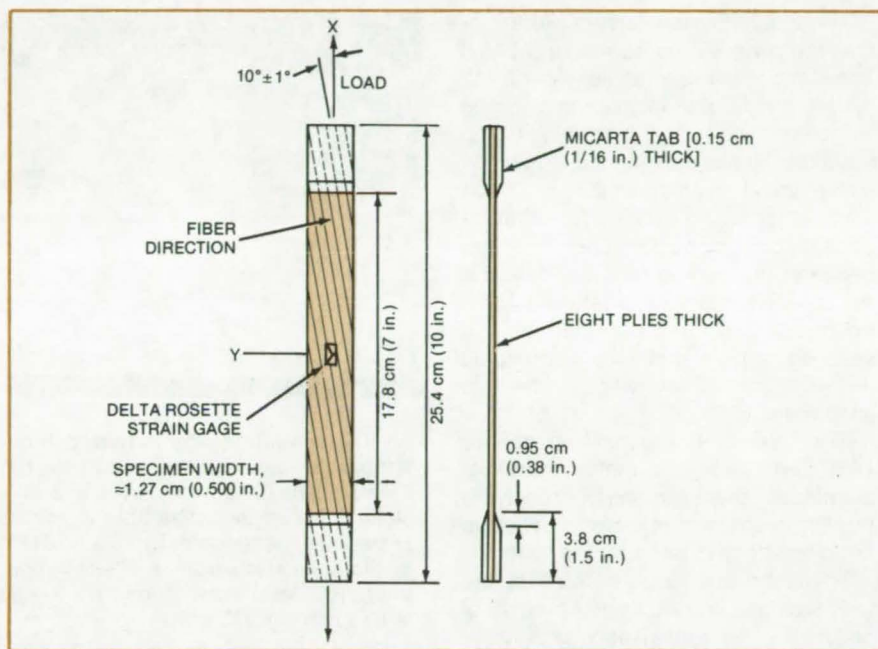
$$\text{Intralaminar shear stress} = \text{coefficient} \frac{\text{tensile load}}{\text{specimen cross section}}$$

and

$$\text{Intralaminar shear strain} = \sum_{i=1}^3 c_i \epsilon_{gi}$$

where the c_i are coefficients and the ϵ_{gi} are strain-gage readings. Equations have been derived for rectangular-rosette and 60°-delta-rosette strain gages.

The initial shear modulus is determined from the slope of the initial tangent to the shear stress-vs.-strain curve. The shear modulus at any other



Test Setup is shown for the 10°-off-axis specimen recommended for developing data on the intralaminar shear characteristics of unidirectional fiber composites. The load is applied at a 10° angle with the fiber orientation, and the strain gage is placed midlength at the center of the specimen. Two, back-to-back delta-rosette strain gages are recommended to account for out-of-plane bending.

point (tangent shear modulus) may be determined from the slope of the tangent to the curve at that point. The secant shear modulus is determined from the slope of a line connecting the origin with the fracture point. The ply intralaminar shear strength equals the shear stress calculated at the fracture load. The ply intralaminar fracture strain is the shear strain calculated at the fracture load.

Theoretical investigation of the technique showed, among other things, that for this tensile-test setup the major stress contribution to fracture is intralaminar shear, and the test will be sensitive to errors greater than 1° in fiber orientation. Experimental data indicated that at specimen midlength fracture strains and Poisson's (transverse) strains are higher at the edges than at the center for some materials, but most measurements are not overly sensitive to small variations in the strain-gage location.

Experimental data compared reasonably well with structural-axis shear

strain as predicted by finite-element analysis. Experimental results from 10°-off-axis specimens for initial-tangent intralaminar shear moduli and fracture stresses are within the range of values reported in the literature.

Its consistency with theory and with other experimental methods, the variety of data yielded, and its relatively straightforward procedures suggest that the 10°-off-axis specimen be considered as a standard test for intralaminar shear characterization of unidirectional fiber composites.

This work was done by Christos C. Chamis and John H. Sinclair of **Lewis Research Center**. Further information may be found in NASA TN-D-8215 (N76-22314/NSP), "10° Off-Axis Tensile Test for Intralaminar Shear Characterization of Fiber Composites" (\$6.00). A copy may be purchased (prepayment required) from the National Technical Information Service, Springfield, Virginia 22161.

LEW-13011



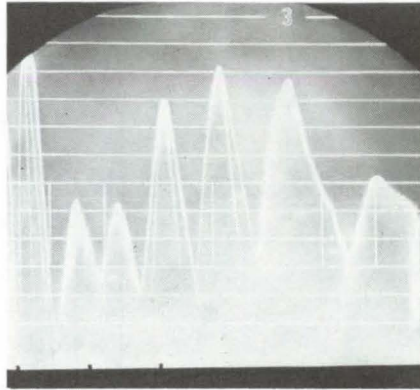
Fresnel Lenses for Ultrasonic Inspection

Fresnel lenses are easily coupled to the test object.

Lyndon B. Johnson Space Center, Houston, Texas

Ultrasonic Fresnel lenses are effective focusing elements with potential applications in ultrasonic "contact" testing for defects in materials. Since a Fresnel lens is flat (with a serrated surface), there is little difficulty in filling the lens/test-object interface with a coupling medium. With a conventional concave lens, the gap between the curved lens surface and the object is not always saturated with couplant; and residual trapped air severely attenuates the ultrasonic wave before it ever reaches the test specimen.

The ultrasonic Fresnel lenses are cast from epoxy in molds made of aluminum, brass, rubber, or polyester. Prototype lenses were attached to flat piezoelectric transducers, and the intensity on the "image" side of the lens was measured as a function of distance. Several reasonably-well-defined intensity maximums were recorded (see figure).



An **Ultrasonic Intensity Pattern** demonstrates the dynamic response of a flat Fresnel lens in contact with a piezoelectric transducer. The time exposure shows the sound intensity as a function of distance away from a reflector near the lens. The distance along the x-axis is about 10 in. (25 cm).

Although contact transducers have been used for inspection testing without a focusing lens, focusing is desirable because it increases the ultrasonic-wave intensity within the test object and thus improves the signal-to-noise ratio.

Ultrasonic beams focused by concave lenses are used successfully with immersion transducers, for which the test object is immersed in a water bath. However, for large objects, objects that are already installed, objects on production lines, and objects that can be damaged by water, contact testing is more practical than immersion.

This work was done by Calvin C. Kammerer of Rockwell International Corp. for Johnson Space Center. No further documentation is available. MSC-18469

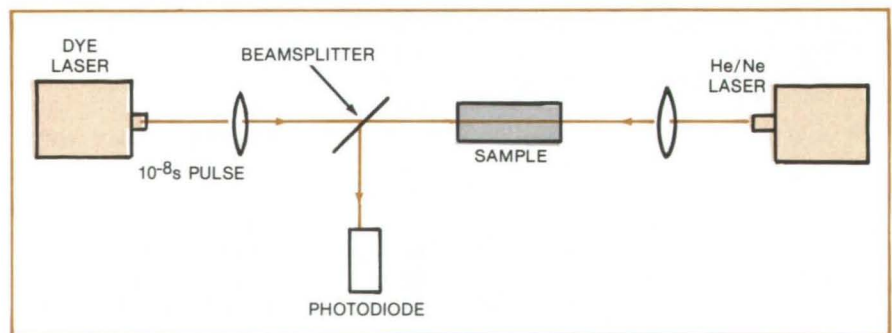
Changes in "Thermal Lens" Measure Diffusivity

A new double-beam method rapidly measures thermal diffusivity.

NASA's Jet Propulsion Laboratory, Pasadena, California

In an extension of the "thermal-lens" effect to new applications and better resolution, two laser beams combine to rapidly measure thermal diffusivity and other molecular dynamic properties. The new double-beam technique can handle very small samples, unlike classical techniques for measuring diffusivity; and it can be used for measurements on samples undergoing stress, making it applicable to data collection for structural engineering.

The thermal lens is set up when heat from an ultrashort burst of pulsed-laser energy introduces inhomogeneity in the refractive index of a



Two Laser Beams, one pulsed and one continuous, measure the thermal diffusivity and the properties of a test sample. The high-energy pulsed laser changes the sample refractive index, which is probed by the low-energy continuous beam. For opaque samples, the continuous beam can be reflected off the sample surface.

test sample. In the double-beam method, a low-power continuous laser probes the sample as it is heated by the high-energy pulse. The continuous beam monitors changes in the optical characteristics, which are related to temperature inhomogeneities and to microscopic dynamic processes. By varying the pulse width of the high-energy laser, it is possible to determine the relationship between the rate of formation of the thermal lens and lattice relaxation processes. The decay time of the lens is related to the thermal diffusivity.

The test setup shown in the figure has measured the thermal properties of polymethylmethacrylate. Using a dye laser with 10-nanosecond pulse width and variable wavelength (360 to 380 nanometers), less than 10^{-8} joule is deposited in the sample during each dye-laser pulse. Estimates of the temperature rise are about 10^{-3}°C or less.

A computer plot of the lens formation, generated by averaging 5,000 scans, took 10 minutes to complete. A trace of the lens decay yielded a value for the thermal diffusivity of $1.0 \times 10^{-3} \text{ cm}^2/\text{s}$, in good

agreement with measurements using classical methods.

This work was done by Amitava Gupta, Su-Don Hong, and Jovan Moacanin of Caltech for NASA's Jet Propulsion Laboratory. For further information, Circle 58 on the TSP Request Card.

This invention is owned by NASA, and a patent application has been filed. Inquiries concerning nonexclusive or exclusive license for its commercial development should be addressed to the Patent Counsel, NASA Resident Legal Office-JPL [see page A5]. Refer to NPO-14657.

Passive Wing/Store Flutter Suppression

Combination of passive and active elements suppresses aircraft-wing/store flutter by decoupling the vibration modes of the wing and store.

Langley Research Center, Hampton, Virginia

A passive flutter-suppression system has been developed to increase the flutter speed of aircraft wings that are adversely affected by the addition of large masses (stores) to the wings, such as external fuel tanks. Important features of the system are its effectiveness for large variations in the mass of the store as well as the unsensitivity of the system to large changes in the location of the store center-of-gravity.

As illustrated in Figure 1, the store is pivoted near the elastic axis of the wing. A spring and dashpot control the frequency and damping of the system. The manner in which this decoupler increases the flutter speed is shown in Figure 2, where wing frequencies are plotted against airspeed. Flutter usually involves the coupling of at least two vibration modes, one of which involves a torsional or pitching motion of the wing. For a rigidly mounted store, the variation of torsional and bending frequencies with airspeed is shown. When the frequencies of these two modes approach each other, a flutter instability may occur. If the store were mounted with a relatively soft spring as shown in Figure 1, the pitch mode of the store would be virtually decoupled from the wing, and a large increase in flutter speed would be found due to the initial wide separation of the torsion and bending frequencies as shown.

To avoid large static deflections normally associated with a low-frequency suspension system, a feedback control system is used to keep the mean deflection of the store aligned with the wing chord.

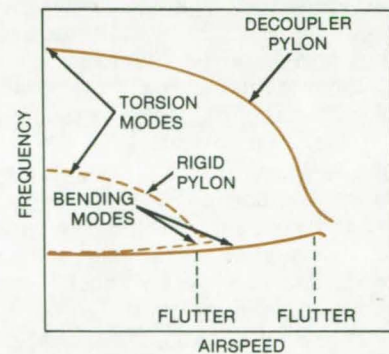


Figure 2. Frequency Separation provided by the decoupler pylon, compared to a rigidly attached store, produces a higher aircraft flutter speed.

This work was done by Jerome T. Foughner, Jr., and Wilmer H. Reed III of Langley Research Center and Harry L. Runyan, Jr., of George Washington University. For further information, Circle 59 on the TSP Request Card.

Inquiries concerning rights for the commercial use of this invention should be addressed to the Patent Counsel, Langley Research Center [see page A5]. Refer to LAR-12468.

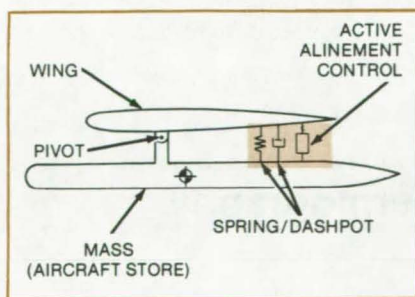


Figure 1. Decoupler Pylon used with aircraft wings carrying stores such as fuel pods uses active and passive elements to isolate the store pitch from wing modes.

Suppressing Buzz-Saw Noise in Jet Engines

Technique promises to reduce annoying fan noise.

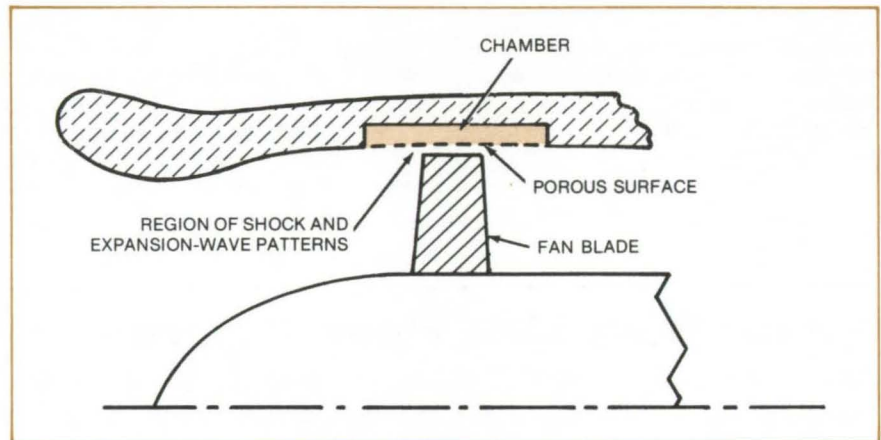
Langley Research Center, Hampton, Virginia

Buzz-saw noise, the most annoying noise component generated by turbofan engines, can be suppressed by installing a porous surface on the duct wall (see figure) directly above the engine fan-blade tip. The porous surface and its housing would reduce the shock-wave reflection from the wall and thus suppress the noise.

Turbofan engine fans produce both tonal and random noises. When the fan-blade tip is supersonic, the tonal noise dominates. Shock- and expansion-wave patterns that constitute the tonal noise are formed at the blade tips. This shock, together with the resulting interacting patterns, rotates inside the duct and propagates out as a strong pulse forming the so-called buzz-saw noise that dominates over the noise produced by the blade-passing frequency and its harmonics.

The proposed approach uses a technique successfully tested in suppressing the jet-noise shock in which a shock wave resulting from a large pressure gradient in the flow originating at the outer tip of the engine nozzle is eliminated. A similar approach can be used to suppress the shock formed by the jet-engine air blade.

The turbofan duct wall in the vicinity of the blade tip would include a porous surface that can suppress direct shock and expansion waves impinging on the wall. Waves reflected from the duct



Buzz-Saw Noise produced by jet engines can be suppressed, if not entirely eliminated, by lining part of the engine duct wall with a porous surface. The combination of porous surface and the chamber above the turbofan blade tip would absorb the shock waves, suppressing the annoying aircraft shrill.

wall are suppressed due to absorption by the porous surface. A chamber behind the porous surface acts like a pressure stabilizer.

Aerodynamically, a shock impinging on the porous surface reflects as an expansion wave, while it reflects as a shock over the nonporous part of the surface. As it is reflected, the resulting interacting patterns (compression and expansion waves) cancel each other's contributions. This effect has been observed experimentally.

This work was done by Lucio Maestrello of Langley Research

Center. Further information may be found in NASA TM-78802 [N79-13820/NSP] "Initial Results of a Porous Plug Nozzle for Supersonic Jet Noise Suppression" [\$5]. A copy may be purchased [prepayment required] from the National Technical Information Service, Springfield, Virginia 22161.

Inquiries concerning rights for the commercial use of this invention should be addressed to the Patent Counsel, Langley Research Center [see page A5]. Refer to LAR-12645.

Detection of Tanker Defects With Infrared Thermography

IR scanner locates internal defects of LNG tank wall.

Langley Research Center, Hampton, Virginia

An infrared scanning technique for finding defects in the secondary barrier of a liquid natural gas (LNG) tank has been successfully tested on a ship under construction at the Newport News Shipbuilding and Dry Dock

Company. The company is currently building a number of LNG tankers to transport Algerian LNG to the east coast of the United States. These ships must be constructed with exact care because of the volatility and hazard-

ous nature of the fuel being transported. Langley Research Center was asked to assist in the detection of flaws by nondestructive methods to determine whether a defect existed in the secondary barrier of one tank of

the first ship of the LNG tanker class being built at the shipyard.

The secondary barrier was located inside the tank wall. The tank itself was already assembled inside the ship. Therefore, a nonstandard, non-destructive evaluation method was required. Probe techniques were found usable, but the large internal surface area of the tank together with the small size of the defects made such methods inadequate. Ultrasonic techniques using computer enhancement to detect defects and their locations were proposed but were found unworkable since normal random ship noise would null or obscure the noise caused by a slight diffusion leak.

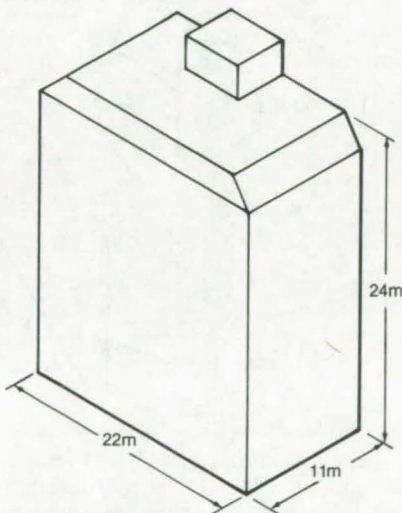


Figure 1. Rectangular LNG Tank with trapezoidal dome must be free of defects because of the hazardous nature of LNG.

The LNG tank is a rectangular structure with a trapezoidal-shaped dome, as shown in Figure 1, with walls of stainless steel corrugated for strength. The inside wall is shown in Figure 2. The inner wall of the tank has a layer of stainless steel (the primary barrier). The tank is tested to ensure that no cryogenic liquid can penetrate this layer, and all welds are finished, polished, and thoroughly examined to ensure leakproof conditions. There are additional layers of balsa, plywood, and insulation. The 3.4-mm plywood sheet is called the secondary barrier and forms a fuel-tight boundary between the stainless-steel wall and

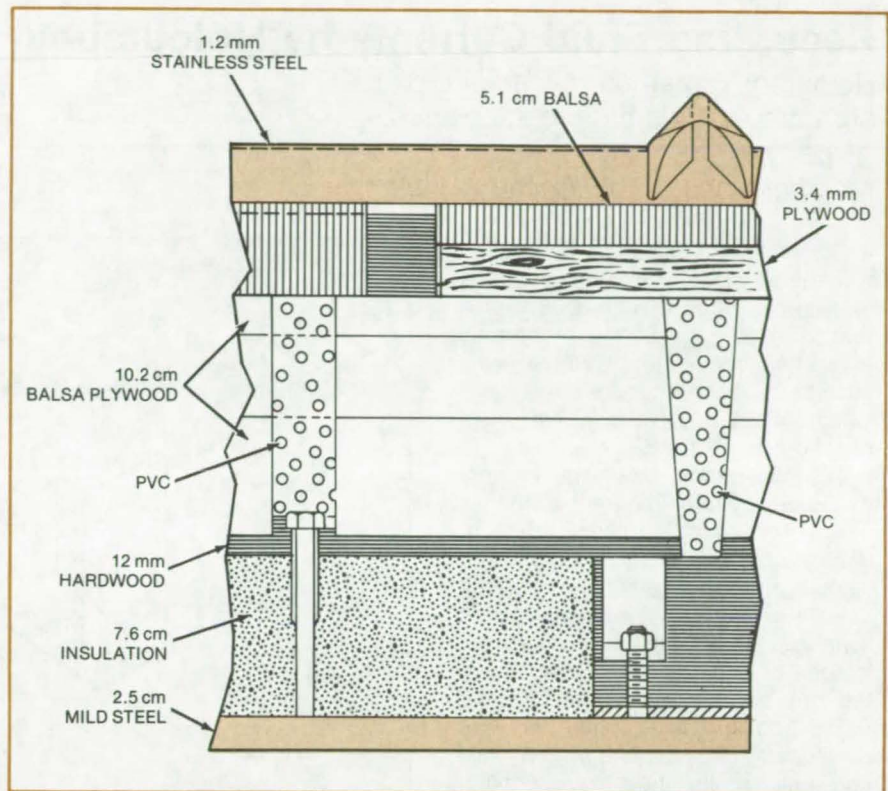


Figure 2. LNG Tank Wall consists of several layers that include steel and wood construction and insulation.

the outer mild-steel wall. The criteria for the tank to pass inspection require that neither the stainless-steel nor the mild-steel walls leak and that only a certain rate of diffusion of gas occurs across the secondary barrier.

The equipment used for the infrared scans is commercially-available AGA 680 camera systems with 8°, 25°, and 45° lenses. These systems operate over a spectral range of 3 to 5.6 μm using a liquid-nitrogen-cooled InSb detector; they have a temperature resolution of 0.2 K at 303 K. If the regions between the primary and outer barriers of the tank wall are evacuated and very cold nitrogen gas is inserted into the outer area (between the outer wall and the secondary barrier) while the primary barrier is observed with the infrared scanner, the secondary barrier leakage will show as a cold spot on the primary barrier. To accentuate this effect, the inner wall is heated to 310 K or greater using a large airhose to bring in hot air.

Several defects were found. Even though none of the holes detected

reached a total of integrated defect size of 2.5 cm in diameter in wall area of 1,280 m^2 , (the criteria for tank acceptance required no hole larger than 2.5 cm diameter, which was exceeded in this tank) the infrared system was able to resolve them because of the diffusion and spreading effect at the primary boundary. These defects were confirmed by the use of ultrasonic and thermometer probe devices. Needed repairs were made at these areas.

The infrared technique has proved itself an efficient method of determining defects in this application with minimal expenditure of time and manpower. These tests could be repeated during the life of the tanker and make more complicated testing unnecessary. The tests also confirmed that the tank did not have any major defects, and the tank was certified.

This work was done by Andronicos G. Kantsios of Langley Research Center. For further information, Circle 60 on the TSP Request Card. LAR-12655



Recording Fluid Currents by Holography

Holographic method reveals the paths of microparticles in time exposures.

Marshall Space Flight Center, Alabama

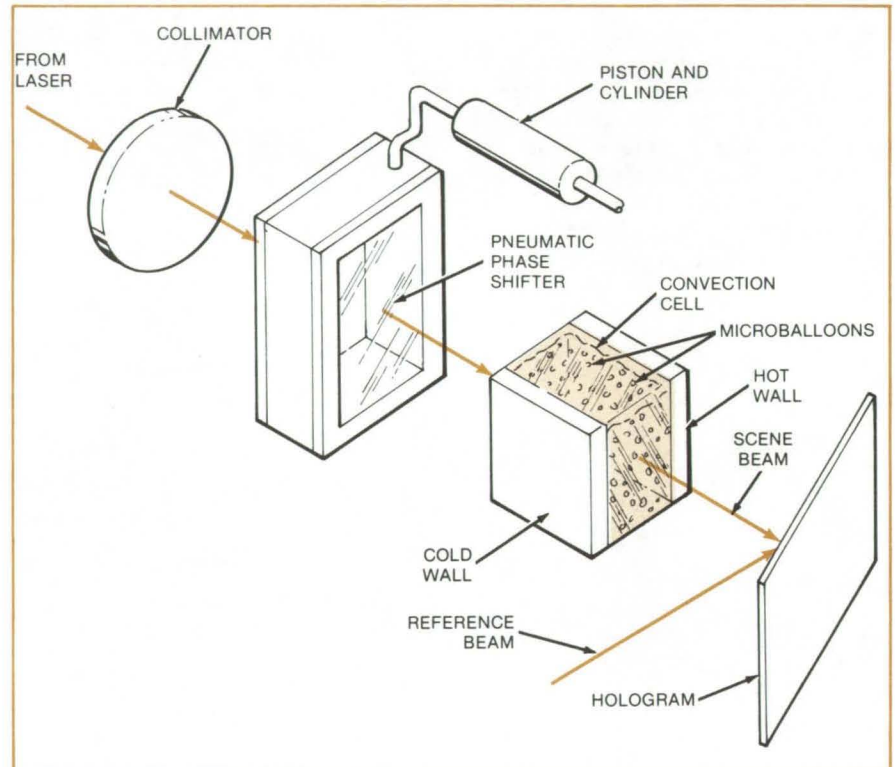
Convection in fluids can be studied with the aid of a holographic apparatus that reveals the three-dimensional motion of the fluid. The apparatus eliminates images of fixed particles such as dust on windows and lenses, which might mask the behavior of moving fluid particles.

The holographic flowmeter records multiple-exposure holographic images of "microballoon" particles intentionally introduced in the fluid. The velocity and direction of streams in the fluid are found by measuring the distances between reconstructed images of a particle and dividing by the time between exposures.

The holographic apparatus was developed for experiments on fluid convection cells under zero gravity. The principle is adaptable to the study of a variety of fluid processes — for example, electrochemical plating and combustion in automotive engines.

In the present form of the apparatus, microballoons (100- μm -diameter, neutrally-buoyant, hollow glass particles) are suspended in a water-filled cell that has four transparent plastic sides and two aluminum sides (see figure). One of the aluminum sides is heated while the other is cooled, so that convection currents are created in the water. A beam from a helium/neon laser passes through the cell and strikes a photographic film. A reference beam from the same laser also strikes the film, without passing through the cell. The two beams produce interference patterns that contain information about the positions of the microballoons in the cell.

The film is exposed four times; the first two exposures are separated by 2 seconds, the second and third by 8 seconds, and the third and fourth by 4 seconds. When the holographic image on the film is reconstructed, the multiple exposures show the successive positions of microballoons as they are moved by convection currents.



The **Key to Noise-Free Recording** of moving-particle positions is a shift in phase of the laser beam passing through the convection cell. Although simply rotating a glass plate from a plane normal to the beam will shift the phase, the proposed pneumatic phase shifter shown here would be more precise. Altering the pressure of the air in the shifter alters the phase of the light passing through it.

The velocities of the microballoons are computed from the distances between successive images and the known interval between exposures.

Between the second and third exposures, the beam passing through the cell is shifted in phase by 180° . This phase shift cancels images of fixed particles that may have been recorded on the film during the first two exposures. Without this background "noise," the moving particles are much easier to discern.

A simple glass microscope slide serves as the phase shifter. Rotation of the glass from a position normal to the scene beam to a new position 3° away from the normal changes the

path of the beam by $1/2$ wavelength, corresponding to a 180° phase shift.

In a planned phase shifter, the primary beam would be passed through an air cell before passing through the convection cell. The pressure in the air cell is varied by a piston, and the light passing through it is advanced or retarded in phase. A pressure change of 0.115 atmosphere ($0.16 \times 10^5 \text{ N/m}^3$) in a cell with windows separated by 1 cm is sufficient to shift the phase by 180° .

This work was done by Lee O. Heflinger and Ralph F. Wuerker of TRW, Inc., for Marshall Space Flight Center. For further information, Circle 61 on the TSP Request Card.
MFS-25373

Downhole Pressure Sensor

Pressure sensor for oil and gas wells is not affected by temperature.

NASA's Jet Propulsion Laboratory, Pasadena, California

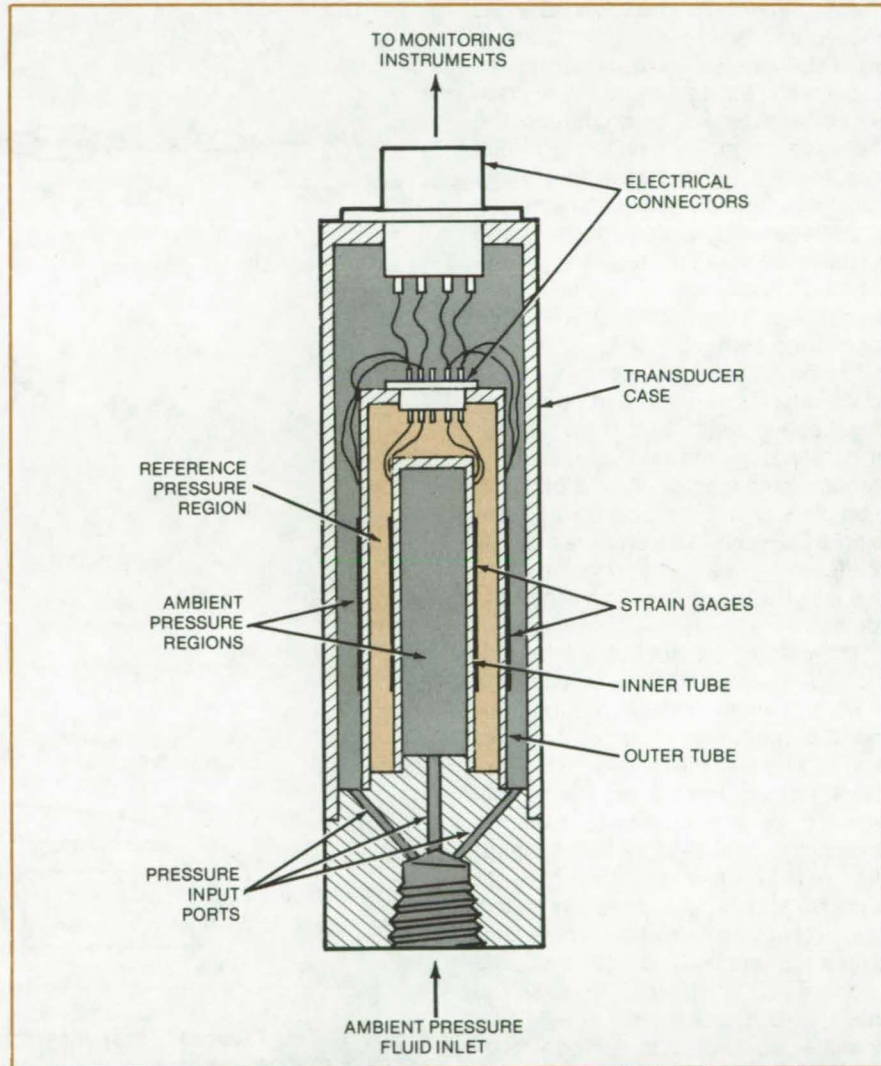
A proposed downhole pressure sensor remains accurate in spite of varying temperatures. Very accurate, sensitive, and stable downhole pressure measurements are needed for a variety of reservoir engineering applications, such as deep petroleum reservoirs, especially gas reservoirs, and in areas of high geothermal gradient.

Pressures in these applications may reach 15,000 psi ($103.5 \times 10^6 \text{ N/m}^2$), and instruments must measure pressure changes of less than 1 psi ($6.9 \times 10^3 \text{ N/m}^2$) occurring gradually over a period of weeks. The accuracy of conventional pressure sensors is too much affected by the relatively high temperatures (180° to 350° C) involved in the recovery of heavy oil.

The sensor has two concentric tubes made of the same material that contract and expand in opposite directions in response to pressure changes. The strain (see figure) difference is detected by strain gages mounted on each tube. Both tubes are mounted on a common base, and each is exposed to ambient pressure. Since the tubes have the same expansion coefficient, their relative motion is determined solely by the ambient pressure. Temperature changes affect both to the same extent, and the thermal effect is canceled.

If the ambient pressure is higher than the reference pressure, the outer tube contracts and the inner tube elongates; the ambient displacement produces twice the change of a sensor with a single tube. The opposite happens when the ambient pressure is lower than the reference. Small tube displacements are easily detected by the sensitive strain gages. These gages produce large indications for small pressure changes.

The electrical transducer for the sensor is a Wheatstone bridge with four active strain gages of the vacuum sputtered type. Since all four gages are



Proposed Pressure Sensor is unaffected by temperature changes. It utilizes strain gages to measure the downhole pressures in petroleum reservoirs. The inner and outer tubes are made of identical material and move in opposite directions in response to pressure. That doubles the displacement, making the instrument sensitive to relatively small pressure changes. The temperature effects are canceled because both tubes respond in the same way to any temperature change.

subjected to identical strains from temperature effects, bridge output is not altered as a result of the temperature changes.

This work was done by C. Martin

Berdahl of Caltech for NASA's Jet Propulsion Laboratory. For further information, Circle 62 on the TSP Request Card.

NPO-14729

Oceanic-Wave-Measurement System

An inexpensive system accurately records wave heights.

Marshall Space Flight Center, Alabama

A barometer mounted on a buoy has been proposed as a way of sensing wave heights. As wave motion raises and lowers the barometer, the pressure differential will be proportional to the wave height. A monitoring circuit samples the barometer output every half cycle of wave motion and adds the magnitudes of adjacent positive and negative peaks. The resulting output signals, proportional to the wave height, are transmitted to a central monitoring station.

The barometer as shown in Figure 1 is mounted on a mast and supported by a floating platform; e.g., a buoy or ship. Static air pressure is measured through small holes in a horizontal tube that is always pointed into the wind by a vane. The entire assembly rotates on a sealed bearing around a hollow shaft feeding into the barometer.

The electrical output of the barometer is coupled to the processing circuit shown in Figure 2. An integrating filter produces a flat response for signal periods in the range of 5 to 20 s, which is considered to be the normal range of periods for ocean waves in fully developed seas. After filtering, the signal passes through an amplifier/scaler that produces 1 volt per meter of wave motion. The scaler output is applied to positive and negative peak detectors. Each of these incorporates an operational amplifier connected to a diode feedback. The diodes are connected so that each detector responds only to its portion of the cycle.

As a wave rises, a signal is fed to a holding circuit comprising capacitor C_1 and resistor R_1 . This stored value, controlled by relay, is then applied to an isolation amplifier that feeds the signal to the differential amplifier. The latter combines the inputs from the positive and negative detectors to produce a signal corresponding to the peak wave height.

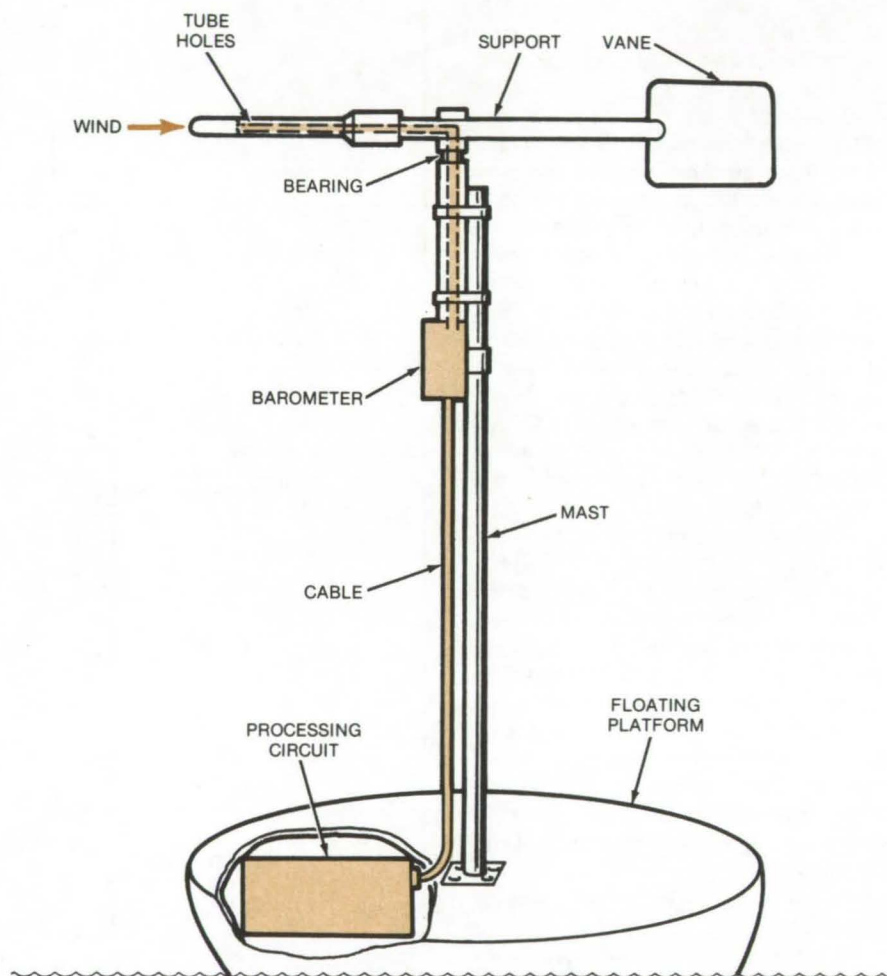


Figure 1. This **Proposed Wave-Measurement System** uses a barometer sensing pressure changes via holes in a tube pointed into the wind. Different air pressures are sensed as the platform is bobbing up and down with the waves. The signals are fed to an electronic processing circuit, which produces signals proportional to wave height.

Both peak detectors are timed by a circuit consisting of zero-crossing detector and Schmitt trigger. The zero-crossing detector responds only to the positive half of the barometer excursion cycle, activating the Schmitt trigger to produce a positive square-wave output with a period identical to the positive barometer cycle. The

Schmitt trigger output is fed to two inverting-amplifier branches, each connected to the respective detector relay. Each relay is alternately energized by its inverting-amplifier branch. For example, the positive detector relay is energized during the initial 10 percent of the positive cycle, as determined by the RC constant of the first

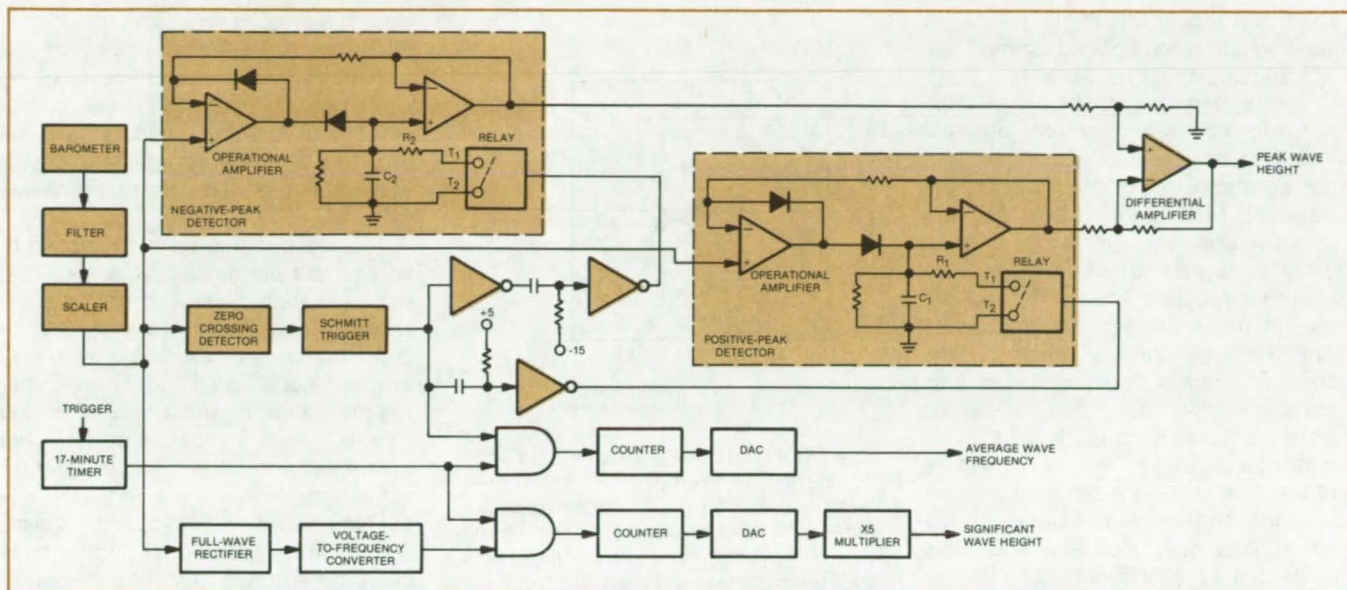


Figure 2. An **Electronic Processing Circuit** detects peak-to-peak barometer readings via positive and negative peak detectors. The detector outputs are synchronized by Schmitt trigger to produce peak wave-height output from the differential amplifier. The average wave frequency and significant wave height are processed by digital circuits shown on the bottom of the diagram.

amplifier branch, while the second relay is similarly energized during the trailing portion of the positive cycle via the double inverting branch. The storage capacitors are thus alternately discharged only during the short portion of the positive cycle, leaving sufficient time to recharge.

The average wave frequency is measured using a 17-min timer

feeding an AND gate. This input, combined with the Schmitt trigger output, is fed to a counter and digital-to-analog converter. Significant wave height is measured through a separate branch during the same 17-min period.

This work was done by John F. Holmes and Ronald T. Miles of Computer Sciences Corp. for

Marshall Space Flight Center. For further information, Circle 63 on the TSP Request Card.

This invention is owned by NASA, and a patent application has been filed. Inquiries concerning nonexclusive or exclusive license for its commercial development should be addressed to the Patent Counsel, Marshall Space Flight Center [see page A5]. Refer to MFS-23862.

Electrofluidic Accelerometer

Electrical sensors in a fluid measure thermal distributions caused by acceleration.

Langley Research Center, Hampton, Virginia

An electrofluidic accelerometer developed at Langley Research Center senses components of a linear or angular acceleration field and provides an analog signal as a direct function of each component. A typical application is as an active controlling element in an airplane autopilot.

Acceleration-measuring devices typically employ damped mass-and-spring systems to sense the acceleration; a strain gage, piezoelectric crystal, or optical sensors provide the output analog signal. Many devices are relatively complex and therefore

relatively expensive. Also, some conventional accelerometers are delicate and can be easily broken or thrown out of calibration. In contrast, an electrofluidic accelerometer is lightweight, small, inexpensive, rugged, and requires little power.

The figure shows the basic arrangement of a single-axis electrofluidic accelerometer. In this basic form, a hollow chamber contains a gas or liquid. Suspended within the chamber are two, identical, small, temperature-sensing devices. The two sensors are spaced a few diameters apart along

the housing axis, which is the sensitive axis for the device. A source of heat is required. This can be provided by a single, small filament midway between the sensors or by the sensors themselves if they generate heat as a byproduct of their operation, such as is the case with thermistors.

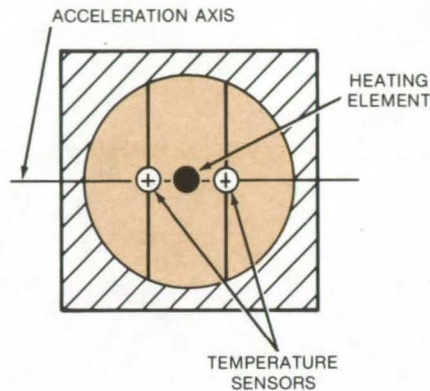
The illustrated arrangement is used to sense acceleration along a single axis. Additional pairs of sensors with properly oriented axes can sense other components of a linear acceleration field relative to the reference axes of the device. In the case of a
(continued on next page)

rotational acceleration field, two linear sensing devices spaced some distance apart could be used as a unit.

The primary function of the sensors is to detect the temperature gradient created by the influence of the acceleration field on the fluid. In the case of zero acceleration or zero effective gravity as might exist with an orbiting spacecraft, heat from the source is radiated and conducted into the fluid equally in all directions. Although the fluid closest to the source is much hotter and has less mass density than that at some distance, there is no tendency for this hotter fluid mass to move because all of the fluid is weightless.

If the sensor is accelerated, the hotter fluid near the heat source is subjected to a buoyant force in the direction of the acceleration because its mass reaction to the acceleration, or its weight, is less than that of the cooler and more dense fluid.

Therefore, the hotter fluid is forced away from the source in the direction of the acceleration, and the thermal gradient pattern is distorted. A finite output differential will be obtained



Electrofluidic Accelerometer consists of two temperature sensors in fixed equidistant positions on opposite sides of a heating element. The single pair of sensors shown above measures the temperature gradient in the surrounding fluid along a single axis. If the device is accelerated, the gradient changes because of the buoyant force on the hotter (thus lighter) portion of the fluid.

from a pair of sensors aligned with the direction of the acceleration. In the case of an acceleration directed along some intermediate axis, the output differential of the sensors will be proportional to the components of that acceleration aligned with the sensitive axis.

This accelerometer is composed of very simple elements and contains no moving mechanical parts. Its size, weight, complexity, and cost of construction appear to be relatively low. It could also be made very rugged, allowing it to be operated where a more delicately constructed instrument would be ill-suited.

Limited tests have shown this accelerometer will work. However, neither the operational limits have been determined nor the theory of operation been substantiated.

This work was done by Donald E. Hewes of Langley Research Center. No further documentation is available.

Inquiries concerning rights for the commercial use of this invention should be addressed to the Patent Counsel, Langley Research Center [see page A5]. Refer to LAR-12493.

Flashback-Free Combustor

All-zirconia construction prevents fuel in the supply line from igniting.

Langley Research Center, Hampton, Virginia

An all-zirconia combustion chamber for testing fuels prevents "flashback" — accidental extension of the flame into the fuel supply line. The chamber consists of a hemispherical injector on a base surrounded by a hemispherical cap (see figure). A fuel/air mixture feeding through the transition tube enters the chamber combustion cavity through 40 injector holes. The combustion products are exhausted through 25 holes in the cap. The cap has two additional ports for thermocouple and gas-sampling probes.

Previously, the injector was made of iron/nickel alloy or quartz. However,

these materials passed enough heat through the injector wall to ignite the fuel/air mixture within the injector, particularly at or near stoichiometric fuel-to-air ratios. The zirconia-injector thermal resistance prevents the flashback without special cooling procedures (such as diluting the fuel/air mixture with nitrogen).

The zirconia injector operates at higher temperatures and lasts longer than the quartz injectors (which were superior to the nickel-alloy version). Moreover, zirconia is not subject to solid-state diffusion to the same extent as the quartz. The two materials,

zirconia and quartz, tend to inter-diffuse when in contact at high temperature, which degrades the ultimate lifetime of the quartz injector.

The combustor base, cap, and injector are cast from commercial zirconia powder. The injector is cast in two split molds — one for the core and one for the external surface. The molded injector is cured at 1,800° F (980° C). It is then placed in the combustor hemisphere, and the complete combustor assembly is cured at 3,000° F (1,650° C).

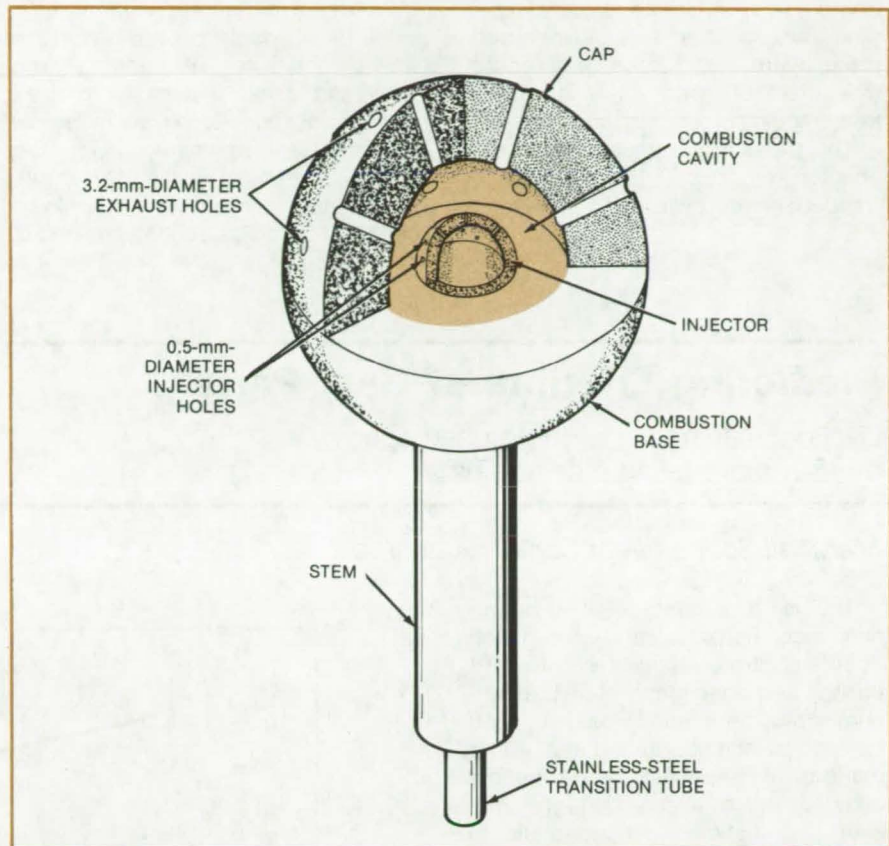
The combustor burns both gaseous and liquid fuels. Liquid fuels are

supplied from closed vessels pressurized with nitrogen and are mixed by adjusting the flow rates from the individual reservoirs. The liquids are atomized in nozzles located close to the combustor to prevent high-boiling-point fractions from condensing in the supply line.

The combustion-cavity flame temperature is measured by a traversing iridium/iridium-rhodium thermocouple. Gas samples are withdrawn for analysis through a water-cooled stainless-steel probe. The NO and NO_x contents of the samples are determined by chemiluminescence.

This work was done by Swen G. Anderson and Noel T. Wakelyn of Langley Research Center. Further information may be found in NASA TP-1472 [N79-28259/NSP] "Chemical Kinetic Modeling of Benzene and Toluene Oxidation Behind Shock Waves" [56]. A copy may be purchased [prepayment required] from the National Technical Information Service, Springfield, Virginia 22161.

Inquiries concerning rights for the commercial use of this invention should be addressed to the Patent Counsel, Langley Research Center [see page A5]. Refer to LAR-12666.



All-Zirconia Combustor used for testing various fuels prevents flashbacks in the fuel supply line. A fuel/air mixture enters the combustion cavity through holes in a hemispherical injector. Combustion products leave the cavity through holes in the hemispherical cap.

Measuring Radiation Effects on MOS Capacitors

Avalanche injection combined with current/voltage technique give a more complete picture about irradiation charging.

NASA's Jet Propulsion Laboratory, Pasadena, California

A major problem of interpreting the effect of ionizing radiation on MOS capacitors stems from the fact that it is difficult to distinguish between the charge at the Si/SiO₂ interface and the charge in the bulk of the oxide. Conventional current-voltage (CV) techniques could not resolve that difference and have led to conflicting reports that shifts of flatband and threshold voltages follow either a square or cube dependence on the oxide thickness. The distinction, however, becomes clearer using electron-avalanche injections to obtain independent information on charge trapping in the oxide.

The electron-injection technique serves as a powerful probe of the resulting trapped-hole distribution after irradiation because it was determined that the electrons only annihilate the trapped holes. Other effects, such as other electron traps and interface state generation, are negligible in the injection range used.

In the avalanche injection, the MOS capacitors are pulsed to produce avalanche breakdown in the depletion region of Si. This process generates energetic minority carriers that are injected into the oxide, surmounting the barrier at the Si/SiO₂ interface. The holes are injected from n-type Si and

the electrons from p-type Si. The voltage shift ΔV of the MOS CV curve due to the trapping of injected carriers is measured as a function of the total density of carriers injected per unit area.

The result for dry oxides indicates a distribution of dominant hole traps that tails off rapidly from the Si/SiO₂ interface with a characteristic distance between 150 and 200 Å (Wet oxides suggest a value of about 400 Å.) These results are consistent with results of previous etch-back photoemission studies.

A large set of data on the CV shift (in the form of effective sheet density of
(continued on next page)

charge) and interface state buildup near midgap is in qualitative agreement with the avalanche-injection measurements and analysis of the hole-trapping process in the oxide.

The trapping parameters for holes, and for electrons in the presence of trapped holes, have been measured

from a set of wafers with different oxide thickness processed under controlled conditions. The trap cross sections and densities indicate at least three trap species: (1) an interfacial species; (2) a dominant bulk species that is determined to tail off from the silicon interface; and (3) a third, lower density and cross-section species that

may be distributed throughout the bulk of the oxide.

This work was done by Mietek Bakowski, Richard H. Cockrum, Joseph Maserjian, and Nasser Zamani of Caltech for NASA's Jet Propulsion Laboratory. For further information, Circle 64 on the TSP Request Card. NPO-14700

Predicting Lifetime of Cast Parts

Cyclical loading tests on notched specimens at 78 K yield reliable design data.

Marshall Space Flight Center, Alabama

The life expectancy of cast aluminum machine parts can be predicted accurately from fatigue tests at 78 K on notched specimens of the aluminum alloy. The method was developed for rocket-engine turbopump parts made of high-strength, heat-treatable alloy with high silicon content; however, the technique is applicable to other aluminum-casting alloys.

The notched specimens produce test results that more accurately reflect actual part performance than do the smooth specimens previously used. In addition, the test data are far less scattered with the notched specimens. Design curves based on the test data predict the lifetime of a part for any stress state and mean stress, over the range of stress concentrations spanned by the data.

Specimens for the tests were taken from a sandcasting of a turbopump part and were machined and heat-treated like the part. A groove was cut around the specimen at its center (see figure). The radius at the bottom of the notch was selected to give the desired stress concentration. For example, with a 0.009-inch (0.229-mm) radius, the elastic stress concentration factor K_t is 3.5. The specimens were subjected to a sinusoidally-varying axial load until they fractured at the notch. The ratio of minimum to maximum alternating stress was -1 (that is, equal but opposite stress) for some specimens, 0 for others (stress alternated between zero and a maximum value without changing direc-

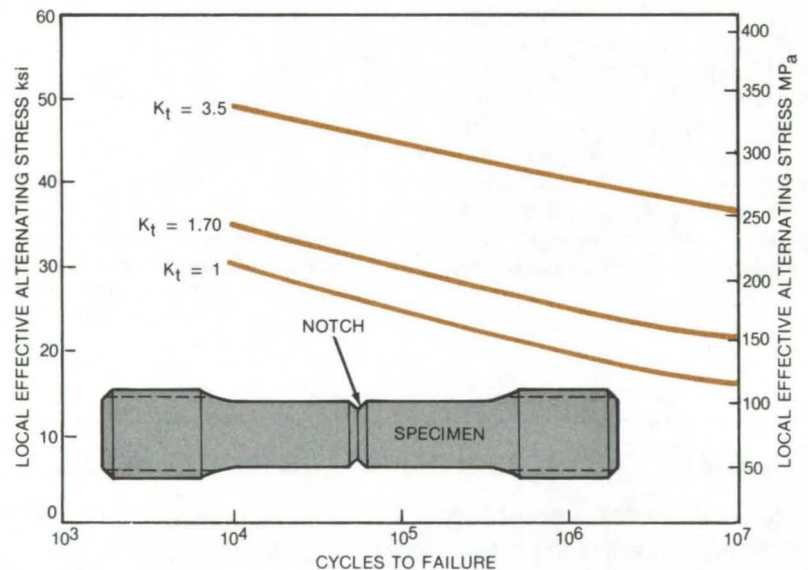
tion), and +0.5 for still others (the minimum stress was one-half the maximum). The specimens were cooled with liquid nitrogen to a temperature of -320° F (78 K) to accelerate failure and thus reduce the time required for the test.

The local effective alternating stress and the peak stress were calculated for each specimen from its geometry and loading. The results were plotted as stress versus cycles to failure.

The same procedure can be used to

develop similar plots for other parts. The only difference is that the notch radius should be altered to correspond to the stress concentration in the part. From such plots, a designer can readily observe the influence of stress and stress concentration on operating life.

This work was done by R. A. Cooper of Rockwell International Corp. for Marshall Space Flight Center. For further information, Circle 65 on the TSP Request Card. MFS-19549



Part Lifetime Increases With Decreasing Stress and Stress Concentration. In this plot, the ratio of minimum to maximum cyclical axial load is -1.0. The values of K_t represent stress concentration, with $K_t = 1$ being the value for an unnotched, smooth specimen.

Detecting Contaminants by Ultraviolet Photography

A simple technique could help prepare clean metal surfaces.

Marshall Space Flight Center, Alabama

The relatively high ultraviolet absorptivity of most organics as compared to metal is suggested as a basis for detecting traces of contamination. By photographing a metal surface in ultraviolet light, contaminants that might otherwise interfere with the adhesion of surface coatings, or with welding and brazing, could be detected and removed. Real-time monitoring of the cleaning process is also possible if an ultraviolet-sensitive television camera is used instead of photographic film.

Most adhesives, solvents, lubricants (except 100-percent aliphatic hydrocarbon oils), and other potential contaminants absorb radiation in the range from about 2,400 to 2,800 Å.

Skin oils as well as various polymers also have this property. On the other hand, metals such as aluminum strongly reflect radiation at these ultraviolet wavelengths. Consequently, an ultraviolet photographic print of a clear metal surface would appear white, and areas of organic contamination would show up as dark spots.

The method would use standard photographic techniques with quartz lenses for the camera. An ultraviolet floodlight would irradiate the area to be inspected.

In a variation of the technique, interference filters would be used to remove the visible spectrum, allowing parts to be inspected in daylight. The

sensitivity of the technique could be enhanced if short-wavelength ultraviolet is used and the detection system is tuned to pick up fluorescence at longer wavelengths. Many absorbers that do not fluoresce in the visible do fluoresce in the ultraviolet portion of the spectrum and would appear as bright spots on the film.

This work was done by David W. Neiswander of Martin Marietta Corp. for Marshall Space Flight Center. No further documentation is available.

Inquiries concerning rights for the commercial use of this invention should be addressed to the Patent Counsel, Marshall Space Flight Center [see page A5]. Refer to MFS-25296.

Detecting Surface Faults on Solar Mirrors

Two tests determine the quality of spherical mirrors.

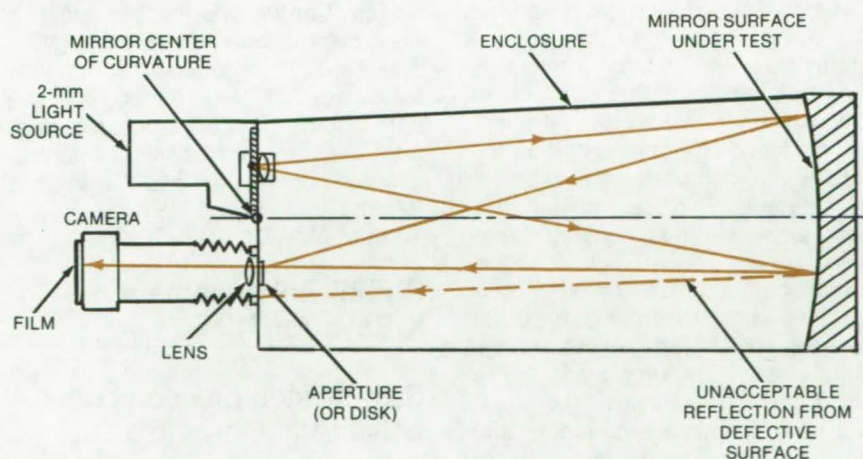
NASA's Jet Propulsion Laboratory, Pasadena, California

Two quality-control tests determine reflectivity and curvature faults of concave solar mirrors. These mirrors have relatively large radii of curvature anywhere from 10 to 500 ft (3 to 150 m) and concentrate solar energy to heat water boilers or other collector surfaces. Acceptable mirrors reflect between 85 to 95 percent of the incident solar energy and focus it into a "spot," or aperture, the size of the surface to be heated.

For economy, the mirrors are not fabricated with great precision, and they are tested without the sophisticated procedures used on high-quality optical-grade mirrors. However, to insure adequate quality control, special tests have been worked out for the production of these mirrors.

The first test, easily adaptable to mass production, tests the mirror reflectivity. A light source illuminates the entire mirror, and a photometer at

(continued on next page)



Curvature Defects in solar mirrors are easily revealed by photographing the mirror surface. A calibrated aperture placed in front of the camera lens admits rays reflecting only from acceptable areas of the mirror, blocking out the diverging rays reflected from the defective areas. The defects can pinpoint problems that may exist in production. The same photograph can be obtained using a calibrated disk instead of the aperture, except that, this time, only the defective areas would be exposed.

the mirror focusing point measures the reflected energy. The reflected intensity is compared with the incident.

The second test is used to study the rejected mirrors to identify possible faults in production. Curvature faults are detected by photographing the mirror surface or by examining it with the photometer. The mirror is mounted on a special frame at the end of a tunnel-like enclosure (see figure). A large-aperture camera and a light source are at the other end.

Light from a 2-mm source illuminates the entire mirror and is reflected

back into the camera. Rays reflected from a correctly curved surface pass at or near the camera axis; rays diverging from faulty surfaces enter through the edge of the camera lens or miss it entirely.

Some divergence is acceptable; e.g., a 3-min deviation from the "perfect" angle of reflection. A calibrated aperture or disk corresponding to acceptable deviation may be placed in front of the camera lens. If the aperture is used, rays reflecting from an acceptable surface will expose the film. The diverging rays will miss the

aperture, leaving unexposed areas on the film. A disk would do just the opposite, producing the same pattern but showing the unexposed areas as acceptable and the exposed areas as faults. An assortment of apertures or disks can be used in one test.

This work was done by Maurice J. Argoud, Michael S. Shumate, Walter L. Walker, and Richard A. Zantesson of Caltech for NASA's Jet Propulsion Laboratory. For further information, Circle 66 on the TSP Request Card. NPO-14684

Books and Reports

These reports, studies, and handbooks are available from NASA as Technical Support Packages (TSP's) when a Request Card number is cited; otherwise they are available from the National Technical Information Service.

Refraction Corrections for Surveying

A mathematical analysis for determining true range and elevation

Optical measurements of range and elevation angles are distorted by the refraction of Earth's atmosphere. Rather than following a straight-line path from source to target, light rays follow an arcing path that gives longer than actual range and larger elevation. The magnitude of the distortion increases with decreasing elevation.

A theoretical discussion of this effect, along with equations for determining exact range and elevation corrections, is presented in a new report. Potentially useful in optical site surveying and related applications, the analysis is easily programmed on a pocket calculator. Input to the equations is the measured range and measured elevation; the output is the true range and true elevation.

The measured data are inserted in a set of three nonlinear differential equations that are derived by applying Snell's law of refraction and assuming that the atmospheric modulus of refraction (1 minus the index of refrac-

tion) decreases exponentially with altitude. The solution of the equations, by Runge-Kutta integration, yields the true range and elevation.

The report includes examples of solutions to the equations and tables of short-, medium-, and long-range corrections. For a measured range of 10 km and a measured elevation of -0.239° , the range correction is 4 meters and the elevation correction is 0.36 milliradian. This translates into a displacement of about 4 meters along the line of sight and a displacement of 3.6 meters in altitude. At 100 km, the displacements are 40 m and 36.7 m, respectively.

This work was done by William M. Lear of TRW, Inc.; for Johnson Space Center. Further information may be found in TM-80803 [N80-10907/NSP], "Refraction Corrections for Surveying" [\$5]. A copy may be purchased [prepayment required] from the National Technical Information Service, Springfield, Virginia 22161. MSC-18664

Digital Enhancement of X-Rays for NDT

Step-by-step procedures for enhancing X-rays in nondestructive tests

A new report is virtually a "cook-book" for the digital processing of industrial X-rays. Computer techniques, previously used primarily in laboratory and developmental research, have been outlined and codified into step-by-step procedures

for enhancing X-ray images. Those involved in nondestructive testing should find the report a valuable asset, particularly if visual inspection is the method currently used to process X-ray images. Whereas the eye has only limited capability to distinguish shades of gray and tends to distort the data, a computer "sees" typically 256 gray shades, without introducing inadvertent distortion.

While no actual software is included in the report, many of the required image-enhancement programs are generally available. (Some are available through COSMIC; see page A8 of this issue of *NASA Tech Briefs*.) Others are described in the report along with their arithmetic statements and algorithms.

The report gives step-by-step procedures for applying the software. For example, the process for deblurring an X-ray to recover edge information and detail is to digitize the image through video averaging to increase the signal-to-noise ratio, then to filter the image through a high-emphasis filter to boost the high spatial frequencies on the original image.

Another example is the method for improving the visibility of image detail and minimizing the effects of some shading nonlinearities. The procedure involves: digitizing, filtering by using a high-pass filter that suppresses the low spatial frequencies, redistributing the gray levels in the filtered image for optimum presentation to the eye by using a contrast stretch filter, and filtering with a low-pass filter to attenuate slightly the highest spatial frequencies if excessive "graininess" exists.

Also included in the report are methods for removing random noise by using a low-pass filter, extracting only edge information utilizing a nine-point gradient, and displaying small gray-level variations using a density slicer routine. Other procedures are for improving the contrast of the X-ray or a particular feature of the X-ray by using a contrast stretch filter and for minimizing the effect of shading nonuniformity by the use of the ramp and background masks and the linear combiner.

All the procedures were successfully tested. The first example mentioned was used to analyze a blurred X-ray of a pump. The second example was used to reveal information about defects in a Space Shuttle solid rocket motor.

This work was done by Robert L. Butterfield of Kennedy Space Center. To obtain a copy of the report, Circle 67 on the TSP Request Card. KSC-11118

Design Considerations for Mechanical Face Seals

Two companion reports cover configuration and lubrication of the seals.

Two companion reports have been published that deal with design considerations for improving the performance of mechanical face seals, one of a family of devices used in the general area of fluid sealing of rotating shafts. One report deals with basic seal configuration and the other with lubrication of the seal.

Basic Configuration

Basically, a mechanical face seal prevents leakage of a fluid along a rotating shaft that passes through a housing or pressure vessel. Sealing is accomplished by a stationary (nonrotating) primary-seal ring that bears against the face of a mating ring (seat) mounted on the shaft. Axial loading, from the sealed pressure and from springs, maintains the contact between the primary ring and the mating ring. Sealing occurs at the primary-seal faces.

Four basic primary-seal assembly configurations and their parts nomenclature are identified: a rotating

primary ring with the sealed liquid at either the outside diameter (O.D.) or the inside diameter (I.D.) and a nonrotating primary ring with the sealed liquid at either the O.D. or the I.D. Occasionally, counterrotating and differential speed applications are encountered where both the primary ring and the mating ring are rotating.

The most common configuration, especially in pumps, is the rotating primary ring configuration. Its principal advantage lies in the relative ease of attachment to straight shaft sections without affecting the seal face alignment. The primary ring assembly is easily attached to the shaft by setscrews, friction fits, or similar means that assemble directly on a smooth shaft diameter.

Nonrotating primary ring configurations are often found in applications where space is limited or where the rotating speeds are high. The principal advantage of the nonrotating primary ring is the absence of centrifugal forces on both the primary and secondary rings.

The rotating primary ring with the sealed liquid at the O.D. has a number of advantages compared to the rotating primary ring with the sealed liquid at the I.D.: (1) centrifugal force tends to retard leakage; (2) centrifugal force tends to centrifuge solid particles away from the primary seal and springs; thus there is a tendency to be self-cleaning; and (3) the sealed pressure tends to put the seal rings into compression.

The rotating primary ring I.D. configuration has advantages in that it is easier to install; and in sealing corrosive fluids, the seal can be designed so that metal parts do not come into contact with the corrosive fluid.

Three basic secondary-seal assembly configurations are described: compression packings, automatic packings, and bellows diaphragm. The principal feature of the compression packing system is that it utilizes a mechanical load on the packing. Automatic packings are all of those packing rings and devices that are self-energized by the sealed pressure and do not normally require an auxiliary load to maintain sealing contact. Bellows diaphragms have no sliding packing surfaces, thus eliminating friction; they also eliminate the

need for separate springs since the bellows serves both the sealing and the face-loading functions.

The technique for seal pressure balancing and its application are described. The PV factor, an arbitrary mathematical relationship used to evaluate the severity of an application, is described and evaluated. Finally, the operating conditions for various applications of low-pressure seals and their failure mode are discussed.

Seal Lubrication

This report reviews the state-of-the-art of liquid-lubricated face seals and summarizes current thinking in regard to seal lubrication. Consideration is primarily given to that class of seals that operate on a full lubricating film.

Face seals operate with a fluid film separating the faces of the primary seals. Within this general class of lubrication there are four different modes of lubrication: Liquid Film Forces, either (a) hydrodynamic due to waviness and angular misalignment (low pressure) or (b) combined hydrodynamic and hydrostatic (low speed, moderate to high pressures); and Liquid/Vapor Film Forces, either (c) thermally induced phase change or (d) thermally induced phase change combined with hydrodynamic and hydrostatic forces.

The report also points out that the lubricating-film thickness is very small (in the range of 1 micron) and therefore small variations in the primary-seal geometry have a dramatic effect on the lubricating process. In general, these small variations in primary-seal geometry are due to unplanned effects of thermal gradients, pressure distortions, wear, etc., which complicate construction of seal performance models.

The report indicates that seal lubrication is a complex mechanism involving many possible primary-seal geometries, liquid vaporization, hydrodynamic forces, hydrostatic forces, inertia and secondary-seal friction. However complex, certain conditions must be met for satisfactory liquid film lubrication: (1) Balance of Axial Forces — the pressure in the fluid film (opening force) must equal the closing force; (2) Positive Axial Film Stiffness — a positive film stiffness is required for stable operation; that is, if the closing force increases for some reason (shock load, etc.), then an

(continued on next page)



increase in the opening force must accompany any decrease in film thickness; and (3) Balance of Moments — the restoring moment generated by the film must be sufficient to balance the moments due to secondary-seal friction, hydrostatic forces, etc.

Current thinking in regard to seal lubrication is reviewed: The effect of energy dissipation in the thin lubricating film separating the sealing faces is pointed out, and the results of vaporization due to heating are illustrated.

Also, hydrodynamic lubrication is reviewed, and an inherent tendency for the seal to operate with angular misalignment is shown. Recent work on hydrostatic effects is summarized, and the conditions for seal instability are discussed. Four different modes of seal lubrication are postulated with the particular mode strongly a function of speed and pressure.

This work was done by Lawrence P. Ludwig of Lewis Research Center and Harold F. Greiner of Sealol, Inc. Further information may be found in: NASA TM-73735 [N78-13439/

NSP], "Design Considerations in Mechanical Face Seals for Improved Performance, I. Basic Configurations" [\$5], and NASA TM-73736 [N77-33518/NSP], "Design Considerations in Mechanical Face Seals for Improved Performance, II. Lubrication" [\$5].

Copies of these reports may be purchased [prepayment required] from the National Technical Information Service, Springfield, Virginia 22161. LEW-13146

Computer Programs

These reports, studies, and handbooks are available from NASA as Technical Support Packages (TSP's) when a Request Card number is cited; otherwise they are available from the National Technical Information Service.

Regenerative Superheated-Steam Turbine Cycles

PRESTO program aids design and analysis of steam turbines.

One of the most important factors in the design of base-load or peak-load powerplants is an accurate analysis of the steam-turbine cycles involved. Several engineering options available in the design of steam-turbine cycles can significantly increase the generating efficiency of these powerplants. Of particular interest are the reheat and regenerative steam-turbine cycles that utilize the superheated steam normally available from large fossil-fueled steam turbines.

The PRESTO computer program was developed to analyze the performance of a wide range of steam-turbine cycles with special attention given to regenerative superheated-steam turbine cycles. PRESTO can be used to model standard turbine cycles, including such features as process steam extraction, induction and feedwater heating by external sources, peaking, and high back pressure. Expansion line efficiencies, exhaust loss, leakages, mechanical losses, and generator losses are used to calculate the

cycle heat rate and the generator output. PRESTO provides the power engineer with a flexible aid for the design and analysis of steam-turbine systems.

PRESTO calculates the expansion line efficiency as a function of volume flow, pressure ratio, initial pressure, initial temperature, and the governing-stage design. This expansion line calculation is used along with packing leakages, valve stem leakages, mechanical losses, exhaust losses, and generator losses to determine the heat rate and generator output.

The PRESTO user specifies the throttle steam thermodynamic properties, the preliminary conditions of the governing stage, system pressure relations, and condenser conditions, as well as the cycle configuration. PRESTO calculates the working parameters for the cycle and executes a performance analysis of the full steam-turbine cycle.

The PRESTO analysis is performed by an iterative procedure that calculates the system operating parameters. All iterations begin at the high-pressure end of the cycle and progress toward the condenser. The use of this iterative procedure allows PRESTO to handle easily such options as parallel or series external heat input, process steam extraction, regressive feedwater heating, and reheaters. PRESTO outputs include cycle heat rate, cycle efficiency, generator output, losses, and other useful system parameters.

This program is written in FORTRAN IV for batch execution and has been implemented on an IBM 360 with a central memory requirement of approximately 230K of 8-bit bytes. PRESTO was developed in 1979.

This program was written by L. C. Fuller and T. K. Stovall of Union Carbide Corp. for Lewis Research Center. For further information, Circle C on the COSMIC Request Card. LEW-13392

Stream-Tube Curvature Analysis

Pressure distribution and flow field at transonic speeds

The Stream-Tube Curvature Analysis Program accurately calculates the inviscid pressure distribution and flow field, including viscous displacement effects, around an arbitrary axisymmetric ducted body at transonic speeds. This computerized flow-field analysis predicts the transonic flow around long and short high-bypass-ratio fan duct nacelles with inlet and outlet flows having appropriate aerothermodynamic properties. The program makes possible parametric studies for evaluating nacelle design criteria and selecting configurations for further experimental investigations.

The inviscid solution technique used is based on a stream-tube curvature method. Engineers frequently rely on one-dimensional compressible flow relationships for a first-order solution to ducted flow. The stream-tube curvature approach is similar except that a number of confluent stream tubes, with slightly different properties, are added together to obtain the total flow in the channel. This method exactly satisfies the inviscid equations of motion in the limit as the size of the individual stream tubes approaches zero.

The program utilizes an automatic grid refinement procedure and solves the flow-field equations with a matrix relaxation technique. The location of incipient turbulent boundary-layer separation is identified when the calculated pressure gradients indicate sufficient cause. Due to its significance to performance predictions, a boundary-layer displacement calculation is coupled with the inviscid analysis.

A compressible turbulent boundary-layer solution is computed using the method of Stratford and Beavers, with turbulent separation predicted by the method of Stratford. Inclusion of these effects allows accurate evaluation of all nacelle forces. The user only needs to supply the program with configuration data, boundary coordinates, and channel flow properties. Program outputs include solution history, flow data, and boundary-layer data. The predicted pressure distributions have been favorably compared with through-flow nacelle test results obtained in wind-tunnel tests.

This program is written in FORTRAN IV and COMPASS for batch execution and has been implemented on the CDC CYBER 175 with a central memory requirement of approximately 108K (octal) of 60-bit words. The Stream-Tube Curvature Analysis Program was developed in 1972 and most recently updated in 1975.

This program was written by D. R. Ferguson and J. S. Keith of General Electric Co. for Langley Research Center. For further information, Circle D on the COSMIC Request Card.
LAR-11535

A Generalized Vortex Lattice Method

Aerodynamic load distributions are calculated for subsonic and supersonic flows.

The several variations of the vortex lattice method that are currently available have proved to be practical and versatile theoretical tools for the aerodynamic analysis and design of planar and nonplanar configurations. The success of the method is due in great part to the relative simplicity of the numerical technique involved and to the accuracy of the results obtained; however, most of the available procedures

are for subsonic flow applications. The VORLAX program was developed to incorporate a direct extension of the vortex lattice method into the supersonic flow regime, thus providing the analyst with a full flow-range capability.

VORLAX has the capability of calculating the aerodynamic load distributions at subsonic and supersonic speeds for arbitrary nonplanar configurations. It is also capable of the inverse process: namely, the computation of the surface warp required to achieve a given load distribution. Correlations with experimental data have shown good agreement in the overall force and moment coefficients due to lift and in the distribution of load coefficients.

If the discrete vortex lattice is considered as an approximation to the surface-distributed vorticity, the generalized principal part of the solution integral yields a residual term to the vorticity-induced velocity field. This term is incorporated into the velocity field generated by the discrete vortex lines, thus making the vortex lattice method valid for supersonic flows. Techniques for simulating nonzerthickness lifting surfaces and fusiform bodies with vortex lattice elements are included in the VORLAX program. Thickness effects of winglike components are simulated by a double (biplanar) vortex lattice layer.

Fusiform bodies are represented by a vortex grid arranged on a series of concentric cylindrical surfaces to simulate volume displacement effects and to compute surface pressure distributions accurately. A special technique was developed for the VORLAX program to perform the analysis of side-slip effects. The technique uses a combination of the skewed-wing approach and the skewed free-stream approach. The formulation utilizes a first-order perturbation solution, which does not involve the geometrical complications of the skewed-wing approach. Inputs to VORLAX consist of data including configuration geometry, free-stream parameters, and solution-control parameters. Outputs include vortex element locations, pressure coefficients, circulation strengths, and computational parameters.

This program is written in FORTRAN IV and COMPASS for batch execution and has been implemented on a CDC CYBER 175 with a central memory requirement of approximately 217K

(octal) of 60-bit words. The VORLAX program was developed in 1977.

This program was written by William M. Baker, Robert D. Elliott, and Luis R. Miranda of Lockheed Aircraft Corp. for Langley Research Center. For further information, Circle E on the COSMIC Request Card.
LAR-12636

Vibration Modes and Frequencies of Structures

Finite-element procedure for coupled mass and stiffness matrices

The program SUDAN, Substructuring in Direct Analysis, analyzes natural modes and frequencies of vibration of structural systems. Based on a direct method of analysis that employs a substructures methodology, the program is used with structures that may be represented as an equivalent system of beams, springs, and rigid bodies.

A finite-element stiffness technique, in combination with a lumped-mass method that allows nondiagonal masses, is used to generate the stiffness and mass matrices for each substructure in a system. User-written constraint equations are used to join analytically the mass and stiffness matrices of the substructures to form the coupled mass and stiffness matrices of the complete structure.

The resulting generalized eigenvalue problem is reduced to symmetric standard eigenvalue form and is solved for all the modes and frequencies of the system. Both the mass and stiffness matrices of the coupled system may be singular simultaneously, in contrast to the usual assumption that one or the other is nonsingular. The SUDAN program has been successfully applied to airframe-vibration analyses.

The program is written in FORTRAN IV and has been executed on CDC 6400/6600 and CYBER 173/175 computers. Only a relatively few changes would be required for conversion to other computers. Development of the public version of SUDAN was completed in 1978.

This program was written by Barbara J. Durling and Raymond G. Kvaternik of Langley Research
(continued on next page)



Center. For further information, Circle F on the COSMIC Request Card. LAR-12647

Predicting Propulsion-System Drag

Axisymmetric nozzle afterbody pressure distributions and drag are predicted at subsonic speeds.

The drag-producing components of an airplane propulsion system are usually installed in areas where the flow field is extremely complex. High body slopes and long boundary-layer runs, especially in the afterbody nozzle region, result in strong viscous effects on the boattail drag. The viscous nature of the jet-exhaust plume further complicates the flow in this region. Because of these strong viscous interactions, most methods used for predicting the installed propulsion-system drag are limited to empirical techniques.

The DONBOL computer program analytically predicts the axisymmetric nozzle afterbody pressure distributions and drag. The predictions are based on a Neumann solution for inviscid external flow coupled with a modified Reshotko-Tucker integral boundary-layer technique, the control volume method of Presz for calculating flow in the separated region, and an inviscid one-dimensional solution for the jet-exhaust flow. Comparisons with experimental data indicate that the program accurately predicts the pressure distributions of boattail afterbodies for which the jet-exhaust plume can be simulated by a solid body. For other configurations, the nozzle pressure drag seems to be significantly under-predicted. This method is limited to subsonic free-stream mach numbers below those for which the flow over the body becomes sonic.

The DONBOL program is based on the assumption that the flow is composed of a viscous layer near the body, an inviscid external flow, and if present, an inviscid jet-exhaust flow. A Neumann solution for incompressible flow, along with a compressibility correction, is used to determine the inviscid external flow.

The inviscid boundary of the jet-exhaust flow is calculated based on one-dimensional isentropic flow theory. Properties of the viscous boundary layer, both attached and separated, and the location of any separation on the nozzle boattail are calculated using the method of Presz, King, and Bateau. The concept of a discriminating streamline is used to avoid singularities in the boundary-layer calculations. However, the boundary-layer displacement thickness, the discriminating streamline shape, and the inviscid jet boundary are functions of the pressure distribution along the body and the jet boundary.

The final flow solution is obtained by iterating between the inviscid outer-flow solution, the inviscid jet-plume solution, and the viscous boundary-layer solution until a specified degree of convergence occurs. Inputs include body geometry, solution-control parameters, free-stream conditions, and jet-exhaust conditions. Outputs include detailed information on the iterative calculations of the flow field.

This program is written in FORTRAN IV for batch execution on a CDC 6600 computer and has an overlaid central memory requirement of approximately 76K (octal) of 60-bit words. The DONBOL program was developed in 1979.

This program was written by Lawrence E. Putnam of Langley Research Center. For further information, Circle G on the COSMIC Request Card. LAR-12619

Heat Conduction in Three Dimensions

Transient and steady-state solutions for complex geometries

A multidimensional heat-conduction program computes the transient temperature history and the steady-state temperatures of complex body geometries in three dimensions. Emphasis is placed on the type of problems associated with the Space Shuttle thermal protection

system, but the program could be used in the thermal analysis of most three-dimensional systems.

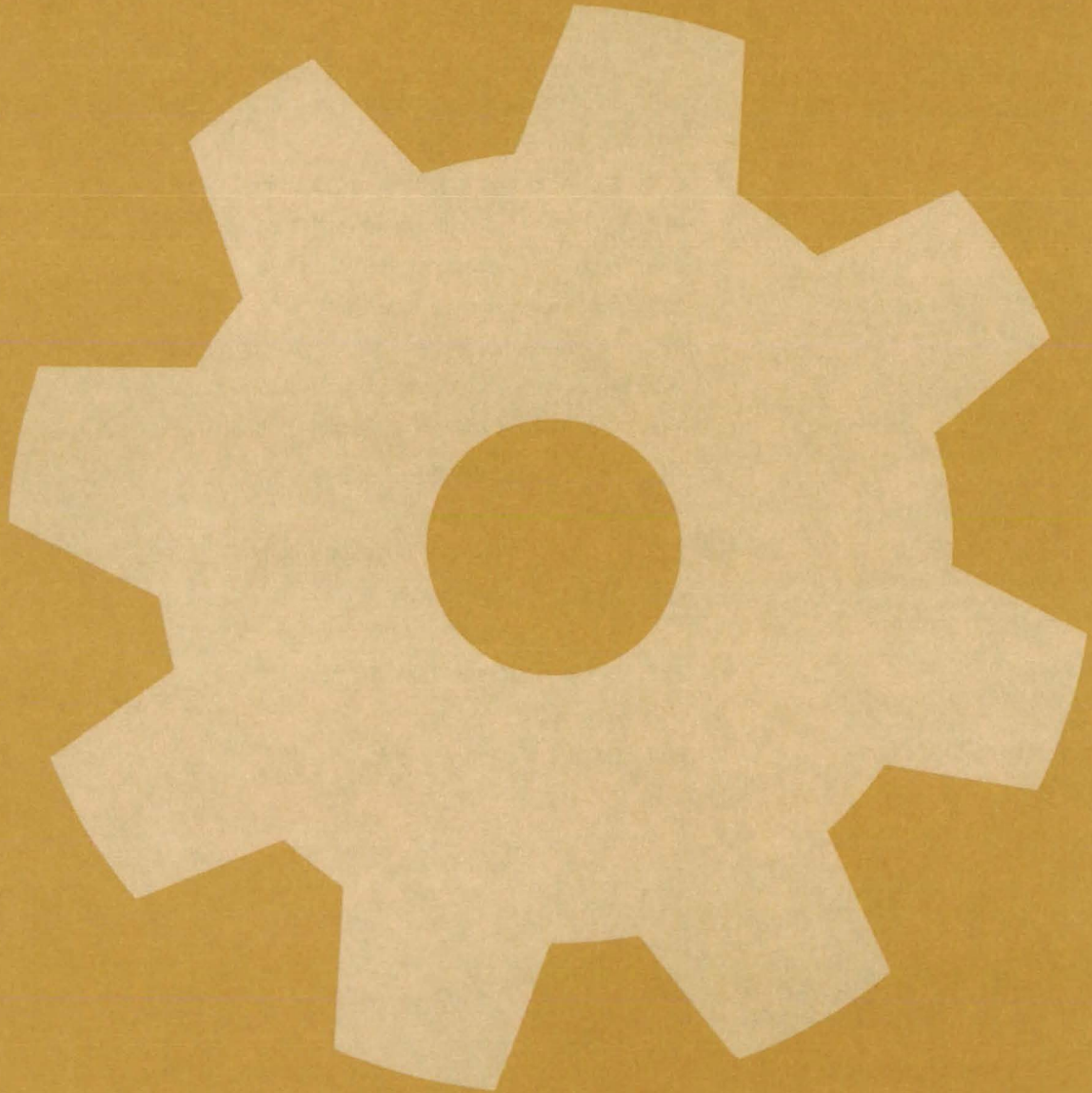
The thermal model is subdivided into sections, or nodes, to a level of approximation that yields the required accuracy. Inputs to the program consist of a geometrical description of the physical system, the material properties, and selected boundary conditions. The boundary conditions account for heat flux, reradiation, radiation interchange, convection, fixed temperatures, and phase changes. The program will accommodate a thermal model with as many as 500 nodes, 4,000 conductors, 3,600 radiation-interchange conductors, and 75 of each type of boundary condition.

The program solves the differential equations describing the transient and steady-state behavior of the model using finite-difference techniques. For the transient analysis, the user may select either a forward-difference method, a midpoint-difference (Crank-Nicolson) method, a backward-difference method, or an alternating-direction method to solve the governing equations numerically. For the steady-state analysis, a modified backward-difference method is available. Program outputs are in the form of temperature-versus-time histories for each section of the thermal model.

The heat-conduction program is available for IBM and CDC machines: The IBM version is written in FORTRAN IV and OS Assembler for batch execution and has been implemented on an IBM 370-series computer with a central memory requirement of approximately 450K of 8-bit bytes. The CDC version is written in all-FORTRAN IV for batch execution and has been implemented on a CDC CYBER 170-series computer with a segmented memory requirement of approximately 230K (octal) of 60-bit words. This heat-conduction program was originally developed in 1976, with the latest update occurring in 1979.

This program was written by Thomas M. Danza, Lloyd W. Fesler, and Richard D. Mongan of Rockwell International Corp. for Johnson Space Center. For further information, Circle H on the COSMIC Request Card. MSC-18616

Machinery



Hardware, Techniques, and Processes

- 213 Flared-Tube Attachment Fitting
- 213 Tube-Flare Inspection Tool
- 214 A Versatile Tunnel Acts as a Flexible Duct
- 215 Mechanical Hand for Gripping Objects
- 216 High-Performance, Multiroller Traction Drive
- 217 Locknut Preload Tool
- 218 Self-Adjusting Mechanical Snubbing Link
- 218 Bayonet Plug With Ramp-Activated Lock
- 219 Heat-Pipe Sensor for Remote Leveling
- 220 Automatic 35-mm Slide Duplicator
- 221 3-D Guidance System With Proximity Sensors
- 222 Automatic Connector Joins Structural Columns
- 222 Test Fittings for Dimensionally Critical Tubes
- 223 Electromechanical Slip Sensor
- 224 X-Ray Beam Pointer
- 225 Handtool Assists in Bundling Cables
- 225 Sleeve Puller Salvages Welded Tubes
- 226 A Linear Magnetic Motor and Generator
- 227 Cryogen-Storage-Tank Support

Computer Programs

- 228 Rotor Transient Analysis

Flared-Tube Attachment Fitting

Tubes are flared first, then installed, with a fitting that can be disassembled and reused.

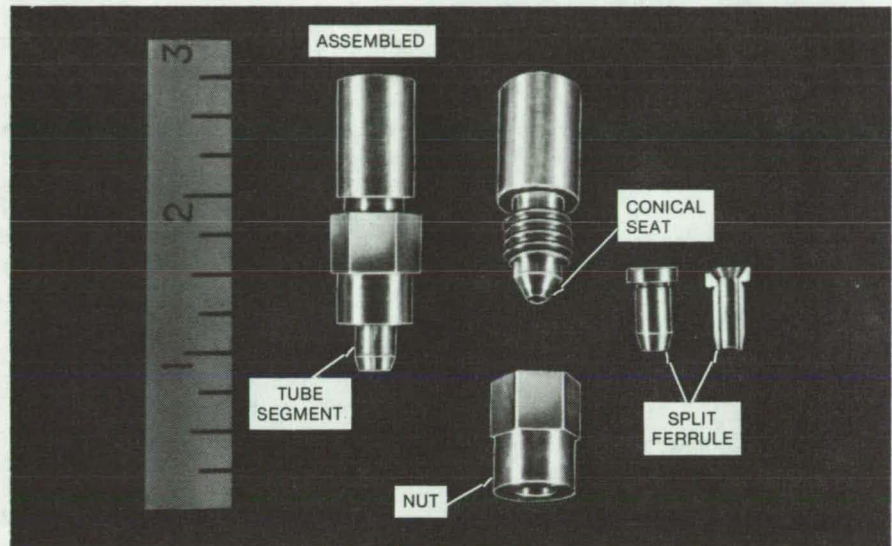
Lyndon B. Johnson Space Center, Houston, Texas

A new fitting for attaching flared tubing to valves and other flow-line components is installed after the tube is flared. In previous designs, the fitting is placed on an unflared tube, then the tube is flared, and finally the tube and fitting are attached to the mating end of the flow-line component.

The new design offers several advantages: First, it allows the installed fitting to be disassembled so that the parts can be inspected; second, the fitting can be salvaged intact and reused or replaced without damaging the flared tube; and third, the tube can be coated, tempered, or otherwise treated after it has been flared, rather than before, as was previously required.

This last feature is particularly valuable for the Space Shuttle entry-air data system, where a silicide-coated columbium tube is attached to the nose-cap penetration fitting. The silicide (mostly columbium silicide) is a ceramic-like layer. Since the brittle coating tends to crack when the tube is flared, it must be applied on an already-flared tube. The ability to disassemble and inspect the connection and coating after installation is also required in the Shuttle system.

As shown in the figure, the fitting consists of a threaded male portion with a conical seating surface, a hexagonal nut with a central hole, and a split ferrule. The conical seating surface is formed on the end of the valve or other component to which the tube is to be attached.



The **Flared-Tube Fitting** is shown assembled (left) and disassembled. The already-flared tube will be inserted through the hole in the hexagonal nut.

To connect the flared-tube end to the threaded male part, the nut is placed on the end of the tube and slid back along its length. The split ferrule is then nested over the flare and is held in place by hand. Finally, the flared end is placed over the conical seat, and the nut is moved into place and screwed onto the threaded male portion. The nut is tightened until the flare presses firmly against the seat.

A key feature of the new design is that the hole in the nut is larger than the outer diameter of the flared end of the tube. This allows the nut to be unscrewed and removed from the tube end when the fitting is disassembled. Also, there is no rubbing motion of the flared end against the seat as the nut

is tightened. Thus, the possibility of damaging a coated tube is reduced.

This work was done by Innis D. Alkire and Julian P. King, Jr., of Rockwell International Corp. for Johnson Space Center. For further information, Circle 68 on the TSP Request Card.

This invention is owned by NASA, and a patent application has been filed. Inquiries concerning nonexclusive or exclusive license for its commercial development should be addressed to the Patent Counsel, Johnson Space Center [see page A5]. Refer to MSC-18416.



Tube-Flare Inspection Tool

Self-aligning pins reveal the flare angle on an optical comparator.

Lyndon B. Johnson Space Center, Houston, Texas

A simple tool, consisting of two stainless-steel pins bonded to a rubber plug, checks flared tube ends for flare angle and symmetry. Its primary func-

tion is to inspect tubes before they are installed, thereby eliminating the expense and inconvenience of repairing leaks caused by imperfect flares.

Other possible uses are in measuring hole tapers, countersink angles, and bearing-face angles.

(continued on next page)

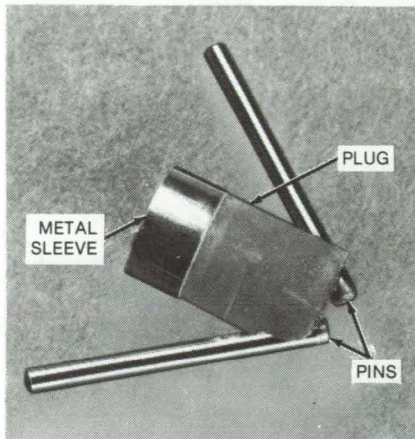


Figure 1. **Steel Pins on a Rubber Plug** conform to the flared end when the plug is inserted in a tube. The fixture dimensions for 1/4-in. (0.63-cm) tubing are: plug length, 1/2 in. (1.27 cm); plug diameter, 0.05 in. (0.13 cm) less than the maximum flare diameter; pin length, 0.75 in. (1.9 cm); pin diameter, 0.062 in. (0.16 cm); and centerline hole diameter, 0.025 in. (0.063 cm). The tool dimensions can be scaled for other tube sizes.

As shown in Figure 1, the two stainless-steel pins rest in slots 180° apart on one end of the plug. Each pin is bonded with rubber cement at an angle of 45° with respect to the plug centerline. A metal sleeve is slipped over the rubber to prevent it from splitting after repeated use.

To measure a flare, the tube is clamped in a V-block on the table of an optical comparator. The shaft of a holding fixture is inserted in the centerline hole of the plug, and the axis of the tool is aligned with the centerline of the tube. The comparator table is adjusted until the shadows of the tube and the tool are visible in the center of the comparator screen (Figure 2).

The rubber plug is gently engaged with the tube so that the rubber "gives" and the pins align with the flare. The shadow of the seated pins on the screen allows the operator to verify that the flare angle is within tolerance. To check for any eccentricity, the operator slightly loosens the clamp holding the tube in the V-block and slowly rotates the tube. The range of

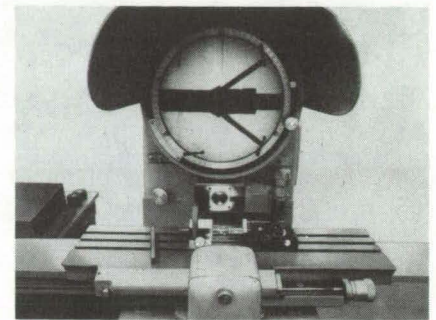


Figure 2. The **Shadows of the Pins** on an optical comparator screen reveal the angle of a flared tube.

movement of the pins is a measure of the symmetry of the flare.

The new tool does not demand any special operator skill. Only a few minutes are required for a measurement.

This work was done by Gerald E. Meunier of Rockwell International Corp. for Johnson Space Center. No further documentation is available. MSC-19636

A Versatile Tunnel Acts as a Flexible Duct

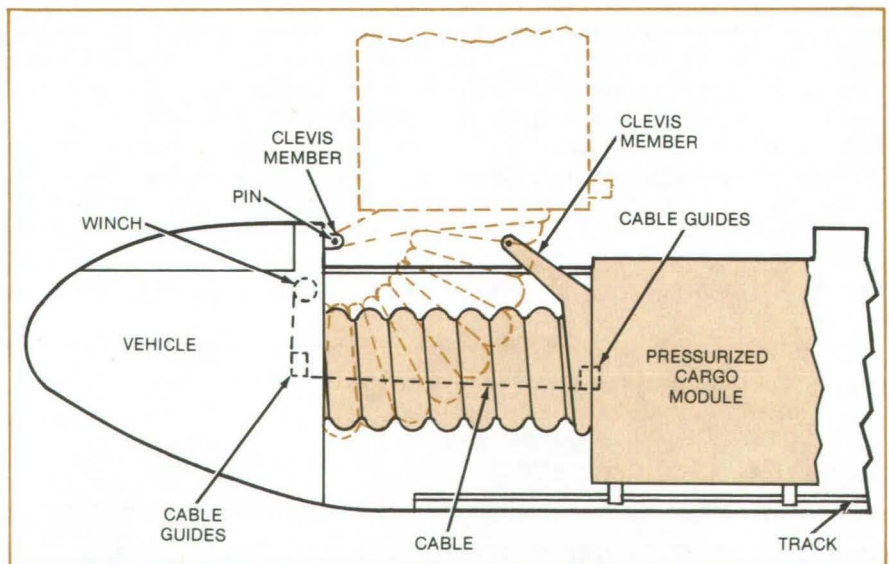
Tunnel duct can be expanded, contracted, and bent

Marshall Space Flight Center, Alabama

A tunnel activated by a cable assembly can be expanded, contracted, and bent similar to a flexible duct without uncoupling at either end. The tunnel was developed to join a reusable space vehicle with a cargo module and could be modified to be used as a hydraulic or a pneumatic hose or duct connecting complex moveable joints in remote manipulators and earth-moving machinery.

Two sets of equal-length cables operated by a single winch control the tunnel length. The cables, guided through rings and pulleys, move in unison regardless of the way the tunnel is deployed.

As shown in the simplified illustration, the tunnel is a bellows tube structure sealed to the module and the vehicle, and the cables run inside it. The module slides on the vehicle tracks and is normally attached to the vehicle by pins inserted through clevis members.



Flexible Tunnel joining a space vehicle with a pressurized cargo module can be contracted, expanded, or bent. The tunnel is inflated by air pressure, its length being controlled by a set of cables. It can be deployed in a straight line or at an angle, depending on how the cargo module is attached to the vehicle.

If the module is deployed in a straight line as shown in the figure, the pins are disconnected, and the cable is paid out. The cables loose, differential pressure (about 1 atm) applied from the module then inflates the tunnel to its maximum length. The tunnel length can be controlled by restraining forces of the cable system.

If the module is to be deployed above the vehicle, the cables are wound up to contract the tunnel until the clevis fixtures align and the

module is secured to the vehicle. The cables are again paid out, and the differential air pressure forces the cargo module upward over the vehicle.

The tunnel and its mechanism might also find applications in the airlines and marine industries. The design could be modified for underwater work.

This work was done by Newton D. Brown, Nicholas C. Costakos, and Gordon L. Jeppesen of Goodyear

*Aerospace Corp. for **Marshall Space Flight Center.** For further information, Circle 69 on the TSP Request Card.*

This invention has been patented by NASA [U.S. Patent No. 3,952,976]. Inquiries concerning nonexclusive or exclusive license for its commercial development should be addressed to the Patent Counsel, Marshall Space Flight Center [see page A5]. Refer to MFS-22636.

Mechanical Hand for Gripping Objects

Remotely operated end effector can grip objects of different sizes and shapes.

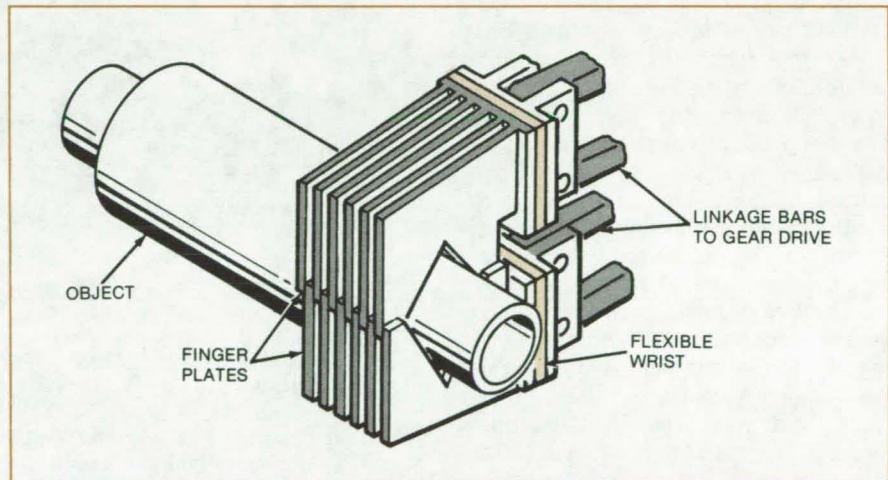
Marshall Space Flight Center, Alabama

An improved end effector serves as a "hand" for a remote-manipulator spacecraft system to grasp objects of various sizes. The device has a built-in flexible wrist-joint "cartilage" for increased gripping force without significant strain on the mechanical connections.

Two identical jaws are used to grip objects (see figure). Each jaw has a set of laterally-spaced finger plates. The plates of one jaw are set off from the other so that they intermesh when the jaws are closed. An object is held by V-shaped notches running across each jaw. These notches allow objects as small as a wire or as large as the notch to be gripped firmly.

Each jaw is driven by a pair of parallel linkage bars coupled to the corresponding wrist joints by a pair of spaced pivots. The pivot support plate is separated from an integral finger backplate by a flexible material such as synthetic rubber. This material, held to the plates by rivets or brads, forms the flexible wrist joint.

The opposite ends of the parallel linkage bars attach to a pair of spaced plates enclosing a gear mechanism. Each inner linkage bar is rigidly joined to a gear plate, and the gear plates



This End Effector has interlocking finger plates to grip the object. The end effector can grasp objects as small as wires and up to the size fitting the V-notches.

mesh with a bevel gear driven by an electric motor directly behind.

The end effector is guided toward a target object by a mechanical arm linked with the central control station. The object is approached with the jaws widely open. Once the jaws are aligned with the object, the bevel gear is activated to close the jaws.

This work was done by Keith H. Clark and James D. Johnston of

Marshall Space Flight Center. For further information, Circle 70 on the TSP Request Card.

This invention is owned by NASA, and a patent application has been filed. Inquiries concerning nonexclusive or exclusive license for its commercial development should be addressed to the Patent Counsel, Marshall Space Flight Center [see page A5]. Refer to MFS-23692.



High-Performance, Multiroller Traction Drive

High power at large gear ratios
using sun-and-planet drives

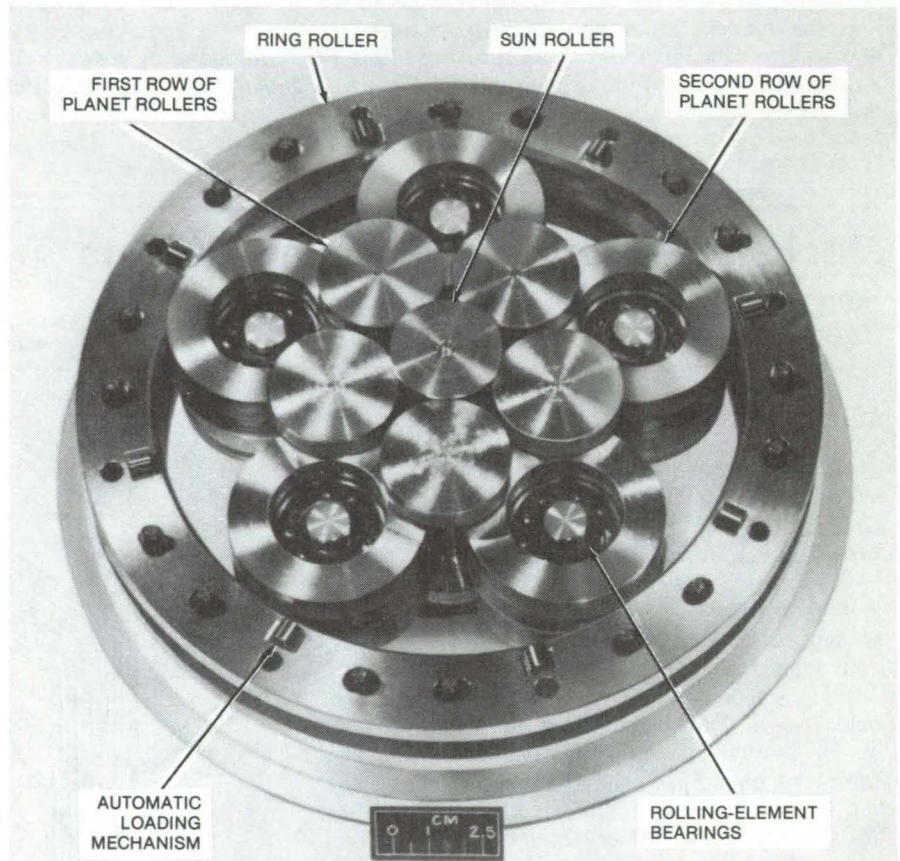
Lewis Research Center, Cleveland, Ohio

A fixed-speed-ratio traction drive (NASVYTRAC) has been developed that can transmit high power across a large speed ratio using a compact cluster of rollers. This traction drive transmits power without gear teeth, through shear forces on the thin lubricant film that separates the drive rollers. An automatic loading mechanism regulates the normal load between rollers so that sufficient normal load is present to transmit the required torque without slip or overloading.

The traction drive, shown in the photo consists of a single-stage planetary roller with two rows of five stepped planet rollers contained between the concentric sun and ring rollers. Either the sun roller or the ring roller may act as the input or output member. Reaction torque is carried to the housing by a pair of rolling-element ball bearings installed in the second (outer) row of planet rollers. The first (inner) row of planet rollers and the sun roller require no bearings, so that the number of total drive bearings is greatly reduced. Furthermore, the reaction torque bearings are located in the optimum position, the outer planet-roller row, where the reaction forces and operating speeds are relatively small. The ring-roller assembly is positioned by its contact with the second row of planet rollers and is splined to the low-speed input/output shaft.

Because the planet rollers in the drive are in three-point contact with adjacent rollers, the roller cluster has a high degree of stability: The first row of planet rollers and the second row of planet rollers (to the extent of bearing internal clearance) will shift under load until a nearly-ideal force balance is established. Consequently, slight mismatches in roller dimensions or housing distortions under load or thermal gradients will have little effect on drive performance other than to cause a slight change in roller orientation. This greatly simplifies manufacturing tolerances.

The number of planet-roller rows, the number of planet rollers in each



Test Drive consists of a single-stage planetary roller with two rows of five stepped planetary rollers contained between concentric sun and ring rollers.

row, and the relative diameter ratios at each contact are variables to be optimized according to the overall speed ratio and the uniformity of contact forces. In general, drives with two planet rows are suitable for speed ratios to about 35 to 1, and drives with three planet rows are suitable for ratios to about 150 to 1. The input or output member can be either the ring or the central roller depending on whether the speed is to be increased or decreased.

Although conventional oils can be used, traction fluid is preferred to lubricate and cool the rollers and to transfer torque. The traction fluid used is a synthetic, high-traction cycloaliphatic hydrocarbon fluid. The traction coefficient of the fluid is approximately 50 percent greater than conventional mineral oils, which

permits a smaller drive to be used. The traction fluid readily becomes a glassylike substance as it is forced between the rollers under high pressure and therefore can transmit a large amount of traction without the rollers actually touching. At the same time, the lubricant forms a protective elastohydrodynamic film that separates the rollers and almost completely eliminates roller wear. This lubricant film, together with the multiple roller elements in highly loaded contact between the flexible ring and the sun roller, provides excellent torsional vibration damping characteristics and promotes quiet performance.

In comparison with conventional transmission gearing, this new traction drive provides large reduction ratios (up to 150:1) at high speeds in a

single stage without differential action. This is unlike conventional gears that require a series of multiple gear meshes. The NASVYTRAC drive can be constructed to transmit 500 horsepower and higher and is quite capable of operating at speeds to 400,000 rpm (roller surface velocities greater than 50,000 fpm). The practical upper speed limit is generally dictated by the other driven or driving mechanical components (bearings, seals, couplings, etc.) in the system.

Parametric tests on a 14.7-to-1 ratio NASVYTRAC drive at speeds to 73,000 rpm showed peak efficiencies

in excess of 95 percent. This compares quite favorably with conventional multistage gearing at equivalent speeds.

The NASVYTRAC drive is capable of transmitting in excess of 7 horsepower per pound of transmission weight, compared to today's best gearboxes, which transmit approximately 4 horsepower per pound.

This work was done by S. Lowenthal, D. A. Rohn, and E. Zaretsky of **Lewis Research Center**, N. E. Anderson of the U.S. Army Research & Technology Laboratories, and A. Nasvytis of **Transmission Research, Inc.** Further

information may be found in NASA TP-1378 [N79-13369/NSP], "Performance of a Nasvytis Multiroller Traction Drive" [\$4.50]. A copy may be purchased [prepayment required] from the National Technical Information Service, Springfield, Virginia 22161.

Inquiries concerning rights for the commercial use of this traction drive should be addressed to NASTEC, Inc., Mr. Richard C. Klein, President, 1700 Ohio Savings Plaza, 1801 East Ninth Street, Cleveland, Ohio 44114, Telephone: [216] 696-5157. LEW-13347

Locknut Preload Tool

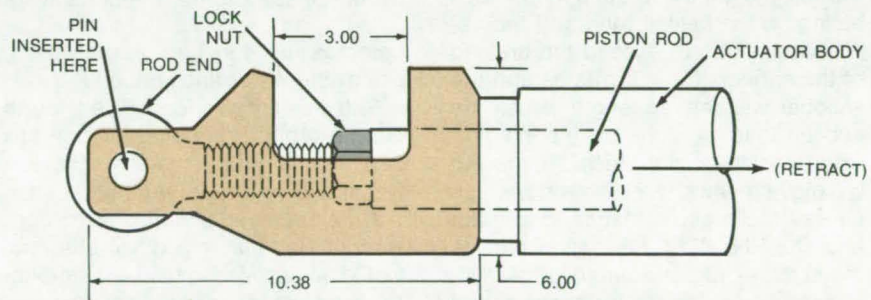
A small tool replaces a large torque wrench for turning locknuts.

Lyndon B. Johnson Space Center, Houston, Texas

Massive locknuts that fix the stroke of hydraulic actuators on the Shuttle engines could previously be turned only with a very large torque wrench — one that could supply the required 1,500 ft-lb (2.0×10^3 N-m) moment. With the assistance of the simple sleeve-like tool shown in the figure, however, it now takes only about 150 ft-lb (199 N-m) to loosen the nuts, a torque small enough to be supplied by more common hand wrenches. Other advantages, such as reduced cost and weight, the ease of manipulation in the cramped space near the actuators, and portability, are also realized with the new tool.

Basically, the preload tool takes advantage of the hydraulic force of the actuator to "stretch" the threaded rod on which the locknut turns. This relieves some of the force on the nut, reducing the amount of torque needed to turn it.

As shown in the figure, the locknut fixes the stroke length of the actuator piston. (The actuator is one of two that control the orientation of each Shuttle engine.) To change the stroke length, the nut is loosened, the rod end is turned, and, when the proper length is set, the nut is retightened.



The **Preload Tool** fits over the rod end, as seen in this simplified drawing of the Shuttle actuator. When the piston rod is retracted, the threaded rod stretches, relieving some of the pressure on the locknut. The nut can then be turned by a small wrench through the cutout slot.

To turn the tightened nut, the preload sleeve is placed over the rod end, which has been removed from its clevis on the engine mount. The actuator is then gradually pressurized (retracted or extended) until the hole in the preload tool aligns with a hole in the rod end bearing. Finally, a pin is inserted through the aligned holes.

With the preload tool in place, the actuator is pressurized in the retraction direction. Since the rod end is pinned to the preload tool, the piston

rod cannot move; and the rod stretches, relieving some of the pressure on the locknut. A small wrench inserted through the slot on the tool turns the nut, while a second wrench holds the piston rod to prevent it from turning.

This work was done by John E. Greenwood and Jerome F. Kauppi of **Rockwell International Corp.** for **Johnson Space Center**. No further documentation is available. MSC-16153



Self-Adjusting Mechanical Snubbing Link

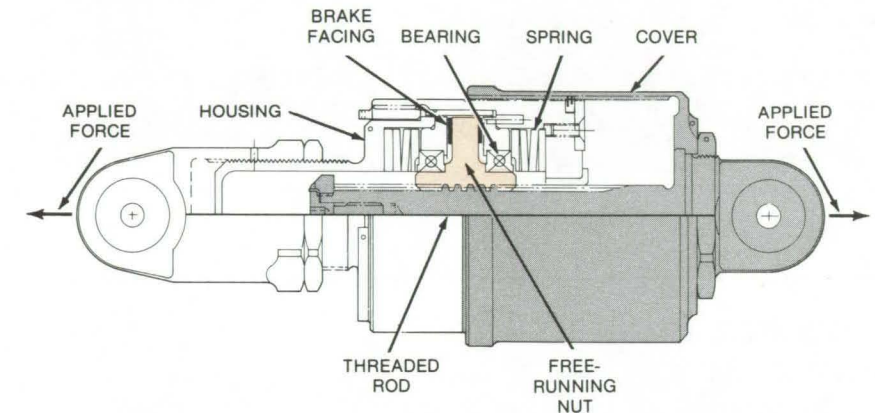
An all-mechanical shock-absorber concept has several advantages over hydraulic devices.

Lyndon B. Johnson Space Center, Houston, Texas

A proposed purely-mechanical load-support link will automatically adjust its length under light loads when the relative motion is slow. It will automatically lock at any position when the onslaught (acceleration) exceeds the design limits for which the link is set. The device will not leak oil or require periodic servicing and inspection common to hydraulic shock absorbers (snubbers).

The concept (see figure) consists of a threaded rod and a free-running nut. The nut is supported between two anti-friction bearings held in position by two opposing preloaded springs. The nut flange has brake surfaces on each side, which are positioned just to clear the mating surfaces of the housing.

When opposing loads are applied to the link, the nut will rotate due to forces acting on the helical thread. If the applied loads do not exceed the preload of the springs, the nut rotates and the snubber will change length. When the applied load exceeds the spring preload (tension or compression), the nut will move relative to the housing, which causes the brake surfaces to contact and stop the nut. This action causes the snubber to act as a solid link. Different lockup forces for tension and



All-Mechanical Snubbing Link utilizes a threaded rod and a nut that rotates under applied low-magnitude loads. Under high loads, the nut moves left or right relative to the housing, until one brake surface bears against the facing surface. With the nut prevented from turning, the mechanism acts as a solid link. In a snubber proposed for the Space Shuttle, the preload springs are 500-lb (2,220-N) disk springs.

compression can be incorporated by using different spring preloads.

The design was conceived for the Shuttle orbiter, requiring support links between structural panels. The links would allow normal thermal, mechanical, or pressure deflections to occur without high loading. When one panel would be exposed to high acceleration, the links would lock rigidly and transmit

loads to other panels without free play.

The concept might be incorporated as a safety device on material handling systems or as an energy absorption device or a governor for machines or equipment.

This work was done by Earl V. Holman of Rockwell International Corp. for Johnson Space Center. No further documentation is available. MSC-16134

Bayonet Plug With Ramp-Activated Lock

Plug and ramped washers are an effective lock at high temperatures.

Lyndon B. Johnson Space Center, Houston, Texas

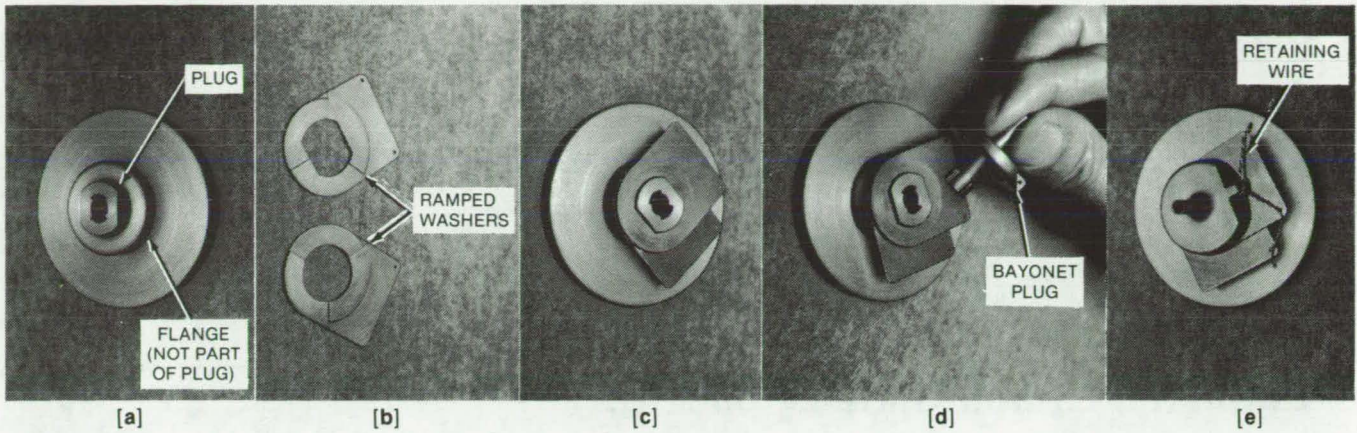
A matched pair of washers with broad surface ramps is the locking mechanism in a new bayonet plug. It can be used where threaded fasteners and springs are impractical because of extreme temperatures or other environmental incompatibility.

The prototype locking mechanism was made for attaching silicon carbide-coated columbium tubes,

which are subjected to temperatures up to 2,600° F (1,427° C) on the Space Shuttle nose cap. At such temperatures, it is difficult to retain complex shapes, such as thread forms. Typically, the silicon carbide coating cracks at the peaks and valleys of the threads, and the substrate columbium is attacked by oxidation. In contrast, the coating on

the broad-surface ramps of the washers is much less susceptible to cracking.

The figure shows the plug fastened to a stepped flange that simulates a portion of the Shuttle nose cap. In (a) the main body of the plug extends through a hole in the flange. A lip (not visible) on the lower surface of the plug matches a bevel on the bottom of



A **Bayonet Plug With Ramped Washers** locks at high temperatures that would deteriorate threaded fasteners. The plug was developed for attaching static-pressure probe tubes to the nose cap of the Space Shuttle. A lip on the inner plug holds the plug in place from below (the lip is not visible in these photos).

the flange. The matched pair of ramped washers shown in (b) is placed on the plug in (c), and in (d) the bayonet is inserted.

The inner slot of one washer matches the contour of the plug; this washer is stationary. The inner slot of the second washer is circular. When

the second washer is rotated, the washers push against the bayonet plug, locking it in place. A retaining wire (e) secures the plug.

This work was done by Kenneth E. Wood of Rockwell International Corp. for **Johnson Space Center**. For further information, Circle 71 on the

TSP Request Card.

This invention is owned by NASA, and a patent application has been filed. Inquiries concerning nonexclusive or exclusive license for its commercial development should be addressed to the Patent Counsel, Johnson Space Center [see page A5]. Refer to MSC-18526.

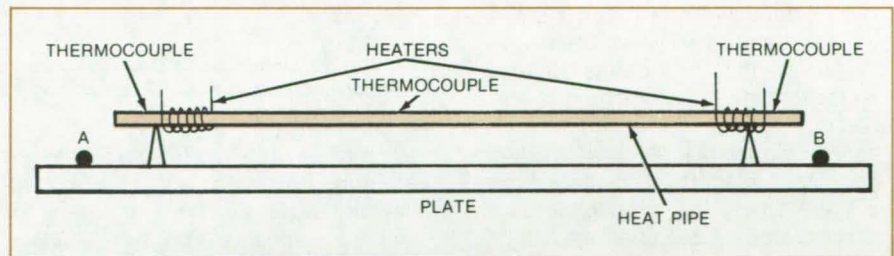
Heat-Pipe Sensor for Remote Leveling

A new system gives level readings in remote locations.

Goddard Space Flight Center, Greenbelt, Maryland

A heat-pipe sensor system permits remote leveling in inaccessible areas without actually "seeing" the object in question. Three thermocouples, on the ends and the middle of the heat pipe, are used to measure temperature differences that arise when the pipe is tilted. When the platform on which the pipe is resting is leveled, the three thermocouple recordings are identical. When the readings are unequal, the platform is leveled by remote control until the readings are identical. The sensor was successfully used on the International Ultraviolet Explorer satellite.

A conventional heat pipe with an axially grooved interior wall is used with ammonia as the working fluid. The pipe is equipped with two heaters and three thermocouples as shown in the illustration.



Proposed Remote-Readout Level Sensor uses a heat pipe equipped with two identical heaters and three monitoring thermocouples. When the platform on which the pipe is resting is level, all three thermocouples produce identical readings. If the platform is tilted, the higher end of the heat pipe would be warmer, and the platform must be leveled by remote control until all the temperature readings are identical.

Once the heaters are turned on, all thermocouples will record a slight rise in temperature. If the platform is level, all three temperature readings are identical. If for example point A is lower than B, the fluid will gravitate to A. The vapors concentrating at B will make

that end warmer. This temperature difference will be recorded by the thermocouples, and the lower end will then be lifted by remote control until all the thermocouples have the same readings. The process would be reversed if point B would be lower than A. (continued on next page)

The system could be easily modified to monitor a platform with two degrees of freedom. It need not be located directly on a platform but can be mounted on a gimbal controlling the platform level. The leveling accuracy is within $\pm 0.25^\circ$, and no calibration is needed.

This system could effectively re-

place the frequently-calibrated expensive optical equipment that can be used only if the object is visible. It can function in cold, in vacuum, and in hot humid environments that produce non-linear expansion and contraction in conventional level-monitoring equipment.

Other potential advantages include low cost, no moving parts, and opera-

tion in toxic environments (e.g., radioactive areas). The system can be customized to operate in steps from -320°F (-195°C) to $+600^\circ\text{F}$ (315°C).

*This work was done by James P. Marshburn of **Goddard Space Flight Center**. No further documentation is available.*

GSC-12095

Automatic 35-mm Slide Duplicator

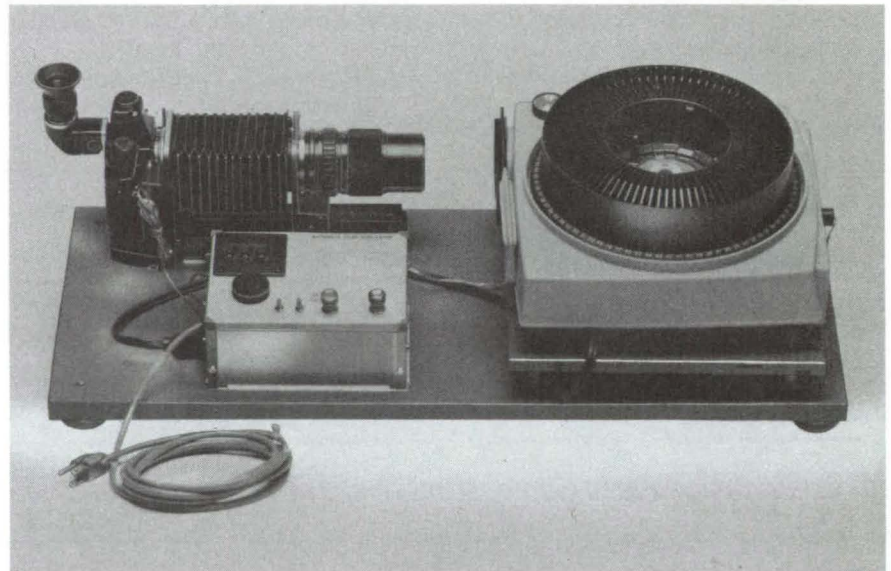
Automatic duplicator is readily assembled from conventional equipment and parts.

Lewis Research Center, Cleveland, Ohio

An automatic 35-mm slide duplicator is easily assembled from conventional inexpensive photographic and electrical components. Duplicates of a series of slides can be exposed automatically without operator attention, eliminating the considerable manual handling and operator processing ordinarily required.

The slide duplicator consists of a conventional single-lens reflex camera and a conventional magazine slide projector electrically coupled through a control unit for automatic operation. The camera, equipped with a bellows extension unit and a 75- to 150-mm zoom lens, a battery-operated film winder, and a right-angle viewer for focusing, is mounted on a baseplate. The slide projector, with lens removed, is mounted with the lens aperture facing the camera. A filter holder is installed on the front of the slide projector to allow compensation for color balance changes. The control unit is assembled from three standard components: a presettable digital counter, a cycle timer, and an audible alarm, plus the requisite switches and cabling.

To operate the slide duplicator, the counter is set to the number of slides to be duplicated, and the electric power is turned on. The timer automatically advances the projector mag-



Automatic 35-mm Slide Duplicator is constructed from a conventional camera and slide projector and a control unit assembled from readily available parts.

azine and injects the first slide into the aperture. Following a slight pause to allow the slide to stabilize, the timer initiates exposure and film winding. The cycle is automatically repeated with the next slide and continues through the entire series. At the end of the programmed exposure sequence, the unit shuts off, and an audible alarm

signals completion of the entire process.

*This work was done by H. F. Seidel and R. E. Texler of **Lewis Research Center**. For further information (schematic, parts list, and assembly instructions), Circle 72 on the TSP Request Card.*

LEW-13399

3-D Guidance System With Proximity Sensors

Proximity sensors help orient a mechanical claw with respect to target fixture.

NASA's Jet Propulsion Laboratory, Pasadena, California

A 3-D guidance system utilizes four proximity sensors on a remotely-controlled mechanical claw. The sensors feed pitch and range information to a manned control station indicating how the claw is oriented relative to a mating fixture it is about to grasp. The operator then aligns the claw so that the fixture is grasped correctly. This system developed for coupling space vehicles can be used in other remote manipulators.

The sensors (see Figure 1) are mounted on the center square frame of the end effector of a four-claw grapple. Each sensor consisting of an LED source and a photodetector is aimed to sense the object parallel to the shaft (the roll axis) supporting the grapple. Thus four sensitive areas are established ahead of the claws. Using the claws to define four corners of a square, the sensors are mounted at midpoints of the sides of the square.

Thus, two orthogonal lines connecting opposite pairs of sensors define the pitch-and-yaw axis of the system.

In the simplest arrangement, each sensor is operated in a two-state binary sensing mode, where a zero indicates a too far state while 1 indicates a too close state when the system is in the vicinity of the target (see Figure 2). The detection distances of sensors B and D are somewhat shorter than of A and C. Thus a success state when the claws are aligned with the target is defined by A signaling 1, B a zero, C a 1, and D a zero. An all-zero state shows that the entire claw is too far from the target and an all-1 that it is too close.

A total of 16 combinations is possible (2^4) indicating various misalignments of yaw and pitch axes with respect to the target. One of the 16 states never occurs, when A and C are zero and B and D 1, because of the detection pattern setup.

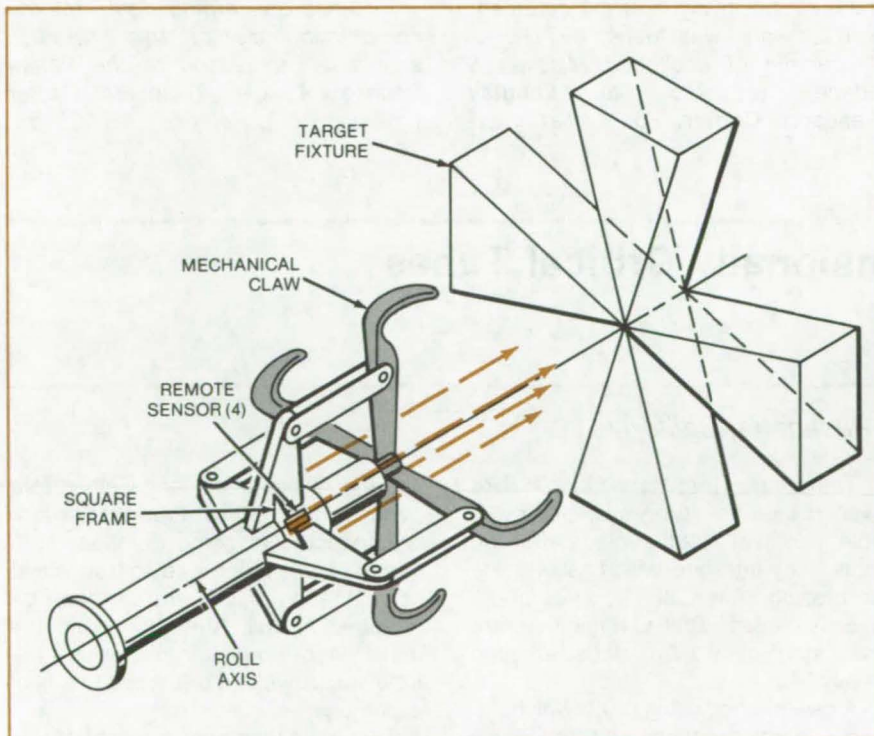


Figure 1. Four Proximity Sensors help to guide the mechanical claw into alignment with the target fixture. Digital signals are used to sense the target distance and to align roll, pitch, and yaw with respect to the target before it is grasped.

A more precise alternative would involve three-state sensing. A signal with a value of 2 would indicate too close, 1 on target, and zero too far. Success would be defined by all 1's, and a total of 75 workable logic states would be possible, giving a more accurate feedback.

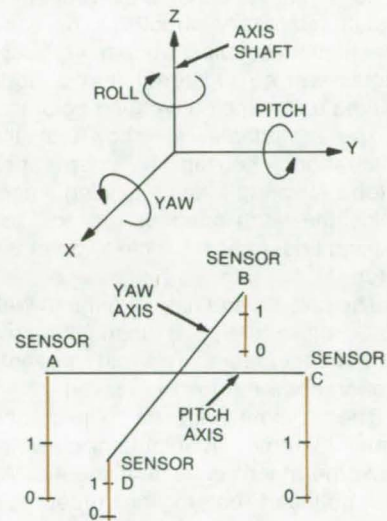


Figure 2. The Sensors are arranged to form the yaw-and-pitch axis of reference for guiding the claw. The sensors generate binary signals of 1 for too close and zero for too far. These signals are fed to the control operator guiding the claw. A similar more-precise alternative uses three states signaling 2 for too close, 1 on target, and zero for too far; and, an even more precise alternative uses continuous calibrated data from the sensors.

This work was done by Antal K. Bejczy of Caltech for NASA's Jet Propulsion Laboratory. For further information, Circle 73 on the TSP Request Card.

This invention is owned by NASA, and a patent application has been filed. Inquiries concerning nonexclusive or exclusive license for its commercial development should be addressed to the Patent Counsel, NASA Resident Legal Office-JPL [see page A5]. Refer to NPO-14521.

Automatic Connector Joins Structural Columns

A connector snap-locks over column ends.

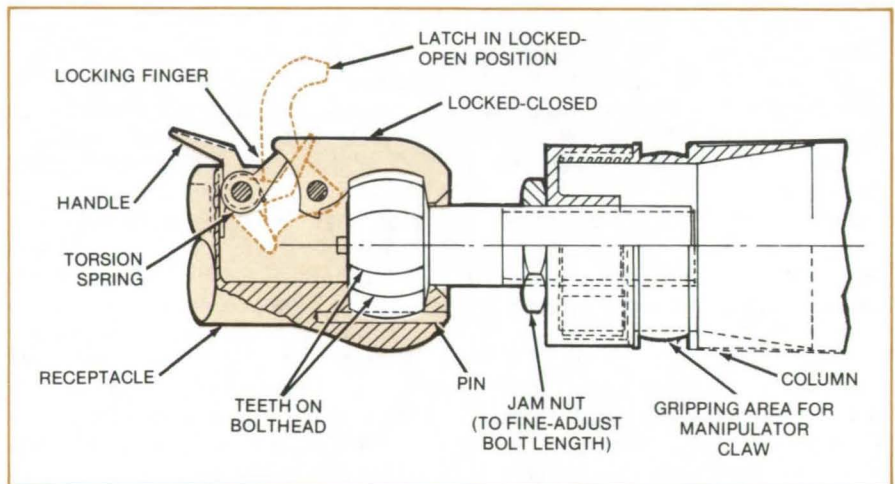
Langley Research Center, Hampton, Virginia

A new connector developed for space application joins 20-m-long columns. At column intersections a latch snaps closed over a toothed bolthead mounted on the column end, forming a rigid joint that will not bend or twist. Developed for quick assembly and disassembly of large space structures, the connector could be used in conventional construction to install temporary structures or as a mechanical coupler. Up to nine receptacles can be clustered into a node joining up to nine converging columns.

The receptacle, as shown in the illustration, houses a snap-action latch. A spring-loaded locking finger holds the latch open or closed. The locking finger has a handle to open the latch.

The column end has a bolthead with sprocketlike teeth that mesh with a pin in the receptacle. This pin prevents torsion once the joint is locked.

The column can be aligned and joined by remote manipulator claws or by some other convenient means. As the bolthead enters the receptacle from the top, a projection on the bolthead depresses the open latch.



Automatic Connector snap-locks columns together to make a truss structure. An unlocked receptacle accepts a bolthead from a column end. When the two are together, the latch snaps over the bolt, locking it in place. The joint is rigidly locked and will not bend or twist.

Once the dead center of the latch is passed, the spring-loaded finger locks the latch positively over the bolthead.

This work was done by G. G. Jacquemin of Lockheed Missiles & Space Co., Inc., for **Langley Research Center**. For further infor-

mation, Circle 74 on the TSP Request Card.

Inquiries concerning rights for the commercial use of this invention should be addressed to the Patent Counsel, Langley Research Center [see page A5]. Refer to LAR-12578.

Test Fittings for Dimensionally Critical Tubes

Fittings prevent damage to tube stubs.

NASA's Jet Propulsion Laboratory, Pasadena, California

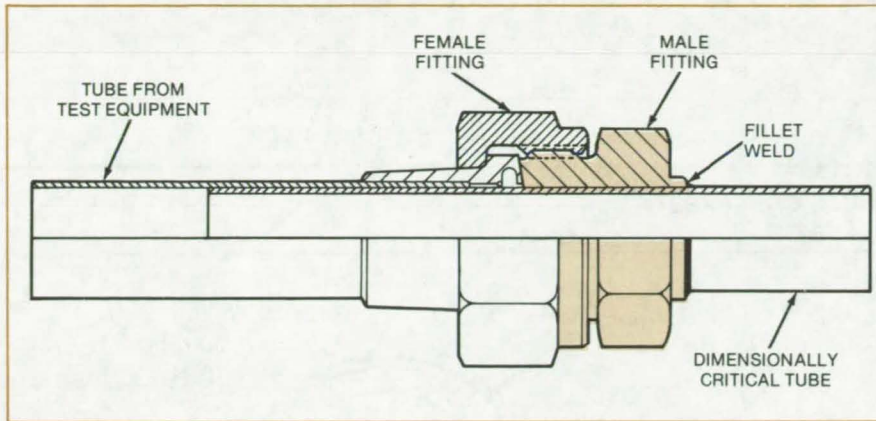
Dimensional tolerances are frequently critical for tubes used in aerospace and aviation fluid-control equipment. These tubes can be easily damaged when components into which they lead are tested and calibrated. For instance, a small offset in the tube dimension can go unnoticed and eventually cause leakage at the manifold joints, creating an expensive repair problem once the component is put into operation.

Temporary test fittings that are slipped over the tube stub are available. However, if left in place after the tests, they interfere with final welding or brazing. Alternatively, integral fittings with face-seal O-rings that are machined onto tube stubs are too heavy.

A new method using a lightweight fitting protects the tubes and tube stubs during testing and through to the final welding. A threaded male fitting (see

figure) is slipped over and welded to a dimensionally critical tube that in turn is connected to some component. A mated female fitting leading from a test or calibration instrument can then be attached at will. After the tests, the male fitting remains in place, and the tube stub is welded or brazed to a final assembly.

The male-fitting inner diameter is slightly larger than the outer diameter of the tube. The fitting is slipped on the



Male Threaded Fitting used as a test connector is welded to a tube stub. The fitting prevents damage to dimensionally critical tubes during the tests and is light enough to be left in place during the final assembly.

tube, positioned at some distance from the stub, and fillet-welded. The female fitting is tightened over the male fitting, forming a temporary leakproof seal. The dimensions of the female fitting and its tube are chosen to be somewhat larger to prevent contact with the tested tube, especially at the tube stub.

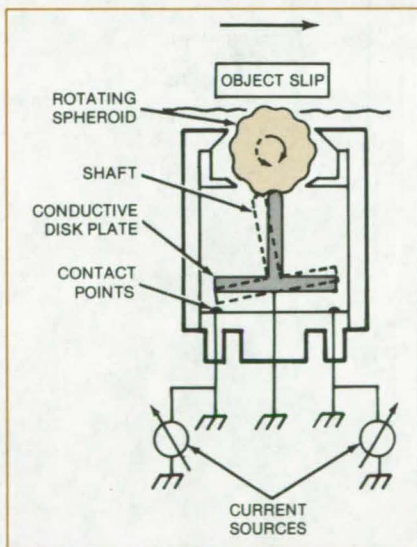
The new approach is adaptable to many types of components, including valves, transducers, and filters. It was applied in ground tests of Voyager 77; and despite numerous qualifications and calibration tests, not a single tube stub or weld had to be reworked.

This work was done by Ray Hagler of Caltech for NASA's Jet Propulsion Laboratory. For further information, Circle 75 on the TSP Request Card. NPO-14399

Electromechanical Slip Sensor

New sensor indicates the direction of slip and slip rate of objects handled by remote manipulators.

NASA's Jet Propulsion Laboratory, Pasadena, California



Slip Sensor uses a freely movable spheroid with a staggered pattern of indentations on its surface. The spheroid rotates in the direction of the slipping body, tilting a shaft with a conductive disk plate. The conductive plate assembly is bent toward the contact corresponding to the direction of slip and is flicked by the indentations at a rate corresponding to slip rate. The slip direction and rate can be determined using LED's arranged in a circular array or a microcomputer with a CRT display.

A new slip sensor system for teleoperator grasping manipulators detects the presence, direction, and rate of slip. Previous sensors were less versatile, detecting only the presence of slip.

The two basic components (see figure) are the sensor on the manipulator and a microcomputer located at a convenient remote location. The sensor incorporates a circular array of 16 contact points corresponding to 16 compass directions relative to the sensor. As the object slips in a certain direction, it rotates a spheroid that in turn tips a shaft in the appropriate direction. A disk base at the bottom of the shaft touches the appropriate contact points. A current flow at those contacts indicates the slip direction.

The spheroid surface has indentations that pulse the shaft at a rate proportional to the slip rate. This generates current pulses that are used to determine the slip rate.

The sensor signals can be direct raw analog LED displays or digitally processed signals on a graphics display. The analog display uses 16 LED's arranged in a circle corresponding to the contact points. A slip in any given direction will pulse the appropriate LED. Since an adjacent LED could also be firing, the operator would visually average out the direction of the slip. The rate of blinking indicates the slip rate.

A microcomputer can process these signals in real time to show the slip rate and direction on a CRT display. The signals are averaged, showing the data in eight compass directions. Slip rate is determined by the frequencies of steps on the display lines.

This work was done by Antal K. Bejczy and Sur Park of Caltech for NASA's Jet Propulsion Laboratory. For further information, Circle 76 on the TSP Request Card. NPO-14654



X-Ray Beam Pointer

Pointer aims X-ray machine for weld radiographs.

Lyndon B. Johnson Space Center, Houston, Texas

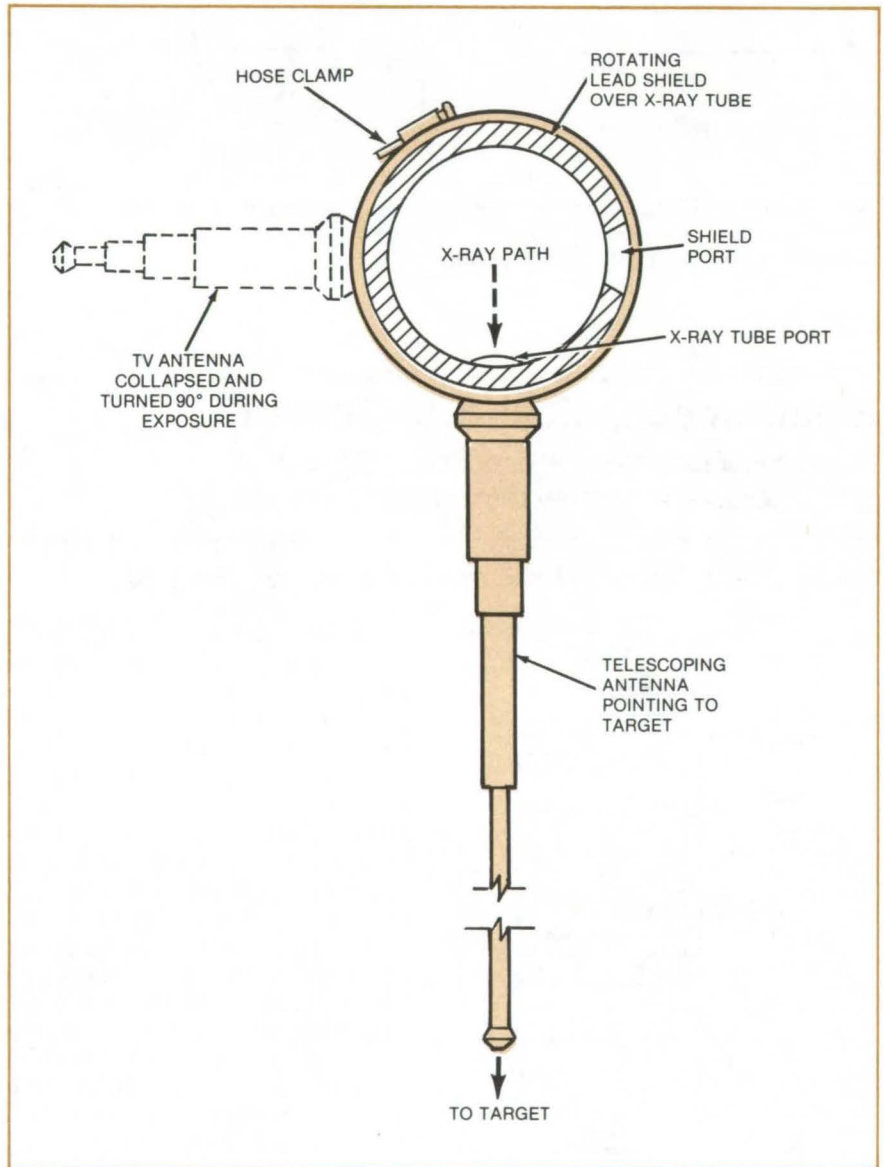
A simple pointer (see figure) indicates the direction the beam will take from a portable X-ray machine. The pointer is an aid in making X-ray photographs of welded assemblies — for example, of complicated plumbing and valve systems.

A conventional, 36-in. (0.9 m) telescoping antenna serves as a pointer to aim the X-ray tube port. The antenna, welded onto a conventional 3-in. (7.6-cm) hose clamp that is tightened around the rotatable X-ray lead shield, extends radially outward.

Before the X-rays are taken, the antenna is extended, and the machine is aligned so that the antenna points to the object and the X-ray film. Once aligned, the antenna is collapsed and moved out of the way by turning the shield to open the X-ray tube port. The open port then faces the target exactly as the antenna pointed.

The pointer is inexpensive and constructed from readily available parts. A plumb bob used previously for vertical alignment and a yardstick used to visualize the X-ray paths at various angles were less convenient and not as accurate. The new pointer cuts the alignment time by one-half and virtually eliminates retakes necessitated by poor alignment. It is estimated that for 3,000 weld radiographs, the pointer will save 300 worker-hours and significant materials costs.

This work was done by C. W. Nelson of Beech Aircraft Corp. for **Johnson Space Center**. For further information, Circle 77 on the TSP Request Card. MSC-18590



Telescoping Pointer shows the direction the X-ray beam will take when the tube shield is opened. Once aligned, the pointer is rotated 90° out of the way, opening the X-ray tube port to face the target. The pointing mechanism is made of inexpensive parts.

Handtool Assists in Bundling Cables

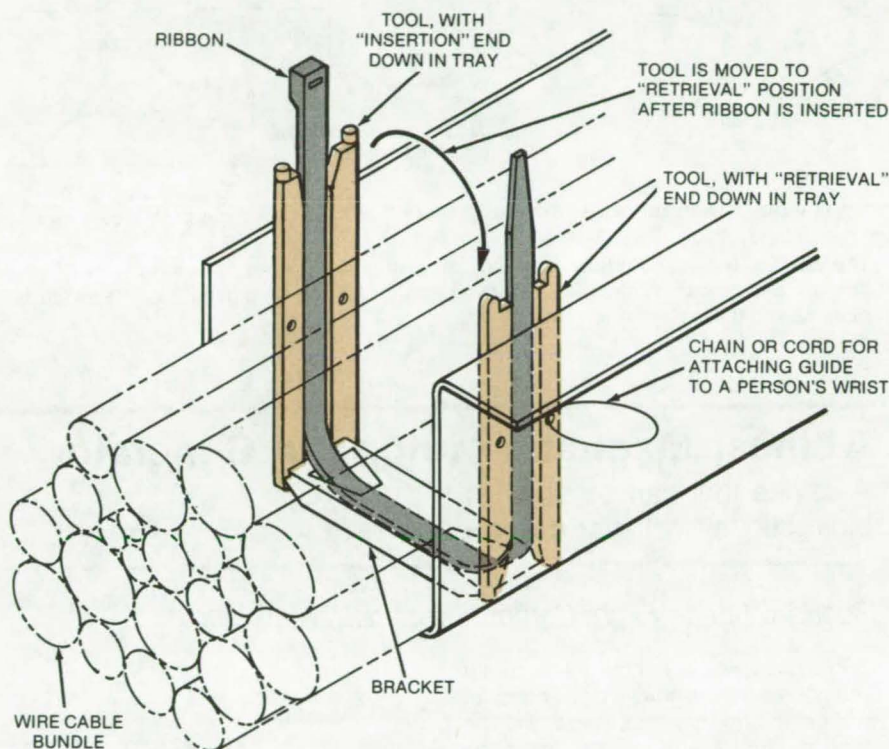
A tool aids in bundling cables together in a restricted space.

Lyndon B. Johnson Space Center, Houston, Texas

A simple tool makes it possible to bundle electrical cables in a channel or "tray" without requiring that the cables be lifted out of the tray. Used with commercially-available plastic ribbons that tie the cables together, the tool guides the ribbon along a tray wall, through a bracket at the bottom of the tray, and up the opposite wall. One end of the ribbon locks in the other end, securing the cable bundle. The procedure is faster and less awkward than the old method of lifting the cables for wrapping.

As shown in the illustration, one inserts the tool gently into the space between the cable and the tray wall, engaging it with a bottom bracket. The ribbon is then slid along a groove in the tool until it threads into the bracket. The operator removes the tool, reinserts it along the other wall so that it engages the bracket at the opposite end, and pushes the ribbon so that it emerges from the tray through the groove in the tool. The ribbon is then cinched with a special gun, and the cable bundle is secured.

This work was done by Eugene J. Stringer of Rockwell International Corp. for Johnson Space Center. For further information, including an engineering drawing of the tool, Circle 78 on the TSP Request Card. MSC-18567



The **Cable-Bundling Tool** helps to insert and then retrieve the ribbon that wraps the cables together. The two ends of the tool are slightly different: The "insertion" end is configured to guide the ribbon into the bottom bracket; the other end (the "retrieval" end) is shaped to guide the ribbon from the bracket into the tool groove. Thus, the tool is inverted when used for the retrieval step.

Sleeve Puller Salvages Welded Tubes

Sleeve remnants are removed nondestructively so tubes can be reused.

Lyndon B. Johnson Space Center, Houston, Texas

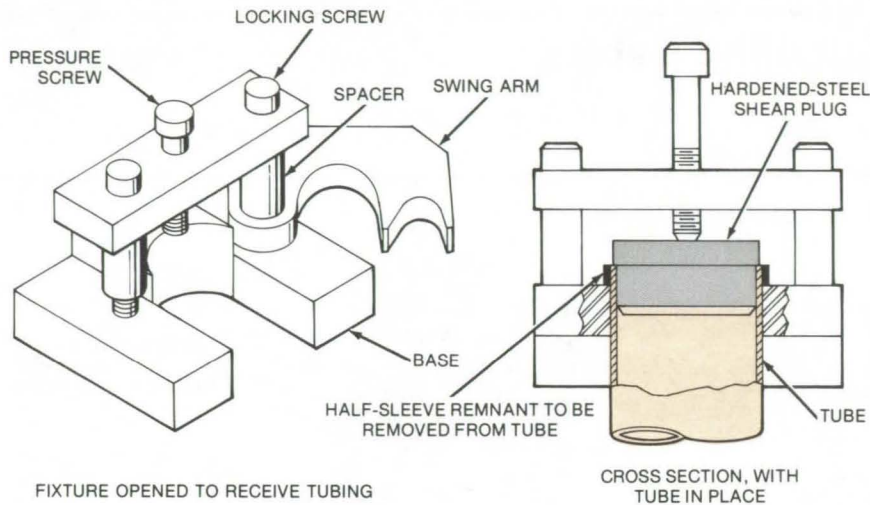
The remnants of sleeves used in welded tube joints are removed without damaging the tube ends by a simple new fixture. Tubes can therefore be reused, saving time, labor, and material in many applications.

The welded tube is salvaged by first sawing through the sleeve and the weld. A half segment of the sleeve remains on each sawed-off section of tube. The end of one tube is then clamped on the fixture, a plug is inserted, and a pressure screw is

advanced to push the tube out of the sleeve segment. The same procedure is repeated for the other tube section. The sleeves are removed without distorting or damaging the tubes, as often happens when the sleeves are removed by pliers or other handtools.

(continued on next page)





As shown in the figure, the fixture consists of a base, two locking screws, two spacers, a swing arm, and a pressure screw. The tube is placed in the cutout in the base, with the sleeve remnant resting on the base. The swing arm is closed around the tube and locked by tightening the two locking screws.

A hardened-steel shear plug, with outside diameter equal to that of the tube, is inserted in the tube end. When the pressure screw is advanced, it pushes the shear plug, which shears the tube segment out of the sleeve.

This work was done by James F. Weaver of Rockwell International Corp. for Johnson Space Center. No further documentation is available. MSC-18686

The **Sleeve-Removal Fixture** consists of a pressure screw, a swing arm, locking screws, and a base. It removes a sleeve remnant from tubing after a welded joint has been sawed through.

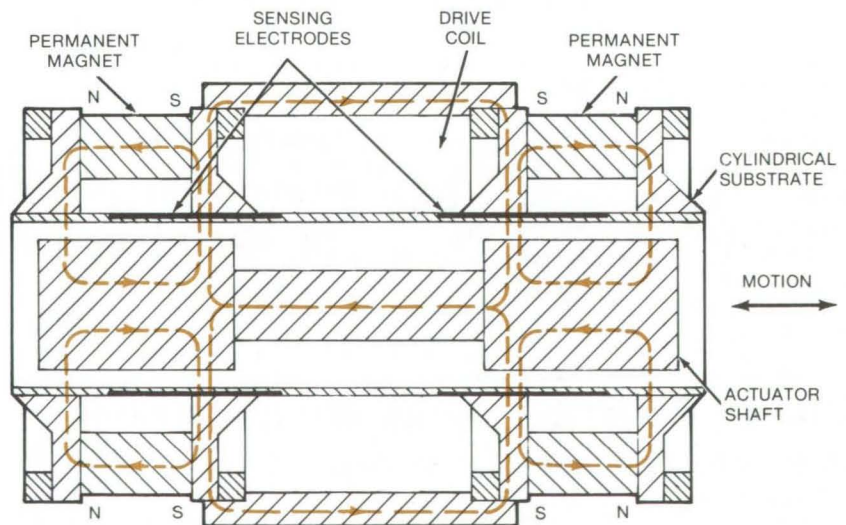
A Linear Magnetic Motor and Generator

A device that can be used as bidirectional motor or ac generator

Goddard Space Flight Center, Greenbelt, Maryland

In a proposed linear magnetic motor and generator, originally developed for cryogenic refrigerators that will be used on future spacecraft, magnetic forces drive a reciprocating shaft along its axis. The actuator shaft, as shown in the figure, is located in the center of a cylindrical body. Support for the shaft may be provided by linear ball bushings, plain bearings, or by noncontacting means such as gas or magnetic bearings. The motor/generator could be applied in remote or hostile environments.

A drive coil between the two permanent-magnet structures controls the linear movement of the actuator. Each of the permanent-magnet structures establishes a flux path passing through the ends of the actuator. The permanent magnets are oriented so that their north poles face axially outward. When the motor/generator operates as a bidirectional motor, the drive coil selectively adds and subtracts magnetic flux to and from these flux paths and thus produces the forces that drive the actuator back and forth along the axis.



Cross Section of Magnetic Motor and Generator shows the actuator shaft and magnetic flux paths (dotted lines). When the system operates as a bidirectional motor, magnetic flux paths established by permanent magnets are altered by the drive coil. The combined forces drive the shaft back and forth along the axis. When the shaft is driven by an external piston, the system induces current in the drive coil and becomes an ac generator.

When the actuator is driven by an external reciprocating engine, the motor/generator becomes an ac generator. In this mode, the actuator coupled to the engine piston moving back and forth along the axis alters flux paths established by the permanent magnets. This induces alternating current within the coil, which can be connected to an external load.

A somewhat modified motor/generator is not cylindrical and has magnetic flux confined to the vertical plane. Its operation is similar to the one described.

This work was done by Philip A. Studer of **Goddard Space Flight Center**. For further information, Circle 79 on the TSP Request Card.

This invention is owned by NASA, and a patent application has been filed. Inquiries concerning nonexclusive or exclusive license for its commercial development should be addressed to the Patent Counsel, Goddard Space Flight Center [see page A5]. Refer to GSC-12518.

Cryogen-Storage-Tank Support

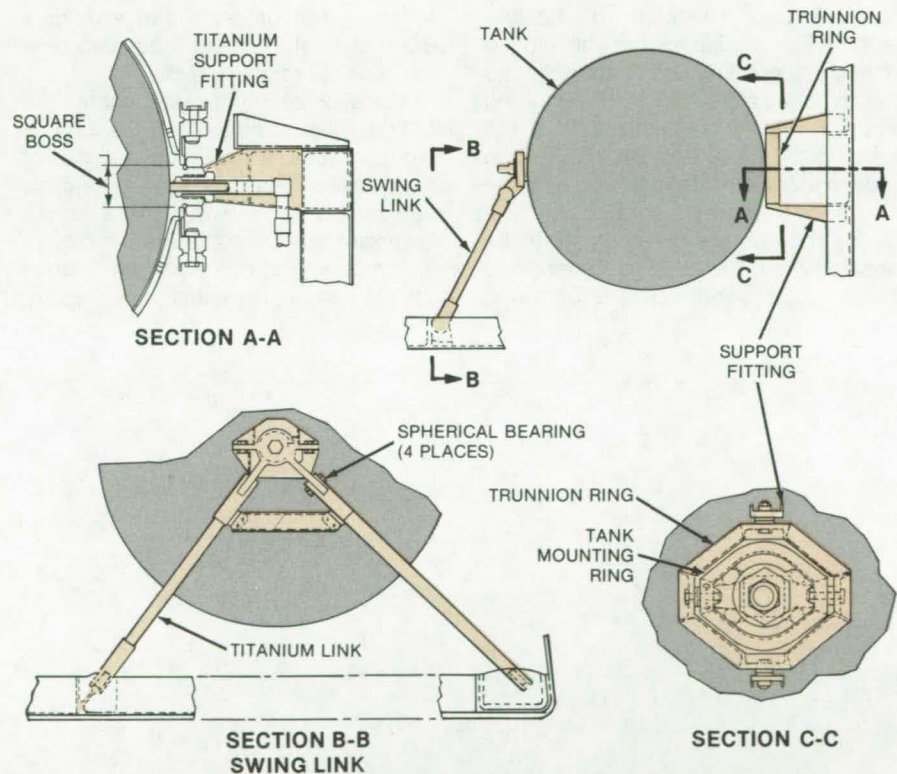
Proposed support isolates the tank from thermal and mechanical loads.

Lyndon B. Johnson Space Center, Houston, Texas

High-pressure helium cryogen tanks supported on structures that are subject to mechanical and thermal loading must be effectively isolated against structural deflection and thermal effects. This problem can be resolved using a proposed, statically determinate support, shown in the figure. The support would isolate the tank from the thermal and mechanical loading by its environment. The tank is supported by an independent mechanism at each end to accommodate changes in tank size due to temperature and pressure variations. This arrangement is self-aligning from the beginning, accommodating manufacturing variations in the tank dimensions as the tank is installed.

On one end the tank is attached to a trunnion ring that can transfer a three-axis load and torque. To isolate the tank thermally, the ring is held away from the structure by titanium fittings. The opposite end of the tank is supported by an A-frame swing-link mechanism clamped around a hub on the tank end. This frame reacts to tank loads in the plane of the frame and allows tank pressure and thermal growth in a direction normal to the frame. The frame also has titanium links for thermal isolation.

This work was done by Gerald H. Wisdom of McDonnell Douglas Corp. for **Johnson Space Center**. No further documentation is available.
MSC-14848



Proposed Tank Support would isolate a cryogen high-pressure helium tank from thermal and mechanical loads imposed on its support structures. This design, using a combination of well-known common mechanisms, would isolate the tank and allow for tank expansion and contraction due to temperature and pressure changes. A similar support method was already used on nitrogen tanks.

Computer Programs

These programs may be obtained at very reasonable cost from COSMIC, a facility sponsored by NASA to make new programs available to the public. For information on program price, size, and availability, circle the reference letter on the COSMIC Request Card in this issue.

Rotor Transient Analysis

Undamped modes approximate the dynamic behavior of rotors and bearings.

Two programs, Modal 1 and Modal 2, have been developed for calculating the transient response of flexible rotors. The modal method developed uses undamped modes to approximate the dynamic behavior of rotor/bearing systems. Modal transformation of the generalized equations of motion into modal equations of motion using the undamped modes significantly reduces the number of equations to be solved without losing the generalities of bearing cross-coupling effects and

influence of gyroscopic moments. This reduction of degrees of freedom greatly reduces the computational effort and cost and thus makes possible the transient analysis of large, complex rotor systems.

Modal 1 is used to calculate the undamped critical speeds and their corresponding mode shapes, damped natural frequencies and their corresponding mode shapes, rotor unbalance response, and transient response of multimass rotor/bearing systems. Special capabilities of this program include asymmetric bearing, bearing rotational damping and stiffness effects, shaft residual bow, and disk skew effects.

Nonlinear bearing forces can also be calculated for each time step during transient analysis with bearing characteristics. The program can also generate plots of transient orbits and time vs. transient response plots.

Modal 2 calculates the undamped critical speeds and their corresponding mode shapes. A maximum number of eight speed cases of transient analysis can be obtained in one single analysis. Transient motion orbits and amplitude vs. time plots at one particular station are generated for every speed case.

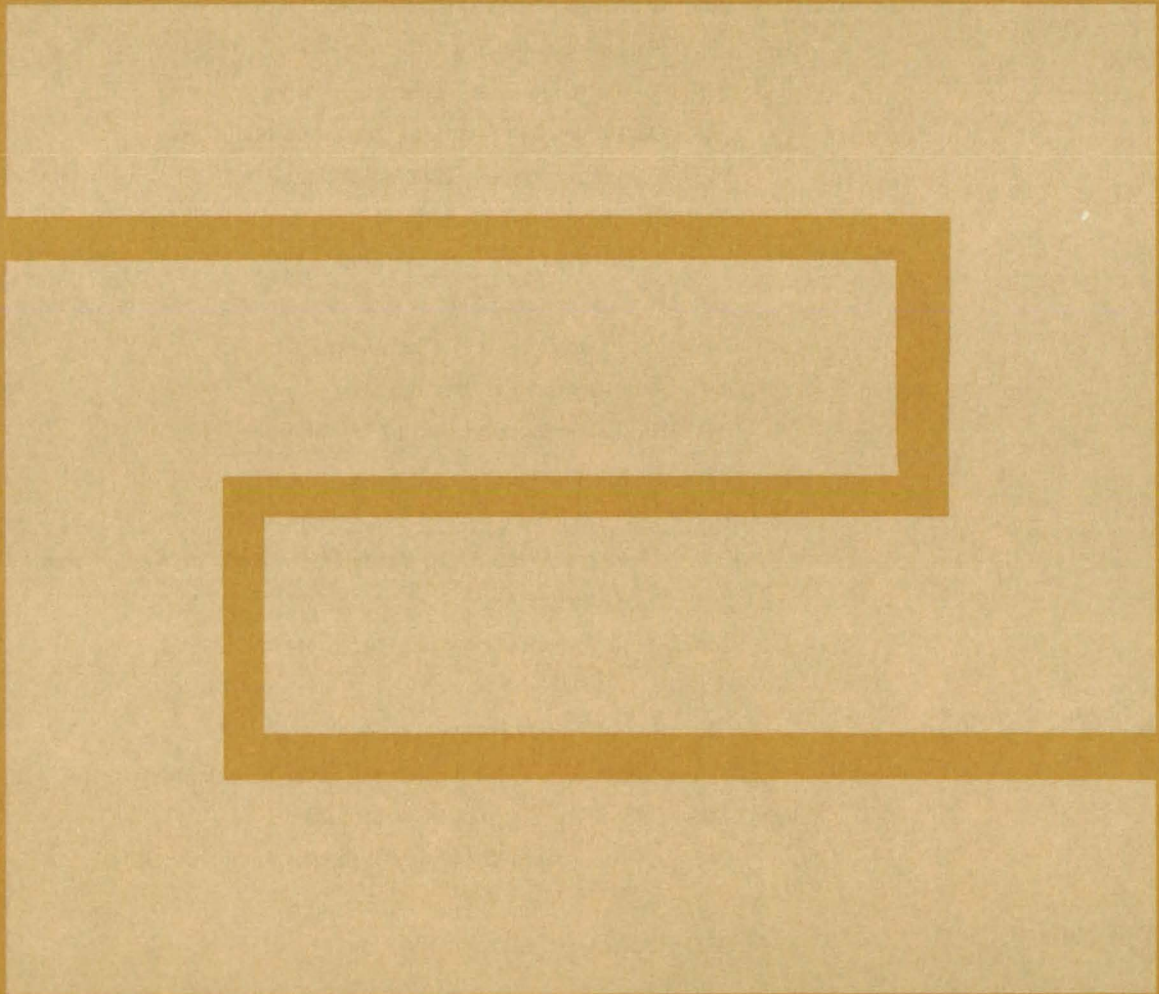
Fast Fourier transformation is used to produce frequency spectrum analysis for every speed case.

The application of modal analysis to uncouple the equations of motion simplifies stability, steady-state unbalance response, and transient response analysis of the system. Nonlinear stability of the system can be predicted by frequency spectra calculated from Fourier transformation of the transient solution. This analysis will provide designers with complete design information, such as critical speed and modes, amplification factors, stability, steady-state and transient forced response, and frequency spectrum of the system, without involving large-scale computational costs. The correlation of experimental data with modal analysis verified the use of modal analysis and numerical Fourier transformation.

These programs are written in FORTRAN IV for use on a CDC 6600 computer.

This program was written by P. E. Allaire, K. C. Choy, and E. J. Gunter of the University of Virginia for Lewis Research Center. For further information, Circle J on the COSMIC Request Card.
LEW-13230

Fabrication Technology



Hardware, Techniques, and Processes

- 231 Photonnitride Passivating Coating for IC's
- 232 Double Metalization for VLSI
- 232 More-Reliable SOS Ion Implantations
- 233 Ohmic Contact to GaAs Semiconductor
- 234 Resistance Welding Graphite-Fiber Composites
- 235 All-Inorganic Spark-Chamber Frame
- 236 Controlling the Shape of Glass Microballoons
- 237 Forming Complex Cavities in Clear Plastic
- 237 Shrinking Plastic Tubing to Nonstandard Diameters
- 238 Thermal Barrier and Gas Seal
- 239 Heat-Shrinkable Sleeve Aids in Installing Universal Joints
- 240 Improved Particulate-Sampling Filter
- 240 Time-Shared RF Brazing
- 241 Producing Gapped-Ferrite Transformer Cores
- 242 Plastic Welder
- 243 Electron-Beam Welder Circle Generator
- 243 "Foreign Material" To Verify Root Fusion in Welded Joints
- 244 Tube-Welder Aids
- 244 Honing Fixture for Weld Electrodes

Books and Reports

- 245 Silicon Nitride Passivation of IC's
- 246 Progress in MOSFET Double-Layer Metalization
- 246 Optimizing Costs of VLSI Circuits
- 246 An Automated Oxide and Diffusion Facility for IC's

Computer Programs

- 247 Predicting Crack Propagation

Photonitride Passivating Coating for IC's

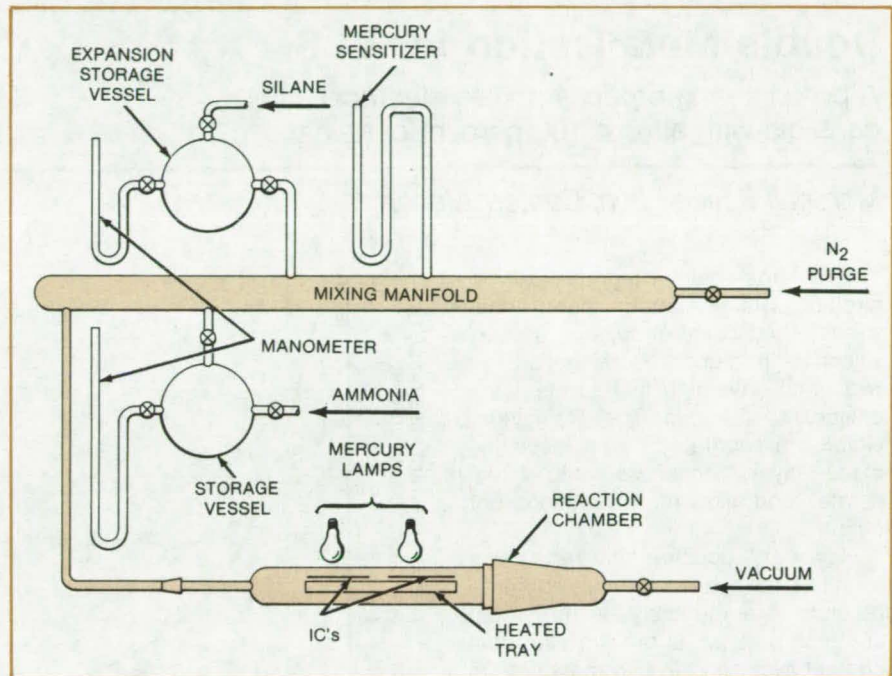
Increased reliability and simplified fabrication result from the postassembly preencapsulation passivation process.

Marshall Space Flight Center, Alabama

The use of low-temperature photochemically-deposited silicon nitride (photonitride) as a final passivation layer over finished metalized semiconductor devices (MOS and bipolar) simplifies their fabrication and enhances their reliability. The photonitride layer is a barrier against moisture and the penetration of mobile ions into sensitive areas of the solid-state devices. The silicon nitride passivation process also inhibits corrosion due to moisture at wire interconnect sites, thus leading to their enhanced reliability. Low-temperature photonitride films are prepared at temperatures from 300° C downward to 100° C. The low temperature makes possible post-assembly passivation of devices containing relatively low-melting-point metalization and bonding wire.

The photonitride coating, several thousand angstroms in thickness, is applied in a reactor that consists of a reaction chamber, metered and controlled sources of reactant gases (silane and ammonia), a pump to move the gases through the chamber at a predetermined flow rate and pressure, and a mercury lamp as a source of ultraviolet radiation (see figure). In the process, the microcircuits to be passivated are placed on a heated tray, and the chamber is evacuated to an acceptable pressure. The flow of reactant gases is started, followed by adjustments of total pressure, gas-flow rates, gas-flow ratios, and substrate temperature.

When the complete system reaches equilibrium, the deposition of silicon nitride is initiated by transmitting ultraviolet radiation through fused-quartz windows that form the top of the deposition chamber. The deposition rate is directly proportional to the intensity of ultraviolet radiation impinging on the substrate surface and is terminated by turning off the mercury lamps positioned over the fused-quartz windows. A programmable control panel allows the selection of automatic or manual operation and associated pneumatic and vacuum



The Photonitride Reaction Chamber receives silane, ammonia, and mercury from a mixing manifold to form the silicon nitride passivating coating on the IC's. Mercury lamps initiate and terminate the reaction in which mercury is a catalyst.

equipment to admit the reactant gases and remove the byproducts.

The low-temperature photonitride films are prepared by the mercury photosensitized reaction of silane (SH_4) and ammonia (NH_3). Only radiation that is absorbed, either by the reactants or by a mercury photosensitizer, can lead to a photochemical reaction. Silane and ammonia absorb radiation significantly only at wavelengths below 2,200 Å. The mercury lamp is the most convenient source of radiation for the chemical processes, but its frequency range is limited to a cutoff wavelength of about 2,000 Å. By saturating the reaction chamber with mercury vapor, the lamp limited-frequency range is overcome; the excited but un-ionized mercury atoms transfer their energy by collision to the chemical reactants within the system, generating free radicals that initiate chain reactions leading to the final silicon nitride product.

The electrical and mechanical compatibility of the photonitride process with microcircuits was examined with various semiconductor devices. Included in the devices examined were an operational amplifier; CMOS, bipolar Schottky, and TTL IC's; and a power transistor. The photonitride deposition process was compatible with all of these wire-bonded lead frame assemblies, with or without initial chip passivation. The survival after the application of photonitride to lead frame assemblies of devices with no chip passivation suggests the possibility of simplifying the device fabrication process by eliminating the chip passivation operation.

The ability of photonitride films to withstand flexure stresses helps to protect IC devices subjected to severe mechanical handling or circuit repair procedures. Tests indicate that leads 75 mils (1.90 mm) in length can be laterally displaced by more than 25 mils (0.63 mm) at the point of

(continued on next page)

maximum curvature without damage to the nitride film.

Significant advantages exist for the photochemical process over other processes, plasma and sputtering, for the deposition of silicon nitride on microelectronics. The advantages are

low deposition temperature and zero stray radiation and ion levels, all of which can change device characteristics. [Also see related article, "Silicon Nitride Passivation of IC's" (MFS-25309), on page 245 of this issue.]

This work was done by T. C. Hall and J. W. Peters of Hughes Aircraft Co. for **Marshall Space Flight Center**. For further information, Circle 80 on the TSP Request Card. MFS-25401

Double Metalization for VLSI

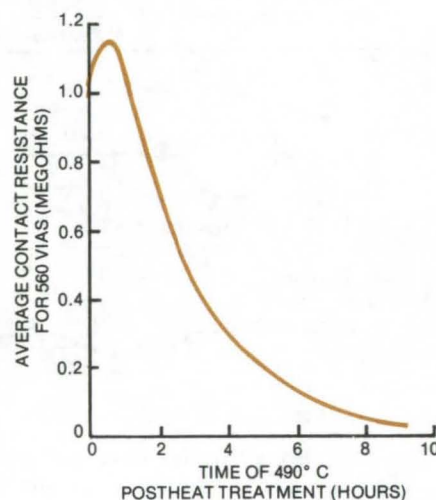
A postsintering process makes electrical contacts with almost 100 percent certainty.

Marshall Space Flight Center, Alabama

Very-large-scale integrated (VLSI) circuits, which contain many thousands of individual circuits on a small silicon chip, benefit from the use of two metal layers to interconnect the devices on the chip. The two layers, which are separated by an insulating oxide layer, conserve chip "real estate" and allow more functions per chip.

However, double-metalized chips for VLSI have been difficult to manufacture reproducibly. The most common problem is making electrical contact between the two metal layers through "vias" (holes) in the oxide insulating layer. The via contacts tend to have excessively high resistance, often to the point of being open circuits. The problem is worse when the number of vias is large (500 or more) and the via size is very small [less than 0.2 mil (5 millimeters) square]. A recently tested sintering procedure carried out after "wet chemistry" processes increased the yield of double-layer metal conductors to more than 98 percent.

The wafers containing the double-metalized chips are sintered (see figure) at 490° C. Apparently the



The **Effectiveness of Postheat Treatment** is clearly demonstrated by the drop in via resistance as a function of heating time. This result was obtained from 560 vias of 0.5 by 0.5 mil in size. The heat treatment usually eliminates most of the open circuits (contact resistance of more than 20 megohms).

aluminum metal layers react with an aluminum oxide film that remains in the via, breaking up the film so that it no longer impedes the electric cur-

rent. Alternately, the recrystallization of both aluminum layers as they cool from the sintering temperature may mechanically disrupt the oxide film. At any rate, the yield of "good" small via — that is, those with low contact resistance — increases dramatically.

The sintering technique was evaluated using 50 specimens. The specimens consisted of a double-layer structure containing 560 vias. The via size varied from 0.5 to 0.2 mil (0.013 to 0.005 mm) square, although only one size was used per specimen. Best results have demonstrated that the technique reduces the number of defective contacts to less than 2 percent — a very respectable figure in this relatively new technology.

This work was done by J. D. Trotter and Thomas E. Wade of Mississippi State University for **Marshall Space Flight Center**. For further information, Circle 81 on the TSP Request Card.

Inquiries concerning rights for the commercial use of this invention should be addressed to the Patent Counsel, Marshall Space Flight Center [see page A5]. Refer to MFS-25149.

More-Reliable SOS Ion Implantations

A conducting layer prevents static charges from accumulating during implantation of silicon-on-sapphire MOS structures.

Marshall Space Flight Center, Alabama

A method for preventing static charges from building up on silicon-on-sapphire (SOS) MOS structures during ion-implantation doping has improved

yields for several LSI circuits. To dissipate the potentially destructive accumulations before they develop, a thin conducting path to ground is

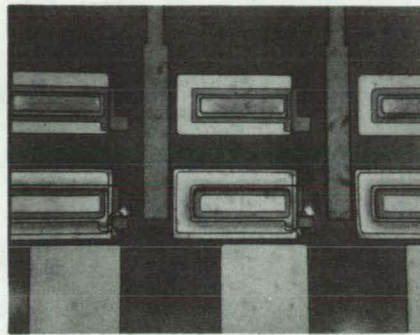
deposited prior to the start of the implantation. Either a very thin conducting film that is essentially transparent to the ions is deposited or a
(continued on next page)

thicker film is used, and gaps are etched in the regions to be doped.

In silicon-on-sapphire technology the silicon layer over the sapphire substrate is selectively etched to form electrically-isolated silicon islands. Then, relatively-heavy ion-implantation doses are applied to dope the MOS subelements to degenerate impurity concentrations on the order of 10^{20} cm^{-3} . The three exposures to an ion beam are required for an all-ion-implantation process: (1) polygate implantation; (2) n^+ implantation with a thick photoresist shield on the PMOS area; and (3) p^+ implantation with a photoresist shield on the NMOS area.

During the heavy source and drain implantations, charges build up on the silicon film. When they reach the breakdown level, the charge flows through neighboring silicon islands or through the sapphire substrate to the ground plate, often damaging the film (see figure) or cracking the sapphire wafer.

Two approaches to reduce charge buildup have been used. In the first, a relatively-thick conducting-shield film, such as aluminum, $1 \mu\text{m}$ in thickness, is deposited. The film is selectively etched to expose areas for implantation, yet it maintains a continuous



Damaged Silicon Films (darkened areas) on sapphire wafers are apparent on these MOS circuit elements. The silicon was damaged during heavy boron-ion implantation at dosages of 5×10^5 cm^{-2} and energies of 70 keV.

electrical path for static charges to dissipate.

In the second approach, a thin conducting layer, such as 200 \AA of aluminum, is deposited. Photoresist is used for shielding, as in the conventional process. The ion current passes through the thin aluminum layer to implant the underlying material.

Previous approaches to prevent charge buildup, such as simultaneously exposing the structure to charges of opposite sign, require extensive equipment modifications that are less practical and more expensive than depositing the conducting layer.

This work was done by D. S. Woo of RCA Corp. for Marshall Space Flight Center. No further documentation is available.

Inquiries concerning rights for the commercial use of this invention should be addressed to the Patent Counsel, Marshall Space Flight Center [see page A5]. Refer to MFS-25322.

Ohmic Contact to GaAs Semiconductor

Multimetallic layers produce stable, low-resistance contacts.

Langley Research Center, Hampton, Virginia

Reliable, low-resistance ohmic contacts to gallium arsenide (GaAs) semiconductor solar cells and lasers have been a constant problem. Often elaborate methods, such as extra p-type GaAs "capping layers," are used to make good contact.

A much easier and more reliable procedure has been developed for contacts to p-type GaAs and p-type GaAlAs devices. The contacts are made by evaporating a layer of magnesium (Mg) 20 to 75 \AA thick, covered by a layer of titanium (Ti) 200 to 400 \AA thick, covered by a layer of palladium (Pd) 200 to 400 \AA thick, covered by a layer of silver (Ag) over $1,000 \text{ \AA}$ thick. The coating system is annealed at 375° to 475° C . Annealing times decrease from 45 to 10 minutes as the

temperature increases. The contact metallurgy may be evaporated through a mask, or liftoff procedures may be used.

This method was used to make ohmic contacts to GaAlAs/GaAs solar cells that were grown by the "saturated-melt" liquid-phase epitaxy method. Slots were etched through the GaAlAs to the underlying GaAs by lithography. Then layers of 20 \AA Mg, 300 \AA Ti, 300 \AA Pd, and $5,000 \text{ \AA}$ Ag were evaporated on the photoresist. Lifting off the photoresist leaves the metallic contacts in the slots. The contacts were annealed at 475° C for 10 minutes in vacuum.

The series resistance of these contacts has been too small to measure at

1 Sun intensity. Also, no leakage problems were encountered, presumably due to the improved contacts and the lower density of Ga droplets in the saturated-melt epitaxy layers. On devices made by the etch-back-epitaxy process, this method of forming contacts has given contact resistances of 7×10^{-4} ohm-cm^2 or less.

The ohmic contact is stable and is expected to meet the 20-year-lifetime requirement at 150° C for GaAs combined photothermal/photovoltaic concentrators.

This work was done by Harold J. Hovel and Jerry M. Woodall of IBM Corp. for Langley Research Center. No further documentation is available. LAR-12466



Resistance Welding Graphite-Fiber Composites

High-strength joints are welded in a few seconds.

Lyndon B. Johnson Space Center, Houston, Texas

Carbon-reinforced thermoplastics, a family of lightweight materials that is finding increasing uses in homes and vehicles, are rapidly bonded together by resistance welding. In recent tests of several methods for joining composite beams for assembly in space, it was found that applying an electric current for a few seconds to melt the thermoplastic locally is the most promising approach. Among other tested methods, adhesive bonding and encapsulation are more time consuming and introduce additional material (the bonding agent) into the joint. Ultrasonic heating shows promise as a bonding method, but it can damage the graphite fibers in the composite.

For resistance welding, the graphite conducts sufficient current to heat and melt the thermoplastic in the vicinity of the joint. By using a spring-loaded electrode, such as that shown in Figure 1, pressure is applied as the thermoplastic softens; and the electrode follows the softening material to maintain contact.

In tests, three rods of graphite/polysulfone at 36 percent by weight of polysulfone were cut into 2-inch (5.08-cm) lengths and stacked as in Figure 2. The rods had square cross sections and were 0.08 in. (0.2 cm) on an edge. Welding was done with an applied force of 2, 3, 4, 5, or 6 lb (9, 13, 17, 22, or 27 N) and 30 to 35 volts dc across the joint. The total energy was 50, 75, or 90 joules, and typical heating times were about 2 seconds.

Excellent tensile strengths were measured for the resistance-welded joints. In the best samples, fibers were pulled from one member of the joint couple when the tensile limit was exceeded. Optimum joining conditions

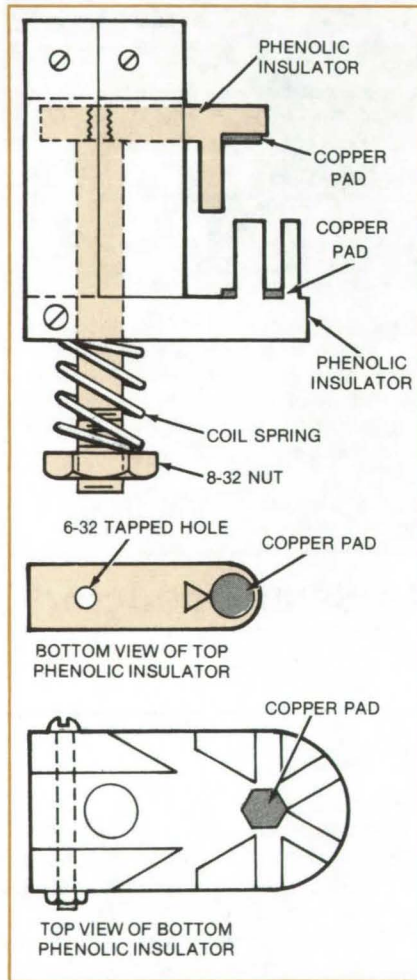


Figure 1. The **Resistance-Welding Electrode** would simultaneously apply heat and pressure to a joint. As the thermoplastic softens, the spring-loaded electrode follows the softening material to maintain contact. The electrode also holds the parts together during the cooling phase.

for the samples tested were 3 lb force at 90 joules and 4 lb at 75 joules. In both cases, the measured joint tensile strengths were above 8.3×10^6 N/m².

Resistance welding can be done in several configurations. In addition to the transverse arrangement of Figure 2, the joint can be heated longitudinally by connecting both power-source electrodes to the center rod and passing current until the thermoplastic softens. Heating by microwaves is also being considered. Thus far, little effort has been devoted to varying the joint surface condition or its size and shape; however, it is expected that optimization of these parameters will further improve the joint strength.

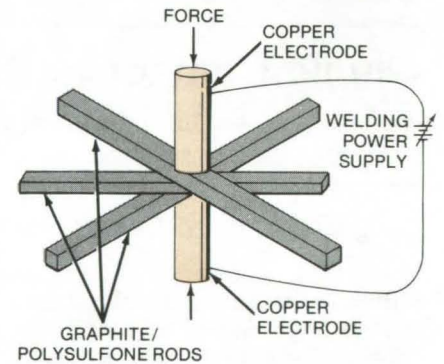


Figure 2. **Heat Is Applied** transverse to the joint to soften the thermoplastic. Since the joint interfaces offer higher resistance than the bulk, they reach softening temperature first.

This work was done by Richard T. Lamoureux of McDonnell Douglas Corp. for Johnson Space Center. For further information, Circle 82 on the TSP Request Card. MSC-18534

All-Inorganic Spark-Chamber Frame

Outgassing is reduced by using ceramic and glass materials exclusively.

Goddard Space Flight Center, Greenbelt, Maryland

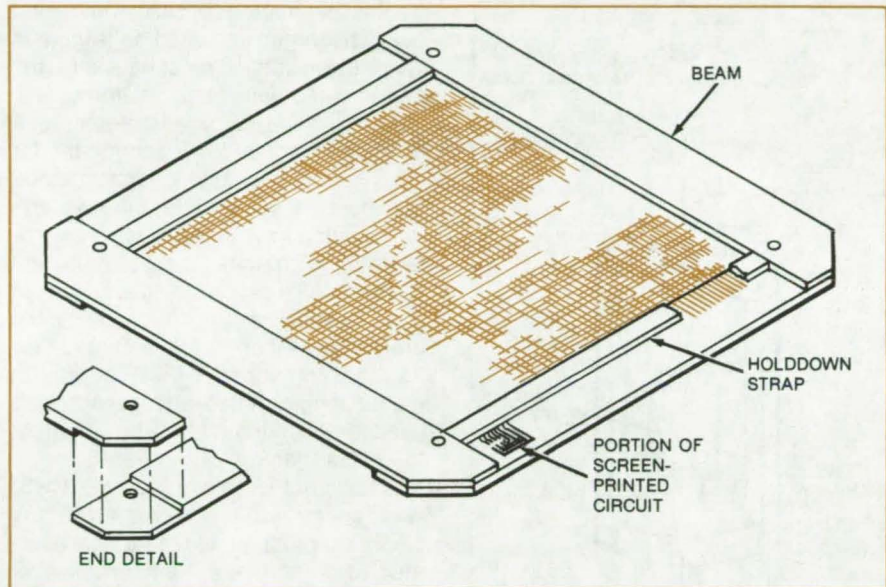
New spark-chamber frames, fabricated without organic-based adhesives or epoxy circuit boards, are less susceptible to contamination by outgassing than previous designs. The all-inorganic frames were developed for gamma-ray studies aboard spacecraft, where stable spark-chamber operation without gas refill is essential. They would offer the same advantage in terrestrial gamma-ray studies, in high-energy physics research, and other applications.

A typical spark chamber is assembled from 40 or 50 stacked frames, each containing hundreds of closely spaced wires (see figure). Within each frame, the wires lie in two adjacent parallel planes, in mutually perpendicular directions, forming a grid.

When a high-energy photon passes in the vicinity of one of the crosspoints of one of the grids, the locally-ionized filler gas conducts current between the two wires at the crosspoint. These wires define the x and y coordinates of the particle trajectory; the z coordinate is defined by the particular frame involved. The ends of the wires of each frame connect to circuits that record the coordinates of the trajectory.

The four ceramic or glass beams that form the edges of the square frame are bonded using a ceramic adhesive. The adhesive is selected for its low vapor pressure and for an expansion coefficient nearly equal to that of the frame material.

Wires are stretched across the frame between the opposing beams. A continuous wire is fed from a spool back and forth across the frame and is secured by holddown straps. After the



New **Spark-Chamber Frames** are assembled from four beams that are rabbeted at their ends. Ceramic or glass adhesives are used exclusively, and the printed circuit is applied by screen printing directly on the beams.

straps are bonded over the wire with a ceramic adhesive, the continuous wire is cut, and the wire ends are connected to a printed circuit overlaid directly on the beams. The circuit is applied by screen-printing silver paste and firing the silver in place.

The frame is assembled on a special wire-wrapping/firing jig. The jig aligns the beams while the ceramic adhesive is fired. Special combs attached to the jig guide the wire as it is wrapped on the frame. An automated wire-wrapping machine is used when attaching the wire.

A key element in the assembly of a satisfactory frame is the proper choice of materials. Effective compositions

for the frame material, the wire, the bonding agent, the silver paste, and the jig have been identified and tested. Data on these materials, and other information, can be obtained by requesting the Technical Support Package referenced below.

*This work was done by Thomas M. Heslin of **Goddard Space Flight Center**. For further information, Circle 83 on the TSP Request Card.*

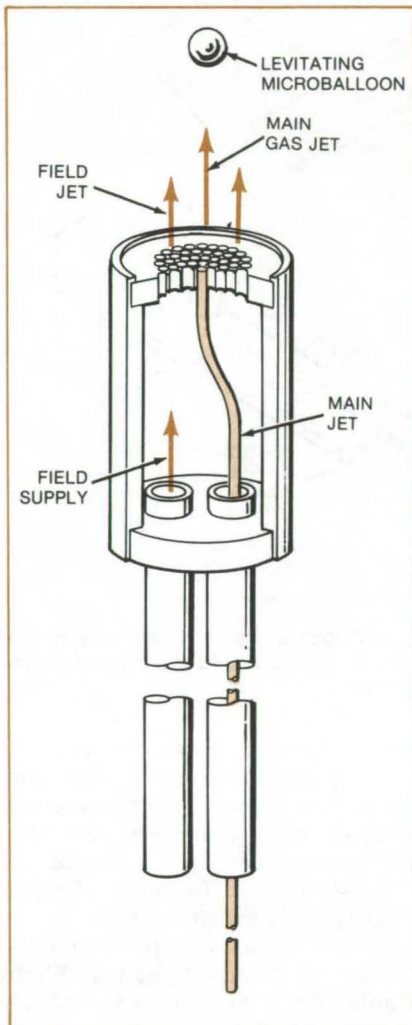
This invention is owned by NASA, and a patent application has been filed. Inquiries concerning nonexclusive or exclusive license for its commercial development should be addressed to the Patent Counsel, Goddard Space Flight Center [see page A5]. Refer to GSC-12354.



Controlling the Shape of Glass Microballoons

Percent yield of "perfect" glass microballoons is increased.

Marshall Space Flight Center, Alabama



Improved Collimated-Hole Structure is made from a platinum/rhodium alloy, making it possible to increase the microlevitating furnace temperature limit to 1,450° C. The levitating gas jets are supplied by two lines: one feeding through the center hole, forming the main jetstream, to support and manipulate the suspended microballoon, and the other feeding the remaining holes to keep the microballoon in the center during the heat treatment. The new structure will speed up the remelting and reshaping of the microballoons, reducing the number of rejects for the laser fusion studies.

Glass microballoons encasing heavy hydrogen and used as targets in laser fusion studies must have a nearly perfect geometry and uniform wall thickness. Only a small fraction of a typical production lot is acceptable for use. Recently an economical method has been developed to improve the microballoon symmetry, using microlevitating furnaces that remelt and reshape the balloons suspended in gas. An analysis of this technology has produced further improvements: new furnace components that operate at higher temperatures and gases to be used for levitation that would not affect the glass materials.

A collimated-hole structure (CHS) was constructed from a refractory platinum/rhodium alloy that can operate at a furnace temperature of 1,450° C. This speeds up the shaping process. Stainless steel used previously limited the upper operating furnace temperature to 1,000° C. In the future, a tungsten CHS may be used. It will withstand furnace temperatures of 2,000° C, further speeding up the process.

The CHS configuration was also modified (see figure) using hexagonally-arranged jet holes for feeding the levitating gas. The central hole feeds the main jetstream, and the rest feed

the field stream. The two flow velocities combine to suspend the microballoon and spin it on a horizontal axis, making it easier to manipulate it in a suspended state. The holes around the center are dimpled to stabilize the lateral-spinning microballoon.

Analysis of heat treatment revealed that oxygen fostered devitrification of the glass materials. Therefore, reducing gases (e.g., nitrogen or hydrogen) are recommended to eliminate this damage to the microballoon walls.

The furnaces, it was found, could also be improved using positive electronic sensing and control to maintain a constant pressure differential across the CHS when the furnace pressure and temperature are changing. This control will retain the microballoon in a stable levitating state.

This work was done by Stanley A. Dunn and Steven Gunter of Bjorksten Research Laboratories Inc. for Marshall Space Flight Center. For further information, Circle 84 on the TSP Request Card.

Inquiries concerning rights for the commercial use of this invention should be addressed to the Patent Counsel, Marshall Space Flight Center [see page A5]. Refer to MFS-25230.

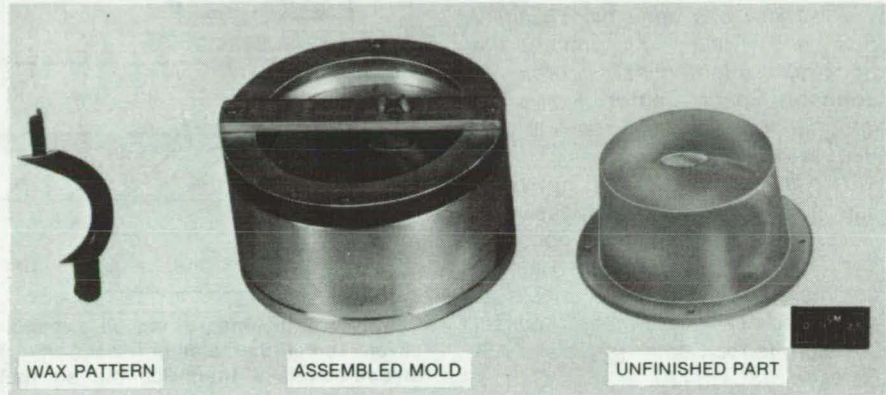
Forming Complex Cavities in Clear Plastic

Lost-wax process is used to mold plastic parts.

Lewis Research Center, Cleveland, Ohio

An increasing number of applications require the use of optically clear components. For example, these components are necessary for the efficient design of systems utilizing complex combustion and manifold systems. A technique has been developed that utilizes standard procedures developed for specialized metal casting. Complex internal cavities are readily formed in clear plastic parts by using elements of the "lost-wax" process.

The size and shape of the desired internal cavity are first replicated in a wax pattern. This pattern is then positioned in an assembly mold that conforms to the exterior requirements of the part. An inexpensive clear epoxy resin is cast into the mold and solidifies around the wax pattern. After curing of the epoxy, the wax is heated until it melts and is poured from the cavity.



Economical Casting Process produces optically-clear plastic components of complex shapes.

The figure shows the wax pattern, the assembly mold, and the finished casting. Substantial savings are obtainable utilizing this technique for the fabrication of parts with complex cavities.

This work was done by T. Riley, G. Matusik, and C. Casterline of Lewis Research Center. No further documentation is available.
LEW-13412

Shrinking Plastic Tubing to Nonstandard Diameters

Process allows larger-than-normal postshrink diameters without splitting.

Lyndon B. Johnson Space Center, Houston, Texas

A new process allows heat-shrinkable plastic tubing to be shrunk to nonstandard sizes or to special contours. The new process for tetrafluoroethylene tubing minimizes temperature fluctuations and monitors the temperature to limit the shrinkage to a value greater than one-half the overexpanded diameter. Formerly, when shrinkage was restricted, the tube wall tended to split because it was too thin to resist the shrinking force at the shrink temperature.

The new method was originally used to prepare a seal for the cargo door of the Space Shuttle. A spring, which gives the seal its proper stiffness, is inserted into the shrunk tubing.

In the new shrinking method, the temperature of the tubing is monitored so that it can be removed from the oven at the proper time. A fiberglass-insulated thick-wall steel pipe is inserted in the shrinking oven to provide a uniform temperature enclosure (see figure). The tubing is slipped over an aluminum mandrel. The mandrel diameter is the same as the diameter required in the tubing. The mandrel is shorter than the tubing so that the ends of the tubing can be held partially closed by clamps that prevent the tubing from shrinking lengthwise. The tubing and mandrel are placed into a supporting coil of aluminum or steel wire. A thermocouple is positioned in the mandrel near one of its ends.

The assembly is slid into the hot steel pipe in the oven, with the thermocouple end nearest the oven door. The coil positions the mandrel and tubing at the center of the pipe.

The oven-temperature setting is kept at about 670° F (354° C) while the thermocouple temperature is monitored. When the thermocouple temperature reaches about 630° F (332° C), the mandrel and tubing are removed from the oven. The tubing will have shrunk to the desired diameter.

With the wire supporting coil and aluminum mandrel removed from the oven, a bolt of fiberglass is wrapped around the supporting coil so that cooling proceeds slowly. When the tube and mandrel have cooled, the

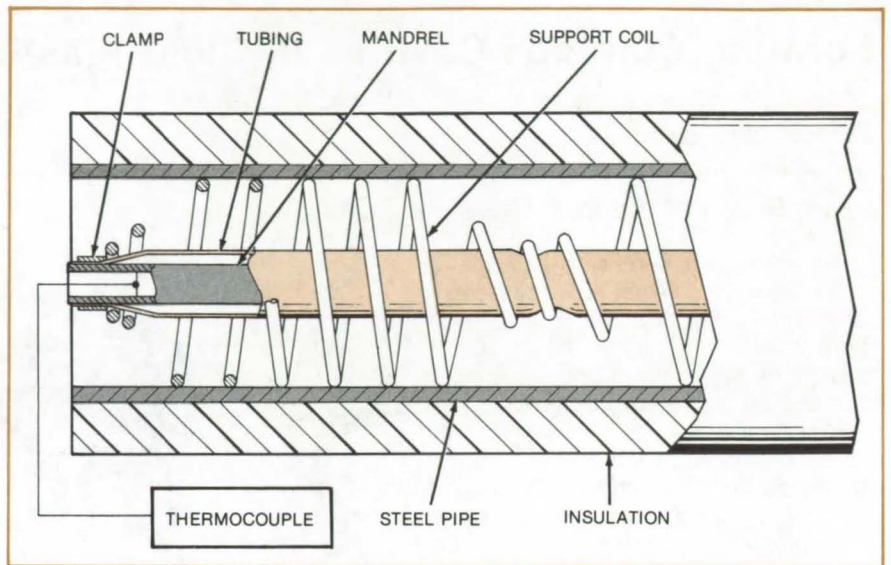
(continued on next page)

thin-tube mandrel is removed by chemical milling.

The method has been used to shrink 9-ft (2.74-m) lengths of 1.25-in. inner-diameter, 0.004-in. wall tubing to 0.75-in. inner-diameter, 0.008-in. wall (3.175-cm inner-diameter, 0.01-cm wall tubing to 1.9-cm inner-diameter, 0.02-cm wall).

This work was done by William V. Ruiz and Conley S. Thatcher of Rockwell International Corp. for Johnson Space Center. For further information, Circle 85 on the TSP Request Card.

This invention is owned by NASA, and a patent application has been filed. Inquiries concerning nonexclusive or exclusive license for its commercial development should be addressed to the Patent Counsel, Johnson Space Center [see page A5]. Refer to MSC-18430.



Tetrafluoroethylene Tubing on a mandrel is supported within a hot steel pipe by several small-diameter coil sections. The rising temperature of the mandrel is measured via a thermocouple so that the assembly can be removed without overshrinking (and splitting) the tubing.

Thermal Barrier and Gas Seal

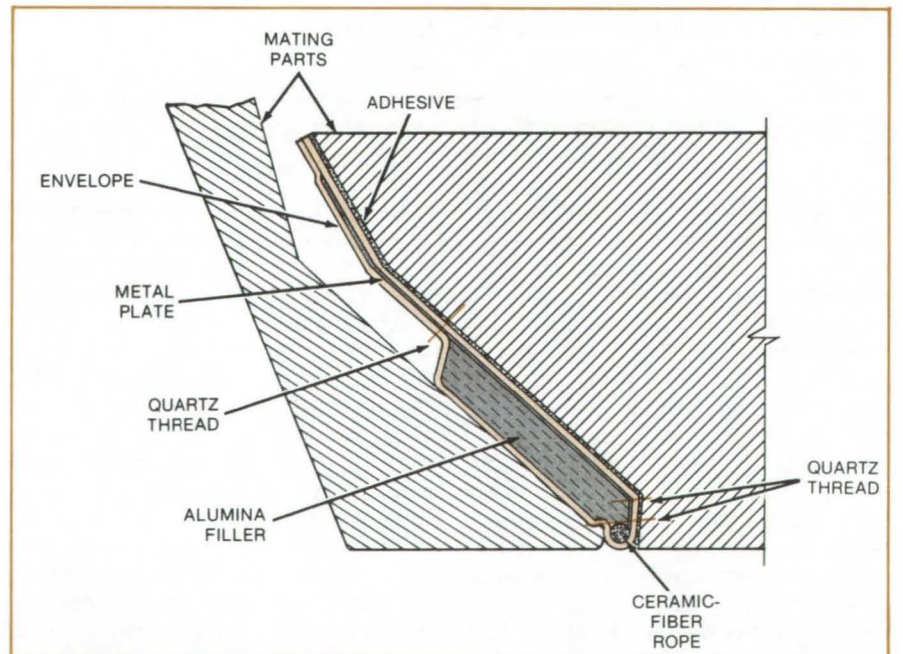
Resilient baglike seal tolerates thousand-degree temperatures.

Lyndon B. Johnson Space Center, Houston, Texas

A high-temperature seal prevents gases from entering gaps between mating parts. The seal withstands temperatures of 2,300° F (1,260° C), or higher, and accommodates small changes in the gap size [width variations of about 0.06 inch (1.5 mm)] without losing its gas-barrier properties. At the same time, the seal maintains a smooth aerodynamic surface across the gap.

Developed for the Space Shuttle, where it closes the gap between the nose landing-gear doors and the forward fuselage, the seal may have high-temperature industrial uses as well, for example, in equipment for the liquefaction or gasification of coal.

As shown in the illustration, the seal contains alumina filler in a woven ceramic-fiber envelope. The alumina both insulates and seals, and the ceramic-cloth envelope stitched together with quartz thread holds the alumina in position between the sealed parts. A metal plate (made of a heat-



High-Temperature Seal includes an alumina filler backed by a metal plate. The alumina-filled envelope is easily handled and installed and can be used in high-temperature industrial processes, such as coal gasification and liquefaction.

resistant material such as nickel alloy) serves as the backbone and helps the seal hold its shape during fabrication, handling, and installation. A ceramic-fiber rope along the bottom of the plate furnishes a stiff rounded edge at the gap opening.

The materials were selected for their low thermal conductivity as well as their resistance to high tempera-

tures. The plate side of the seal is bonded to the adjacent part with a high-temperature adhesive. The mating part then compresses the envelope and filler so that the gap is sealed. The seal changes its shape to conform to small changes in the gap width.

This work was done by John O. Kane and Milo Surbat of Rockwell International Corp. for **Johnson**

Space Center. For further information, Circle 86 on the TSP Request Card.

This invention is owned by NASA, and a patent application has been filed. Inquiries concerning nonexclusive or exclusive license for its commercial development should be addressed to the Patent Counsel, Johnson Space Center [see page A5]. Refer to MSC-18390.

Heat-Shrinkable Sleeve Aids in Installing Universal Joints

Tubing stiffens the joint and protects it from contamination.

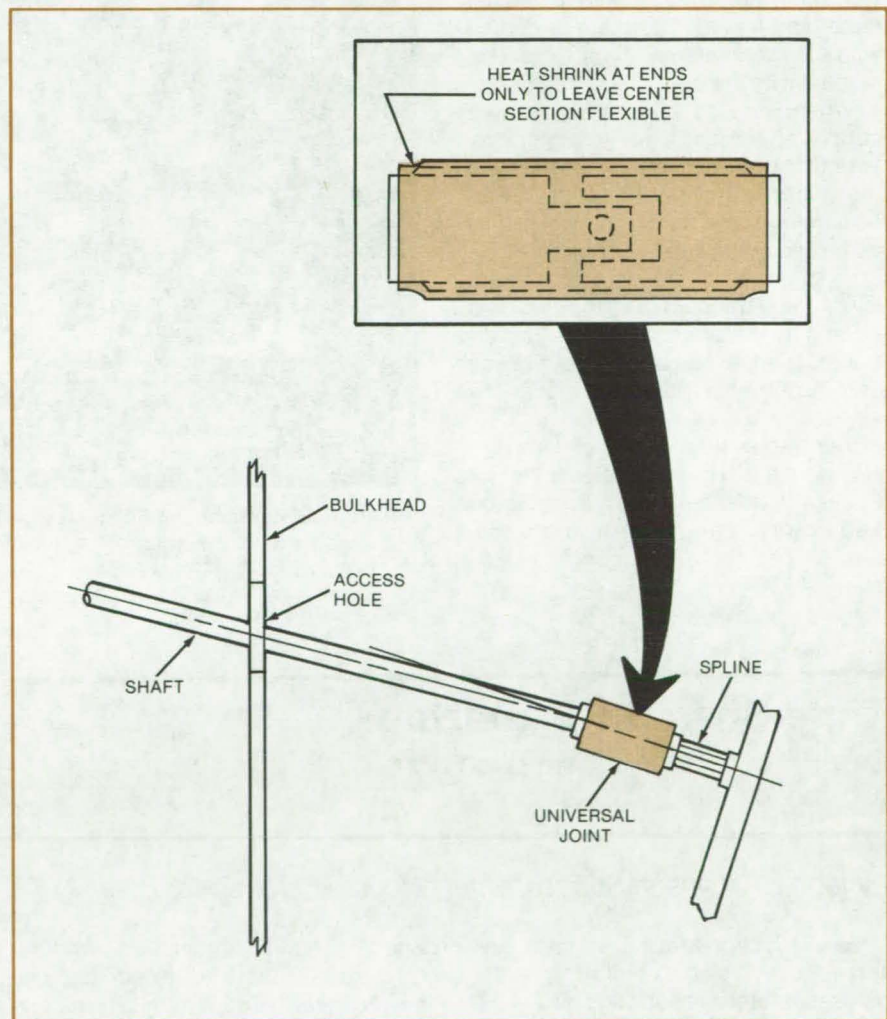
Lyndon B. Johnson Space Center, Houston, Texas

Heat-shrinkable tubing, normally used as electrical insulation on wire and cable, is now being applied in a new and quite different way — to “stiffen” universal joints so they can be attached to other structural members in confined spaces. This innovative technique, which saves considerable time and effort when assembling nonrigid parts, makes it unnecessary to use special holding fixtures or tools. In addition, the tubing also protects the joint from dust and other contamination.

The method was developed for attaching a universal joint on the end of a shaft to a spline fitting, where access to the spline is only through a small hole in a bulkhead (see figure). The tendency of the joint to “droop” under the pull of gravity makes it difficult to align it with the spline.

To overcome this problem, assemblers place a length of heat-shrinkable tubing over the joint, as shown, and apply heat at the ends to shrink it in place. This stiffens the joint sufficiently so that it is easily aligned with the spline. After the parts are joined, the sleeve remains in place as a shield against contamination. It is flexible enough so that it does not interfere with normal motion of the joint.

This work was done by William S. Green and Fredrick W. Thompson of Rockwell International Corp. for **Johnson Space Center.** No further documentation is available. MSC-18685



A **Heat-Shrinkable Sleeve** stiffens this joint so that it can be aligned with a spline fitting. Previously, the unsleeved joint would droop, making it difficult to attach it to the splines.

Improved Particulate-Sampling Filter

Small surface indentations entrain a larger and more representative sampling.

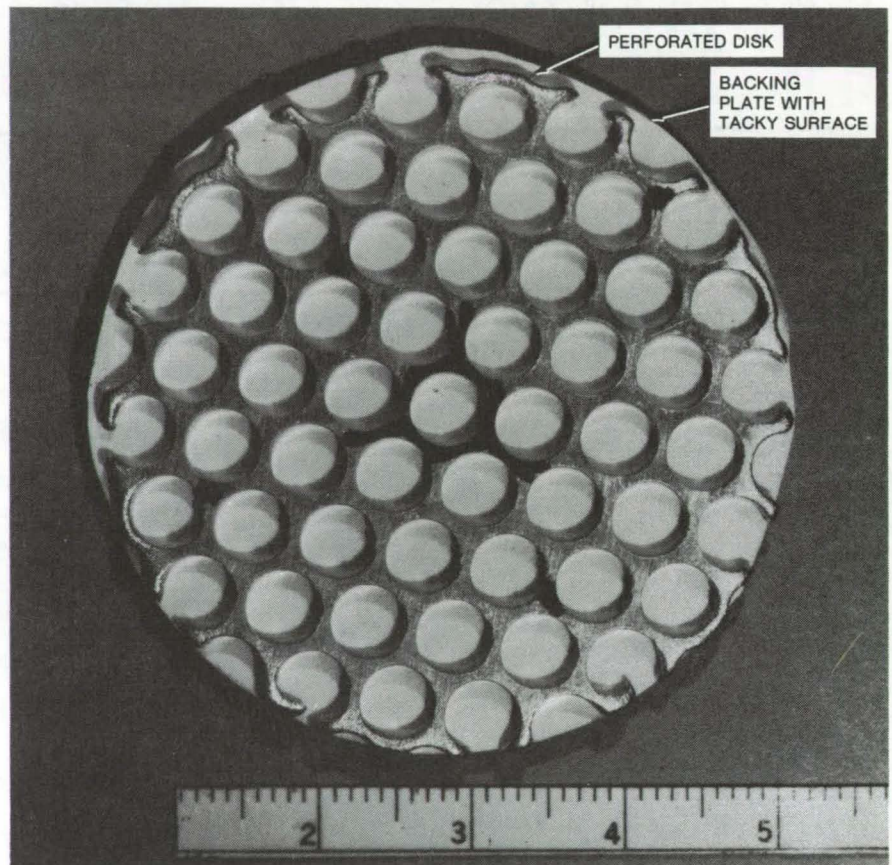
NASA's Jet Propulsion Laboratory, Pasadena, California

A passive filter for sampling the particulates in a gas flow is more efficient because of its indented surface. When tested in the air-purge line of a planetary spacecraft, the indented surface trapped larger and more representative samples than did a petri-dish smeared with a smooth layer of adhesive. Potential applications of the improved filter are in air-quality monitoring at industrial sites, in mines, and in and around nuclear powerplants.

The new filter consists of a perforated aluminum disk backed by a flat plate (see figure). The plate is coated with a sticky material on its surface in contact with the disk.

When installed with its active area parallel to the gas flow, the filter creates tiny eddy currents in and around the "wells" in the perforated disk. Particulates in the eddy currents thus come in contact with the sticky surface for a longer time (with greater probability of being trapped) than they would if flowing over a smooth surface. The extracted sample can be analyzed onsite or transported to a laboratory for analysis.

This work was done by Alan R. Hoffman and Horst W. Schneider of Caltech for NASA's Jet Propulsion Laboratory. For further information, Circle 87 on the TSP Request Card. NPO-14801



The **Particulate-Sampling Filter** is assembled from a perforated disk and a flat backing plate with a sticky surface. The thickness of the perforated disk is about 1/8 inch (0.31 cm).

Time-Shared RF Brazing

One RF generator is controlled from two independent work stations.

Lyndon B. Johnson Space Center, Houston, Texas

Two induction-brazing stations are served by a single radio-frequency (RF) generator with the aid of an RF switch and simple control boxes. The time-shared outlet increases the utilization and productivity of a costly RF power generator.

The two-station system was developed for brazing tubular joints on the

Space Shuttle life-support system. Operators at the brazing stations use power from the generator alternately; while one operator is brazing, the other sets up a new workpiece.

A standard RF switch routes power from a 30-kilowatt generator to either of the stations. The switch is controlled by boxes at the brazing stations

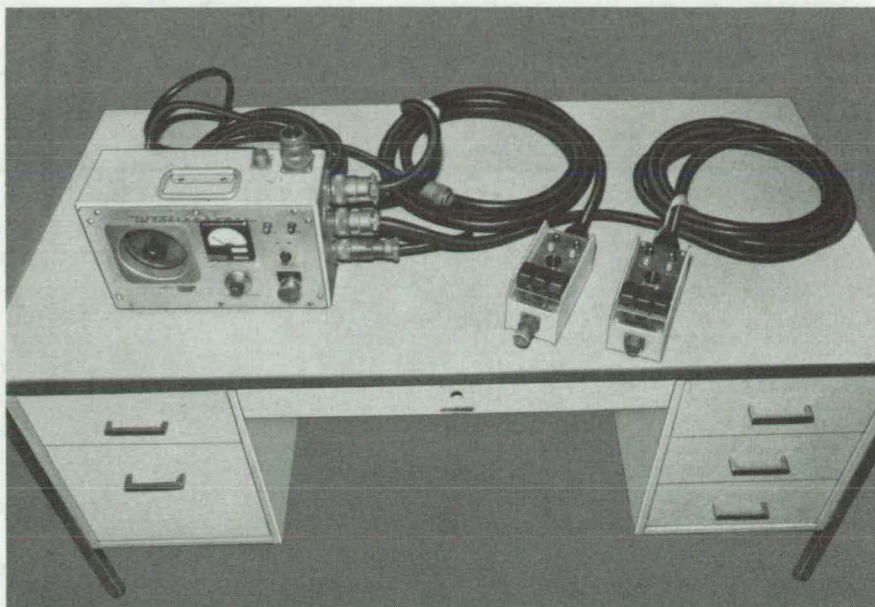
(see figure). When an operator turns on the control box and presses the "station select" switch on that box, the RF switch connects that station to the generator.

A light on each control box indicates which operator has control. When the generator has warmed up, a "ready" lamp lights up. Operator 1 pushes the

“braze” button on control box 1, and RF energy flows to station 1. When the work is finished, operator 1 pushes the “stop” button. The generator is then available to operator 2, who pushes the buttons on control box 2 to braze at station 2.

Brazing may be stopped automatically, instead of manually, by a brazing-temperature controller at the station; or a timer in the RF switch housing may terminate a brazing operation automatically. The RF switch is air-operated with water-cooled contacts. If the switch loses air pressure, the generator is automatically prevented from transmitting power.

This work was done by John A. Stein and Maurice A. Vannasse of Rockwell International Corp. for Johnson Space Center. For further information, Circle 88 on the TSP Request Card.
MSC-18617

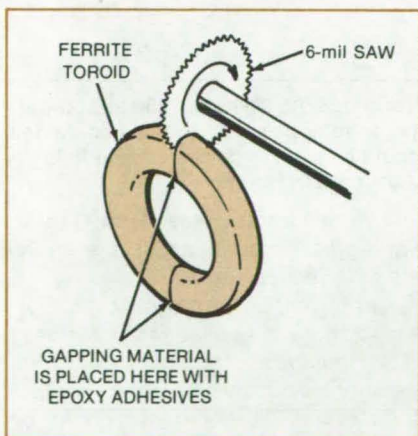


Control Boxes for Stations 1 and 2 connect to the RF switch and RF generator through a master control box (left). The master control must be turned on before the ancillary control boxes can be used.

Producing Gapped-Ferrite Transformer Cores

Improved manufacturing techniques make reproducible gaps and minimize cracking.

NASA's Jet Propulsion Laboratory, Pasadena, California



Molded Unfired Transformer Cores are cut with a thin saw and then fired. The hardened semicircular core sections are then bonded together, placed in an aluminum core box, and fluidized-coated. After the winding is run over the box, the core is potted. This economical method significantly reduces the number of rejects.

New fabricating techniques produce more-uniform ferrite toroidal core inductors with an airgap. In conventional methods, airgaps in transformer cores are produced by partly grinding away the central hollow sections of cup-shaped half cores and then by cementing the halves together. Since this operation is manual, the gaps are frequently not uniform and, because the cores are brittle, many crack apart during winding and potting, resulting in a high reject rate.

In the new method, the cores are molded from fine ferrite powder shaped by means of a volatile binder. As taken from the mold, the toroid is soft and chalklike. Instead of firing the mold to cure the binder, as is normally done, the cores are cut apart radially using a 6-mil (0.2-mm) saw (see figure). The halves are then fired to produce a hard semicircular core section. The toroid is formed when both halves are ce-

mented together using commercially-available gapping material and epoxy adhesive. This allows the final core to be assembled with any required gap size.

Before potting, the cemented halves are placed in an aluminum core box filled with a sealing compound that will surround the assembled core. The box is covered with a washerlike epoxy/fiberglass cover and fluidized-coated. Wiring is then wound over the aluminum box that encases the core. Potting is performed in a conventional way, after the winding; however, this time stresses are relieved because the core is free to adjust itself within the damping compound surrounding the core.

This work was done by Colonel W. T. McLyman of Caltech for NASA's Jet Propulsion Laboratory. For further information, Circle 89 on the TSP Request Card.
NPO-14715

Plastic Welder

Induction heating is used to join plastic parts.

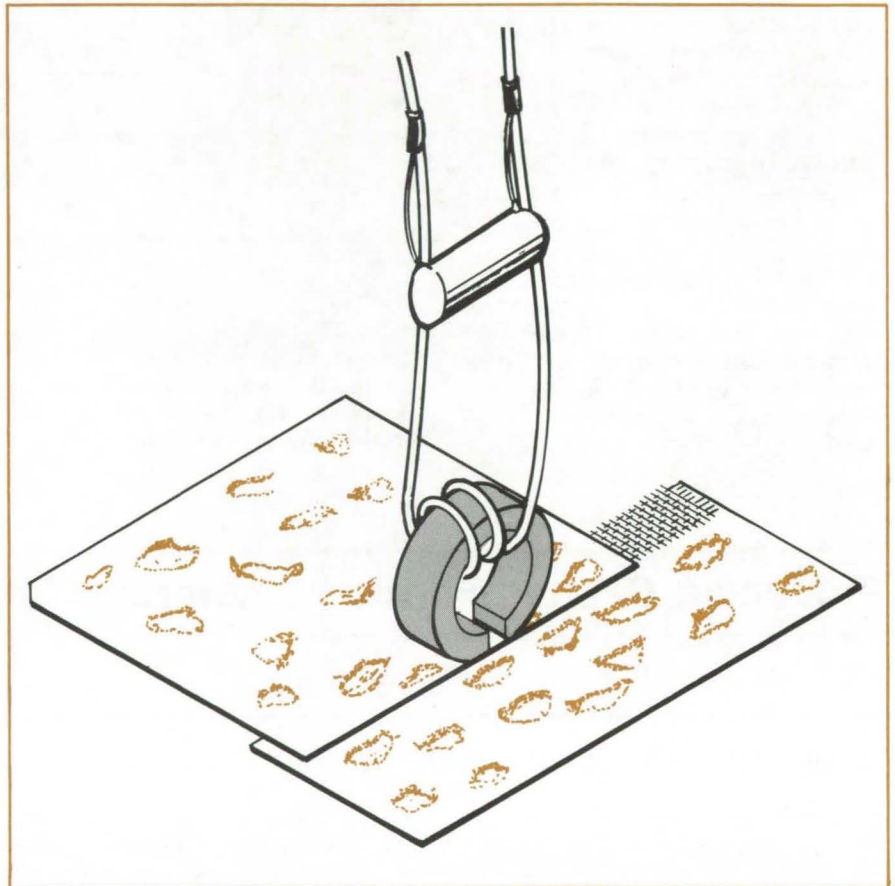
Langley Research Center, Hampton, Virginia

A low-cost, self-contained, and portable welding system developed at Langley Research Center joins plastic parts by induction heating. The device can be used in any atmosphere or in a vacuum, and the plastic components can be joined in situ.

Conventional methods used to join thermoplastics and composites include adhesives, fusing, and mechanical fasteners (e.g., using nuts and bolts or rivets). Adhesives are not reliable when parts are exposed to a vacuum, and fusing often deforms the plastic and causes it to flow around a joint. Mechanical fasteners require hole preparation and special hardware; riveting, if heat is used, can cause hole deformation; and nuts and bolts may require two people for assembly, especially with large sheets. Induction heating, however, causes little or no deformation at the joints, utilizes few component parts, and can be used with almost any type of thermoplastic.

A modified, wound, toroidal inductor core (see illustration) is used to transfer magnetic flux through the thermoplastic to a carbon steel screen. The airgap cut into the toroid diverts the path of the magnetic flux from the toroid to the screen.

Typically the metal screen would be cut into long strips 1/4 in. (0.64 cm) wide and sandwiched between sheets of plastic at a joint to join one sheet of plastic to another or to join a plastic sheet to a structural beam. The airgap of the toroid is placed on one of the plastic surfaces directly above the screen. When the toroid is energized, the alternating current produces inductive heating in the screen, causing the plastic surfaces on either side of the screen to melt and flow into the screen



Inductive-Heating Welder joins plastic sheets thermally. The low, 25- to 100-watt, power required readily permits it to be battery- or solar-powered and self-contained. Various configurations of the plastic welder could be used in the aerospace industry and in the automobile, furniture, and construction industries.

and forming the joint. The temperature of the screen is determined by such factors as the input power, number of coil windings, width of the airgap, and the frequency of the alternating current. The toroid is moved along the seam or joint at a controlled speed to produce optimum joining.

This work was done by John D. Buckley, Robert L. Fox, and Robert J.

Swaim of Langley Research Center. For further information, Circle 90 on the TSP Request Card.

This invention is owned by NASA, and a patent application has been filed. Inquiries concerning nonexclusive or exclusive license for its commercial development should be addressed to the Patent Counsel, Langley Research Center [see page A5]. Refer to LAR-12540.

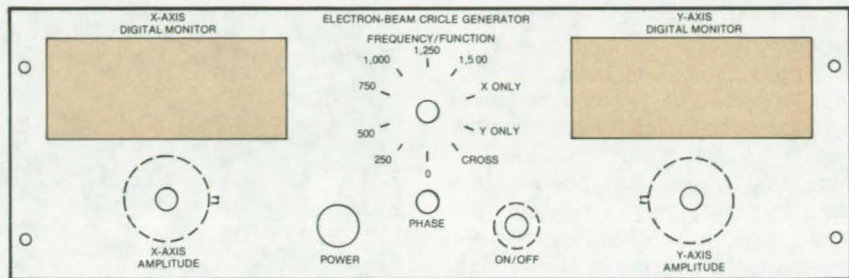
Electron-Beam Welder Circle Generator

A generator rotates an electron beam and performs other convenient functions during the welding process.

Marshall Space Flight Center, Alabama

Conventional electron-beam welders will not rotate the beam in a circular pattern. Circular or arc joints are usually welded by time-consuming techniques relying heavily on the operator's skill. A new circle generator automatically guides the beam in preset circular or elliptical patterns. The generator output is ac coupled to the welder deflection coil to preclude dc offset that could affect the beam alignment.

The generator utilizes two equal-amplitude sinusoidally varying signals set 90° out of phase (see control panel drawing). One signal controls the x-axis displacement, and the other controls the y-axis displacement. The method is identical to that used to produce the well-known Lissajous patterns on oscilloscopes. By varying the phase angle between the two signals, the beam can be made to describe either a circle or an ellipse.



Electron-Beam Circle-Generator Panel has controls to set the beam in circular or elliptical patterns. The panel has x- and y-axis signal amplitude controls and permits phase adjustment between the two signals to weld circular or elliptical joints. A frequency selector on the panel controls the beam travel speed. Two digital readouts monitor the amplitudes of x- and y-axis inputs.

The welding speed can be varied with a frequency selector that ranges from 250 to 1,500 Hz in 250-Hz steps. The amplitudes of the x- and y-axes are varied by adjusting the phase shift. Both high- and low-range adjustments are available, and each axis can be controlled separately. A crosshair is

provided for setup and beam alignments.

This work was done by Richard K. Burley of Rockwell International Corp. for Marshall Space Flight Center. For further information, Circle 91 on the TSP Request Card. MFS-19441

“Foreign Material” To Verify Root Fusion in Welded Joints

A foil or thin wire at the weld root can be used to verify weld penetration.

Marshall Space Flight Center, Alabama

A very thin wire, or foil, placed at the root of an electron-beam weld joint before the welding can verify the fusion of the weld root. The material (e.g., gold or zirconium) is “foreign” to the weld joint; and since only very small amounts are used, it does not affect the joint structure. When the weld is adequately penetrated, the material mixes with the weld, and traces of it diffuse to the top (the weld crown). A chemical analysis (e.g., spectroscopic) of samples taken from the weld crown will identify the foreign material and verify that the root has fused.

Weld roots are difficult to examine because the root is usually inaccessi-

ble to visual inspection. X-ray and ultrasonic inspection techniques, two commonly available methods, are not always reliable.

Using the new method, weld samples can be rapidly prepared without elaborate machining that could delay the production line. Any convenient handtool can be used to remove minute samples from the crown. Also spectroscopic analysis is highly sensitive so that a minimum amount of trace material can be used to avoid degrading the weld. The content of trace foil in the weld crown is predictable from the amount placed at the root and is accurately measurable by spectroscopic elemental analysis.

Currently, computer studies are being made to determine the optimum amount of material to be used without degrading the weld structure. Good results have been obtained using a gold/nickel alloy, which may be even better than gold in minimizing possible weld embrittlement.

This work was done by R. E. Kleint of Rockwell International Corp. for Marshall Space Flight Center. For further information, Circle 92 on the TSP Request Card.

Inquiries concerning rights for the commercial use of this invention should be addressed to the Patent Counsel, Marshall Space Flight Center [see page A5]. Refer to MFS-19496.

Tube-Welder Aids

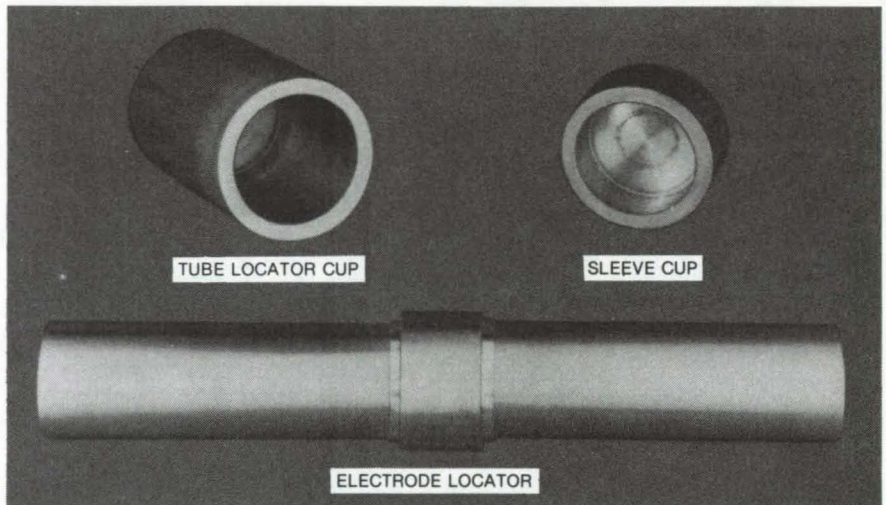
Simple tools assist in setting up and welding tubes.

Lyndon B. Johnson Space Center, Houston, Texas

A new set of tools designed for repeated tube welding can speed up mass production. Each set is made for a specific tube size and weld-joint location and can be compared to templates used in lettering. Once the tools are made, they are easily slipped on the tubes to set an airgap between the welding head and the joint and to mark sleeve and joint positions. Conventional measurements are too slow for mass production and are prone to errors similar to sloppy hand lettering without a template.

The set, as shown in the photograph, includes an electrode locator, a sleeve cup, and a tube-locator cup. The electrode locator incorporates a sleeve that fits over the tube to be joined. The sleeve thickness matches the desired gap between the electrode and the weld joint. The electrode housing is simply slipped over the sleeve, and the electrode is lowered to touch the sleeve surface. This sets the gap, and the electrode is tightened in that position for repeated use without further readjustments.

The sleeve cup is simply slipped over the tube end like a cap. The cup in place, the tube is marked around the cup edge to show where one end of a



Tube-Welder Aids speed up mass-production tube welding. A set of such tools can be easily made to fit a given tube diameter. A finished set can be used repeatedly to fix the electrode-to-weld gap and to mark the sleeve and joint positions.

welding sleeve will join the tube. The same procedure is repeated with a mating tube end to mark the other end of the welding sleeve.

A somewhat similar tube-locator cup is also slipped over a tube end. Its edge marks a stop for a weld-locator tool moved flush against the cup. The weld-locator tool is clamped at that location to show the area where the tube is to be welded.

The tools can be readily made in most tube-manufacturing plants and will more than pay for themselves in a very short time in reduced labor costs and quality control.

This work was done by James F. Weaver of Rockwell International Corp. for Johnson Space Center. For further information, Circle 93 on the TSP Request Card.
MSC-18687

Honing Fixture for Weld Electrodes

A fixture for refacing electrodes mounts directly on the welding machine.

Marshall Space Flight Center, Alabama

Weld quality is improved by a honing fixture that attaches directly to the welding machine. Although developed for refacing the electrodes on a particular commercial welder (Unitek), the fixture could easily be adapted to other resistance welding machines.

The new fixture is used in lieu of manually refinishing the electrodes with emery paper or other abrasive. It produces uniformly flat, parallel electrodes, in contrast to the rounded and skewed faces and generally inconsistent results of the manual approach.

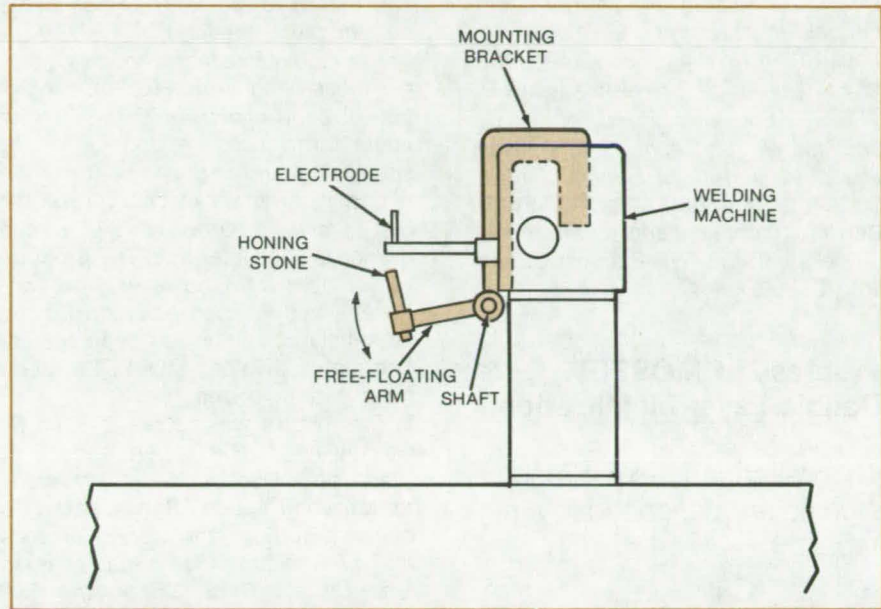
Moreover, it does so in less time, which can translate into significant cost savings on production runs.

As shown in the figure, the honing fixture consists of a free-floating arm that travels along a cylindrical shaft. A special bracket attaches the shaft to the welding machine.

An abrasive stone is clamped in a slot on the free-floating arm. Thus, the fixture allows the operator to move the stone up and down between the electrodes. As long as the stone is flat and the fixture is properly aligned, the flatness and parallelism of the electrode faces are assured.

This work was done by R. F. Nicholas and W. H. Schubert of Rockwell International Corp. for Marshall Space Flight Center. To obtain drawings of the electrode-honing fixture, Circle 94 on the TSP Request Card.

MFS-19537



The Honing Fixture is installed on the welding machine by using a mounting bracket. The up and down movement of the stone against the electrode can be done manually, or a motor drive could be designed.

Books and Reports

These reports, studies, and handbooks are available from NASA as Technical Support Packages (TSP's) when a Request Card number is cited; otherwise they are available from the National Technical Information Service.

Silicon Nitride Passivation of IC's

A feasibility study looks at the effectiveness of a silicon nitride passivation coating against the effects of moisture and mobile ions.

A 49-page report evaluates the effectiveness of depositing low-temperature (100° to 300° C) silicon nitride protective layers on wire-bonded integrated circuits mounted on lead frame assemblies. A feasibility study evaluated the effectiveness of silicon nitride passivation in inhibiting the corrosion due to moisture at wire interconnect sites of plastic-molded

integrated circuits. The study assessed the overall protection given a plastic-encapsulated device containing charge-sensitive microcircuits. A CMOS microcircuit was used in the study.

Two methods of silicon nitride passivation were studied: photonitride passivation and plasma nitride passivation. The devices were passivated (not to be confused with passivation of the chip alone) while still attached to the lead frames. After passivation and encapsulation, the devices were subjected to a sequence of accelerated electrical and environmental tests. The tests included temperature cycling, high-temperature electrical stress, and temperature and humidity exposure. Electrical parameter measurements were made of all devices initially and then at intervals in the course of each test.

From the tests it was concluded that photonitride passivation is compatible with all wire-bonded lead frame assemblies tested, with or without initial chip passivation, and that plasma nitride passivation of lead frame assemblies is possible only if

the chip is passivated before assembly. The survival rate after the environmental-test sequence of devices with a coating of plasma nitride on the chip and a coating of either plasma nitride or photonitride over the assembled device is significantly greater than that of devices assembled with no nitride protective coating over either chip or lead frame. The majority of devices with unpassivated chips and with photonitride over the lead frames survived the environmental test sequence.

Moreover, the report concludes that plastic-encapsulated circuits incorporating a photonitride protective coating exhibit high survival rates. The survival of devices with no prior chip passivation suggests the possibility of simplifying the device fabrication process by eliminating the chip passivation operation.

In addition to descriptions of the passivation processes, the report includes several tables that summarize the results of the tests. There are also figures included that show the effects of flexing on the coatings.

(continued on next page)

[Also see related article on photonitride passivation, "Photonitride Passivating Coatings for IC's" (MFS-25401), on page 231 of this issue.]

This work was done by J. J. Erickson, F. L. Gebhart, T. C. Hall, and J. W. Peters of Hughes Aircraft Co. for Marshall Space Flight Center. To obtain a copy of the report, Circle 95 on the TSP Request Card. MFS-25309

Progress in MOSFET Double-Layer Metalization

Theoretical and experimental studies are described in a new report.

A 237-page report describes a one-year research effort in VLSI fabrication. Four activities are described:

- a theoretical study of two-dimensional diffusion in SOS (silicon-on-sapphire);
- the setup of a sputtering system, furnaces, and photolithography equipment;
- experiments on double-layer metal; and
- an investigation of two-dimensional modeling of MOSFET's (metal-oxide-semiconductor field-effect transistors).

Computer simulations of various phosphorus and boron diffusions in SOS were completed using a diffusion program. The objective was to produce curves of the variation with diffusion time and temperature of the junction depth, sheet resistance, and integrated impurity dose. Data were generated for boron and phosphorus redistributed in nitrogen, dry oxygen, and steam ambients for <111> oriented SOS films, using a model that considers the implanted profile, oxidation, and diffusivity.

In place at the IC-fabrication facility are the furnaces, the photolithography apparatus, and other equipment for double-layer metalization. The only missing apparatus is an SiO₂ reactor.

Previous double-layer metalwork emphasized wet chemistry. By incorporating ultrasonic etching of the vias, premetal cleaning with modified buffered HF, phosphorus-doped SiO₂,

and extended sintering, yields of 98 percent were obtained.

A two-dimensional modeling program has been written for the simulation of short-channel MOSFET's with nonuniform substrate doping. A key simplifying assumption is that the majority carriers can be represented by a sheet charge at the silicon dioxide/silicon interface. The program is not complete; however, the two-dimensional Poisson equation for the potential distribution has been solved. The status of other MOSFET simulations is summarized.

This work was done by J. D. Gassaway, J. D. Trotter, and T. E. Wade of Mississippi State University for Marshall Space Flight Center. To obtain a copy of the report, "Trends and Techniques for Space Base Electronics," Circle 96 on the TSP Request Card. MFS-25239

Optimizing Costs of VLSI Circuits

Various costs of custom VLSI circuits are analyzed.

An 85-page report analyzes the costs of developing and producing low-production-volume, customized VLSI (very-large-scale integrated) circuits. A relationship is developed between the IC cost and an electronic system cost using IC cost models that are based on a design/fabrication approach. The emphasis of this report is in developing an understanding between the cost and volume for custom circuits that will be used by NASA. Reliability is one of the major cost components in these models.

The first of the five report sections states the purpose of this project, summarizes the new models, and presents a brief history of electronic system development. Examples are cited of how the systems have grown in complexity from tube technology to modern VLSI circuits that pack up to 75,000 transistors.

The second section presents a macroscopic model of electronic system cost. The electronic system is assumed to be partitioned into LSI chips composed of distinct subassemblies.

The cost of the entire system is then related to the subassembly cost, the number of subassemblies being variable depending on the integration level.

A macroscopic model of MOS IC chip cost is presented in the third section. The model is developed for IC die cost in terms of manufacturing parameters and the degree of integration as it relates to the die area.

The fourth section discusses die and system cost curves for four cases: (1) a full-custom seven-mask-level CMOS LSI, (2) standard CMOS LSI, (3) semicustom CMOS LSI in double metal, and (4) semicustom CMOS LSI in a single metal.

Four appendix sections conclude the report. Three list some very useful reference literature; the fourth presents a basic-language computer program used in analyzing die and system costs.

The report has a number of plotted curves that show relationships among various cost and circuit parameters. Benefit-to-cost ratio, a popular decisionmaking tool in selecting the most economical system circuits, is also presented.

The presented analysis serves as a solid basis for future cost modeling. As the models become more precise, electronic systems manufacturers will be able to tailor an optimum mix of standard and customized IC's that would go into a particular system.

This work was done by Koy B. Cook, Jr., and David V. Kerns, Jr., of Auburn University for Marshall Space Flight Center. To obtain a copy of the report, "Cost Optimization in Low Volume VLSI Circuits," Circle 97 on the TSP Request Card. MFS-25348

An Automated Oxide and Diffusion Facility for IC's

Totally-automated oxidation and diffusion facility for fabricating the IC's

A 34-page report discusses an IC fabrication facility developed at the Marshall Space Flight Center. [Also see related articles "An Automated Photolithography Facility for IC's" (MFS-25073) and "Automated Ion Implantation for IC's" (MFS-25193) on

page 115 of *NASA Tech Briefs*, Vol. 5, No. 1.] The almost-entirely-automated oxide-growth and diffusion plant will be a part of an overall IC fabrication facility requiring virtually no labor other than process-control monitoring. The facility will produce ultrareliable IC's that will function for 25 years or longer in spaceflights and other critical applications.

The new system will process wafers arriving at the facility on an air track. The wafers will be automatically loaded into a furnace tube, processed, returned to the track, and sent to the next operation. The entire process will be controlled by a computer.

At this stage the system was already installed at the two three-stack furnaces and checked. The following diffusion and oxidation processes were demonstrated: (a) wet and dry oxidation for general use, (b) wet and dry oxidation for gate oxide, (c) boron diffusion, (d) phosphorus diffusion, and (e) sintering.

Part of the system incorporates state-of-the-art components and processes, such as the diffusion furnace

and high-temperature-grown oxide. However, several major innovations have been demonstrated: (a) process controller specifically designed for semiconductor processing; (b) an automatic loading system to accept wafers from an air track, insert them into a quartz carrier, and place the carrier on a paddle for insertion into the furnace; (c) automatic unloading of the wafers back onto the air track; and (d) boron diffusion using diborane.

The system will perform oxidation and diffusion processes as required for PMOS processing. No experience is yet available on the productivity of the design; however, enough data have been gathered to suggest several improvements in future systems. These include a more-flexible real-time process controller with improved capacity, a simpler means of rotating the quartz carrier 90° and laying it on the paddle, boron diffusion using solid boron or boron tribromide, and an adjustable air track that would prevent the wafers from "hanging up."

The overall diffusion system consists of the following:

- a. two existing commercially-available three-stack diffusion furnaces,
- b. two special load stations that incorporate a wafer track and buffer tee,
- c. two automatic wafer-boat elevation systems,
- d. six automatic wafer-boat insertion systems,
- e. a computer-based process controller,
- f. two source cabinets for the gas-blending systems,
- g. eight one-boat loaders,
- h. six gas-blending assemblies, and
- i. expendable materials (quartz, silicon carbide and the like).

The report includes a number of photographs and drawings of the facility. Operating details and parameters are also discussed.

This work was done by Bobby W. Kennedy of Marshall Space Flight Center. To obtain a copy of the report, "Thermally Grown Oxides and Diffusions for Automatic Processing of Integrated Circuits," Circle 98 on the TSP Request Card. MFS-25357

Computer Programs

These programs may be obtained at very reasonable cost from COSMIC, a facility sponsored by NASA to make new programs available to the public. For information on program price, size, and availability, circle the reference letter on the COSMIC Request Card in this issue.

Predicting Crack Propagation

Flaw growth under load is predicted in two dimensions.

Structural flaws and cracks may grow under fatigue-inducing loads and, upon reaching a critical size, cause structural failure. The growth of flaws and cracks may occur at load levels well below the ultimate load-bearing capability.

The Advanced Crack Propagation Predictive Analysis Program, FLAGRO4,

aids in predicting the growth of preexisting flaws and cracks. FLAGRO4 provides fracture mechanics analysts with a computerized method of evaluating the "safe crack-growth life" of structural components. FLAGRO4 could also be used to evaluate the damage tolerance of a structure.

The propagation of a crack is governed by the stress field in the vicinity of the crack tip. The "stress intensity factor" is defined in terms of the relationship between the stress field magnitude and the crack size. The propagation of the crack becomes catastrophic when the local stress intensity factor equals the fracture toughness of the material.

FLAGRO4 uses a two-dimensional model that predicts flaw growth in two directions independently, based on the calculation of stress intensity factors. The analyst may specify that the growth rate be controlled by Collipriest's equation, Forman's equation, Paris' equation, or by tabulated, user-supplied

data. FLAGRO4 can model part-through, through, and corner cracks located on panels, on panel edges, at open holes, at pin-loaded holes, at pin-loaded lugs, and on tub or bar surfaces. The modeling of the crack growth may be continued until propagation becomes catastrophic. FLAGRO4 can accommodate part-through to through crack transitions, stress gradients across the width and thickness, cold-worked hole residual stresses, material property variations due to environmental changes, and Willenberg retardation.

Input to FLAGRO4 consist of initial crack definition (which can be defined automatically), rate-solution type, flaw type and geometry, material properties (if they are not in the built-in material table), load-spectrum data, load-stress functions, and design-limit stress levels. FLAGRO4 outputs include echoes of the inputs with any errors or warning messages and a life-history profile of the crack propagation.

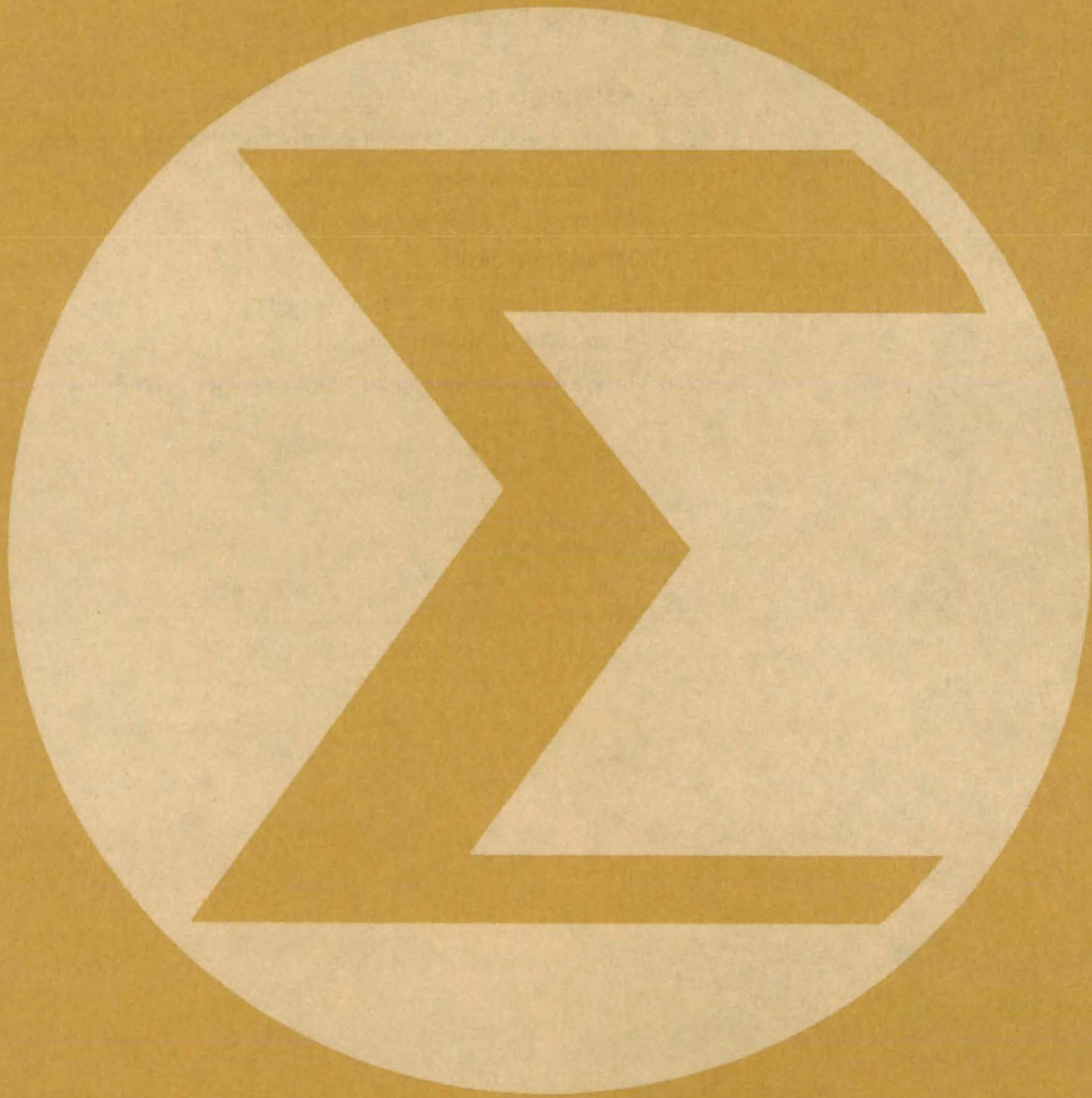
(continued on next page)

FLAGRO4 is written in FORTRAN IV for batch execution and is available for CDC and IBM machines: The CDC version (MSC-18718) has been implemented on a CDC 6000-series machine with a central memory requirement of approximately 150K (octal) of

60-bit words. The IBM version (MSC-18721) has been implemented on an IBM 360-series machine with a central memory requirement of approximately 260K (octal) 8-bit bytes. The FLAGRO4 program was developed in 1979.

*This program was written by Tianlai Hu of Rockwell International Corp. for **Johnson Space Center**. For further information, Circle K on the COSMIC Request Card.
MSC-18718 and MSC-18721*

Mathematics and Information Sciences



**Hardware,
Techniques, and
Processes**

251 An Approximation to Student's t-Distribution

252 Low-Cost Landsat Processing System

Computer Programs

252 NASA PERT Time II

253 Linear Stochastic Optimal Control and Estimation Problem

254 Multiple Linear Regression Analysis

254 Structured FORTRAN Preprocessor

254 MBASIC Processor

255 Basic Cluster Compression Algorithm

255 System Time-Domain Simulation

256 Image-Based Information, Communication, and Retrieval

An Approximation to Student's t-Distribution

Three equations relate Student's t-distribution to the standard normal distribution.

Langley Research Center, Hampton, Virginia

During the development of a computer subroutine, an approximation to Student's t-distribution was needed that would be accurate for all degrees of freedom yet would not occupy much memory space. The set of equations in Figure 1 was tested and found to satisfy these requirements. They give a maximum error of less than 0.8 percent and a typical error of less than 0.01 percent.

Equation (1) expresses the t variable of Student's t-distribution as a function of the variable z of the standard normal distribution function and the number of degrees of freedom ν . The equation is thus a prescription for converting standard normal distribution tables to Student's t-distribution tables. In this approximation, t approaches z when ν is large, and t equals z for $\nu = \infty$.

Since no error estimates are given in the reference for equation (1), several values of t were computed and compared with exact values listed in a table of probability distributions. The comparison indicated that the approximation is excellent for degrees of freedom larger than 6. It is inadequate, however, for degrees of freedom equal to 1 and 2. Fortunately, equations (2) and (3) give exact solutions for these cases.

The three equations were used to calculate values of t for values of probability equal to 0.995, 0.99, 0.975, 0.90, 0.80, 0.70, and 0.60 for each degree of freedom up to 120. These levels of probability correspond to z values of 2.5758, 2.3263, 1.9600, 1.2816, 0.8420, 0.5240, and 0.2533, respectively. The calculated t values were compared with exact values, and the errors are shown in Figure 2. The table shows that the set of equations covers the entire range with excellent accuracy. Since the approximation for

$$t = z + \frac{g_1(z)}{\nu} + \frac{g_2(z)}{\nu^2} + \frac{g_3(z)}{\nu^3} + \frac{g_4(z)}{\nu^4} \quad (1)$$

where

$$g_1(z) = \frac{1}{4}(z^3 + z)$$

$$g_2(z) = \frac{1}{96}(5z^5 + 16z^3 + 3z)$$

$$g_3(z) = \frac{1}{384}(3z^7 + 19z^5 - 15z)$$

$$g_4(z) = \frac{1}{92,160}(79z^9 + 776z^7 + 1,452z^5 - 1,920z^3 - 945z)$$

$$t = \cot [\pi(1 - P)] \quad \text{for } \nu = 1 \quad (2)$$

$$t = \sqrt{\frac{1}{2P(1-P)}} - 2 \quad \text{for } \nu = 2 \quad (3)$$

Figure 1. **Three Equations** approximate Student's t-distribution. Equation (1), used for $\nu > 2$, expresses the t variable in terms of the standard normal variable z. For $\nu = 1$ and 2, equations (2) and (3) express t exactly in terms of probability P. Equation (1) is listed in Handbook of Mathematical Functions, AMS 55, National Bureau of Standards, U.S. Government Printing Office (1964).

ν	PROBABILITY, P							
	0.60	0.70	0.80	0.90	0.95	0.975	0.99	0.995
1						0	0	0
2						0	0	0
3						0.005	-0.016	-0.044
4						0.001	-0.003	-0.004
5							-0.001	-0.002
6	MAXIMUM ERROR ≤ 0.0005							
7								
.								
.								
120								

Figure 2. The **Error of the Approximation** (where error is the difference between true and approximate values for t) is tabulated for ν between 1 and 120 and for several probabilities.

t in equation (1) monotonically approaches the exact values as ν goes to infinity, the error of the approximation is greater at any value of ν than it is for larger ν values.

This work was done by Donald R. Rummler and Columbus W. Stroud of Langley Research Center. No further documentation is available. LAR-12238



Low-Cost Landsat Processing System

Study shows Landsat analysis system can be assembled at a relatively low cost.

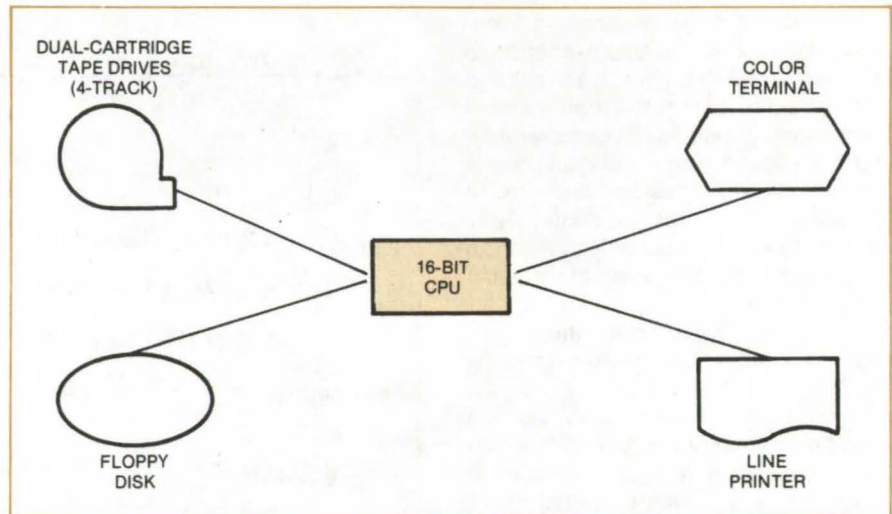
Marshall Space Flight Center, Alabama

Many potential users of Landsat data, such as state agencies and universities, do not have enough funds to purchase an automated Landsat data-analysis system. Most commercial units cost between \$400,000 and \$1,000,000, and even the assembled low-cost systems can be from \$75,000 to \$100,000. A recent study, however, has shown that a small-scale analysis system can be put together for about \$30,000 — an affordable price for many potential users.

The proposed system would consist of a central processing unit (CPU) and memory, a dual floppy disk and dual-drive magnetic tape, a console and interface, an output device, and an interactive display, all commercially available. The key components are shown on the block diagram.

The CPU would be a minicomputer with 32 kilowords of core memory. The floppy disk would have a 0.5-megabyte storage capacity. The magnetic-tape drive would be a 1,600-bits/in. (340-bits/cm), 4-track dual tape drive with 2.88 megabytes of storage capacity. The interaction display would be a 256- by 256-pixel display with a minimum of 6 bits of information per pixel (equivalent to a 64-color display). A cursor and zoom are highly-recommended display options that will make the analysis more accurate and convenient.

A number of processing programs written in FORTRAN IV is available for analyzing the Landsat data. Individual programs can process training-field selection, maximum-likelihood classi-



Small-Scale Landsat Data-Processing System can be assembled from commercially available components. The proposed system could be used by state agencies and universities that cannot afford expensive processing systems currently offered on the market.

fication, linear classification, unsupervised classification, coordinate transformation, polygon extraction, rectification/sampling, and geographic data bases; and can also extract polygonal data that encompass parts of two Landsat scenes.

The proposed system can process Landsat data for subscene areas on a repetitive basis. With additional hardware enhancements, such as the floating-point processor and hardware multiply/divide, the system could process entire scenes of Landsat data in less than 2 days, not counting training-sample-selection time. Without these improvements, a full-scene

classification for approximately 60 classes would take about 20 to 25 days of constant processing, assuming no equipment malfunction or power losses. The amount of time required for processing decreases linearly with the number of classifications desired (e.g., a full-scene classification with approximately 15 classes would take about a week of constant processing).

This work was done by Nickolas L. Faust, Nancy J. Hooper, and G. William Spann of Metrics, Inc., for Marshall Space Flight Center. For further information, Circle 99 on the TSP Request Card.
MFS-25396

Computer Programs

These programs may be obtained at very reasonable cost from COSMIC, a facility sponsored by NASA to make new programs available to the public. For information on program price, size, and availability, circle the reference letter on the COSMIC Request Card in this issue.

NASA PERT Time II

IBM 370 version of a versatile management tool

The planning and management of a large engineering project, where the interrelationships between activities and functional areas are numerous

and involved, can become so complex that it is difficult to visualize as a whole. This potential problem readily lends itself to the employment of computerized data management systems. The Program Evaluation and Review Technique (PERT) is defined as a disciplined management technique involving computer processing.

NASA PERT Time II was developed as a computerized aid in the planning and control of project development variables, namely time and performance measurements. NASA PERT Time II can give the project manager an insight into current and future project development, as well as forewarning of potential problem areas. A formalized evaluation and planning system cannot replace good management; therefore, the usefulness of NASA PERT Time II is entirely dependent on analysis and judgment by the project manager. NASA PERT Time II can prove to be a very valuable aid, offering the project manager a better overview of the project as a whole.

The NASA PERT Time II program utilizes a modular technique. The module for computer system requirements is called a subnet; it is a subset or portion of a project-network activities. The program user will usually see this module as a "fragnet." A fragnet is defined as a meaningful portion of a project network. There is no significant difference between a subnet and a fragnet. A fragnet allows the user to represent project entities such as a subdivision of work, a contractor, an organization, a mission, a summary, or an integration network. Each fragnet will contain some events that are identical to events in other fragnets that make up the project network. These events are defined as interface events and identify the relations between fragnets.

Once all aspects of a project have been described in terms of fragnets, a control network is automatically generated. This control network is made up of control activities obtained by condensing all paths between control network events. Control network events are made up of interface events and all start and end events.

The program determines both expected and allowed dates for each control network event. Finally, the program generates reports on expected and allowed activity dates for fragnets specified by the user. As a project progresses, event and time variables in the fragnets and control network may be updated and new reports generated.

There are no well-defined limits on the size of the project that may be analyzed. The size of the project that may

be analyzed depends mainly on the computer resources available and the level of detail used in the fragnets. The program is currently designed to handle a maximum of 50 fragnets with each fragnet containing a maximum of 2,160 activities, 2,000 events, and 500 starts, ends, and interfaces.

This program is written in FORTRAN IV and OS Assembler for batch execution and has been implemented on an IBM 370 with a minimum central memory requirement of approximately 350K of 8-bit bytes. (The original NASA PERT Time II program was developed in 1965 for use on the IBM 7094 and was adapted for use on the IBM 370 in 1979.)

This program was written by Ross C. Bainbridge, Frank Funicelli, Daniel J. Hirsch, Eugene A. Pallat, Elizabeth Ryan, and Joseph D. Walker of Lewis Research Center and Hans Bremmer of Goddard Space Flight Center. For further information, Circle L on the COSMIC Request Card.
LEW-13145

Linear Stochastic Optimal Control and Estimation Problem

IBM 360 version of LSOCE program

The linear stochastic optimal control and estimation problem (LSOCE) involves the design of controls for a linear time-invariant system that is disturbed by white noise in such a way as to minimize a performance index. These controls must be designed to use system measurements that are corrupted by white noise. The solution to the LSOCE problem is a Kalman filter coupled through a set of optimal regulator gains to produce the desired control signal.

The key to solving the LSOCE problem is the solution of the matrix Riccati differential equation. This equation occurs in solving for both the finite-time optimal linear regulator gains and the finite-time optimal linear estimator (Kalman filter) gains. A computer program, LSOCE, was developed to solve effectively the LSOCE problem for a wide range of practical

applications. It has been used to design numerous control systems including the controls for supersonic inlets.

In solving the general LSOCE problem, it is helpful to study the infinite-time LSOCE problem in which the main equations to be solved use algebraic matrix Riccati equations. In practice, the solution of the algebraic equation is used in obtaining the solution to the more general differential equation. In this package, both the algebraic and differential equations are solved using an extension of the eigenvector method. For the infinite-time case, various system covariance matrices and mean-square values are computed as a measure of the control-system effectiveness.

The state-covariance matrix is obtained by solving the system Lyapunov equation, and the covariance of the error in system estimates is given by a Riccati equation. The program also offers the user the ability to solve common variations on the LSOCE problem including noise-free regulator problems and open-loop plant-covariance matrices problems. The LSOCE program is structured to handle any number of state variables and is restricted only by computer core availability. The program is currently dimensioned to handle up to 12 system state variables.

This program is written in FORTRAN IV for batch execution and has been implemented on an IBM 360 with a central memory requirement of approximately 77K of 8-bit bytes. The LSOCE program was originally developed in 1975 with the current version being released in 1979.

This computer program written in FORTRAN IV for use on the IBM 7094 computer, reference LEW-12505, and for use on the UNIVAC 1110/EXEC 8 computer, reference LEW-12540, was published previously in *NASA Tech Briefs*, Vol. 1, No. 4 page 657 (LEW-12540/LEW-12505).

This program was written by Lucille C. Geyser and F. K. Bruce Lehtinen of Lewis Research Center. For further information, Circle M on the COSMIC Request Card.
LEW-13206



Multiple Linear Regression Analysis

Rapid calculation of best-suited coefficients

A major problem in linear regression calculations is selection of the best set of coefficients. A computer program (MRA) for a multiple linear regression analysis automatically selects the best-suited set of coefficients. It uses an algorithm based on a procedure developed by Efraymson that proceeds one step at a time with statistical testing at each step. Since only the statistically most significant terms are considered, the best-suited coefficients can be calculated rapidly. The statistical testing incorporates a modification suggested by Draper and Smith to increase efficiency. The user need supply only the vectors of independent and dependent data and specify the confidence level required in the analysis.

The program uses a stepwise statistical procedure for relating a minimal set of variables to a particular set of observations. This is accomplished by introducing independent variables into the regression one at a time and ordering the selection of the next variable entered into the regression according to the magnitude of its partial correlation coefficient. The partial correlation coefficient gives the proportion of the variation of the dependent variable due to each of the independent variables not presently in the regression.

Once a variable has been added to the regression, all of the independent variables in the regression are tested for their statistical significance by calculating the added regression sum-of-squares due to each term. A variable that entered the regression at an earlier step may now prove to be statistically insignificant due to the influence of later terms. This insures that the final regression contains the statistically most significant set of coefficients.

This program is written in FORTRAN IV for batch execution and has been implemented on the NOVA 1200 with a core requirement of approximately 32K of 16-bit words. The MRA program was developed in 1977.

This program was written by Thomas R. Edwards of Marshall Space Flight Center. For further

*information, Circle N on the COSMIC Request Card.
MFS-23764*

Structured FORTRAN Preprocessor

Structured-programing features simplify software design.

The NASA Structured FORTRAN Preprocessor was developed to assist programmers in constructing reliable software. The preprocessor features "structured-programing" control structures that can be used to facilitate program design, coding, documentation, and debugging. The FORTRAN programmer needs to learn only a few control statements to code his program in a structured format that is easy to debug and maintain. By freeing the programmer from the flow constraints of standard FORTRAN, the preprocessor simplifies the design and coding of difficult logic flows and helps to improve software reliability.

The principal control structures supported by the preprocessor include the IF THEN ELSE, OR IF, DO WHILE, FOR, and TEST CASE statements. The first three are well-known structured-programing features that have previously been unavailable to the FORTRAN programmer. With these features, codes can be structured without confusing the logical flow of the program with a large number of GO TO statements.

The FOR construct is a special iterative construct allowing code repetition by testing an index for a specified termination value. In the TEST CASE construct, the specified expression is checked for a match in the parameter string of a CASE statement. When a match is detected, the segment of code associated with the CASE statement is executed, and then execution is returned to the statement following the TEST CASE construct.

Input to the preprocessor may be a mixture of standard FORTRAN and structured control statements. The output is a standard FORTRAN program that is the logical equivalent of the input program and is ready for compilation and execution. During debugging, updating, and maintenance, the programmers need to con-

cern themselves only with the easy-to-follow structured program. Once any changes are made, the structured program is preprocessed and compiled again.

This software is written in ANSI FORTRAN and should be compatible with any machine supporting a FORTRAN compiler that accepts ANSI statements. The preprocessor has been implemented on an IBM 370-series computer with a central memory requirement of approximately 90K of 8-bit bytes. The preprocessor was developed in 1977.

This program was written by S. Austin, B. Buckles, and J. P. Ryan of Science Applications, Inc., for Marshall Space Flight Center. For further information, Circle P on the COSMIC Request Card.

Inquiries concerning rights for the commercial use of this invention should be addressed to the Patent Counsel, Marshall Space Flight Center [see page A5]. Refer to MFS-23813.

MBASIC Processor

UNIVAC and DEC-10 processors for a flexible efficient language

MBASIC, an advanced version of the BASIC language developed at Dartmouth College, is a high-level interactive computer language that reduces the time required to program a task for computer execution. Like BASIC and FORTRAN, MBASIC combines English and simple algebra to give instructions to the computer; however, MBASIC results in shorter, simpler programs that are easier to write and understand. In addition, practically all system commands needed for management information processing are available in MBASIC. This feature makes it unnecessary for MBASIC users to learn executive commands or to rewrite MBASIC programs to accommodate system changes. MBASIC should provide a powerful computing language for technical or management information processing and for scientific and engineering applications.

The conversational nature of MBASIC allows the user to interact with the program as it is being developed.

Each MBASIC statement is analyzed for errors as it is entered. Diagnostic error messages and versatile editing features make corrections quicker and easier. Any portion of a program may be executed before it is completely assembled. This ability is one of the fundamental design features of MBASIC and is the principal reason why MBASIC has truly conversational capabilities. Although individual statements may be syntactically correct, erroneous expressions can cause an interruption during program execution. If an interruption occurs, a diagnostic message is printed, and control is returned to the user. If necessary, the user may enter direct statements and execute them immediately. After program corrections have been made, execution can be resumed at any appropriate statement, including the statement in which the interruption occurred.

The power of MBASIC lies in its capacity to direct a computer to perform a large variety of complex tasks while the user supplies only a few simple English or algebraic instructions. The program instructions are written like sentences, resulting in a program that is easy to read and write. These instructions are combined into program modules that are written as paragraphs. Comments may be included to document module functions.

The outstanding features that contribute to the power of MBASIC include: multiple assignments in a single instruction; conditional, assignment, and repetitive statement modifiers; multiple statements in a single instruction; and excellent string-handling capabilities. Excellent array-handling capabilities are available, including assigning values while dimensioning, matrix algebra written like simple algebra, and combining simple and array expressions in a single instruction. The programmer may use expressions to refer to statement numbers and may access magnetic tapes through terminals during program execution. The availability of these and other features leads naturally to a simplification of the program design process.

Two machine versions of the MBASIC processor are available, UNIVAC and DEC-10. The UNIVAC

version is written in reentrant Assembler code for interactive execution under EXEC 8 and has a memory requirement of approximately 15K of 36-bit words. The UNIVAC MBASIC processor was developed in 1973. In 1977, an MBASIC processor was developed for use on the DEC System-10. The DEC-10 version is written in reentrant Assembler code for interactive execution under TOPS-10 and requires approximately 14K of 36-bit words. MBASIC is a trademark of the California Institute of Technology.

This program was written by R. Booth Hartley and Robert E. Holzman of Caltech for NASA's Jet Propulsion Laboratory. For further information, Circle R on the COSMIC Request Card.

NPO-14245

Basic Cluster Compression Algorithm

Feature extraction and data compression of Landsat data

The Basic Cluster Compression Algorithm (BCCA) program reduces the costs associated with transmitting, storing, distributing, and interpreting Landsat multispectral image data. This preprocessing algorithm uses feature extraction and data compression techniques to represent the information in the image data efficiently. The format of the preprocessed data allows simple lookup-table decoding and direct use of the extracted features. This reduces user computation needed for image reconstruction or computer interpretation of the image data.

The algorithm uses spatially local clustering to extract features from the image data to describe spectral characteristics of the data set. These features may be used to form a sequence of scalar numbers that define each picture element in terms of the cluster features. The sequence, called the feature map, may be represented efficiently by using source encoding concepts. It is possible to make various extensions on the Basic Cluster Compression Algorithm to obtain different types of compression characteristics.

The Basic Cluster Compression Algorithm was derived from the standard

iterative approach to clustering. This approach requires only simple repetitive computations, and parallel processing can be used for very high data rates. The only user supervision required for the BCCA is the specification of the number of clusters desired. Initial cluster centers are selected to be well scattered throughout the set of all data vectors, and the BCCA is somewhat insensitive to the choice of initial cluster centers. Data vectors are assigned to clusters dependent on the relative distance between the data vector and the cluster center. The clustering is terminated whenever the clustering converges or whenever a specified number of iterations has been performed.

This program is written in FORTRAN IV for batch execution and has been implemented on an SEL 32/55 with a central memory requirement of approximately 27K of 32-bit words. The BCCA program was developed in 1977.

This program was written by Edward E. Hilbert and Jun-Ji Lee of Caltech for NASA's Jet Propulsion Laboratory. For further information, Circle S on the COSMIC Request Card.

NPO-14816

System Time-Domain Simulation

Complex systems can be simulated by engineers without extensive computer experience.

The System Time Domain (SYSTID) Simulation Program is a powerful tool for the transient simulation and analysis of complex systems. SYSTID requires little computer experience and has been used to simulate and analyze a wide range of systems, including communications systems and spacecraft power systems.

The analyst uses a free-form engineering-oriented language to input a topological "black-box" description of a system. SYSTID automatically generates the appropriate algorithms and proceeds with the simulation. The user has enormous flexibility in the representation of system elements;

(continued on next page)



any element may be defined in terms of the extensive SYSTID library of models, as a user-developed SYSTID model, or as a FORTRAN-coded algorithm. Models can be nested, and one can build a model library from a basic set. Furthermore the program can easily be linked to postprocessing routines for detailed analysis of the simulation results.

The basic SYSTID library consists mainly of routines that aid in the simulation of continuous functions. The technique of the bilinear z-transform representation of transform functions is used and may be defined in terms of poles and zeros or in terms of the classical functions, such as Bessel and elliptic functions.

SYSTID is designed to execute as a multipass processor in a batch or demand mode of operation. The first phase reads the user-input description of the system along with supporting models and performs a variety of error checks. This phase also formulates the FORTRAN algorithms corresponding to the system description. SYSTID can be viewed as a FORTRAN program generator that converts non-procedural topological input into an executable computer program. If the first phase is completed successfully, the FORTRAN routines are compiled and linked with the SYSTID library and the simulation executed. For multiple simulations of the same system, the first phase needs to be completed only once. Simulation results are output as graphs and tables. Linking the simulation program to a postprocessor allows the user to access the time histories of any node or variable for further analysis.

The SYSTID program is written in FORTRAN IV for batch execution and has been implemented on a UNIVAC 1110 under control of EXEC 8, Level 31. The basic SYSTID system has a central memory requirement of approximately 60K of 36-bit words. This release of SYSTID was developed in 1977.

This program was written by Carroll T. Dawson, Theodore W. Eggleston, and Andy C. Goris of Johnson Space Center; Mike Fashano and Dale Paynter of Hughes Aircraft Co.; and William H. Tranter of the University of Missouri — Rolla. For further information, Circle T on the COSMIC Request Card.
MSC-18333

Image-Based Information, Communication, and Retrieval

IBIS/VICAR system combines video image processing and information management.

The IBIS/VICAR system is a powerful system for analyzing, manipulating, and managing image data. It combines the JPL IBIS (Image-Based Information System) geographic information management system and the JPL VICAR (Video Image Communication and Retrieval System) image-processing system. The IBIS/VICAR system has extensive general-purpose image-processing capabilities, and an information management system that accepts, converts, and operates on vector (graphical) and tabular data.

The system can be used to perform various image-processing functions on any type of digitized image data, including remotely sensed data such as Landsat multispectral scanner data. The image-processing functions available include picture comparison, picture expansion with noise elimination, convolution filtering, geometric transformations, Fourier transformations, and many other manipulation and enhancement procedures. In addition, the information management system handles image-related data and merges image data with other types of data files.

The IBIS system analyzes geographical problems by grouping selected functions from the IBIS library for investigation of a variety of spatial phenomena. Tabular and graphical data can be stored in registration with imagery data in the form of overlaid data planes. Information may be derived from simple associations and comparisons between two or more data files or from more complex procedures, including polygon overlay and spatial cross tabulation. The VICAR program library can be readily used to generate, input, output, and process image data for the IBIS system.

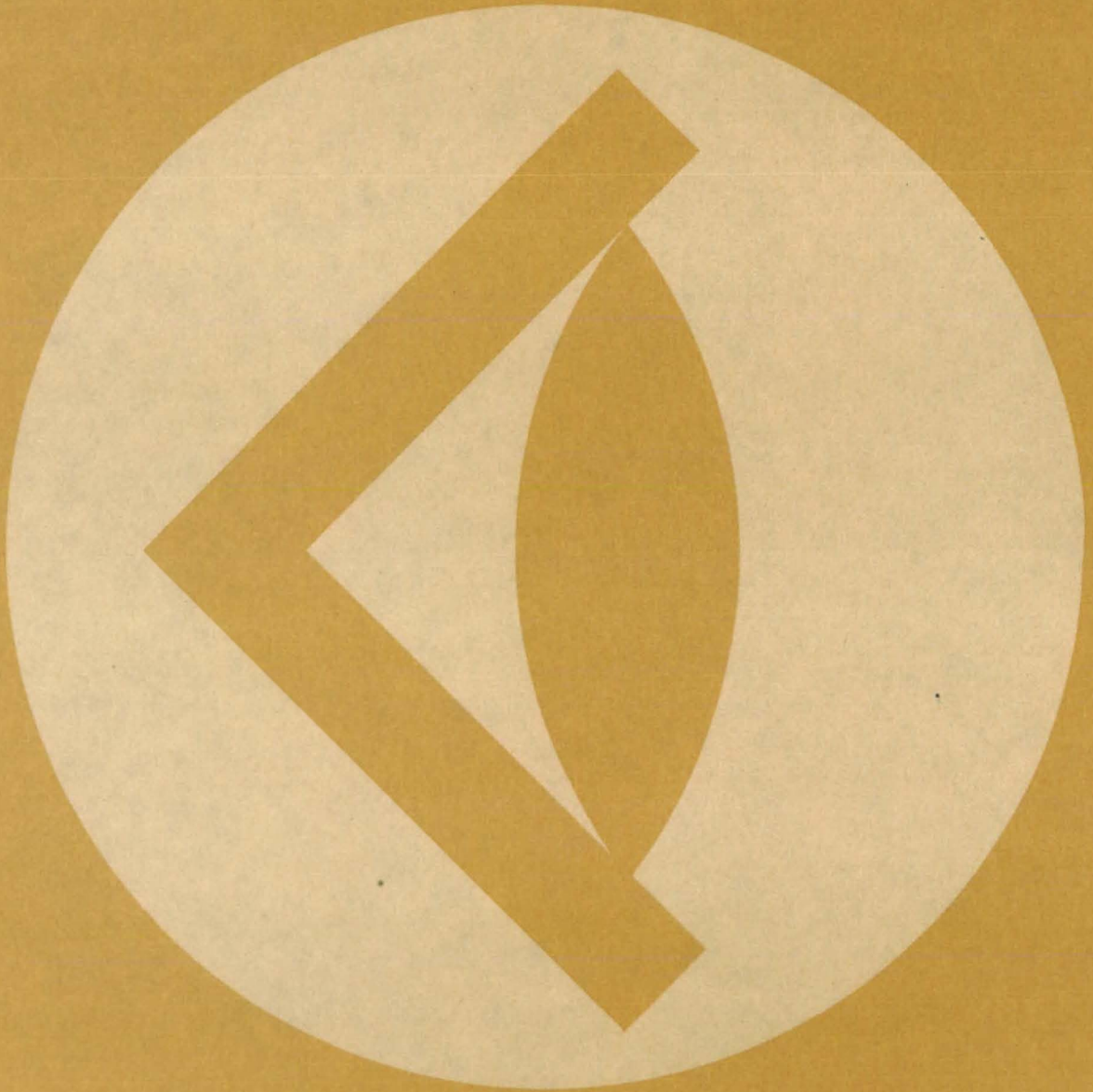
The IBIS/VICAR system, which requires minimal inputs, can be used by analysts with only elementary programming knowledge and a simple understanding of the system operation. The analyst calls for the automatic execution of one or more of the system programs, including the requisite image-data management services, through a set of command instructions. The flexible programs require that the user supply only the parameters specific to a particular application. Special-purpose input/output routines efficiently transfer image data with reduced memory requirements. New applications programs can be easily incorporated as they are developed.

The IBIS/VICAR system is a system of programs and control procedures written in FORTRAN IV, Assembler, and OS JCL for batch execution. The IBIS/VICAR system has been implemented on an IBM 360-series computer with a minimum central memory requirement of approximately 150K of 8-bit bytes. The IBIS/VICAR system was released in 1979.

This program was written by Nevin A. Bryant and Albert L. Zobrist of Caltech for NASA's Jet Propulsion Laboratory. For further information, Circle U on the COSMIC Request Card.

NPO-14893

SUBJECT INDEX



ABSORBERS [EQUIPMENT]			
Self-adjusting mechanical snubbing link page 218	MSC-16134		
AC GENERATORS			
Energy saving in ac generators page 134	MFS-25302		
ACCELEROMETERS			
Electrofluidic accelerometer page 201	LAR-12493		
ACOUSTIC SIMULATION			
Low-cost calibration of acoustic locators page 169	LAR-12632		
AERODYNAMIC DRAG			
Grooves reduce aircraft drag page 192	LAR-12599		
AIR QUALITY			
Improved particulate-sampling filter page 240	NPO-14801		
AIRCRAFT ENGINES			
Composites for aeropropulsion page 183	LEW-13438		
ALGAE			
Laser-fluorescence measurement of marine algae page 187	LAR-12282		
ALGORITHMS			
Basic cluster compression algorithm page 255	NPO-14816		
ALIGNMENT			
X-ray beam pointer page 224	MSC-18590		
ANGULAR ACCELERATION			
Electrofluidic accelerometer page 201	LAR-12493		
ATMOSPHERIC REFRACTION			
Refraction corrections for surveying page 206	MSC-18664		
AUGMENTATION			
Digital enhancement of X-rays for NDT page 206	KSC-11118		
BASIC [PROGRAMMING LANGUAGE]			
MBASIC processor page 254	NPO-14245		
BRAZING			
Time-shared RF brazing page 240	MSC-18617		
BUBBLES			
Removal of hydrogen bubbles from nuclear reactors page 180	LAR-12597		
BUNDLES			
Handtool assists in bundling cables page 225	MSC-18567		
CALIBRATING			
A temperature fixed point near 58° C page 179	MFS-25304		
Low-cost calibration of acoustic locators page 169	LAR-12632		
Optical calibrator for TDL spectrometers page 164	GSC-12562		
CAMERAS			
Camera add-on records time of exposure page 168	LAR-12635		
CAPACITORS			
Measuring radiation effects on MOS capacitors page 203	NPO-14700		
CASTINGS			
Predicting the lifetime of cast parts page 204	MFS-19549		
CATHODE RAY TUBES			
Real-time film recording from stroke-written CRT's page 154	LAR-12529		
CAVITIES			
Forming complex cavities in clear plastic page 237	LEW-13412		
CHARGE COUPLED DEVICES			
Better-quality CCD-array images page 153	NPO-14426		
CIRCLES [GEOMETRY]			
Electron-beam welder circle generator page 91	MFS-19441		
COAL			
Position monitor for mining machines page 141	MFS-25342		
COATINGS			
Improved adherence of TiC coatings to steel page 181	LEW-13169		
Photonitride passivating coating for IC's page 231	MFS-25401		
Selective optical coatings for solar collectors page 173	MFS-23589		
COLUMNS [SUPPORTS]			
Automatic connector joins structural columns page 222	LAR-12578		
COMBUSTION CHAMBERS			
Flashback-free combustor page 202	LAR-12666		
Methane/air flames in a concentric-tube combustor page 184	LEW-13388		
COMPOSITE MATERIALS			
Composites for aeropropulsion page 183	LEW-13438		
Efficient measurement of shear properties of fiber composites page 193	LEW-13011		
Plasticizer for polyimide composites page 180	LAR-12642		
Resistance welding graphite-fiber composites page 234	MSC-18534		
COMPUTER PROGRAMMING			
DDL: digital systems design language page 146	MFS-25352		
MBASIC processor page 254	NPO-14245		
Structured FORTRAN preprocessor page 254	MFS-23813		
COMPUTERIZED SIMULATION			
System time-domain simulation page 255	MSC-18333		
CONDUCTIVE HEAT TRANSFER			
Heat conduction in three dimensions page 210	MSC-18616		
CONTACT RESISTANCE			
Ohmic contact to GaAs semiconductors page 233	LAR-12466		
CONTAMINANTS			
Detecting contaminants by ultraviolet photography page 205	MFS-25296		
CONTROLLERS			
Final report on development of a programable controller page 171	MFS-25388		
CONVECTION			
Recording fluid currents by holography page 198	MFS-25373		
CORROSION PREVENTION			
Photonitride passivating coating for IC's page 231	MFS-25401		
Silicon nitride passivation of IC's page 245	MFS-25309		
COST ANALYSIS			
Low-cost Landsat processing system page 252	MFS-25396		
Optimizing costs of VLSI circuits page 246	MFS-25348		
COUPLINGS			
Automatic connector joins structural columns page 222	LAR-12578		
Flared-tube attachment fitting page 213	MSC-18416		
CRACK PROPAGATION			
Predicting crack propagation page 248	MSC-18718		
CRYOGENIC EQUIPMENT			
Cryogen-storage-tank support page 227	MSC-14848		
CURVATURE			
Stream-tube curvature analysis page 208	LAR-11535		
DATA COMPRESSION			
Basic cluster compression algorithm page 255	NPO-14816		
DATA PROCESSING EQUIPMENT			
RAM-based parallel-output controller page 150	GSC-12447		
DECODERS			
11-line to 512-line decoder page 141	MSC-19751		
DECOUPLING			
Quasi-passive vibration decoupler page 195	LAR-12468		
DEFECTS			
Detection of tanker defects with infrared thermography page 196	LAR-12655		
DIGITAL DATA			
11-line to 512-line decoder page 141	MSC-19751		
DIGITAL FILTERS			
Aliasing filter for multirate systems page 137	MSC-18472		
DIGITAL TO ANALOG CONVERTERS			
Smoothing the output from a DAC page 144	FRC-11025		
DIMENSIONAL STABILITY			
Test fittings for dimensionally critical tubes page 222	NPO-14399		
DIRECTIONAL ANTENNAS			
Dual-frequency bidirectional antenna page 138	GSC-12501		
DISCONNECT DEVICES			
Automatic connector joins structural columns page 222	LAR-12578		
DISTRIBUTION FUNCTIONS			
An approximation to Student's t-distribution page 251	LAR-12238		
DOPPLER EFFECT			
A microcomputer for Doppler data processing page 151	GSC-12448		
Instrument remotely measures wind velocities page 163	NPO-14524		
DRAG			
Grooves reduce aircraft drag page 192	LAR-12599		
Predicting propulsion system drag page 210	LAR-12619		
DROPS [LIQUIDS]			
Holographic drop-size analyzer page 166	NPO-14676		
Photographic measurement of droplet density page 167	MFS-25326		
DUCTS			
A versatile tunnel acts as a flexible duct page 214	MFS-22636		
DYNAMIC CHARACTERISTICS			
Frequency response of multiple-sampling-rate systems page 158	MSC-18473		
ELECTRIC GENERATORS			
A linear magnetic motor and generator page 226	GSC-12518		
ELECTRIC MOTORS			
Torque control for electric motors page 155	MSC-18635		



ELECTRICAL FAULTS Model for MOS field-time-dependent breakdown page 145	NPO-14701	FLUORESCENCE Fluorescent radiation converter page 166	GSC-12528	HEATING EQUIPMENT A hot-water system tested onsite — Togus, Maine page 175	MFS-25435
ELECTROCARDIOGRAPHY Testing EKG electrodes on-line page 187	MSC-18696	FORMING TECHNIQUES Forming complex cavities in clear plastic page 237	LEW-13412	A reliable solar-heating system — Huntsville, Alabama page 175	MFS-25431
ELECTRODES Testing EKG electrodes on-line page 187	MSC-18696	FORTRAN Structured FORTRAN preprocessor page 254	MFS-23813	A solar-energy system in Minnesota page 175	MFS-25428
ELECTRON BEAM WELDING Electron-beam welder circle generator page 91	MFS-19441	FRACTURE MECHANICS Predicting crack propagation page 248	MSC-18718	A solar-energy system in Pennsylvania page 173	MFS-25427
ELECTRONIC EQUIPMENT TESTS Testing EKG electrodes on-line page 187	MSC-18696	FREQUENCY ANALYZERS Frequency response of multiple-sampling-rate systems page 158	MSC-18473	A test program for solar collectors page 174	MFS-25433
ENERGY CONVERSION EFFICIENCY Energy saving in ac generators page 134	MFS-25302	FREQUENCY CONTROL Frequency-controlled voltage regulator page 156	NPO-13633	Final report on development of a programable controller page 171	MFS-25388
Improved power-factor controller page 133	MFS-25323	FREQUENCY CONVERTERS Fluorescent radiation converter page 166	GSC-12528	Finned-absorber solar collector page 173	MFS-25385
ENERGY DISTRIBUTION Far-field radiation pattern of tunable diode lasers page 164	LAR-12631	FREQUENCY STANDARDS Integral storage-bulb and microwave cavity for masers page 170	GSC-12542	Fresnel lens tracking solar collector page 172	MFS-25419
EQUATIONS OF STATE An equation of state for liquids page 161	NPO-14821	FRESNEL DIFFRACTION Fresnel lens tracking solar collector page 172	MFS-25419	Installation guidelines for the Pennsylvania system page 175	MFS-25424
EXPOSURE Camera add-on records time of exposure page 168	LAR-12635	Fresnel lenses for ultrasonic inspection page 194	MSC-18469	Operational tests of a solar-energy system in Georgia page 174	MFS-25420
FASTENERS Bayonet plug with ramp-activated lock page 218	MSC-18526	FRICION REDUCTION Lubrication handbook page 183	MFS-25158	Operational tests of a solar-energy system — Florida site page 174	MFS-25423
Handtool assists in bundling cables page 225	MSC-18567	FUEL INJECTION Flashback-free combustor page 202	LAR-12666	Outdoor tests of the concentric-tube collector page 172	MFS-25398
FATIGUE TESTS Predicting the lifetime of cast parts page 204	MFS-19549	GALLIUM ARSENIDES Ohmic contact to GaAs semiconductors page 233	LAR-12466	Selective optical coatings for solar collectors page 173	MFS-23589
FEEDBACK CONTROL Temperature-compensating dc restorer page 136	LAR-12549	GAPS Producing gapped-ferrite transformer cores page 241	NPO-14715	Solar-heating and cooling demonstration project page 176	MFS-25443
FIELD EFFECT TRANSISTORS Progress in MOSFET double-layer metalization page 246	MFS-25239	GASEOUS DIFFUSION An automated oxide and diffusion facility for IC's page 246	MFS-25357	HIGH RESOLUTION High-resolution double-pass interferometer page 162	NPO-14448
FILTRATION Improved particulate-sampling filter page 240	NPO-14801	GEOLOGICAL SURVEYS Refraction corrections for surveying page 206	MSC-18664	HOLOGRAPHY Holographic drop-size analyzer page 166	NPO-14676
FITTINGS Flared-tube attachment fitting page 213	MSC-18416	GLASS Controlling the shape of glass microballoons page 236	MFS-25230	Recording fluid currents by holography page 198	MFS-25373
Test fittings for dimensionally critical tubes page 222	NPO-14399	GROOVING Grooves reduce aircraft drag page 192	LAR-12599	HYDROGEN Removal of hydrogen bubbles from nuclear reactors page 180	LAR-12597
FLAME PROPAGATION Methane/air flames in a concentric-tube combustor page 184	LEW-13388	GUIDANCE SENSORS 3-D guidance system with proximity sensors page 221	NPO-14521	IMAGE ENHANCEMENT Better-quality CCD-array images page 153	NPO-14426
FLARED BODIES Flared-tube attachment fitting page 213	MSC-18416	HEAT PIPES Heat-pipe sensor for remote leveling page 209	GSC-12095	Digital enhancement of X-rays for NDT page 206	KSC-11118
Tube-flare inspection tool page 213	MSC-19636	HEAT SHIELDING Thermal barrier and gas seal page 238	MSC-18390	IMAGERY Image-based information, communication, and retrieval page 256	NPO-14893
FLASHBACK Flashback-free combustor page 202	LAR-12666	HEAT TRANSFER Automatic thermal switches page 191	GSC-12553	Low-cost Landsat processing system page 252	MFS-25396
FLICKER Real-time film recording from stroke-written CRT's page 154	LAR-12529	Heat conduction in three dimensions page 210	MSC-18616	INDUCTION MOTORS Improved power-factor controller page 133	MFS-25323
FLOW DISTRIBUTION A generalized vortex lattice method page 209	LAR-12636	HEATING Computer-controlled warmup circuit page 139	NPO-14815	INFRARED INSPECTION Detection of tanker defects with infrared thermography page 196	LAR-12655
Stream-tube curvature analysis page 208	LAR-11535			INSTALLATION MANUALS Installation guidelines for the Pennsylvania system page 175	MFS-25424
FLUID FLOW Recording fluid currents by holography page 198	MFS-25373			INSTALLING Heat-shrinkable sleeve aids in installing universal joints page 239	MSC-18685
				INTERFACES Input/output interface module page 143	MSC-18180

INTERFEROMETERS

High-resolution double-pass interferometer
page 162 NPO-14448

INVISCID FLOW

Stream-tube curvature analysis
page 208 LAR-11535

ION EXCHANGING

Hybrid microspheres
page 182 NPO-14462

ION IMPLANTATION

More-reliable SOS ion implantations
page 232 MFS-25322

JET ENGINES

Suppressing buzz-saw noise in jet engines
page 196 LAR-12645

JOINTS [JUNCTIONS]

Heat-shrinkable sleeve aids in installing universal joints
page 239 MSC-18685

KLYSTRONS

Computer-controlled warmup circuit
page 139 NPO-14815

LANDSAT SATELLITES

Image-based information, communication, and retrieval
page 256 NPO-14893

Low-cost Landsat processing system
page 252 MFS-25396

LARGE SCALE INTEGRATION

An automated oxide and diffusion facility for IC's
page 246 MFS-25357

Double metalization for VLSI
page 232 MFS-25149

LSI logic for phase control rectifiers
page 144 MFS-25208

More-reliable SOS ion implantations
page 232 MFS-25322

Optimizing costs of VLSI circuits
page 246 MFS-25348

Photonitride passivating coating for IC's
page 231 MFS-25401

Progress in MOSFET double-layer metalization
page 246 MFS-25239

Silicon nitride passivation of IC's
page 245 MFS-25309

LASER APPLICATIONS

Changes in "thermal lens" measure diffusivity
page 195 NPO-14657

Laser-fluorescence measurement of marine algae
page 187 LAR-12282

LASERS

Far-field radiation pattern of tunable diode lasers
page 164 LAR-12631

LENSES

Fresnel lenses for ultrasonic inspection
page 194 MSC-18469

LEVEL [HORIZONTAL]

Heat-pipe sensor for remote leveling
page 209 GSC-12095

LIFE [DURABILITY]

Predicting the lifetime of cast parts
page 204 MFS-19549

LIGHTING EQUIPMENT

Direct-current converter for gas-discharge lamps
page 140 MSC-18407

LINEARIZATION

Linearizing dc transducer output
page 152 NPO-14617

LIQUIDS

An equation of state for liquids
page 161 NPO-14821

LOCKS [FASTENERS]

Bayonet plug with ramp-activated lock
page 218 MSC-18526

LUBRICATION

Design considerations for mechanical face seals
page 183 LEW-13146

Lubrication handbook
page 183 MFS-25158

MACHINE ORIENTED LANGUAGES

DDL: digital systems design language
page 146 MFS-25352

MAGNETIC CORES

Producing gapped-ferrite transformer cores
page 241 NPO-14715

MANAGEMENT SYSTEMS

NASA PERT time II
page 252 LEW-13145

MANIPULATORS

Electromechanical slip sensor
page 223 NPO-14654

End effector for gripping objects
page 215 MFS-23692

MARINE TECHNOLOGY

Laser-fluorescence measurement of marine algae
page 187 LAR-12282

MASERS

Integral storage-bulb and microwave cavity for masers
page 170 GSC-12542

MATERIALS HANDLING

End effector for gripping objects
page 215 MFS-23692

MECHANICAL DRIVES

High-performance, multiroller traction drive
page 216 LEW-13347

MERCURY LAMPS

Direct-current converter for gas-discharge lamps
page 140 MSC-18407

METAL MATRIX COMPOSITES

Composites for aeropropulsion
page 183 LEW-13438

METAL OXIDE SEMICONDUCTORS

Measuring radiation effects on MOS capacitors
page 203 NPO-14700

Model for MOS field-time-dependent breakdown
page 145 NPO-14701

METAL SURFACES

Detecting contaminants by ultraviolet photography
page 205 MFS-25296

METALLIZING

Double metalization for VLSI
page 232 MFS-25149

Progress in MOSFET double-layer metalization
page 246 MFS-25239

METHANE

Methane/air flames in a concentric-tube combustor
page 184 LEW-13388

MICROPARTICLES

Controlling the shape of glass microballoons
page 236 MFS-25230

MICROWAVE EQUIPMENT

Computer-controlled warmup circuit
page 139 NPO-14815

Integral storage-bulb and microwave cavity for masers
page 170 GSC-12542

MINING

Position monitor for mining machines
page 141 MFS-25342

MIRRORS

Detecting surface faults on solar mirrors
page 205 NPO-14684

MOTORS

A linear magnetic motor and generator
page 226 GSC-12518

NOISE REDUCTION

Suppressing buzz-saw noise in jet engines
page 196 LAR-12645

NONDESTRUCTIVE TESTS

Digital enhancement of X-rays for NDT
page 206 KSC-11118

NONLINEARITY

Linearizing dc transducer output
page 152 NPO-14617

NOZZLE DESIGN

Predicting propulsion system drag
page 210 LAR-12619

NUCLEAR REACTORS

Removal of hydrogen bubbles from nuclear reactors
page 180 LAR-12597

NUTS [FASTENERS]

Locknut preload tool
page 217 MSC-16153

OCEAN SURFACE

Oceanic-wave-measurement system
page 200 MFS-23862

OPTICAL DATA PROCESSING

Better-quality CCD-array images
page 153 NPO-14426

OPTICAL EQUIPMENT

Optical calibrator for TDL spectrometers
page 164 GSC-12562

OPTICAL MEASUREMENT

Detecting surface faults on solar mirrors
page 205 NPO-14684

OXIDATION

An automated oxide and diffusion facility for IC's
page 246 MFS-25357

PARALLEL PROCESSING

Input/output interface module
page 143 MSC-18180

PARTICLE DENSITY

Photographic measurement of droplet density
page 167 MFS-25326

PARTICULATE SAMPLING

Improved particulate-sampling filter
page 240 NPO-14801

PASSIVITY

Photonitride passivating coating for IC's
page 231 MFS-25401

Silicon nitride passivation of IC's
page 245 MFS-25309

PERFORMANCE TESTS

A test program for solar collectors
page 174 MFS-25433

Operational tests of a solar-energy system in Georgia
page 174 MFS-25420

Outdoor tests of the concentric-tube collector
page 172 MFS-25398

PHASE CONTROL

LSI logic for phase control rectifiers
page 144 MFS-25208

PHOTOCHEMICAL REACTIONS

UV actinometer film
page 165 NPO-14479

PHOTOGRAPHIC MEASUREMENT

Photographic measurement of droplet density
page 167 MFS-25326



PHOTOGRAPHIC PROCESSING			
Automatic 35-mm slide duplicator	page 220	LEW-13399	
PHOTOGRAPHY			
Camera add-on records time of exposure	page 168	LAR-12635	
PHOTOVOLTAIC CELLS			
A survey of photovoltaic systems	page 171	MFS-25397	
PIEZOELECTRIC TRANSDUCERS			
Low-cost calibration of acoustic locators	page 169	LAR-12632	
PIPES [TUBES]			
Flared-tube attachment fitting	page 213	MSC-18416	
Shrinking plastic tubing to nonstandard diameters	page 237	MSC-18430	
Sleeve puller salvages welded tubes	page 225	MSC-18686	
Test fittings for dimensionally critical tubes	page 222	NPO-14399	
Tube-flare inspection tool	page 213	MSC-19636	
Tube-welder aids	page 244	MSC-18687	
PLASTICIZERS			
Plasticizer for polyimide composites	page 180	LAR-12642	
PLASTICS			
Forming complex cavities in clear plastic	page 237	LEW-13412	
Plastic welder	page 242	LAR-12540	
POLARIZED RADIATION			
Dual-frequency bidirectional antenna	page 138	GSC-12501	
POLYIMIDES			
Plasticizer for polyimide composites	page 180	LAR-12642	
POLYMERIC FILMS			
UV actinometer film	page 165	NPO-14479	
POSITION [LOCATION]			
A microcomputer for Doppler data processing	page 151	GSC-12448	
Position monitor for mining machines	page 141	MFS-25342	
POWER EFFICIENCY			
Energy saving in ac generators	page 132	MFS-25302	
Improved power-factor controller	page 133	MFS-25323	
POWER SUPPLY CIRCUITS			
Frequency-controlled voltage regulator	page 156	NPO-13633	
PRESSURE SENSORS			
Downhole pressure sensor	page 199	NPO-14729	
PROGRAMMING LANGUAGES			
MBASIC processor	page 254	NPO-14245	
PROJECT MANAGEMENT			
NASA PERT time II	page 252	LEW-13145	
PROPULSION SYSTEM CONFIGURATIONS			
Predicting propulsion system drag	page 210	LAR-12619	
PROXIMITY			
3-D guidance system with proximity sensors	page 221	NPO-14521	
PYLONS			
Quasi-passive vibration decoupler	page 195	LAR-12468	
RADIATION EFFECTS			
Measuring radiation effects on MOS capacitors	page 203	NPO-14700	
RADIATION MEASURING INSTRUMENTS			
All-inorganic spark-chamber frame	page 235	GSC-12354	
RADIO FREQUENCY HEATING			
Time-shared RF brazing	page 240	MSC-18617	
RANDOM ACCESS MEMORY			
RAM-based frame synchronizer	page 149	GSC-12430	
RAM-based parallel-output controller	page 150	GSC-12447	
RECTIFIERS			
LSI logic for phase control rectifiers	page 144	MFS-25208	
REDUNDANT COMPONENTS			
A redundant regulator control with low standby losses	page 157	NPO-13165	
REGENERATION [ENGINEERING]			
Regenerative superheated steam-turbine cycles	page 208	LEW-13392	
REGRESSION ANALYSIS			
Multiple linear regression analysis	page 234	MFS-23764	
REMOTE HANDLING			
End effector for gripping objects	page 215	MFS-23692	
REMOTE SENSORS			
Heat-pipe sensor for remote leveling	page 209	GSC-12095	
REPRODUCTION [COPYING]			
Automatic 35-mm slide duplicator	page 220	LEW-13399	
REUSE			
Sleeve puller salvages welded tubes	page 225	MSC-18686	
ROTORS			
Rotor transient analysis	page 228	LEW-13230	
SEALS [STOPPERS]			
Design considerations for mechanical face seals	page 183	LEW-13146	
Thermal barrier and gas seal	page 238	MSC-18390	
SHEAR PROPERTIES			
Efficient measurement of shear properties of fiber composites	page 193	LEW-13011	
SHOCK ABSORBERS			
Self-adjusting mechanical snubbing link	page 218	MSC-16134	
SHRINKAGE			
Shrinking plastic tubing to nonstandard diameters	page 237	MSC-18430	
SIGNAL PROCESSING			
Smoothing the output from a DAC	page 144	FRC-11025	
SILICON NITRIDES			
Photonitride passivating coating for IC's	page 231	MFS-25401	
Silicon nitride passivation of IC's	page 245	MFS-25309	
SLEEVES			
Heat-shrinkable sleeve aids in installing universal joints	page 239	MSC-18685	
Sleeve puller salvages welded tubes	page 225	MSC-18686	
SLIDING			
Electromechanical slip sensor	page 223	NPO-14654	
SOLAR CELLS			
A survey of photovoltaic systems	page 171	MFS-25397	
Improved multispectral solar-cell array	page 169	HQN-10937	
Ohmic contact to GaAs semiconductors	page 233	LAR-12466	
"Peeled-film" solar cells	page 135	NPO-14734	
SOLAR ENERGY			
A hot-water system tested onsite — Togus, Maine	page 175	MFS-25435	
A reliable solar-heating system — Huntsville, Alabama	page 175	MFS-25431	
A solar-energy system in Minnesota	page 175	MFS-25428	
A solar-energy system in Pennsylvania	page 173	MFS-25427	
A survey of photovoltaic systems	page 171	MFS-25397	
A test program for solar collectors	page 174	MFS-25433	
Detecting surface faults on solar mirrors	page 205	NPO-14684	
Final report on development of a programmable controller	page 171	MFS-25388	
Finned-absorber solar collector	page 173	MFS-25385	
Fresnel lens tracking solar collector	page 172	MFS-25419	
Installation guidelines for the Pennsylvania system	page 175	MFS-25424	
Operational tests of a solar-energy system in Georgia	page 174	MFS-25420	
Operational tests of a solar-energy system — Florida site	page 174	MFS-25423	
Outdoor tests of the concentric-tube collector	page 172	MFS-25398	
Selective optical coatings for solar collectors	page 173	MFS-25389	
Solar-heating and cooling demonstration project	page 176	MFS-25443	
SPARK CHAMBERS			
All-inorganic spark-chamber frame	page 235	GSC-12354	
SPECTRAL ENERGY DISTRIBUTION			
Improved multispectral solar-cell array	page 169	HQN-10937	
SPECTROMETERS			
High-resolution double-pass interferometer	page 162	NPO-14448	
Optical calibrator for TDL spectrometers	page 164	GSC-12562	
SPHERES			
Hybrid microspheres	page 182	NPO-14462	
STANDARDS			
A temperature fixed point near 58° C	page 179	MFS-25304	
STATIC DISCHARGERS			
More-reliable SOS ion implantations	page 232	MFS-25322	
STATISTICAL ANALYSIS			
Multiple linear regression analysis	page 234	MFS-23764	

STATISTICAL DISTRIBUTIONS			
An approximation to Student's t-distribution	page 251	LAR-12238	
STEAM TURBINES			
Regenerative superheated steam-turbine cycles	page 181	LEW-13392	
STEELS			
Improved adherence of TiC coatings to steel	page 181	LEW-13169	
STORAGE TANKS			
Thermal stratification in liquid-storage tanks	page 171	MFS-25416	
STOCHASTIC PROCESSES			
Linear stochastic optimal control and estimation problem	page 253	LEW-13206	
STRATIFICATION			
Thermal stratification in liquid-storage tanks	page 171	MFS-25416	
STRUCTURAL ANALYSIS			
Predicting crack propagation	page 248	MSC-18718	
STRUCTURAL MEMBERS			
Automatic connector joins structural columns	page 222	LAR-12578	
STRUCTURAL VIBRATION			
Vibration modes and frequencies of structures	page 209	LAR-12647	
STUDENT'S t-DISTRIBUTION			
An approximation to Student's t-distribution	page 251	LAR-12238	
SUPPORTS			
Cryogen-storage-tank support	page 227	MSC-14848	
SUPPRESSORS			
Suppressing buzz-saw noise in jet engines	page 196	LAR-12645	
SURFACE DEFECTS			
Detecting surface faults on solar mirrors	page 205	NPO-14684	
SWITCHES			
Automatic thermal switches	page 191	GSC-12553	
SYNCHRONIZERS			
RAM-based frame synchronizer	page 149	GSC-12430	
SYSTEMS ANALYSIS			
System time-domain simulation	page 255	MSC-18333	
TANKER SHIPS			
Detection of tanker defects with infrared thermography	page 196	LAR-12655	
TELECOMMUNICATION			
Dual-frequency bidirectional antenna	page 138	GSC-12501	
TELEMETRY			
RAM-based frame synchronizer	page 149	GSC-12430	
TEMPERATURE COMPENSATION			
Temperature-compensating dc restorer	page 136	LAR-12549	
TEMPERATURE CONTROL			
Automatic thermal switches	page 191	GSC-12553	
TEMPERATURE DISTRIBUTION			
Heat conduction in three dimensions	page 210	MSC-18616	
Thermal stratification in liquid-storage tanks	page 171	MFS-25416	
TEMPERATURE SCALES			
A temperature fixed point near 58° C	page 179	MFS-25304	
THERMAL DIFFUSIVITY			
Changes in "thermal lens" measure diffusivity	page 195	NPO-14657	
THERMAL INSULATION			
Thermal barrier and gas seal	page 238	MSC-18390	
THERMOPLASTIC RESINS			
Plastic welder	page 242	LAR-12540	
Resistance welding graphite-fiber composites	page 234	MSC-18534	
THERMOSTATS			
Automatic thermal switches	page 191	GSC-12553	
THIN FILMS			
"Peeled-film" solar cells	page 135	NPO-14734	
TIME SHARING			
Time-shared RF brazing	page 240	MSC-18617	
TIMING DEVICES			
Camera add-on records time of exposure	page 168	LAR-12635	
TITANIUM CARBIDES			
Improved adherence of TiC coatings to steel	page 181	LEW-13169	
TOOLS			
Handtool assists in bundling cables	page 225	MSC-18567	
Locknut preload tool	page 217	MSC-16153	
Tube-flare inspection tool	page 213	MSC-19636	
Tube-welder aids	page 244	MSC-18687	
TORQUE			
Locknut preload tool	page 217	MSC-16153	
Torque control for electric motors	page 155	MSC-18635	
TRACTION			
High-performance, multiroller traction drive	page 216	LEW-13347	
TRANSDUCERS			
Linearizing dc transducer output	page 152	NPO-14617	
TRANSFER TUNNELS			
A versatile tunnel acts as a flexible duct	page 214	MFS-22636	
TRANSFORMERS			
Producing gapped-ferrite transformer cores	page 241	NPO-14715	
TRANSIENT RESPONSE			
Rotor transient analysis	page 228	LEW-13230	
TURBINES			
Regenerative superheated steam-turbine cycles	page 208	LEW-13392	
ULTRASONIC TESTS			
Fresnel lenses for ultrasonic inspection	page 194	MSC-18469	
ULTRAVIOLET PHOTOGRAPHY			
Detecting contaminants by ultraviolet photography	page 205	MFS-25296	
ULTRAVIOLET SPECTROPHOTOMETERS			
UV actinometer film	page 165	NPO-14479	
VIBRATION MODE			
Vibration modes and frequencies of structures	page 209	LAR-12647	
VIBRATORY LOADS			
Quasi-passive vibration decoupler	page 195	LAR-12468	
VIDEO EQUIPMENT			
Real-time film recording from stroke-written CRT's	page 154	LAR-12529	
VOLTAGE CONVERTERS [DC TO DC]			
Direct-current converter for gas-discharge lamps	page 140	MSC-18407	
VOLTAGE REGULATORS			
A redundant regulator control with low standby losses	page 157	NPO-13165	
Frequency-controlled voltage regulator	page 156	NPO-13633	
VORTEX SHEETS			
A generalized vortex lattice method	page 209	LAR-12636	
WATER WAVES			
Oceanic-wave-measurement system	page 200	MFS-23862	
WEATHER DATA RECORDERS			
A microcomputer for Doppler data processing	page 151	GSC-12448	
WELD TESTS			
"Foreign material" to verify root fusion in welded joints	page 243	MFS-19496	
WELDED JOINTS			
Tube-welder aids	page 244	MSC-18687	
WELDING			
Electron-beam welder circle generator	page 91	MFS-19441	
Plastic welder	page 242	LAR-12540	
Resistance welding graphite-fiber composites	page 234	MSC-18534	
WELLS			
Downhole pressure sensor	page 199	NPO-14729	
WIND VELOCITY MEASUREMENT			
Instrument remotely measures wind velocities	page 163	NPO-14524	
X RAY INSPECTION			
Digital enhancement of X-rays for NDT	page 206	KSC-11118	
X-ray beam pointer	page 224	MSC-18590	



National Aeronautics and
Space Administration

Washington, D.C.
20546

Official Business
Penalty for Private Use, \$300

THIRD-CLASS BULK

THIRD-CLASS BULK RATE
POSTAGE & FEES PAID
NASA
WASHINGTON, D.C.
PERMIT No. P-154

NASA

Lightweight metalized plastic blankets are now a familiar sight at the finish lines of distance races, where runners use them to prevent loss of body heat. An outgrowth of early NASA work on metalization technology for spacecraft, the blankets are just one of a broad line of related products with industrial and consumer-oriented applications. [See the bottom of page A1.]

